6-18-2018 2:00 PM

The Incorporation of Phosphorus into Block Copolymers and Their Self-Assembly

Benjamin F. Hisey
The University of Western Ontario

Supervisor
Ragogna, Paul J.
The University of Western Ontario Joint Supervisor
Gillies, Elizabeth R.
The University of Western Ontario

Graduate Program in Chemistry
A thesis submitted in partial fulfillment of the requirements for the degree in Doctor of Philosophy

Abstract

The content of this thesis focuses on the incorporation of phosphorus into amphiphilic block copolymers (BCPs) for the realization of interesting properties in the solution phase self-assembled materials derived from the BCPs. The incorporation was achieved through attachment of phosphorus to the terminus of already existing BCPs or the synthesis of BCPs from prepared or commercially available phosphorus-containing monomers. The phosphorus-containing polymers exhibited properties due to the presence of the phosphorus in the BCPs. The first example of this is the modification of poly(ethylene oxide)-*b*-poly(ε-caprolactone) (PEO-*b*-PCL) copolymers by the attachment of tetraalkyl phosphonium salts with varying alkyl chains to the PEO chain end. The resulting nanoscale assemblies displayed antibacterial activity against *Escherichia coli* and *Staphylococcus aureus*. The nano-assemblies were also able to encapsulate and release the hydrophobic drug tetracycline. The second example from this work is the incorporation of phosphorus into the side chains of an amphiphilic polystyrene-*b*-poly((4-vinylbenzyl)tributylphosphonium) (PS-*b*-P(P+X-)) BCP. The BCP was used to study the effect of the counter-ion (X-) on aqueous self-assembly of the material through variation of the anion in the monomer. Anions investigated in the work included chloride, bromide, nitrate and trifluoromethylsulfonate, and while maintaining the same degree of polymerization, the change in the anion prior to self-assembly resulted in a significant difference in the resulting nanoparticles. The third example of the incorporation of phosphorus into a BCP features a poly(4-diphenylphosphino styrene)-*b*-poly((4-vinylbenzyl)tributylphosphonium chloride). This block copolymer features phosphorus as a phosphine and as a phosphonium salt. The phosphine block was able to form the core of self-assembled nano-particles and was shown to coordinate Pd, W and Mo. The corona underwent salt metathesis to coordinate $AuCl_4^-$. The final work is the synthesis of functional end-group containing polymers by the inclusion of phosphorus in reversible addition-fragmentation chain transfer (RAFT) agents. The incorporation of a phosphonium salt onto the end-group of poly(butyl acrylate) polymers demonstrates that the presence of the phosphonium salt allows the material to self-assemble in aqueous solution.

Keywords

Phosphonium salts, synthetic block copolymers, amphiphilic block copolymers, metal loaded nanoparticles, solution phase self-assembly

Co-Authorship Statement

The first chapter was written by Benamin Hisey and edited by Paul J. Ragogna and Elizabeth R. Gillies.

The work described in chapter two was coauthored by Benjamin Hisey, Paul J. Ragogna and Elizabeth R. Gillies and was published in *Biomacromolecules*, **2017**, *18*, 914-923. Benjamin Hisey wrote the first draft of the manuscript and all authors contributed to the editing process of the published work.

The work described in chapter three was coauthored by Benjamin Hisey, Jasmine V. Buddingh, Elizabeth R. Gillies and Paul J. Ragogna and was published in *Langmuir*, **2017**, *33*, 14738-14747. Benjamin Hisey was the main experimentalist on the work and Jasmine V. Buddingh, an undergraduate who Benjamin Hisey mentored, contributed via the synthesis of 4-vinylbenzyltributylphosphonium trifluoromethylsulfonate and the self-assembly of poly(styrene)-*b*-poly(4-vinylbenzyltributyl phosphonium chloride) as well as the characterization of those assemblies. Benjamin Hisey authored the manuscript and all authors contributed to the editing process of the published work.

Chapters 4, 5 and 6 were written by Benjamin Hisey and edited by Paul J. Ragogna and Elizabeth Gillies.

Dedication

I wish to dedicate this thesis to the memory of a dear friend, Kelly Larose. Kelly did not have the opportunity to continue her education. Her efforts were an enduring demonstration of her tenacity and ability to overcome obstacles. Kelly had the makings of an intelligent researcher and dedicated scientist, the Canadian scientific community lost someone promising the day she passed.

It's like forgetting the words to your favourite song
You can't believe it
You were always singing along
It was so easy and the words so sweet
Eet by Regina Spektor

Acknowledgements

My supervisors Paul Ragogna and Elizabeth Gillies have offered an education that cannot be described on this page. Their commitment to me as their student has continually exceeded my expectations and they have passed on such a wealth of knowledge and wisdom that I shall never be able to repay them.

My peers in the Ragogna and Gillies groups have contributed greatly to my success and ability to perform my work. Without the cohesive group of people willing to share in the trials and triumphs of one another, science could not progress in the way it has. My groups made my work as a chemist possible.

The various staff of the chemistry department at Western make studying and doing chemistry here possible, their excellence in their fields has allowed me to pursue excellence in mine.

My parents, Harold and Cecilia, and my siblings, Thomas and Andrew, have always shown support for my aspirations, and this has been no different for my time at Western. My in-laws Glen and Jackie have never hesitated to support me as one of their own children and my sisters-in-law, Jenna and Katie, have never failed to remind me of their desire to see me succeed.

I assure the reader that I could not have undertaken such a task as graduate school and found the success that I have without the consistent and incredible support that I receive from my wife Nicole. She is undoubtedly the largest contributor to my fight through the frustrations of graduate-level research. Her own career has served as an admirable and shining example of the value of hard-work and perseverance.

Lastly I thank my committee for their timely advice and guidance during my yearly reports and my examiners for the careful attention paid to my written and spoken defence of my work. As the final gate keepers to the coveted title of “doctor” your insurance that my knowledge is adequate, and my reasoning sound, provide the assurance that my degree was earned and not simply given.

To all of the above, thank you.

Table of Contents

List of Tables

List of Figures

List of Schemes

List of Equations

List of Abbreviations

°C	degrees Celsius
AIBN	azobisisobutyronitrile
ATCC	American type culture collection
ATRP	atom transfer radical polymerization
BCP	block copolymer
CAC	critical aggregation concentration
CFU	colony forming unit
CTA	chain transfer agent
CRP	controlled radical polymerization
CuAAC	copper-assisted alkyne azide click
Đ	dispersity
diBCP	diblock copolymer
DLC	drug loading content
DLS	dynamic light scattering
DP	degree of polymerization
DSC	differential scanning calorimetry
EE	encapsulation efficiency
E. coli	*Escherichia coli*
ESI	electrospray ionization
f_A	volume fraction
FTIR	Fourier-transform infrared spectroscopy
g	grams
HRMS	high-resolution mass spectrometry
Hz	hertz
IR	infra-red
kJ	kilojoules
M	moles-per-litre
M_n	number average molecular weight
M_w	weight average molecular weight
MBC	minimum bactericidal concentration
mL	millilitre
MRI	magnetic resonance imaging
MSA	methane sulfonic acid
MW	molecular weight
macroRAFT agent	macromolecular RAFT agent
mol	moles
N_A	number of repeat units
NMP	nitroxide mediated polymerization

NMR	nuclear magnetic resonance
PAA	poly(acrylic acid)
PDI	polydispersity index
PEO	poly(ethylene oxide)
PET	poly(ethylene terephthalate)
PCL	poly(ω-caprolactone)
PS	polystyrene
PTFE	poly(tetrafluoroethylene)
RAFT	reversible addition-fragmentation chain transfer
ROP	ring-opening polymerization
S. aureus	*Staphylococcus aureus*
SA	self-assemble/self-assembly
SEC	size-exclusion chromatography
T_c	melting temperature
T_g	glass transition temperature
TEM	transmission electron microscopy
TGA	thermal gravimetric analysis
χ	Flory-Huggins parameter

Chapter 1

Introduction

1.1 Introduction to Polymers

Polymeric materials have been used by humans throughout the course of our history. The earliest materials were unmodified natural polymers such as plant fibers, which were used for clothing or tools. The arrival of synthetic polymers had a profound impact on human society. For example, the introduction of moisture-proof cellophane (chemically modified cellulose) led to significant changes in how people interacted with their food (see Figure 1-1).[1] The trend of polymer materials shaping our society has continued to the present day and is expected to continue as researchers develop polymers able to impact future technologies such as nano-medicine,[2] robotics,[3] and even space exploration.[4]

Figure 1-1 A Dupont advertisement demonstrates how a currently ubiquitous product changed how people interact with their food.[1]

Polymers are defined as macromolecules composed of large numbers of much smaller molecules, or repeat units, linked together.[5] The molecular weights of polymers often range from the thousands of g/mol to millions of g/mol, and the length of individual polymer molecules in a sample can vary, unlike small molecules for which the molecular formulae and molecular weights are fixed. The high molecular weights and molecular weight distribution are responsible for the differences in physical properties observed between polymer samples and small molecules. The chemical structure of polymers contributes to their physical properties, as does the dispersity and absolute sizes of the polymer chains in the sample. Polymers thus require different ways to define their molecular weight than small molecules in order that scientists can explain differences between two chemically identical, but physically different polymer samples.

There are several definitions of polymer molecular weight that have arisen from a necessity to compare structurally similar polymer samples with different physical and chemical characteristics. The simplest measure of molecular weight is the number average molar mass, or M_n (Equation 1.1), of a polymer sample. M_n emphasizes the average chain length in the sample. The weight average molar mass, M_w (Equation 1.2), emphasizes the larger polymer chains in a sample, as these tend to dominate the physical properties of a polymer sample. The dispersity of a polymer sample, *Đ* (Equation 1.3), is defined as the ratio of the M_w to the M_n. The value of *Đ* is always greater than 1 as a consequence of how it is calculated. In the equations below, N_x is the number of molecules at a specific molecular weight and M_x is that molecular weight.

$$M_n = \frac{\sum N_x M_x}{\sum N_x} \qquad \text{Equation 1.1}$$

$$M_w = \frac{\sum N_x M_x^2}{\sum N_x M_x} \qquad \text{Equation 1.2}$$

$$Đ = {M_w}/{M_n} \qquad \text{Equation 1.3}$$

While small molecules are characterized by three major thermal transitions, polymers are characterized by two, the *glass transition temperature* (T_g) and the *crystalline melting temperature* (T_m). The T_m of a polymer is the onset temperature at which the crystalline domains in the polymer sample melt. This value is strictly greater

than T_g, if it is present. Not all polymers exhibit a T_m, because not all polymers are able to pack into crystalline domains. The T_g is the temperature at which the non-crystalline domains of the polymer transition from the glassy state to the rubbery state. In the glassy state polymer chains do not contain sufficient energy to overcome intermolecular interactions to organize into the equilibrium orientations on experimentally relevant timescales and so, the polymer chains behave like a solid. Polymers do not undergo a phase transition between their glassy state and their rubbery-viscous state.[6] As a polymer transitions into the rubbery-viscous state at the T_g, its physical properties go through a continuous transition and so, the transition is not considered a phase transition.[6] The polymer in the rubbery state has sufficient energy for the material to achieve the equilibrium orientations of the polymer chains on experimentally relevant timescales and the sample behaves like an extremely viscous liquid.

1.2 Block Copolymers

Polymers have found applications in an extremely diverse range of technologies. Many commercial polymers are termed homopolymers (Figure 1-2A), polymers that consist of a single kind of repeating unit. Examples of homopolymers include poly(ethylene terephthalate) (PET) used in water bottles and poly(tetrafluoroethylene) (PTFE), or commercially TEFLON, the common "anti-stick" coating.

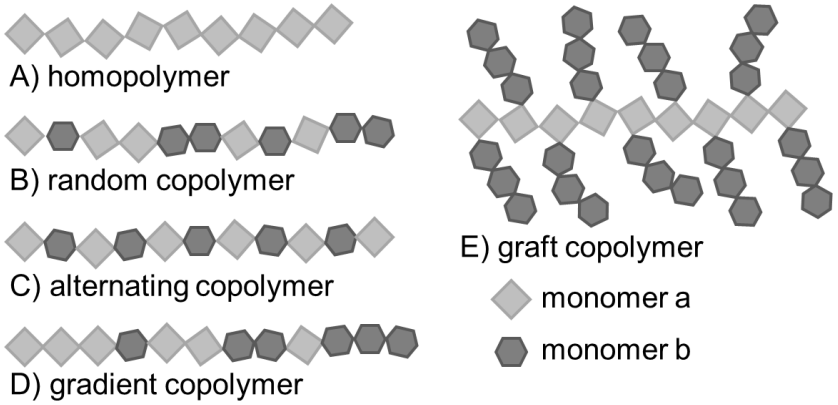

Figure 1-2. A) Linear homopolymer consisting of a single kind of repeat unit. B) Copolymer consisting of different repeat units randomly positioned. C) Copolymer consisting of alternating repeat units. D) Copolymer consisting of two polymers with two gradients across the backbone. E) Graft copolymer consisting of a backbone of one repeat unit with side chains of another.

Polymers that consist of more than one kind of repeat unit are called copolymers. The number and manor of incorporation of the different repeat units determines how the copolymer is classified. The simplest case is a copolymer consisting of two different repeat units with a random distribution of the repeat units along the backbone as demonstrated in Figure 1-2B, these copolymers are known as random copolymers. Copolymers can also incorporate two monomers that alternate along the backbone (Figure 1-2C) or appear in some predictable pattern. These are classified as statistical copolymers, as the monomers are present in some fixed distribution along the backbone. Another way that monomers may be incorporated is presented in Figure 1-2D. This copolymer has one end rich in monomer A, a gradient segment where the appearance of A decreases as B becomes increasingly prevalent and finally, a segment of monomer B. Graft copolymers (Figure 1-2E) consist of a backbone of one variety of repeat unit with side chains bearing polymers, one can also think of these materials as consisting of polymeric repeat units.

The last class, are block copolymers (BCPs). Several architectures of BCPs are demonstrated in Figure 1-3. BCPs are characterised by the presence of several segments, or blocks, of different repeat units that are covalently joined along the backbone. The number of blocks, sequences, and points of attachment of the blocks can result in a vast diversity of BCP architectures. The simplest case to envision is that of a linear diblock copolymer as depicted in Figure 1-3A. However, more blocks can be present and may be made of the same or different repeat units, so long as a block of a different repeat unit separates two blocks of the same repeat unit. Figure 1-3B illustrates a triblock copolymer composed of three chemically distinct blocks. While linear BCPs are often the most common examples, blocks can be attached at a central point, thus giving rise to the class of star polymers. The special case of Miktoarm star copolymers (Figure 1-3C) is used to describe star polymers with chemically dissimilar arms.

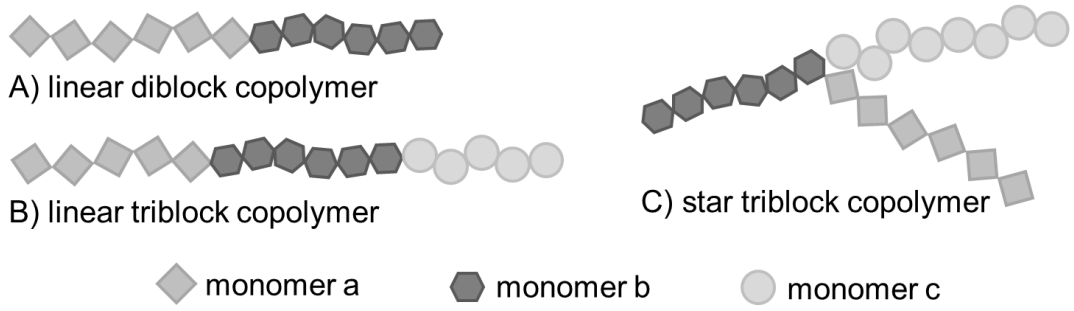

Figure 1-3 A) BCP consisting of two block adjoind at one end. B) BCP consisting of three blocks adjoined at their ends. C) BCP consisting of three blocks joined at a common point

The properties of copolymers are determined not only by the properties of the individual repeat units and the lengths of the chains, but also by the way the different repeat units are organized along the polymer backbone, and by the ratios of the repeat units. This means that BCPs with the same chemical components can have significantly different physical and chemical properties.

1.3 Polymer Synthesis

There are two main methods for assembling monomers to build polymers: step growth polymerization and chain growth polymerization. Step growth polymerization features the growth of the polymer chain at random points along the backbone. These events concatenate smaller monomers and oligomers into the polymer. Chain growth polymerization, the primary method utilised in this dissertation, involves the addition of monomers at the growing end of the polymer chain. While many differences exist in the reactions used in the two methods, the main feature that separates the two methods is the relationship between polymer molar mass and monomer consumption. Figure 1-4 shows that at low monomer conversion, the molar mass of the polymer chains in a chain growth sample is high and remains that way throughout the polymerisation. The step-growth mechanism, however, has low polymer molar masses up until very high monomer conversions. This is due to the conversion of monomers into small oligomers, and only when enough oligomers are present does the molar mass of the polymer chains become significant as they concatenate.[5]

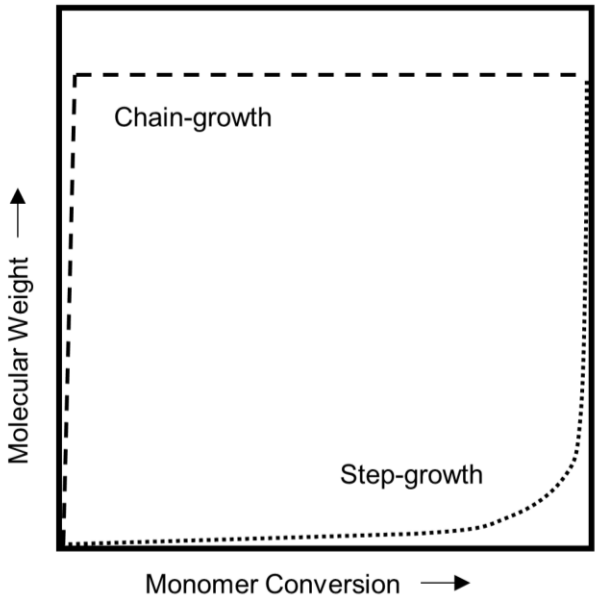

Figure 1-4 An important difference between chain-growth and step-growth polymerization is the appearance time of high molecular weight polymers during the conversion of monomer to polymer.

1.4 Radical Polymerization

The most common form of chain growth polymerization is radical polymerization. Radical polymerization uses a radical mechanism to convert monomers into polymer chains and has found widespread application for several reasons. Perhaps the most important reason is the variety of monomers polymerizable by this technique, among which the most common functional group is the alkene. The carbon-carbon double bond is often activated by the presence of adjacent functional groups such as carbonyls (such as the acrylates) or phenyl rings (such as the styrenic monomers). Radical chemistry converts the n carbon-carbon double bonds of n monomers into 2n carbon-carbon single bonds, an approximately 85 kJ/mol gain in bond energy. This large enthalpic change between the products and reactants is what drives the polymerization.

Radical polymerizations require radical initiators, compounds that undergo homolytic bond cleavage to produce reactive radical species. The bond cleavage is often initiated by light or heat, and the reactive radical goes on to react with a monomer unit, beginning the chain growth process in the initiation phase. Monomers add to the end of the growing polymer chain in an uncontrolled fashion during the propagation phase. When free monomer is nearly exhausted the prevalence of side reactions between the

polymer radicals results in the quenching of the reactive radical and the end of chain growth. The quenching may also be performed deliberately to end polymerization.

1.5 Controlled Radical Polymerization

While free radical polymerization can create high molecular weight polymers in a small amount of time, the method also produces polymer samples with large *Đ* values. To circumvent this, researchers have developed several methods for controlling the polymerization of monomers using radical mechanisms. Controlled radical polymerizations (CRP) utilize a dormant state species to limit the number of growing polymer chains present in the reaction mixture. The limitation of growing polymer chains reduces termination events involving these radicals and so samples of low *Đ* are produced (Figure 1-5).

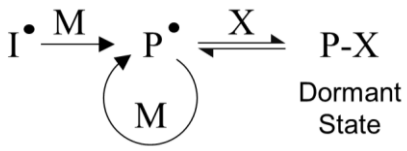

Figure 1-5 Idealized equilibrium of a controlled radical polymerization

CRP offers the ability to not only produce polymer samples with *Đ* close to 1, in many cases they also allow the isolation of the dormant species, which can subsequently be re-initiated to produce polymers of increasing complexity. Many techniques have been developed to control the radical polymerization of monomers. Some of the most widely utilized are stable free radical polymerization (often nitroxide mediated polymerization (NMP, Figure 1-6A)), atom transfer radical polymerization (ATRP, Figure 1-6B), and reversible addition-fragmentation chain transfer (RAFT, Figure 1-6C) polymerization. These methods involve the addition of an agent other than the initiator and monomer into the polymerization mixture in order to produce the dormant state.

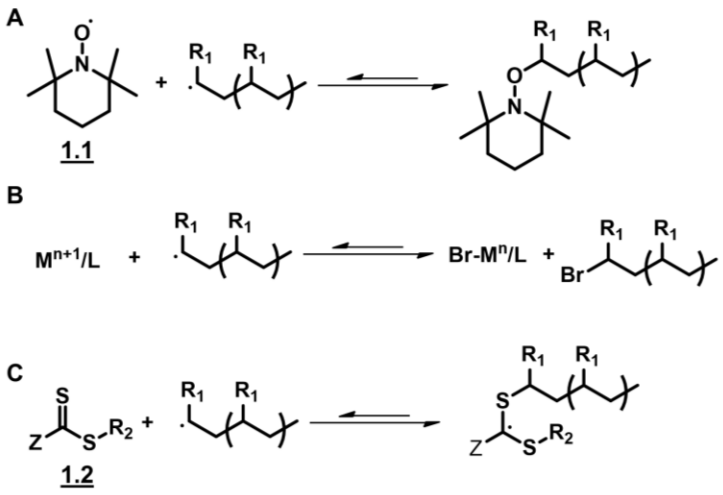

Figure 1-6 Three popular examples of controlled radical polymerization. A) NMP. B) ATRP. C) RAFT polymerization.

1.6 RAFT Polymerization

RAFT polymerization was first described in 1998 in a patent filed to the world intellectual property office[7], and first published in the same year in *Macromolecules* by the Commonwealth Scientific and Industrial Research Organization in Australia.[8] RAFT is separated from other forms of controlled radical polymerizations as it utilizes a degenerative chain transfer and does not rely on the existence of a persistent radical effect.[9] The RAFT process depends on the establishment of an equilibrium between actively growing polymer chains and dormant stable polymer chains. Because the RAFT process does not involve a change in the number of radicals present during polymerization the process is termed degenerative.[10] Figure 1-7 shows a detailed proposed mechanism of the RAFT process. The RAFT process is also unique in controlled radical polymerizations as it ideally does not affect the kinetics of the polymerization reaction that it controls, although in practice it can have an effect on the rates of polymerization.[11] This is because the growth of chains occurs while the polymer chain is unbound to the RAFT agent, and species **1.3** and **1.5** are ideally short-lived compared to species **1.2**, **1.4**, and **1.6**. It is important to note that, while the number of radicals does not change throughout the polymerization, the number of actively growing chains is reduced due to the formation of species **1.4** and **1.6** and this limits the prevalence of side reactions.

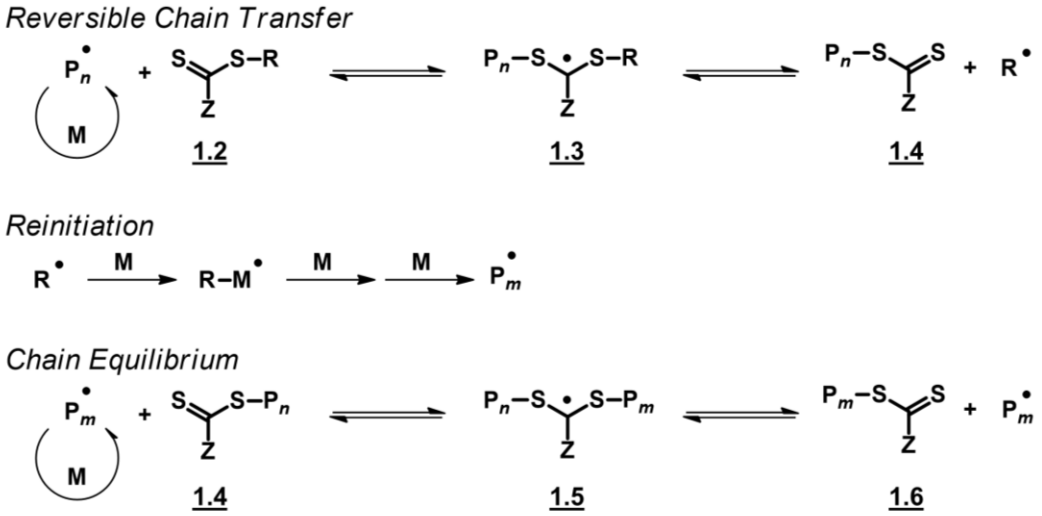

Figure 1-7. Proposed mechanism of RAFT polymerization demonstrating steps affected by the presence of the RAFT agent.[11] M ≡ monomer, P_n ≡ polymer.

RAFT polymerization has been used to control the polymerization of a wide range of monomers. This is due in part to the tolerance of most functional groups toward RAFT agents, but also the extensive variability available in RAFT agents.[12] Compound **1.2** demonstrates the general design of a thiocarbonylthio RAFT agent, where the groups Z and R can be rationally chosen to provide optimal control over the desired monomer.[13] The Z group affects the stability of the dormant state radical[11] and controls the rate at which the macroradical is added to or removed from the thiocarbonylthio unit of the RAFT agent. Better control of most monomers is generally achieved with the following order of Z groups: aryl > alkyl > S-alkyl > O-alkyl > N,N-alkyl.[13–15] RAFT agents in which there is an element with a lone pair conjugated to the carbonylthio group have low transfer coefficients.[13] The transfer coefficient refers to the propensity of a RAFT agent to go from **1.3** to **1.4**. This however can be altered by the presence of an electron-withdrawing group connected directly to the atom adjacent to the carbonylthio group.[14]

The choice of R group is also important in RAFT agent design, as it must balance being a good homolytic leaving group and a good reinitiator of the monomer.[11,15] The structure of the R group determines preference for **1.3** to fragment into products or return to the starting materials.[12] A good R group favours the formation of the R radical. The R group also determines the reinitiation rate of the monomer. If re-initiation does not occur,

retardation of the polymerization can occur, which results in a loss of control over the dispersity and molecular weight of the resulting polymer sample.[11,12,15] The chosen R group can also not simply be an analogue of the monomeric propagating radical. For example, when R is 2-ethoxycarbonyl-2-propyl (Figure 1-8), the RAFT agent provides poor control over the polymerization of methyl methacrylate, its monomeric analogue.[16] This is the result of 2-ethoxycarbonyl-2-propyl being a poor homolytic leaving group with respect to the poly(methyl methacrylate).[12] If the macroradical is an equivalent or better homolytic leaving group than the R group, then initiation from the RAFT agent R group occurs much later in the polymerization, resulting in poor control.

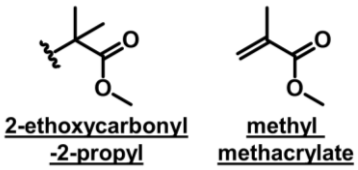

Figure 1-8. Comparison of structural similarities of the 2-ethoxycarbonyl-2-propyl RAFT agent R group and the monomer methyl methacrylate.

1.6.1 RAFT Polymerization to Produce Block Copolymers

RAFT has been used extensively to generate BCPs with varying degrees of complexity.[17–19] The simplest method to generate BCPs using RAFT polymerization is to make use of a polymer generated by RAFT as a macroRAFT agent. A macroRAFT agent has a polymeric R group. This R group can be initiated the same way as traditional RAFT polymerization, but when a different monomer is added to the chain end, a BCP is generated. This technique is known as *chain extension*. As RAFT polymerization installs a thiocarbonylthio group at the end of any living polymer chains, these can be purified between monomer additions and reinitiated in the presence of a radical source to yield BCPs.[17] Ideally this technique leads to true BCPs, and not gradient copolymers, as the macroRAFT agent can be isolated and purified between each monomer addition. When generating BCPs with this method the order of polymerization must be considered, as the preceding polymerized monomer becomes the reinitiating radical species, and so must have a good initiation of the following monomer to maintain control.[12] The Z group of the RAFT agent must also be able to provide good control over the equilibrium between **1.2**

and **1.3**, as well as **1.3** and **1.4**, favouring the formation of **1.4**.[17] There are also several other important practical considerations, such as the solubility of the macroRAFT agent and subsequent monomers, as well as the BCP generated.

Alternative methods of BCP generation also exist using RAFT polymerization. For example, polymers generated by alternative polymerization techniques can be incorporated onto the Z or R groups of the RAFT agent. This technique is different from *chain extension* because the fundamental kinetics of the RAFT process depicted in Figure 1-7 should ideally not be altered by the presence of a polymeric species not directly bonded to the thiocabronylthio unit. Alternatively, BCPs can be generated by the inclusion of reactive functional groups on the Z or R groups of the RAFT agent, such as 'clickable' units. Subsequent reaction of a RAFT-generated polymer with another polymer featuring reactive end-groups can then be used to generate the BCP.

1.7 Self-Assembly of Diblock Copolymers

Blends of materials with different physical properties tend towards phase separation when they have more thermodynamically favourable interactions amongst the same polymers than between the two different polymers.[20] The existence of distinct polymer blocks covalently joined in BCPs results in the inability for the polymers to *macro*phase-separate as they relax into equilibrium configurations. Most diblock copolymers (diBCPs), however, tend to *micro*phase separate due to differences in the chemical structures of each block.[21] The following discussion focuses on diBCPs as they have played a central role in BCP self-assembly. Given appropriate conditions, polymeric materials adopt the most thermodynamically favoured configuration.[22–24] Researchers have exploited the ability of BCPs to self-assemble to generate a wide array of bulk, thin film, and solution phase microphase separated materials. Descriptions of systems that undergo spontaneous self-assembly must consider several different energies of interactions. Most prominent however, are the interactions between blocks of different repeat units, and the interactions between the polymer blocks and the environment.[22–24]

1.7.1 Self-Assembly of diBCPs in Bulk

The morphologies adopted are based on the chemical structures of the blocks, their relative volume fractions (f_A), degrees of polymerization (N_A), and the connectivity of the blocks to one another. The first consideration is often expressed through the Flory-Huggins parameter (χ). The Flory-Huggins parameter is a measure of the incompatibility between a polymer and the molecules that are interacting with it.[20,22] While χ was used initially to describe the interaction between a polymer chain and solvent molecules, it can be used in an analogous way to describe generalized interactions between a polymer and another substance, such as another polymer block composed of different repeating units.[20] The χ varies inversely with temperature and the degree of microphase separation (for diblock copolymers) depends on χN_A, the segregation product.[22] The volume fractions of the blocks are important in determining what block forms the continuous phase of the bulk material as shown in Figure 1-9. The block with the greater f_A will often form the continuous phase of the bulk self-assembled material. Bulk phase self-assembly of BCPs has been used for a variety of applications such as photonic materials,[25] inorganic templates,[26,27] nanoporous membranes,[28] and many others.[26]

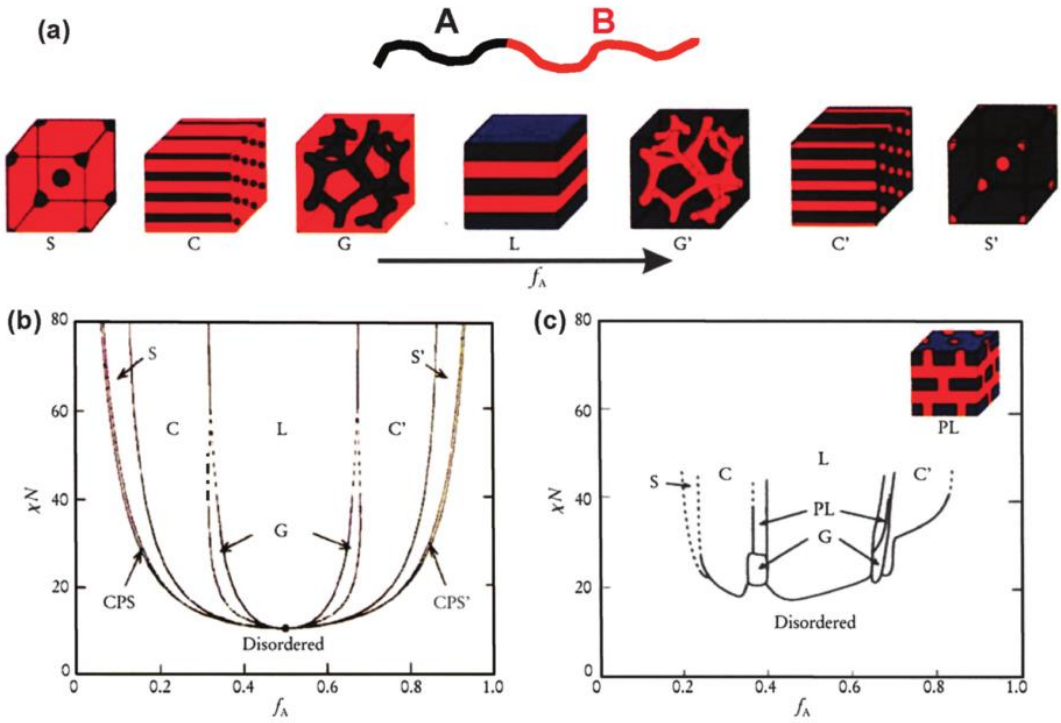

Figure 1-9. a) Bulk phase morphologies of self-assembled BCPs. b) Theoretical morphological diagram of bulk phase morphologies. c) Experimental morphological diagram.[22] Reproduced with permission of the publisher (Appendix E).

1.7.2 Self-Assembly of diBCPs in Solution

The self-assembly of diBCPs in the solution phase is controlled largely by three factors: packing of the core forming blocks, the interfacial energy between the core and the solvent, and repulsive interactions between coronal chains.[22] BCPs that are able to undergo solution phase self-assembly are described as amphiphilic[29] and to a smaller extent double-hydrophilic.[30–33] Nanoprecipitation is the common technique to cause the self-assembly of amphiphilic BCPs. It involves dissolution of the BCP in a non-selective solvent (a solvent that dissolves both blocks) and then the combination of this solution with a selective solvent (often water).[22] Double-hydrophilic BCPs, however, rely generally on a change in temperature,[30,31] change in pH,[33] ionic strength changes or the addition of a complexation agent.[32]

In order for BCPs to aggregate in solution, the concentration of the BCP must exceed the critical aggregation concentration (CAC).[23] Below the CAC, BCP chains are freely dissolved in solution, and above the CAC there is an equilibrium between chains in and out of aggregates (as long as the core is above the T_g). The CAC is primarily influenced by the length of the hydrophobic block in amphiphilic BCPs, as this is the portion of the BCP which induces self-assembly.[23] Materials formed through solution phase self-assemblies of BCP are often on the nanometer scale and are generally spherical. The most common morphology is the true micelle,[22,23,34] defined as a spherical particle with a corona and a core, the diameter of which does not exceed the total length of two polymer chains stretched end-to-end. Higher order morphologies observed are illustrated in Figure 1-10 and include rods, worm-like micelles, vesicles, lamellae and high-order bilayer structures.

The morphology generated by the self-assembly of the BCP depends on several factors. The packing of the core chains influences the CAC, but also governs the curvature that the aggregate is able to adopt. The curvature of the surface of the aggregate limits the available morphologies, as demonstrated in Figure 1-10. Eisenberg *et al.* have extensively studied the differences in how the relative block lengths influence the thermodynamic morphology formed in polystyrene-*b*-poly(acrylic acid) (PS-*b*-PAA) BCPs.[29,35–37] In those works, the authors showed that the relative block lengths of PAA to PS influenced the morphologies, with a tendency for relatively shorter PAA chains to

result in higher-order morphologies. This is attributed to the ability of these BCP aggregates to adopt a lower interfacial curvature due to smaller coronal chain interactions and the packing of the PS core forming blocks.[36,37] The interfacial energy between the core and the solvent influences the morphologies largely in the early stages of their formation. As water is added, the energy of packing of the core chains is minimized through arrangement of the particles into different morphologies, if the core chains are sufficiently swelled by non-selective solvent.[22] The interchain interactions of the corona chains also influence the morphology in two ways. They influence the association of the BCP as the aggregates are forming from dissolved chains, and they influence the curvature that the aggregate can adopt.[22]

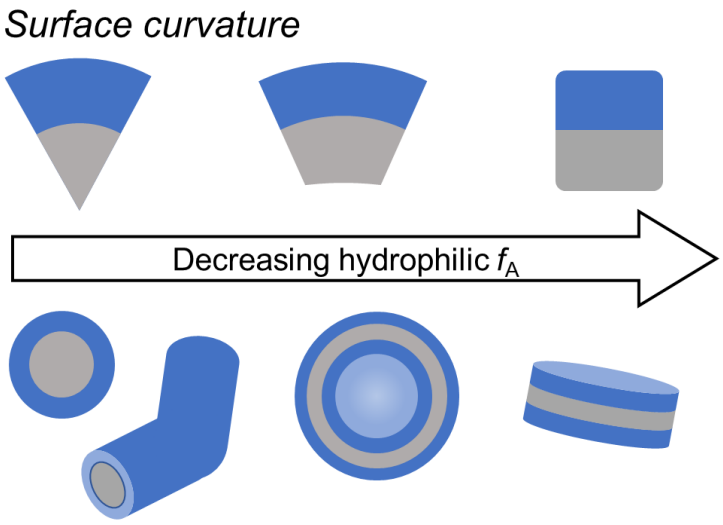

Figure 1-10. Influence of interfacial curvature on the available morphologies to diBCP aggregates. Morphologies on the bottom from left to right: micelle, rod-like micelle, vesicle, lamella.

Nanomaterials prepared by the self-assembly of BCPs continue to receive broad commercial and research interest. Amphiphilic block copolymers are used most widely as non-ionic polymeric surfactants for aqueous solutions.[38]

1.7.3 Biomedical Applications of BCP Aggregates

The ability of amphiphilic diBCP assemblies to encapsulate hydrophobic materials into their cores has made them materials of high interest to the drug delivery community.[39–43] DiBCP aggregates have favourable properties relative to low molecular

weight surfactant-based drug delivery vehicles as they often have greater loading capacities, greater drug stabilization, high aggregate stability, and longevity.[40] Aggregates designed for drug delivery systems also often make use of poly(ethylene oxide) (PEO) as the hydrophilic block, as this has 'stealth' like properties. The PEO does not result in the detection of the particles by the body's immune system, allowing PEO-stabilized aggregates to have increased circulation time.[43] In the years since diBCPs have been investigated for drug delivery, many new techniques have been developed to improve their stability, drug release rates, and targeting capabilities. One approach has been to add cross-linkable groups to the BCP or to add a targeting group to the corona, which are illustrated in Figure 1-11.[43] By cross-linking portions of the aggregate, the particles do not dissolve into free polymer chains even at low concentrations. Cross-linking can also increase release times. The targeting groups allow for drug carriers to accumulate at therapeutic targets. In one example of targeted drug delivery, Prabaharan and coworkers designed a BCP micellar system that used hydrazone bonds to conjugate doxorubicin, a common anti-cancer drug, to the hydrophobic poly(L-aspartate) block of a poly(L-aspartate)-*b*-PEO BCP.[44] The hydrazone linkage is labile in low pH environments, the environment common around tumors, and so in the presence of tumors the doxorubicin will release.[44] This is an example of passive targeting as there is no method to accumulate drug carrier in the presence of the tumor, yet the drug releases much faster in the presence of the tumor.[43] In another example Chen *et al.* conjugated a short cyclic peptide which binds to an overexpressed membrane protein in some tumor cells to the hydrophilic block terminus.[45] The particles with the targeting peptide had increased intracellular concentrations in cells overexpressing the targeted protein compared to non-targeting micelles.[45]

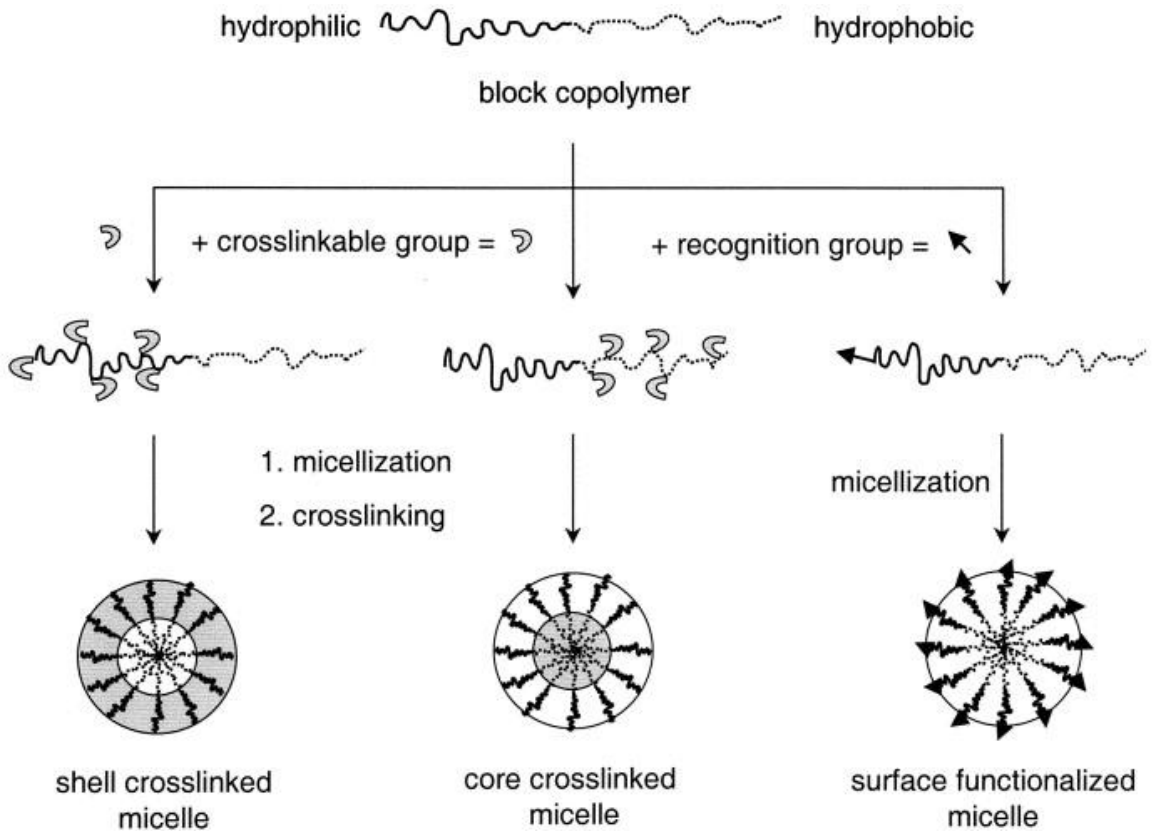

Figure 1-11. Cartoon illustrating the various ways that BCP aggregates have been functionalized to improve their uses as biomedical nanotechnology.[43] Reproduced with permission from Elsevier (Appendix E)

While drug delivery capabilities of BCP aggregates have received wide and varied attention, researchers have also employed self-assembled BCPs in imaging and diagnostic applications. Imaging capabilities have included MRI contrast enhancement,[46–48] X-ray computed tomography, and others.[46] Self-assembled BCP aggregates offer several advantages over traditional small molecule contrast agents such as prolonged residence times in the blood and high localized concentrations due to targeting abilities of BCP aggregates.[48] The enhancement of imaging techniques is often achieved through the loading of the particles with contrast agents such as lanthanide particles into the core to improve imaging in computed tomography.[39,46,49]

1.7.4 Other Solution Phase Applications of BCP Aggregates

BCP aggregates have been exploited in unique and varied research applications. This is largely due to the library of techniques available to synthetic polymer chemists to control finely the architecture of BCPs.[23] An active area of research is the use of BCP

aggregates as nanoreactors.[50–58] BCP aggregates provide an excluded volume from the solvent. This volume has a different polarity and a different chemical environment than the external solution allowing for reactions to occur in media that have been historically difficult. For example, Boucher-Jacobs and coworkers demonstrated the ability to use aqueous dispersed BCP micelles loaded with a non-aqueous soluble Pd catalyst to polymerize ethylene.[56] While the efficiency of the catalyst in the micelles was lower than that in an organic solvent, the stability of the system and the performance compared to traditional aqueous methods was favourable.[56]

BCP solution phase aggregates have also been employed as templates for the formation of mesoporous inorganic materials.[59–63] The ability to associate inorganic precursor material to the core or coronas of BCP aggregates allows for the controlled spatial deposition of the materials onto surfaces, where the BCP is removed and the precursor transformed into the desired mesoporous material. One recent example of this strategy was demonstrated by the Mai and Feng groups, who reported the formation of mesoporous polypyrrole layers with embedded Fe_2O_3 nanoparticles templated on either side of reduced graphene nanosheets by PS-*b*-PEO BCP micelles.[61] The prepared material served as a supercapacitor electrode material with desirable properties, but could be further pyrolyzed to produce 'sandwich-like' mesoporous N-doped carbon/Fe_3O_4/rGO material. This material was effective as a catalyst for an oxygen reduction reaction comparable to commercially available Pt/C catalysts.[61]

The applications of solution phase BCP aggregates continue to grow as novel polymer architectures are investigated and modern techniques allow the study of increasingly complex systems. Several reviews demonstrate the breadth of this area of research.[23,24,26]

1.8 Phosphorus-Containing BCPs

The incorporation of phosphorus into polymeric materials has resulted in an expanded scope of applications for polymeric materials. The design of synthetic polymers has incorporated phosphorus to impart improved functionality. For example, phosphorus has been used in dental resins for its ability to bind to tooth enamel,[64] anticorrosion coatings for metals,[65] bone adhesives,[66] anti-fouling surfaces with phosphorylcholines,[67]

and antibacterial phosphonium-containing polymers.[68] The incorporation of phosphorus into BCPs has also yielded many interesting and practical results. For example, side chain metal-containing aggregates,[69] main chain metal-containing BCPs,[70–72] biocompatible BCP nanoparticles,[73,74] ion transport materials,[75–77] novel flame-retardant materials,[78,79] oxygen sensing materials,[80] nanoreactors,[81] and many others.[64,82–88]

There are two main strategies for incorporating phosphorus into BCPs. Post-polymerization functionalization involves the reaction of the polymeric material with a phosphorus-containing reagent. This allows for ready access to materials with novel properties, while using traditional polymerization techniques. For example, in 2000 Persigehl and coworkers synthesized a phosphine-containing amphiphilic BCP able to undergo self-assembly through a Pd catalyzed P-C coupling reaction.[89] The authors used living cationic polymerization to prepare a poly(2-methyl-2-oxazoline)-*b*-poly((2-heptyl-2-oxazoline)-*co*-(4-iodophenylheptyl-2-oxazoline)) BCP (**1.7** in Figure 1-12). The I-C bond was replaced by a Pd cross-coupling of diphenylphosphine with the polymer, a reaction developed by Stelzer *et al.*[90] The authors showed that the complete exchange of I-C bonds to P-C bonds was possible within 48 hours at a 0.2 mol% catalyst loading.[89]

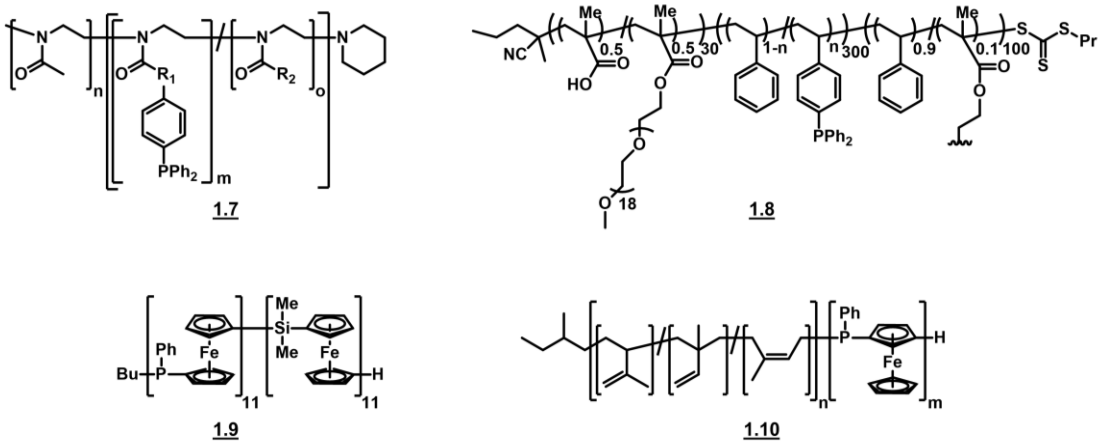

Figure 1-12. Phosphorus containing BCPs.

The second method of incorporation uses phosphorus-containing monomers, either in the side chain or polymerizable group. Side chain phosphorus-bearing monomers can be polymerized through traditional polymerization techniques as the polymerizable group is often well known. For example, Lobry and coworkers prepared an amphiphilic triblock copolymer through RAFT polymerization of commercially available monomers,

including 4-diphenylphosphino styrene.[91] The resulting poly(methacrylic acid-*co*-poly(ethylene oxide)methyl ether methacrylate)-*b*-poly(styrene-*co*-4-diphenylphosphino styrene)-*b*-poly(styrene-*co*-di(ethylene glycol) dimethacrylate) (**1.8**) was able to coordinate Rh in the core of the polymerization-induced self-assembled nanogels. The Rh loaded nanogels showed little to no Rh leaching and were able to catalyze the hydroformylation of 1-octene.[91]

Incorporating phosphorus into the backbone of the BCP has been achieved either through reactivity involving the phosphorus, such as is the case in polyphosphazenes[92,93] or the ring-opening polymerization (ROP) of [1]ferrocenophanes.[70–72] The poly(ferrocenylphosphine) BCPs have been prepared by the Manners group. They make use of the relatively weak bond in [1]ferrocenophane to promote the anionic ROP to yield a living polymer chain. The addition of [1]ferrocenosilane resulted in a poly(ferrocenylphosphine)-*b*-poly(ferrocenylsilane) BCP (**1.9**).[71] In subsequent work others demonstrated that it is also possible to form poly(ferrocenylphosphine)-*b*-polyisoprene (**1.10**) that can self-assemble in hexane.[72] This material was able to coordinate Au(I) in the poly(ferrocenylphosphine) core of the micelles. The Gates group has also contributed several studies to the field of phosphorus-containing block copolymers.[94-96] Most recently they have demonstrated the ability of a poly(isoprene)-*b*-poly(phosphine) BCP to undergo self-assembly and coordinate a low valent Au(I) species.[96] They were able to fine-tune the morphology by changing the relative lengths of the block copolymer.

1.9 Scope of Thesis

This dissertation focuses on the incorporation of phosphorus into amphiphilic BCPs to impart interesting functionality to these materials in the solution phase aggregates. Chapter 2 of this work illustrates the biological activity that can result from the incorporation of trialkyl-(4-pentynyl)phosphonium chloride salts onto the corona of micelles formed from poly(ethylene oxide)-*b*-poly(caprolactone) (PEO-*b*-PCL) BCPs. The resulting aqueous dispersible micelles showed bactericidal activity against *Escherichia coli* (*E. coli*) and *Staphylococcus aureus* (*S. aureus*). The material also had the ability to encapsulate and release the hydrophobic antibacterial drug tetracycline.

Chapter 3 explores the effect of the anion on the self-assembly of a polystyrene-*b*-poly(4-vinylbenzyltributyl phosphonium) BCP. While the self-assembly of polyelectrolyte BCPs has been extensively investigated over their research history, there was a lack of investigation into the effect the counterion had on the resulting aggregates formed from the aqueous self-assembly of polyelectrolyte BCPs. By changing the identity of the anion and maintaining all other relevant properties of the BCPs, the effect of the anion on the size of aggregates was determined.

Chapter 4 reports the first synthesis of poly(4-diphenylphosphino styrene)-*b*-poly(4-vinylbenzyltributyl phosphonium chloride), a BCP containing a phosphine and a phosphonium block. This polymer has demonstrable ability to incorporate two different metals through different interactions with the phosphorus species. By coordination of the phosphine to metals, the core of the aqueous phase BCP nano-particles can be loaded with Pd, W, or Mo. These aggregates can undergo anion exchange with $HAuCl_4$ in aqueous solution. These bimetallic species offer an interesting path into metal-containing nanoscale aggregates or ceramics.

Chapter 5 reports progress in the synthesis of phosphorus-containing RAFT agents. The versatility of RAFT polymerization offers unique advantages to other forms of CRP. By incorporating phosphorus into RAFT agents, phosphorus can be introduced into a wide variety of materials and impart new functionalities to polymeric systems. This work shows the ability to synthesize a phosphonium salt-containing RAFT agent that can control the polymerization of *n*-butyl acrylate. The resulting polymer can undergo aqueous self-assembly, with the particles being stabilized in water by the presence of the single end-group phosphonium salt.

1.10 References

1. Bernat, C. (2011). *Food culture, supermarkets, and packaging: A researcher's perspective*. [online] O Say Can you See?. Available at: http://americanhistory.si.edu/blog/2011/10/food-culture.html [Accessed 29 Nov. 2017].
2. G. Chen, I. Roy, C. Yang, P. N. Prasad, *Chem. Rev.*, 2016, **116**, 2826–2885.
3. Rossiter, J. (2018). *Robotics, Smart Materials, and Their Future Impact for*

Humans. [online] OpenMind. Available at: https://www.bbvaopenmind.com/en/article/robotics-smart-materials-and-their-future-impact-for-humans/?fullscreen=true [accessed January 16, 2018].

4. I. Kondyurina, A. Kondyurin, B. Lauke, Ł. Figiel, R. Vogel, U. Reuter, *Adv. Sp. Res.*, 2006, **37**, 109–115.
5. G. Odian, *Principles of Polymerization*, John Wiley & Sons, Inc., New Jersey, fourth edition, 2004.
6. P. G. Debenedetti, F. H. Stillinger, *Nature*, 2001, **410**, 259–267.
7. T. P. Lee, G. Moad, E. Rizzardo, S. H. Thang, WO 98/01478 1998.
8. J. Chiefari, Y. K. Chong, F. Ercole, J. Krstina, J. Jeffery, T. P. T. Le, R. T. A. Mayadunne, G. F. Meijs, C. L. Moad, G. Moad, E. Rizzardo,S. H. Thang, *Macromolecules*, 1998, **31**, 5559-5562.
9. C. Barner-Kowollik, In *Handbook of RAFT Polymerization*, C. Barner-Kowollik, Ed.; Wiley-VCH Verlag GmbH & Co., Darmstadt, Germany, 2008, ch. 1, pp. 1–4.
10. S. Perrier, *Macromolecules*, 2017, **50**, 7433–7447.
11. Moad, G., Barner-Kowollik, C. In *Handbook of RAFT Polymerization*, C. Barner-Kowollik, Ed.; Wiley-VCH Verlag GmbH & Co., Darmstadt, Germany, 2008, ch. 3, pp. 51–104.
12. D. J. Keddie, G. Moad, E. Rizzardo, S. H. Thang, *Macromolecules*, 2012, **45**, 5321–5342.
13. M. Destarac, *Polym. Rev.*, 2011, **51**, 163–187.
14. J. Chiefari, R. T. A. Mayadunne, C. L. Moad, G. Moad, E. Rizzardo, A. Postma, S. H. Thang, *Macromolecules*, 2003, **36**, 2256–2272.
15. E. Rizzardo, G. Moad, S. H. Thang, In *Handbook of RAFT Polymerization*, C. Barner-Kowollik, Ed.; Wiley-VCH Verlag GmbH & Co., Darmstadt, Germany, 2008, ch. 6, pp. 189–234.
16. B. Y. K. Chong, J. Krstina, T. P. T. Le, G. Moad, A. Postma, E. Rizzardo, S. H. Thang, *Macromolecules*, 2003, **36**, 2256–2272.
17. M. H. Stenzel, In *Handbook of RAFT Polymerization*, C. Barner-Kowollik, Ed.; Wiley-VCH Verlag GmbH & Co., Darmstadt, Germany 2008; pp. 315–372.

18. D. J. Keddie, *Chem. Soc. Rev.*, 2014, **43**, 496–505.
19. W. B. Farnham, M. T. Sheehan, In *Directed Self-assembly of Block Co-polymers for Nano-manufacturing* Elsevier 2015, ch. 1, pp. 27–45.
20. I. W. Hamley, *Introduction to Soft Matter Revised Edition*, John Wiley & Sons, Ltd., Padstow, Great Britain, 2007.
21. S. F. Bates, *Science*, 1991, **251**, 898–905.
22. Y. Mai, A. Eisenberg, *Chem. Soc. Rev.*, 2012, **41**, 5969–85.
23. I. W. Hamley, *Block Copolymers in Solution: Fundementals and Applications*, John Wiley & Sons, Inc., Chichester, 2005.
24. H. Feng, X. Lu, W. Wang, N.-G. Kang, J. Mays, *Polymers*, 2017, **9**, 494.
25. Y. Kang, J. J. Walish, T. Gorishnyy, E. L. Thomas, *Nat. Mater.*, 2007, **6**, 957–960.
26. J. K. Kim, S. Y. Yang, Y. Lee, Y. Kim, *Prog. Polym. Sci.*, 2010, **35**, 1325–1349.
27. J. K. Kim, J. I. Lee, D. H. Lee, *Macromol. Res.*, 2008, **16**, 267–292.
28. L. Chen, W. A. Phillip, E. L. Cussler, M. A. Hillmyer, *J. Am. Chem. Soc.*, 2007, **129**, 13786-13787.
29. D. E. Discher, A. Eisenberg, *Science.*, 2002, **297**, 967-973.
30. O. Casse, A. Shkilnyy, J. Linders, C. Mayer, D. Häussinger, A. Völkel, A .F. Thünemann, R. Dimova, H. Cölfen, W. Meier, H. Schlaad, A. Taubert, *Macromolecules*, 2012, **45**, 4772–4777.
31. Z. Ge, D. Xie, D Chen, X. Jiang, Y. Zhang, H. Liu, S. Liu, *Macromolecules*, 2007, **40**, 3538-3546.
32. H. Cölfen, *Macromol. Rapid Commun.*, 2001, **22**, 219–252.
33. G. Mountrichas, S Pispas, *Macromolecules* 2006, **39**, 4767-4774.
34. P. Alexandridis, B. Lindman, *Amphiphilic Block Copolymers: Self-Assembly and Applications*, Elsevier Science B.V., Amsterdam, 2000.
35. A. Eisenberg, J. S. Kim, *Introduction to Ionomers*, John Wiley & Sons, Inc., New York, 1998.
36. L. Zhang, A. Eisenberg, *J. Am. Chem. Soc.*, 1996, **118**, 3168–3181.
37. L. F. Zhang, A. Eisenberg, *Polym. Adv. Technol.*, 1998, **9**, 677–699.

38. I. W. Hamley, In *Block Copolymers in Solution: Fundamentals and Applications* John Wiley & Sons, Ltd., Chichester 2005, ch. 6, pp. 241–283.
39. S. Movassaghian, O. M. Merkel, V. P. Torchilin, *Wiley Interdiscip. Rev. Nanomedicine Nanobiotechnology*, 2015, **7**, 691–707.
40. Z. Ahmad, A. Shah, M. Siddiq, H. B. Kraatz, *RSC Adv.*, 2014, **4**, 17028–17038.
41. E. Busseron, Y. Ruff, E. Moulin, N. Giuseppone, *Nanoscale*, 2013, **5**, 7098.
42. S. A. Senevirathne, K. E. Washington, M. C. Biewer, M. C. Stefan, *J. Mater. Chem. B*, 2016, **4**, 360–370.
43. A. Rösler, G. W. Vandermeulen, H. Klok, *Adv. Drug Deliv. Rev.*, 2001, **53**, 95–108.
44. M. Prabaharan, J. J. Grailer, S. Pilla, D. A. Steeber, S. Gong, *Biomaterials*, 2009, **30**, 5757–5766.
45. G. Chen, L. Wang, T. Cordie, C. Vokoun, K. W. Eliceiri, S. Gong, *Biomaterials*, 2015, **47**, 41–50.
46. V. P. Torchilin, *Adv. Drug Deliv. Rev.*, 2002, **54**, 235–252.
47. E. Nakamura, K. Makino, T. Okano, T. Yamamoto, M. Yokoyama, *J. Control. Release*, 2006, **114**, 325–333.
48. M. Theerasilp, P. Sunintaboon, W. Sungkarat, N. Nasongkla, *Appl. Nanosci.*, 2017, **7**, 711–721.
49. C. Cruje, J. Dunmore-Buyze, J. P. MacDonald, D. W. Holdsworth, M. Drangova, E. R. Gillies, *Biomacromolecules*, 2018, **19**, 896–905.
50. C. H. Braun, T. V. Richter, F. Schacher, A. H. E. Müller, E. J. W. Crossland, S. Ludwigs, *Macromol. Rapid Commun.*, 2010, **31**, 729–734.
51. Q. Chen, H. Schönherr, G. J. Vancso, *Small*, 2009, **5**, 1436–1445.
52. M. S. Bakshi, *Adv. Colloid Interface Sci.*, 2014, 213, 1–20.
53. P. Khullar, V. Singh, A. Mahal, H. Kumar, G. Kaur, M. S. Bakshi, *J. Phys. Chem. B*, 2013, **117**, 3028–3039.
54. C. Bouilhac, E. Cloutet, D. Taton, A. Deffieux, R. Borsali, H. Cramail, *J. Polym. Sci. Part A Polym. Chem.*, 2009, **47**, 197–209.
55. G. Zhang, S. Tang, A. Li, L. Zhu, *Langmuir*, 2017, **33**, 6353–6362.
56. C. Boucher-Jacobs, M. Rabnawaz, J. S. Katz, R. Even, D. Guironnet, *Nat.*

Commun., 2018, **9**, 841.

57. B. H. Lipshutz, S. Ghorai, A. R. Abela, R. Moser, T. Nishikata, C. Duplais, A. Krasovskiy, R. D. Gaston, R. C. Gadwood, *J. Org. Chem.*, 2011, **76**, 4379–4391.
58. X. Zhang, A. F. Cardozo, S. Chen, W. Zhang, C. Julcour, M. Lansalot, J. F. Blanco, F. Gayet, H. Delmas, B. Charleux, E. Manoury, F. D'Agosto, R. Poli, *Chem. Eur. J.*, 2014, **20**, 15505–15517.
59. E. Isarain-Chávez, M. D. Baró, E. Pellicer, J. Sort, *Nanoscale*, 2017, **9**, 18081–18093.
60. H. Tian, S. Zhu, F. Xu, W. Mao, H. Wei, Y. Mai, X. Feng, *ACS Appl. Mater. Interfaces*, 2017, **9**, 43975–43982.
61. S. Zhu, H. Tian, N. Wang, B. Chen, Y. Mai, X. Feng, *Small*, 2018, **14**, 1702755.
62. S. Tanaka, Y. V. Kaneti, R. Bhattacharjee, M. N. Islam, R. Nakahata, N. Abdullah, S. I. Yusa, N. T. Nguyen, M. J. A. Shiddiky, Y. Yamauchi, M. S. A. Hossain, *ACS Appl. Mater. Interfaces*, 2018, **10**, 1039–1049.
63. D. Zhao, J. Feng, Q. Huo, N. Melosh, G. H. Fredrickson, B. F. Chmelka, G. D. Stucky, *Science*, 1998, **279**, 548–552.
64. Y. Lei, T. Wang, J. W. Mitchell, L. Zaidel, J. Qiu, L. Kilpatrick-Liverman, K. Le, J. Hedger, F. Qi, M. Anderson, B. Rutherford, B. Wu, S. Tetradis, W. Shi, *RSC Adv.*, 2014, **4**, 49053–49060.
65. S. Banerjee, M. Wehbi, A. Manseri, A. Mehdi, A. Alaaeddine, A. Hachem, B. Ameduri, *ACS Appl. Mater. Interfaces*, 2017, **9**, 6433–6443.
66. V. Bhagat, E. O'Brien, J. Zhou, M. L. Becker, *Biomacromolecules*, 2016, **17**, 3016–3024.
67. X. Lin, K. Fukazawa, K. Ishihara, *ACS Appl. Mater. Interfaces*, 2015, **7**, 17489–17498.
68. A. Kanazawa, T. Ikeda, T. Endo, *J. Polym. Sci. Part A Polym. Chem.*, 1993, **31**, 335–343.
69. M. Hadadpour, J. Gwyther, I. Manners, P. J. Ragogna, *Chem. Mater.*, 2015, **27**, 3430–3440.
70. S. K. Patra, G. R. Whittell, S. Nagiah, C. L. Ho, W. Y. Wong, I. Manners, *Chem.*

Eur. J., 2010, **16**, 3240–3250.

71. C. H. Honeyman, T. J. Peckham, J. A. Massey, I. Manners, *Chem. Commun.*, 1996, **0**, 2589.
72. L. Cao, I. Manners, M. A. Winnik, *Macromolecules*, 2001, **34**, 3353–3360.
73. Y. P. Borguet, S. Khan, A. Noel, S. P. Gunsten, S. L. Brody, M. Elsabahy, K. L. Wooley, *Biomacromolecules*, 2018,**19**, 1212-1222.
74. J. J. Yuan, A. Schmid, S. P. Armes, A. L. Lewis, *Langmuir*, 2006, **22**, 11022–11027.
75. R. Perrin, M. Elomaa, P. Jannasch, *Macromolecules*, 2009, **42**, 5146–5154.
76. F. Schönberger, G. Qian, B. C. Benicewicz, *J. Polym. Sci. Part A Polym. Chem.*, 2017, **55**, 1831–1843.
77. W. Zhang, Y. Liu, A. C. Jackson, A. M. Savage, S. P. Ertem, T. H. Tsai, S. Seifert, F. L. Beyer, M. W. Liberatore, A. M. Herring, E. B. Coughlin, *Macromolecules*, 2016, **49**, 4714–4722.
78. H. Chen, Y. Luo, C. Chai, J. Wang, J. Li, M. Xia, *J. Appl. Polym. Sci.*, 2008, **110**, 3107–3115.
79. H.-B. Chen, L. Chen, X. Dong, L. J. Li, Y.-Z. Wang, *Polymer*, 2012, **53**, 3520–3528.
80. R. Ruffolo, C. E. B. Evans, X. H. Liu, Y. Ni, Z. Pang, P. Park, A. R. McWilliams, X. Gu, X. Lu, A. Yekta, M. A. Winnik, I. Manners, *Anal. Chem.*, 2000, **72**, 1894–1904.
81. K. J. T. Noonan, B. H. Gillon, V. Cappello, D. P. Gates, *J. Am. Chem. Soc.*, 2008, **130**, 12876–12877.
82. T. Zhang, Z. Song, H. Chen, X. Yu, Z. Jiang, *J. Biomater. Sci. Polym. Ed.*, 2008, **19**, 509–524.
83. X.-Z. Yang, Y.-C. Wang, L.-Y. Tang, H. Xia, J. Wang, *J. Polym. Sci. Part A Polym. Chem.*, 2008, **46**, 6425–6434.
84. Y. Su, C. Li, *React. Funct. Polym.*, 2007, **67**, 233–240.
85. G. H. Li, S. H. Kim, C. G. Cho, T.-J. Park, Y. Kim, *Macromol. Res.*, 2006, **14**, 504–509.

86. K. J. Sykes, S. Harrisson, D. J. Keddie, *Macromol. Chem. Phys.*, 2016, **217**, 2310–2320.

87. B. Laszkiewicz, *J. Appl. Polym. Sci.*, 1967, **11**, 2295–2301.

88. Z. Wang, J. Parrondo, V. Ramani, *J. Electrochem. Soc.*, 2017, **164**, 1216–1225.

89. P. Persigehl, R. Jordan, O. Nuyken, *Macromolecules*, 2000, **33**, 6977–6981.

90. O. Herd, A. Heßler, M. Hingst, M. Tepper, O. Stelzer, *J. Organomet. Chem.*, 1996, **522**, 69–76.

91. E. Lobry, A. F. Cardozo, L. Barthe, J.-F. Blanco, H. Delmas, S. Chen, F. Gayet, X. Zhang, M. Lansalot, F. D'Agosto, R. Poli, E. Manoury, C. Julcour, *J. Catal.*, 2016, **342**, 164–172.

92. J. M. Nelson, A. P. Primrose, T. J. Hartle, H. R. Allcock, I. Manners, *Macromolecules*, 1998, **31**, 947-949.

93. S. Rothemund, I. Teasdale, *Chem. Soc. Rev.*, 2016, **45**, 5200–5215.

94 T. J. Peckham, J. Massey, D. P. Gates, I. Manners, *Phosphorus Sulfur Silicon Relat. Elem.*, 1999, **144**, 217-220

95 K. J. T. Noonan, D. P. Gates, *Angew. Chem. Int. Ed.*, 2006, **45**, 7271-7274

96 K. J. T. Noonan, B. H. Gillon, V. Cappello, D. P. Gates, *J. Am. Chem. Soc.*, 2008, **130**, 12876-12877

Chapter 2

Hisey, B; Ragogna, P. J.; Gillies, E. R. *Biomacromolecules*, **2017**, *18(3)*, pp 914-923.

Phosphonium Functionalized Polymer Micelles with Intrinsic Antibacterial Activity.

2.1 Introduction

Polymeric nanocarriers, self-assembled nanoscopic materials with domains of different hydrophilicity, have been extensively investigated due to their abilities to encapsulate biomedically relevant cargo and to provide a chemically tunable platform.[1–4] Common nanocarrier morphologies are spherical micelles[5], cylindrical micelles,[6,7] bilayer structures (e.g. vesicles)[8] and in some circumstances more complex architectures that can be obtained using unconventional polymers or intermolecular interactions.[9] Amphiphilic BCPs are often the structural components of polymeric nanocarriers, due to the control they provide over the morphology and the well-established chemistry used to synthesize and functionalize them. By encapsulating hydrophobic compounds into the hydrophobic domains of nanomaterials, these water-insoluble molecules can be dispersed in aqueous solutions.[4,10,11] BCP nanocarriers have been and continue to be investigated for the delivery of a large variety of compounds including small molecule drugs, therapeutic nucleic acids, imaging contrast agents, and antibacterial compounds.[1,4,12]

An increase in the occurrence of pernicious antibiotic-resistant bacteria is currently motivating a search for novel ways of combating bacterial infections. The World Health Organization warns that in order to avoid a return to the ‘pre-antibiotic’ age, researchers and health professionals need to employ new and varied antibiotic treatments of bacterial infections.[13] The ability to incorporate hydrophobic antibacterial compounds into aqueous dispersible nanocarriers allows for increased availability of the drugs at the site of infection.[14] The use of nanocarriers has allowed researchers to utilize traditional antibacterial compounds with improved efficacy. For example, intracellular bacterial infections are often resistant to antibacterial treatment due to the localization of

the bacteria in the eukaryotic cells. Maya and coworkers were able to target intracellular *S. aureus* by encapsulating tetracycline in chitosan nanoparticles.[15] Li *et al.* demonstrated the encapsulation of antibacterial agents into polymer vesicles that enzymatically degraded in the presence of target bacteria to deliver the antibacterial cargo.[16] Furthermore, Liu and coworkers have recently demonstrated the ability of triclosan-loaded micelles to penetrate into biofilms and to kill the *S. aureus* residing in the biofilms with greater efficacy than free triclosan.[17] There are many other examples that demonstrate the increase in desirable properties that can be achieved by loading antibacterial small molecules into nanocarrier systems.[10,12,18] This approach may also allow for the use of new poorly water-soluble antibacterial compounds in the combat of antibacterial resistance.

Far fewer examples exist of nanocarriers with inherently antibacterial units. This is somewhat surprising given the extensive research that has been performed on incorporating functionality into nanocarrier design.[2,19] The incorporation of silver nanoparticles[20–22] and/or polymers such as chitosan[23,24] or other polyammonium cations,[25–28,] has been explored as an approach for imparting antibacterial activity to nanocarriers. Previously unexplored is the use of phosphonium cations to impart antibacterial activity to polymeric nanocarriers. Phosphonium cations, like ammonium cations, are thought to interact with the negatively charged structural biopolymers and phospholipids on the outer surfaces of bacteria cell walls, leading to penetration of the cell wall, ultimately resulting in cell death.[28–30] Gram-positive bacteria such as *S. aureus* have teichoic acid polymers on the cell wall that confer a negative charge and Gram-negative bacteria such as *E. coli* have lipopolysaccharides that are responsible for the negative charge of the cell surface. Previous research has demonstrated that phosphonium salts as well as their corresponding polymers have improved antibacterial efficacy compared to analogous ammonium compounds.[31–33] This can arise from the differences in charge distribution between the larger phosphonium cation and smaller ammonium cation. In this context, the Ragogna and Gillies groups have recently demonstrated the efficacy of surfaces and semi-interpenetrating networks containing phosphonium cations against Gram-positive and Gram-negative bacteria.[34,35]

Here I explore the synthesis and self-assembly of phosphonium end-capped PEO-*b*-PCL copolymers. To the best of my knowledge, this represents the first example of phosphonium-functionalized BCP assemblies in aqueous solution. I also demonstrate the antibacterial properties of the assemblies against *S. aureus* and *E. coli*. Furthermore, it was shown that the antibiotic tetracycline can be incorporated into the micelles, potentially providing orthogonal modes of action, where the traditional antibiotic targets specific pathways in bacteria while the phosphonium cation provides membrane disruption. While work exists demonstrating the benefit of combining antibacterial nanoparticles with traditional antibacterial small molecules[24,36] the deliberate encapsulation of a traditional antibacterial agent within an intrinsically antibacterial polymeric nanocarrier has not been reported.

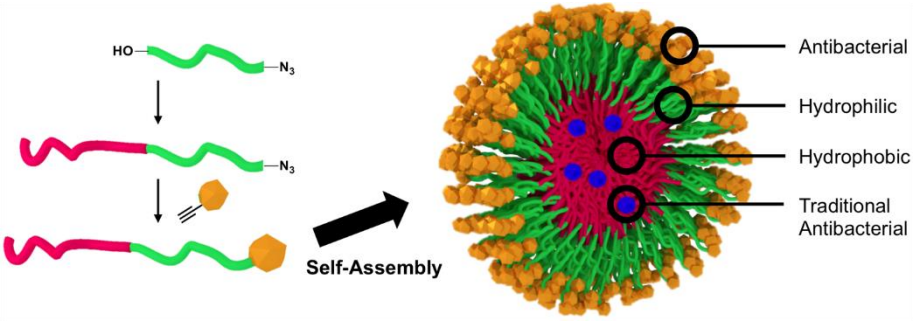

Figure 2-1. Schematic illustrating a phosphonium-functionalized micelle loaded with antibiotic.

2.2 Results and Discussion

2.2.1 Synthesis of PEO-*b*-PCL Copolymers

PEO-*b*-PCL copolymers were selected because of their established biocompatibility and low toxicity in drug delivery applications.[37] An azide terminal group on the PEO was selected for the conjugation of the phosphonium moiety via a copper-assisted azide-alkyne cycloaddition (CuAAC). Methoxy- and azide-terminated PEO-*b*-PCL copolymers, **MeO-BCP** and **N_3-BCP** respectively, were synthesized according to our previously reported procedure.[38] Briefly, PEO monomethyl ether (**MeO-PEO**) or PEO monoazide (**N_3-PEO**) were used as macroinitiators to polymerize caprolactone in toluene using methanesulfonic acid (MSA) as a catalyst (Scheme 2-1).[38] This method yields copolymers with very low molar mass *Đ*. Low *Đ* is important for good control over the morphology of the self-assemblies.[39,40] From previous research it is known that a mass

ratio of PCL:PEO of 1.3:1 yields micellar nanocarriers.[38] Therefore, using a PEO macroinitiator of ~2000 g/mol, a degree of polymerization (DP) of ~24 caprolactone repeat units was targeted. The resulting BCPs were characterized by ^{1}H NMR spectroscopy and size-exclusion chromatography (SEC). ^{1}H NMR spectroscopy confirmed that the DPs were ~24 for each of **MeO-BCP** and **N_3-BCP**, corresponding to an M_n of ~4700 g/mol (Figure A-1 and A-2). By SEC relative to PEO standards, **MeO-BCP** had a M_n of 5750 g/mol and *Đ* of 1.11, while **N_3-BCP** had an M_n of 5950 g/mol and *Đ* of 1.12 (Figure A-3). The differences in M_n of these copolymers measured by SEC likely arose from their different terminal groups.

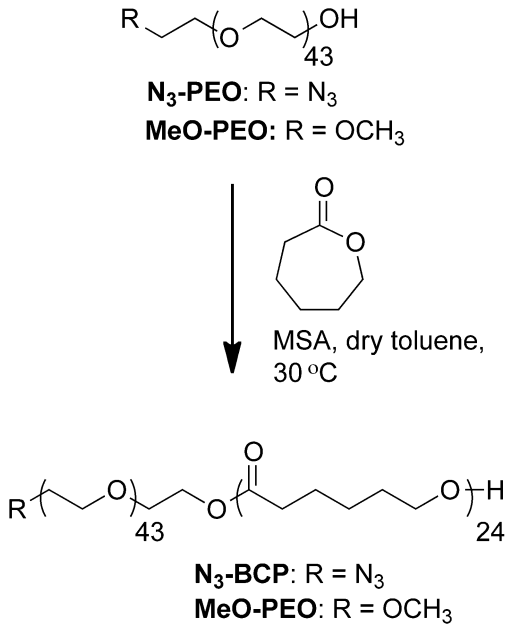

Scheme 2-1. Synthesis of **MeO-BCP** and **N_3-BCP**.

2.2.2 Synthesis of Alkyne-Functionalized Phosphonium Salts

Alkyne-functionalized phosphonium centres were required for conjugation to **N_3-BCP**. The lengths of the alkyl chains on phosphonium and ammonium salts are known to affect the antibacterial activity of the small molecules,[31] so it was desirable to explore this in the context of phosphonium-functionalized polymer assemblies. Initial attempts to prepare the alkyne-functionalized phosphonium salts by reaction of trialkylphosphines with propargyl bromide resulted in complex and inseparable product mixtures. This is due

to side reactivity of the phosphonium salt with the unreacted phosphine.[41] While addition of hydrobromic acid to the reaction reduced the number of products, isolation of the desired product remained elusive. On the other hand, use of 5-chloro-1-pentyne led to the conversion of triethylphosphine and tri-*n*-butylphosphine into single products **Et$_3$P-yne** and **Bu$_3$P-yne**, respectively (Scheme 2-2). The synthesis of **Oct$_3$P-yne** yielded a mixture of products and silica gel column chromatography was used for purification. This was attributed to the extended heating time required to convert the starting material into product as this phosphine is more sterically hindered. In each case, the pure product was characterized by multinuclear magnetic resonance spectroscopy and high-resolution mass spectrometry. The ^{1}H NMR spectra of the products showed characteristic peaks corresponding to the alkyne proton at 2.03 ppm (Figure 2-2), demonstrating successful quaternization of the phosphine to the phosphonium salt.

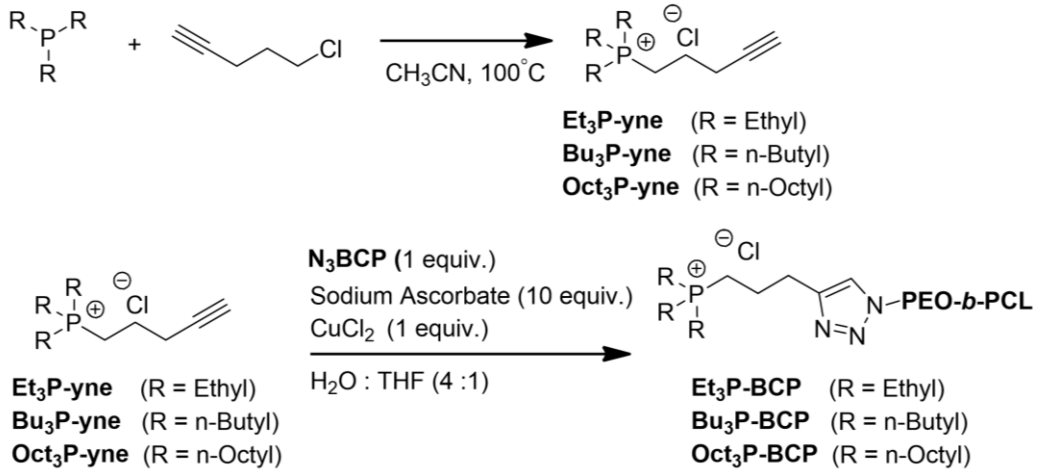

Scheme 2-2. Synthesis of the phosphonium salts and the phosphonium capped polymers.

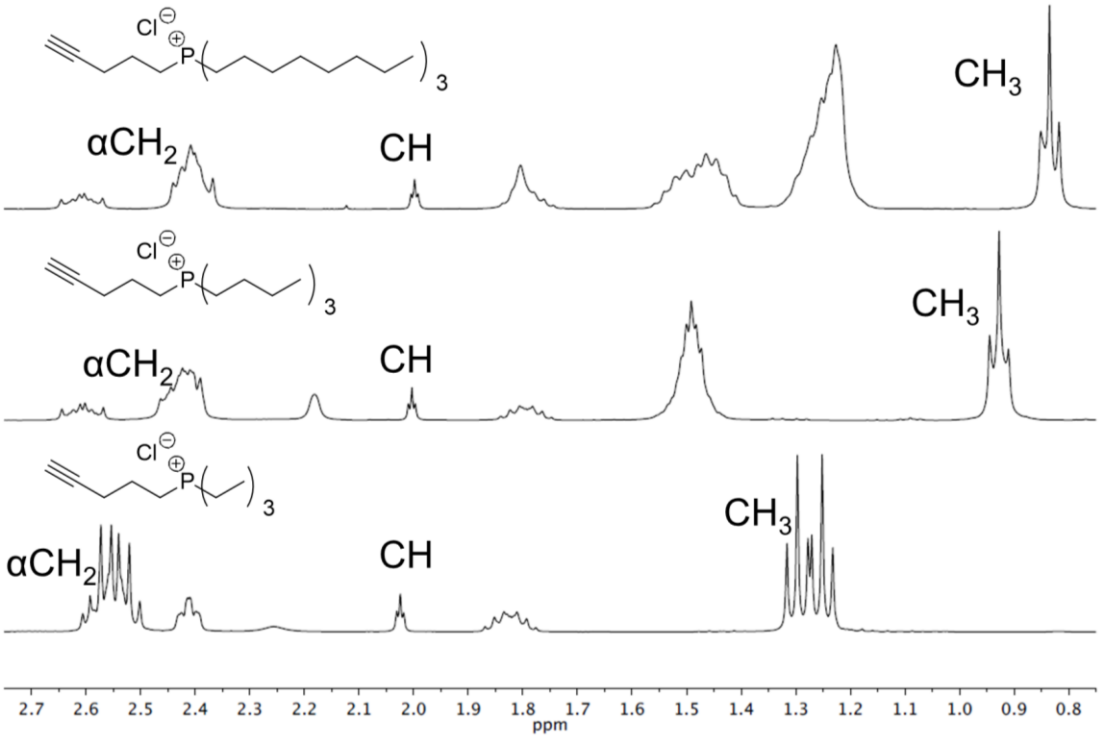

Figure 2-2. ^{1}H NMR ($CDCl_3$, 400 MHz) spectra of the phosphonium salts with selected peaks labeled. The peaks at 1.85, 2.20 ppm and 2.25 ppm from top to bottom are residual water.

2.2.3 Conjugation of the Phosphonium Cations to the BCP

Attachment of the phosphonium salts to **N_3-BCP** was achieved using CuAAC in 4:1 H_2O:THF with $CuCl_2$ and sodium ascorbate to afford **Et_3P-BCP**, **Bu_3P-BCP**, and **Oct_3P-BCP** (Scheme 2-2). Due to the subsequent use of the polymer in anti-bacterial testing it was imperative that any residual copper be removed from the functionalized materials. The reaction mixtures were therefore dialyzed against large volumes of 0.5 M NaCl solution, followed by water. The dialysis against aqueous NaCl was important to ensure that the phosphonium counterion remained chloride as there are reports in the literature that ascorbate may have antibacterial activity, thus we needed to preclude the chance of anion exchange.[42] As shown in Figure 2-3, IR spectra of the **N_3-BCP** had an azide stretch at 2100 cm^{-1}, whereas the triazole product formed from the CuAAC reaction had no peak present in that region. Integration of the ^{1}H NMR signals corresponding to the methyl protons on the phosphonium groups relative to the terminal methylene group of the PEO block adjacent to the first repeat unit of the PCL block were consistent with

complete conversion of the azides (Figure A-11 - A-13). Peaks characteristic of the proton on the triazole ring were also observed above 7.00 ppm in the ^{1}H NMR spectra of the tributyl- and triethyl phosphonium salt functionalized polymers (Figure A-11 - A-13). The methylene peak adjacent to the triazole ring was also present in the ^{1}H NMR spectra of all the phosphonium salt functionalized BCPs at 4.5 ppm.

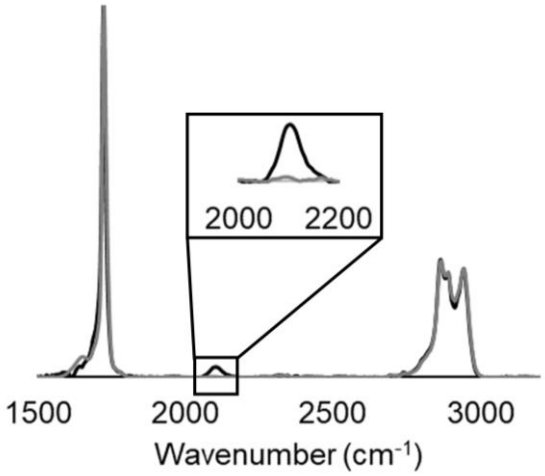

Figure 2-3**.** ATR-IR spectra of the starting **N_3-BCP** (black spectrum) and **Bu_3P-BCP** (grey spectrum) showing the disappearance of the azide stretch following the CuAAC reaction.

2.2.4 Micelle Preparation and Characterization

The micelles were prepared from **MeO-BCP**, **Et_3P-BCP**, **Bu_3P-BCP**, and **Oct_3P-BCP** by nanoprecipitation of a polymer solution in THF into water, which is a selective solvent for the PEO block of the copolymers. The rapid decrease in solubility of the PCL block in the solvent mixture causes the polymers to SA into nano-sized cores surrounded by PEO. Figure 2-4 shows representative TEM images of the resulting assemblies. Assemblies prepared from the phosphonium cation-capped polymers were stained using auric acid (Figure 2-4 B-D). In this case, the aurate can undergo anion exchange to bind to the positively charged phosphonium ion.[43] In each case, solid spherical particles were observed. The sub-50 nm diameters of the **MeO-BCP**, **Et_3P-BCP**, and **Bu_3P-BCP** assemblies suggests that they were largely true micellar structures, whereas some larger 50 – 100 nm assemblies were observed for **Oct_3P-BCP**, suggesting that some compound micelles or aggregates of micelles were also present. The **Oct_3P-yne** is not soluble in

water and so installation of this hydrophobic end group on the hydrophilic block may cause this aggregation.

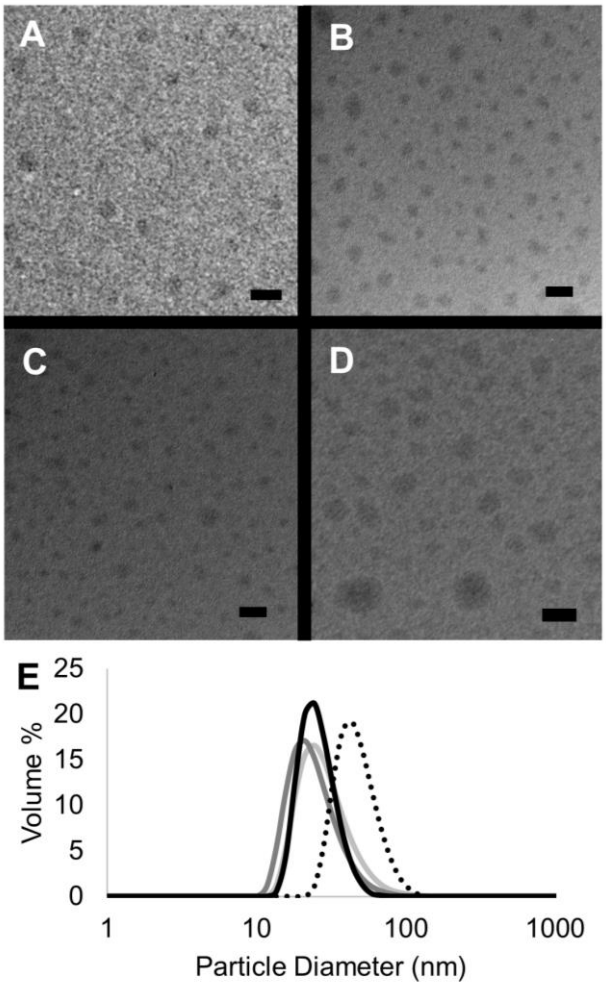

Figure 2-4. A – D) TEM micrographs of the assemblies prepared by nanoprecipitation (scale bar represents 100 nm): A) **MeO-BCP** micelles, B) **Et$_3$P-BCP** micelles, C) **Bu$_3$P-BCP** micelles, D) **Oct$_3$P-BCP** assemblies. All **Alk$_3$P-BCP** samples (B-D) were stained with auric acid. E) Volume distributions of the assembly diameters measured by DLS (**MeO-BCP** = solid black; **Et$_3$P-BCP** = light grey; **Bu$_3$P-BCP** = dark grey; **Oct$_3$P-BCP** = dotted black).

As shown in Figure 2-4E and Table 2-1, the hydrodynamic diameters measured by dynamic light scattering (DLS) were in good agreement with the sizes observed by TEM. **MeO-BCP**, **Et$_3$P-BCP**, and **Bu$_3$P-BCP** micelles had z-average diameters ranging from 30 – 45 nm and **Oct$_3$P-BCP** assemblies had a z-average diameter of 59 nm. ζ-potentials of the micelles were also measured. **MeO-BCP** micelles had a ζ-potential of -23 mV. This is typical for assemblies with PEO coronas.[44] On the other hand, all the

phosphonium-functionalized micelles had positive ζ-potentials, and these ranged from 19 to 30 mV. This supports that the phosphonium cations reside on the surface of the micelles.

	Z-average diameter (nm)	Polydispersity index (PDI)	ζ-potential (mV)
MeO-BCP micelles	29.5 ± 0.8	0.122 ± 0.027	-23.2 ± 5.2
Et_3P-BCP micelles	45.0 ± 2.5	0.072 ± 0.003	19.0 ± 2.4
Bu_3P-BCP micelles	39.6 ± 3.7	0.213 ± 0.025	26.8 ± 7.7
Oct_3P-BCP assemblies	58.9 ± 2.8	0.110 ± 0.020	29.7 ± 0.5

Table 2-1**.** Hydrodynamic diameters and ζ-potentials measured for the polymer assemblies by dynamic light scattering.

2.2.4 Antibacterial Properties of Phosphonium-Functionalized Assemblies

The antibacterial efficacies of the phosphonium-functionalized micelles and their corresponding small molecule phosphonium salts were evaluated by measuring their minimum bactericidal concentrations (MBC). The MBC is the concentration required to kill 99% of bacteria in the assay. This assay involved inoculating varying concentrations of the assemblies or small molecules in pH 7.4 phosphate buffer with a bacterial suspension containing 10^5 colony forming units (CFU)/mL of either Gram-negative *E. coli* (ATCC 29425) or Gram-positive *S. aureus* (ATCC 6538). The inoculated samples were incubated at 37 °C for 4 hours, then the resulting suspensions were plated on agar, incubated overnight and then the bacterial colonies were counted. The percent reduction, and thus MBC, was calculated by comparing the number of colonies counted after incubation with the sample compared to those of bacteria exposed to only phosphate buffer with no polymer or small molecule added.

As shown in Table 2-2, the small molecule phosphonium cations had relatively high MBC values against both *E. coli* and *S. aureus*. The low aqueous solubility of **Oct_3P-yne** made testing the MBC of the salt unfeasible, but **Et_3P-yne** had a MBC greater than 45 mM, the highest concentration tested, against *S. aureus* and *E. coli*. **Bu_3P-yne**

was more bioactive, with MBC values of 4.1 mM and 33 mM for *S. aureus* and *E. coli*, respectively. **MeO-BCP** micelles were also studied and the MBC was not observed at 1.1 mM (concentration of polymer), which was the highest concentration tested. Thus, the block copolymers themselves are not antibacterial under the test conditions. The ethyl and butyl phosphonium salt functionalized micelles had MBC values lower than the corresponding small molecule phosphonium salts. This demonstrates the increased efficacy of the phosphonium salts in multivalent systems. Interestingly there was no observed difference in MBC between the **Et_3P-BCP** micelles and **Bu_3P-BCP** micelles with *S. aureus* (0.13 mM for both alkyl chain lengths) as one might expect from previous work,[31-33] but there was with *E. coli* (0.26 mM and 0.13 mM, respectively). The **Oct_3P-BCP** assemblies had the lowest MBC against *S. aureus* with an MBC of 0.031 mM, and the highest MBC of the phosphonium-functionalized assemblies against *E. coli* at 0.49 mM.

Compound	MBC against *S. aureus* (mM)	MBC against *E. coli* (mM)
Et_3P-yne	> 45	> 45
Bu_3P-yne	4.1	33
MeO-BCP micelles	> 1.1	> 1.1
Et_3P-BCP micelles	0.13	0.26
Bu_3P-BCP micelles	0.13	0.13
Oct_3P-BCP micelles	0.031	0.49

Table 2-2. MBC values for the phosphonium salts and phosphonium-functionalized assemblies against *S. aureus* and *E. coli*. For the block copolymers, the concentrations correspond to the concentrations of polymer chains, and thus the concentration of the terminal phosphonium groups.

Except for **Bu_3P-BCP** micelles, higher MBC values were found for *E. coli*. The lower efficacy against *E. coli* was expected based on previous research and can be attributed to differences in the cell wall structures of Gram-positive and Gram-negative bacteria.[45] Gram-positive bacteria such as *S. aureus* have a plasma membrane surrounded by a periplasmic space and a peptidoglycan layer, whereas Gram-negative bacteria such as *E. coli* have an additional outer membrane surrounding the peptidoglycan layer. The mode of action of mono-cationic and polycationic biocides is generally accepted to include the following processes: 1) biocide adsorption to the cell surface, 2) biocide diffusion through the cell wall, 3) adsorption to the cytoplasmic membrane, 4) cytoplasmic membrane disruption, and 5) loss of cytoplasmic components, resulting in cell death.[30] Thus, Gram-negative bacteria have an additional barrier through which the biocide must diffuse, and disrupt, which may explain why higher concentrations of micelles were generally required to kill *E. coli*.

It was also noted that different trends with respect to alkyl chain length were observed for the different strains of bacteria. **Oct_3P-BCP** micelles had the lowest MBC for *S. aureus* whereas **Bu_3P-BCP** micelles had the lowest MBC for *E. coli*. While phosphonium groups with longer alkyl chains have been previously demonstrated to show greater antibacterial activity in general,[33] there are also datum to suggest that the relationship between alkyl chain length and antibacterial efficacy is not linear.[46] As hydrophilic cationic groups promote attachment to the bacterial membrane and hydrophobic alkyl chains insert into membranes to disrupt them, the hydrophilicity and hydrophobicity must be balanced to match the characteristics of the different bacterial membranes.[47] It is also possible that the larger size of the **Oct_3P-BCP** assemblies plays a role. The larger size of the individual assemblies results in fewer particles for a given polymer/phosphonium concentration and thus fewer assemblies to interact with the bacteria.[48] Additionally, the diminished rate of diffusion at the surface of the Gram-negative *E. coli* may slow the interaction of phosphonium domains in the **Oct_3P-BCP** compound micelles with the bacteria cell wall.[45] In comparing small molecule cationic biocides with polycationic biocides, the small molecules typically have higher rates of diffusion through the cell wall, while the multivalent nature of polycationic biocides

increases the adsorption to the cell surface and the cytoplasmic membrane, often leading to increased rates and occurrences of cytoplasmic membrane disruption.[30]

The phosphonium-functionalized assemblies can also be compared with other antibacterial polymer assemblies. For example, Du and co-workers demonstrated the preparation of Ag nanoparticle-decorated micelles and vesicles with antibacterial activity.[20] These assemblies had a low MBC of 8.69×10^{-2} mM of Ag. However, it is unclear whether the activity of the system arose from nano-silver associated with the micelles or dissociated Ag^{+} ions released into solution that were not associated with the micellar corona.[20] The mechanism of bacterial killing by nano-silver, while controversial,[49] is also different and is thought to involve the inactivation of the bacterial DNA and ribosomes by silver ions.[50,51] Later, the same group reported the preparation of antibacterial nano-assemblies composed of poly[2-(2-methoxyethoxy)ethyl methacrylate]$_{20}$-*block*-poly[2-(*tert*-butylaminoethyl) methacrylate]$_{20}$.[25] The polyamine block ionizes in solution to yield positively charged particles. Vesicles prepared from the above polymer were reported to have MBC values of 0.63 mM of amine against both *E. coli* and *S. aureus*.[25] Later, multicompartment polymer vesicles prepared from the same polymers were reported to have improved antibacterial efficacy with MBC values of 0.1 mg/mL or 1.27×10^{-2} mM of amine, a value lower than their measured minimum inhibitory concentration (MIC) values for the same material.[26] As the MIC corresponds to the concentration required to inhibit bacterial growth but not necessary kill the bacteria, MIC values are not generally expected to be higher than MBC values. Du and coworkers also reported that low MIC values in the μM range could be achieved against *E. coli* and *S. aureus* using polypeptides as the hydrophilic block of a vesicle forming polymeric amphiphile.[52]

2.2.5 Hemolysis of Red Blood Cells

A challenge often encountered with membrane-active antibacterial agents is that in addition to lysing bacterial cell membranes, they can also lyse the membranes of red blood cells, resulting in non-specific toxicity. Therefore, to evaluate the potential of the phosphonium-functionalized micelles to lyse red blood cells, a hemolysis assay was performed. Briefly, following a previously reported procedure,[53] red blood cells were

obtained from defibrinated sheep blood and were incubated with **MeO-BCP**, **Et$_3$P-BCP**, **Bu$_3$P-BCP**, **Oct$_3$P-BCP** micelles in PBS for 2 hours. As a positive control, red blood cells were suspended in deionized water, resulting in the immediate lysis of the cells. The absorbance of the supernatant at 540 nm after the intact blood cells were pelletized was measured. Percent hemolysis was determined according to equation 2.1 below.

$$\text{Percent Hemolysis} = \frac{A_{\text{sample}} - A_{\text{micelles}} - A_{\text{negative control}}}{A_{\text{positive control}} - A_{\text{negative control}}} \times 100\%$$

Equation 2.1

As shown in Figure 2-5, only 0.53 mM of **Et$_3$P-BCP** micelles exhibited any hemolytic activity, with 7% hemolysis observed. Interestingly, this system was the least active of the 3 systems against both strains of bacteria, so this result was unexpected. While there is not a complete understanding of all the factors influencing selectivity for eukaryotic and prokaryotic membranes[45] it is likely that the hydrophilic balance of the **Et$_3$P-BCP** micelles results in its higher activity against red blood cell membranes.[53] Nevertheless, the overall results suggest that the phosphonium-functionalized micelles have good potential to kill bacteria selectively. While further studies would be required to elucidate the *in vitro* and *in vivo* toxicity, previous studies have shown that phosphonium compounds exhibit low *in vitro*,[35,54] and *in vivo*[54] toxicity.

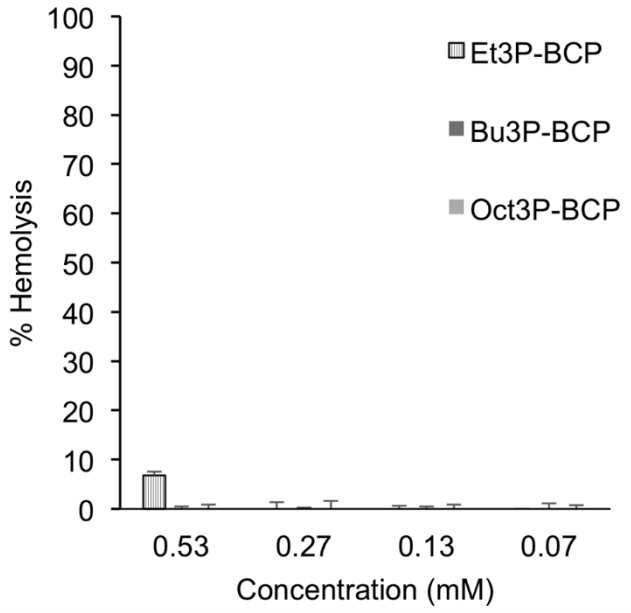

Figure 2-5. Hemolysis of red blood cells from defibrinated sheep blood. 0% hemolysis corresponds to the control of red blood cells in PBS while 100% hemolysis corresponds to the positive control of red blood cells in purified water. % hemolysis was determined by equation 2.1.

2.2.6 Encapsulation and Release of Tetracycline

The antibacterial efficacy of the phosphonium-functionalized assemblies can potentially be enhanced through encapsulation of a small molecule antibiotic that acts through a mechanism other than membrane disruption, thereby targeting multiple different stages of the infection process. Such an approach has not been explored in the context of antibacterial polymer assemblies to the best of our knowledge. Tetracycline (Figure 2-6) was chosen as the antibiotic as it is widely used and is hydrophobic, resulting in low aqueous solubility and the possibility to encapsulate it in the hydrophobic PCL cores of the micelles. Tetracycline acts by binding to the bacterial ribosome and preventing the production of new proteins.[55] It was encapsulated in the micelles through co-dissolution with the polymer in $CHCl_3$, followed by the addition of water with rapid stirring and heating at 30 °C overnight to evaporate the $CHCl_3$. Unencapsulated drug was then removed by centrifugal ultrafiltration (Figure A14). This procedure was performed for both **MeO-BCP** and **Bu_3P-BCP** to determine the effect of the phosphonium moieties on the drug loading and release. This afforded assemblies with diameters of 65 ± 5 nm for **MeO-BCP** as measured by DLS (Figure A15). The amount of drug loaded into the assemblies was determined as the difference between the drug added during assembly and the unencapsulated drug removed by ultrafiltration, which was determined by UV-vis spectroscopy. The encapsulation efficiency (equation 2.2, below) and drug loading content (equation 2.3, below) were determined to be 31 ± 7 % and 2.0 ± 0.2 % for **MeO-BCP** and, 42 ± 3 % and 3.1 ± 0.3 % for **Bu_3P-BCP,** respectively. The higher EE and DLC observed in the **Bu_3P-BCP** system may result from ionic interactions between the ionized tetracycline and the phosphonium ions on the micelles.

$$EE = \frac{\text{Mass of Drug in Particles}}{\text{Mass of Drug Added}} \times 100\%$$

Equation 2.2

$$DLC = \frac{\text{Mass of Drug in Particles}}{\text{Mass of Loaded Particles}} \times 100\ \%$$

Equation 2.3

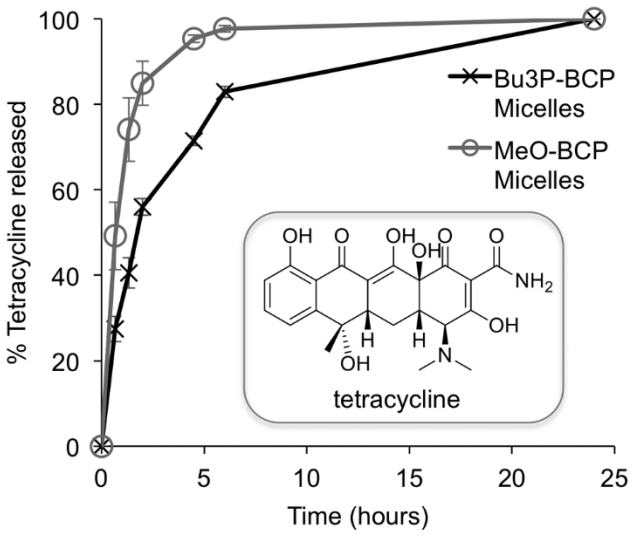

Figure 2-6. Release profiles of tetracycline from **MeO-BCP** micelles and **Bu$_3$P-BCP** micelles. Inset: tetracycline structure

The release rate of tetracycline from the **MeO-BCP** and **Bu$_3$P-BCP** micelles was then studied by incubating the drug-loaded micelles at 37 °C in pH 7.2 phosphate buffer. At each time point, centrifugal ultrafiltration was used to separate the micelles from the released drug and the concentration of the released drug was measured. As shown in Figure 2-6, all the encapsulated tetracycline was released from the **MeO-BCP** micelles in ~5 hours. The release of tetracycline was somewhat slower from the **Bu$_3$P-BCP** micelles, with ~70% of the drug being released over the first 5 h and 100% release over 24 h. The differences in release rates between the two systems is likely due to the presence of the phosphonium end cap. Upon release from the hydrophobic micelle core into the phosphate buffer, tetracycline may become ionized and undergo electrostatic interactions with the phosphonium cations on the surfaces of the micelle, thereby slowing its release.

Antibacterial assays with *E. coli* were performed to examine the added effect of the tetracycline in the micelle core. At the tetracycline loadings described above, the activity of the **Bu$_3$P-BCP** micelles was dominated by the phosphonium groups and the same MBC value was determined. No activity was observed for tetracycline-loaded **MeO-BCP** micelles over a 4-hour incubation at a concentration of 0.26 mM of polymer. This can be attributed to the bacteriostatic effects of tetracycline. On the time scale of the experiment, the tetracycline would not kill bacteria but instead just inhibit its ability to

produce new proteins.[55] Thus, these experiments were not able to reveal an additive or synergistic effect of the drug and phosphonium on the bacteria. However, this does not preclude the possibility of observing one *in vivo* where the released drug could exhibit significantly different biodistribution than the assemblies and may reach sites not accessible to the polymer assemblies. Further studies will be needed to investigate this possibility.

2.3 Conclusions

In conclusion, this study demonstrated the synthesis and self-assembly of three new phosphonium-functionalized PEO-*b*-PCL copolymers with varying alkyl chain lengths on the phosphonium. **Et_3P-BCP**, **Bu_3P-BCP**, and the control **MeO-BCP** self-assembled into micelles with diameters less than 50 nm, while **Oct_3P-BCP** formed larger micelles or aggregates. All the phosphonium-functionalized assemblies had positive ζ-potentials, whereas the **MeO-BCP** micelles had a negative ζ-potentials. Despite relatively low loadings of the antibacterial component (only a single phosphonium unit per polymer chain), sub-mM MBC values were obtained against both *E. coli* and *S. aureus* and the activities of the different systems depended on the bacterial stain due to differences in their cell wall structures. In comparing the MBC values for the assemblies with those of the corresponding phosphonium small molecules, the assemblies were much more effective in killing bacteria, presumably due to their multivalent interactions with the bacteria. The low loadings of the phosphonium groups on the assemblies also allowed then to exhibit excellent hemolytic stability, with only the highest concentration of **Et_3P-BCP** micelles showing any hemolytic activity, above the MBC for both *S. aureus* and *E. coli*. It was also demonstrated that the intrinsically antibacterial **Bu_3P-BCP** micelles could encapsulate and release tetracycline, providing the potential for an orthogonal mechanism of attack against bacteria.

2.4 Experimental

General procedures and materials

MeO-BCP and **N_3-BCP** were prepared as previously reported[38] and the characterization data for the specific batches used in the current work are included in Appendix A4-A10. Briefly, they were prepared from the ROP of freshly distilled ε-caprolactone in dry toluene initiated by the PEO monomethyl ether or PEO monoazide. Methanesulfonic acid was used as a catalyst, and the product was obtained by precipitation in cold hexanes. Solvents were dried using an MBraun Solvent Purification System. Dried solvent was collected under vacuum in a flame-dried Straus flask and stored over 4Å molecular sieves. Purified water was obtained using a Barnstead™ EASYPure® II ultra pure water system (ThermoFisher Scientific). Nuclear Magnetic Resonance (NMR) spectroscopy was conducted on a Varian INOVA 400 MHz spectrometer (Agilent Technologies, Santa Clara, CA; ^{1}H 400 MHz, $^{31}P\{^{1}H\}$ 162 MHz, $^{13}C\{^{1}H\}$ 100 MHz) unless otherwise noted. All ^{1}H NMR spectra were referenced relative to the residual solvent peak ($CHCl_3$; ^{1}H δ = 7.27). The chemical shifts for $^{31}P\{^{1}H\}$ NMR spectroscopy were referenced using an external standard (85% H_3PO_4; δ_P = 0). All $^{13}C\{^{1}H\}$ NMR spectra were referenced relative to the residual solvent peak ($CDCl_3$; ^{13}C δ = 77.0). Infrared (IR) spectra were obtained using a Bruker Tensor 27 spectrometer using attenuated total internal reflectance mode (ATR) on a ZnSe crystal. High Resolution Mass spectrometry (HRMS) were obtained on a Finnigan MAT 8400 mass spectrometer using electron impact ionization. Dynamic light scattering (DLS) and ζ-potential measurements were performed on a Zetasizer Nano ZS from Malvern Instruments equipped with a 633 nm laser. A polymer concentration of ~0.1 mg/mL of polymer were used in DLS measurements. Ultraviolet-visible (UV-vis) spectroscopy was performed using a Varian Cary 300 Bio UV-visible spectrophotometer. The size exclusion chromatography (SEC) instrument was equipped with a Viscotek GPC Max VE2001 solvent module (Malvern Instruments Ltd., Malvern, UK). Samples were analyzed using the Viscotek VE3580 RI detector operating at 30 °C. The separation technique employed two Agilent Polypore (300 × 7.5 mm) columns connected in series and to a Polypore guard column (50 × 7.5 mm) (Agilent Technologies). Samples were dissolved in tetrahydrofuran (THF) (glass distilled grade) at a concentration of approximately 5 mg/mL, filtered through 0.22 μm syringe filters, and

then injected using a 100 μL loop. The THF eluent was filtered and eluted at 1 mL/min for a total of 30 min. The instrument was calibrated with PEO standards. Dialysis was performed using Spectra/Por® 6 pre-wetted dialysis tubing (Spectrum Laboratories Inc.).

*Synthesis of tri-n-butyl(1-pentynyl)phosphonium chloride (**Bu_3P-yne**)*

Tributylphosphine (5.00 g, 24.5 mmol, 1.0 equiv.) was dissolved in dry CH_3CN in a pressure tube inside a glovebox. 5-chloro-1-pentyne (2.80 g, 27.3 mmol, 1.1 equiv.) was then added dropwise to the stirring phosphine solution. The pressure tube was sealed and then heated at 100 °C. The reaction was monitored by $^{31}P\{^1H\}$ NMR spectroscopy. Upon exhaustion of the tributyl phosphine the volatile components were removed *in vacuo*. The crude product was dissolved in CH_2Cl_2 and precipitated into a rapidly stirring solution of cold hexanes (0 °C) to afford an off-white powder. The product was recovered by vacuum filtration. Yield = 6.31 g, 84%. ^1H NMR (400 MHz, $CDCl_3$): δ = 2.70 – 2.68 (m, 2H), 2.53 – 2.42 (m, 8H), 2.05 (t, $^4J(H,H)$ = 2.73 Hz, 1H), 1.90 – 1.79 (m, 2H), 1.61 – 1.47 (m, 12H), 0.97 (t, $^3J(H,H)$ = 7.23 Hz, 9H). $^{13}C\{^1H\}$ (100.52 MHz, $CDCl_3$): δ = 82.0, 70.5, 23.9 (d, $^3J(P,C)$ = 15.3 Hz), 23.7 (d, $^2J(P,C)$ = 5.3 Hz), 21.0 (d, $^2J(P,C)$ = 3.8 Hz), 19.4 (d, $^3J(P,C)$ = 16.8 Hz), 19.0 (d, $^1J(P,C)$ = 47.5 Hz), 18.2 (d, $^1J(P,C)$ = 49.0 Hz), 13.4. $^{31}P\{^1H\}$ NMR (161.82 MHz, $CDCl_3$): δ = 34. ATR-IR: 2105 cm^{-1} (w, C≡C), 2960 cm^{-1} (s, CH). HRMS calculated for $C_{17}H_{34}P$ $[M]^+$: 269.2398; Found: 269.2400.

*Synthesis of triethyl(1-pentynyl)phosphonium chloride (**Et_3P-yne**)*

The same procedure described above for the synthesis of ***Bu_3P-yne*** was used except that triethylphosphine was used as the starting material. The product was obtained as a light brown powder. Yield = 80%. ^1H NMR (400 MHz, $CDCl_3$): δ = 2.62 – 2.47 (m, 8H), 2.41 (ddt, $^3J(H,H)$ = 3.6 Hz, $^4J(H,H)$ = 2.7 Hz, $^4J(P,H)$ = 0.8 Hz, 2H), 2.02 (t, $^4J(H,H)$ = 2.7 Hz, 1H), 1.87 – 1.77 (m, 2H), 1.28 (dt, $^3J(H,H)$ = 7.6 Hz, $^3J(P,H)$ = 18.0 Hz, 9H). $^{13}C\{^1H\}$ (100.52 MHz, $CDCl_3$): δ = 82.1, 70.9, 21.0 (d, $^2J(P,C)$ = 3.7 Hz), 19.6 (d, $^3J(P,C)$ = 16.5 Hz), 17.1 (d, $^1J(P,C)$ = 48.6 Hz), 12.5 (d, $^1J(P,C)$ = 48.7 Hz), 6.2 (d, $^2J(P,C)$ = 5.5 Hz). $^{31}P\{^1H\}$ NMR (161.82 MHz, $CDCl_3$): δ = 39. ATR-IR: 2105 cm^{-1} (w, C≡C), 2960 cm^{-1} (s, CH). HRMS calculated for $C_{11}H_{21}P$ $[M]^+$: 184.1381; Found: 184.1379.

*Synthesis of tri-n-octyl(1-pentynyl)phosphonium chloride (**Oct$_3$P-yne**)*

Tri-n-octylphosphine (1.00 g, 2.70 mmol, 1.0 equiv.) was dissolved in dry dioxane in a pressure tube inside a glovebox. 5 mg of NaI was added to the reaction mixture. 5-chloro-1-pentyne (0.300 g, 2.92 mmol, 1.1 equiv.) was then added dropwise to the stirring phosphine solution. The pressure tube was sealed and then heated at 100 °C. The reaction was monitored by $^{31}P\{^{1}H\}$ NMR spectroscopy. At approximately 50% conversion of the starting phosphine, the excess phosphine, 5-chloropentyne and solvent were removed *in vacuo*. The resulting colourless oil was washed twice with excess hexanes. The crude product was purified on a silica gel column using 1:1 CH_2Cl_2:MeOH as the eluent. Fractions were checked for purity by $^{31}P\{^{1}H\}$ NMR spectroscopy, pure fractions were combined, and the solvent was removed *in vacuo* to provide a light brown viscous oil. Yield = 12%. ^{1}H NMR (400 MHz, $CDCl_3$): δ = 2.70 – 2.57 (m, 2H), 2.44 – 2.34 (m, 8H), 2.00 (t, $^{4}J(H,H)$ = 2.6 Hz, 1H), 1.84 – 1.76 (m, 2H), 1.54 – 1.41 (m, 12H), 1.27 – 1.22 (m, 24H), 0.83 (t, $^{3}J(H,H)$ = 6.8 Hz, 9H). $^{13}C\{^{1}H\}$ (100.52 MHz, $CDCl_3$): δ = 81.9, 70.4, 31.5, 30.7 (d, $^{1}J(P,C)$ = 14.1 Hz), 28.8, 22.4, 21.7 (d, $^{3}J(P,C)$ = 4.0 Hz), 21.0 (d, $^{3}J(P,C)$ = 4.0 Hz), 19.3 (d, $^{1}J(P,C)$ = 17.1 Hz), 19.2 (d, $^{2}J(P,C)$ = 46.2 Hz), 18.2 (d, $^{2}J(C,H)$ = 49.2 Hz), 13.9 (s, CH_3). $^{31}P\{^{1}H\}$ NMR (161.82 MHz, $CDCl_3$): δ = 33.9. ATR-IR: 1460 cm^{-1} (m, P-C_nH_m), 2120 cm^{-1} (w, C≡C), 2920 cm^{-1} (s, CH). HRMS calculated for $C_{29}H_{58}P$ $[M]^+$: 437.4276; Found: 437.4267.

*Synthesis of **Alk$_3$P-BCP***

N$_3$-BCP (100 mg, 21 μmol, 1 equiv.) was suspended in purified water (2 mL) with stirring. The trialkyl(1-pentynyl)phosphonium chloride (42 μmol, 2.0 equiv.) as a solution in THF (0.5 mL), and Cu(II)Cl_2 (4 mg, 23 μmol, 1 equiv.) were added. A 50 mM aqueous solution of sodium ascorbate (2 mL, 210 μmol, 10 equiv.) was added with rapid stirring and the reaction flask was sealed. After 18 hours, the reaction mixture was dialyzed using a 10 kg/mol molecular weight cut-off (MWCO) membrane first against 1 L of a 0.5 mM aqueous NaCl solution for 18 hours, then against 1 L of purified water for 12 hours twice. The sample was then lyophilized to obtain the phosphonium-functionalized polymer as a white powder in approximately quantitative yield.

Et_3P-BCP: ^{1}H NMR (400 MHz, $CDCl_3$): 7.70 (s, 1H), 4.50 (t, ^{3}J(H,H) = 4.9 Hz, 2H), 4.02 (t, ^{3}J(H,H) = 6.6 Hz, 52H), 3.60 (m, 180H), 2.90 (t, ^{3}J(H,H) = 6.4 Hz, 2H), 2.49 (dq, ^{2}J(H,P) = 13.0 Hz, ^{3}J(H,H) = 8 Hz, 6H); 2.29 (t, ^{3}J(H,H) = 7.6 Hz, 52H), 1.66-1.56 (m, 104H), 1.40 – 1.30 (m, 52H), 1.25 (dt, ^{3}J(H,P) = 18.0 Hz, ^{3}J(H,H) = 7.6 Hz, 9H). ^{31}P{^{1}H} NMR (161.82 MHz, $CDCl_3$): δ = 38.7. ATR-IR: 1105 cm^{-1} (m, CH_2-O-CH_2); 1190 cm^{-1} (m, *O-C*=O); 1720 cm^{-1} (s, C=O); 2800 – 2900 cm^{-1} (m, C-H).

Bu_3P-BCP: ^{1}H NMR (400 MHz, $CDCl_3$): δ = 7.72 (s, 1H); 4.50 (t, ^{3}J(H,H) = 5.2 Hz, 2H), 4.03 (t, ^{3}J(H,H) = 6.6 Hz, 52H), 3.61 (m, 180H), 2.90 (m, 2H), 2.65 (m, 2H), 2.37 (m, 8H), 2.27 (t, ^{3}J(H,H) = 7.6 Hz, 52H), 1.66-1.56 (m, 104H), 1.48 (m, 12H), 1.40 – 1.30 (m, 52H), 0.94 (t, ^{3}J(H,H) = 6.4 Hz). ^{31}P{^{1}H} NMR (161.82 MHz, $CDCl_3$); δ = 33.3. ATR-IR: 1105 cm^{-1} (m, CH_2-O-CH_2); 1190 cm^{-1} (m, *O-C*=O); 1720 cm^{-1} (s, C=O); 2800 – 2900 cm^{-1} (m, C-H).

Oct_3P-BCP: ^{1}H NMR (400 MHz, $CDCl_3$): δ = 7.72 (s, 1H), 4.50 (t, ^{3}J(H,H) = 5.2 Hz, 2H), 4.03 (t, ^{3}J(H,H) = 6.6 Hz, 52H), 3.61 (m, 180H), 2.90 (m, 2H), 2.65 (m, 2H), 2.37 (m, 8H), 2.27 (t, ^{3}J(H,H) = 7.6 Hz, 52H), 1.66-1.56 (m, 104H), 1.48 (m, 12H), 1.40 – 1.30 (m, 52H); 0.94 (t, ^{3}J(H,H) = 6.4 Hz, 20H). ^{31}P{^{1}H} NMR (161.82 MHz, $CDCl_3$); δ = 33.3. ATR-IR: 1105 cm^{-1} (m, CH_2-O-CH_2); 1190 cm^{-1} (m, *O-C*=O); 1720 cm^{-1} (s, C=O); 2800 – 2900 cm^{-1} (m, C-H).

Self-assembly of BCPs

Copolymer (5 mg) was dissolved in glass distilled THF (0.5 mL) that had been passed through a 0.22 μm polytetrafluoroethylene filter. The copolymer solution was then added to rapidly stirring purified water (2 mL) that had been passed through an Acrodisc® Syringe Filter (0.45 μm Supor® Membrane) (Pall Life Sciences). The resulting suspension was placed in a 30 °C sand bath overnight to evaporate the THF.

Transmission electron microscopy (TEM)

TEM images were obtained using a Philips CM 10 Transmission Electron Microscope. Self-assembly samples were loaded onto Formvar-coated copper grids by placing the grid on a clean filter paper and dropping 10 μL of a 0.5 – 1.0 mg/mL solution onto the grid and repeating after 30 seconds. The grid was allowed to dry overnight on the filter paper

and was imaged the next day. The **Alk$_3$P-BCP** nanocarriers were stained by adding 100 μL of a 1 wt% aqueous auric acid solution to the stock TEM solution and allowing it to stir for one hour to exchange chloride anions with aurate. The sample was then loaded onto the grid as described above.

Determination of the minimum bactericidal concentration (MBC)

The bacteria used were *E. coli* (ATCC 29425) and *S. aureus* (ATCC 6538). After inoculation of 10 mL of 0.3 mM pH 7.4 phosphate buffer, the bacteria were cultured overnight in nutrient broth in an incubator-shaker at 37 °C. They were then pelletized by centrifugation and the broth was decanted. 10 mL of phosphate solution was then used to resuspend the pellet. The bacteria were again pelletized by centrifugation. This process of resuspension and centrifugation was repeated twice more. For *S. aureus*, a suspension with an optical density of 0.3 at 600 nm, corresponding to 10^7 CFU/mL was prepared. For *E. coli*, a suspension with an optical density of 0.2 at 600 nm, corresponding to 10^8 CFU/mL was prepared. These stock solutions were then diluted to ~2×10^5 CFU/mL.

Samples for testing were prepared at the highest concentration for testing in 0.3 mM pH 7.4 phosphate buffer and serial two-fold dilutions were performed to achieve lower concentrations. All molecules and assemblies were sterilized by irradiation with UV light in a UV light cabinet for 30 minutes prior to testing. Tests were performed in 96 well plates. Sample wells contained 100 μL of the sample material in phosphate buffer and 100 μL of the bacterial suspension at 10^5 CFU/mL. Control wells contained 100 μL of phosphate buffer and 100 μL of the bacterial suspension at 10^5 CFU/mL. The phosphate buffer was also tested for sterility. Samples and controls were measured in triplicate. The wells were mixed for 4 hours at ambient temperature using a Tecan infinite M1000 Pro (Tecan Trading AG, Switzerland) plate reader. The suspensions were then diluted by adding 100 μL of the well contents into 9.9 mL of phosphate buffer to give a resulting bacterial concentration of approximately 10^3 CFU/mL. 100 μL of this suspension was then pour plated on nutrient agar and incubated overnight at 37 °C. The nutrient agar was prepared by dissolving 25 g of LB broth (Miller's modification) (Alfa Aesar, Reston, United States) and 15 g of Agar Powder $(C_{12}H_{18}O_9)_x$ (Alfa Aesar, Reston, United States) in 1 L of hot water (85°C). The following day the bacterial colonies were

counted. The MBC was determined as a 99% reduction in the number of bacterial colonies on the plate.

Hemolysis assay

The hemolytic activity of the nanocarriers was determined using sterile defibrinated sheep's blood (Cedarlane Labs, Burlington Ontario, Canada). The blood was pelletized by centrifuging 1 mL of the blood and washing the pellet four times with 0.9 % saline. The pellet was resuspended in 1 mL of a phosphate buffered saline (PBS) consisting of 0.32 mM NaH_2PO_4 and 140.40 mM NaCl maintained at a pH of 7.4 to create the red blood cell (RBC) suspension. A concentrated solution of the micelles was diluted with 750 µL of the PBS to the highest concentration for the assay. The micelle solutions were diluted two-fold serially with PBS to achieve the desired concentrations. To the micelle solutions 25 µL of the RBC suspension was added. A negative control of 25 µL of the RBC suspension in 1000 µL of the PBS and a positive control of 25 µL of the RBC suspension in 1000 µL purified water. Nanocarrier background controls were made consisting of the same concentration of the nanocarrier in PBS to eliminate absorbance or scattering contributions from the nanocarriers themselves. The samples were incubated at room temperature for 2 hours and afterward the samples were centrifuged to re-pelletize the blood cells. 200 µL of the supernatant of each sample and control were placed into wells in a 96 well plate and the absorbance (A) at 540 nm was measured. The percent hemolysis was determined with the following equation:

$$\text{Percent Hemolysis} = \frac{A_{\text{sample}} - A_{\text{micelles}} - A_{\text{negative control}}}{A_{\text{positive control}} - A_{\text{negative control}}} \times 100\%$$

Equation 2.1

Tetracycline encapsulation

500 µL of a solution of tetracycline (0.5 mg/mL in $CHCl_3$) was used to dissolve either **MeO-BCP** or **Bu_3P-BCP** (5 mg). With rapid stirring 2 mL of purified water was added and stirring was continued overnight at 30 °C. The sample was covered with aluminum foil to allow evaporation of $CHCl_3$ while at the same time preventing exposure to ambient light. The resulting suspension was then introduced into a Microsep™ Advance Centrifugal Device with a 10 kg/mol MWCO (Pall Life Sciences) and the solvent was

reduced to 1/5 its initial volume. The concentrated suspension was diluted to 2 mL of purified water, and centrifugation was performed again. The filtrate was combined and the concentration of tetracycline in the filtrate was measured by UV-visible spectroscopy (ε = 14,075 $M^{-1}cm^{-1}$ in water at 363 nm) to determine the EE of tetracycline as:

$$EE = \frac{\text{Mass of Drug in Particles}}{\text{Mass of Drug Added}} \times 100\%$$

Equation 2.2

The DLC of the assemblies could then be calculated as:

$$DLC = \frac{\text{Mass of Drug in Particles}}{\text{Mass of Loaded Particles}} \times 100\ \%$$

Equation 2.3

Tetracycline release study

Assemblies containing encapsulated tetracycline were prepared as described above except that 0.3 mM, pH 7.2 phosphate buffer was used. A volume of 2 mL each of tetracycline-loaded **MeO-BCP** or **Bu_3P-BCP** micelles was then placed on a wrist-action shaker. At measurement time points, centrifugal ultrafiltration was performed as described above to separate released tetracycline from the suspension and the concentrated suspension was diluted again to 2 mL with the phosphate buffer. The absorbance of the filtrate was measured and the concentration of tetracycline in the filtrate was determined based on an ε = 14,075 $M^{-1}cm^{-1}$ in the same buffer at 363 nm.

2.5 References

1 G. Chen, I. Roy, C. Yang, P. N. Prasad, *Chem. Rev.*, 2016, **116**, 2826–2885.

2 S. Mura, J. Nicolas, P. Couvreur, P. *Nat. Mater.*, 2013, **12**, 991–1003.

3 N. Kamaly, B. Yameen, J. Wu, O. C. Farokhzad, *Chem. Rev.*, 2016, **116**, 2602–2663.

4 R. Duncan, *Nat. Rev. Drug Discov.*, 2003, **2**, 347–360.

5 I. W. Hamley, *Block Copolymers in Solution: Fundementals and Applications*, John Wiley & Sons, Inc., Chichester, 2005.

6 Y. Kim, P. Dalhaimer, D. A. Christian, D. E. Discher, *Nanotechnology*, 2005, **16**, 484–491.

7 N. P. Truong, J. F. Quinn, M. R. Whittaker, T. P. Davis, *Polym. Chem.*, 2016, **7**, 4295–4312.

8 S. R. Mane, N. V. Rao K. Chaterjee, H. Dinda, S. Nag, A. Kishore, J. Das Sarma, R. Shunmugam, *Macromolecules*, 2012, **45**, 8037–8042.

9 S. Wieczorek, A. Dallmann, Z. Kochovski, H. G. Börner, *J. Am. Chem. Soc.*, 2016, **138**, 9349–9352.

10 A. Rösler, G. W. M. Vandermeulen, H.-A. Klok, *Adv. Drug Deliv. Rev.*, 2012, **64**, 270–279.

11 Y. Mai, A. Eisenberg, *Chem. Soc. Rev.*, 2012, **41**, 5969–5985.

12 P. Gao, A. Nie, M. Zou, Y. Shi, G. Cheng, *J. Antibiot.*, 2011, **64**, 625–634.

13 World Health Organization. WHO | Global action plan on antimicrobial resistance http://www.who.int/drugresistance/global_action_plan/en/ (accessed Jun 14, 2016).

14 M. Moreno-Sastre, M. Pastor, C. J. Salomon, A. Esquisabel, J. L. Pedraz, *J. Antimicrob. Chemother.*, 2015, **70**, 2945–2955.

15 S. Maya, S. Indulekha, V. Sukhithasri, K. T. Smitha, S. V. Nair, R. Jayakumar, R. Biswas, *Int. J. Biol. Macromol.*, 2012, **51**, 392–399.

16 Y. Li, G. Liu, X. Wang, J. Hu, S. Liu, *Angew. Chem. Int. Ed.*, 2016, **55**, 1760–1764.

17 Y. Liu, H. J. Busscher, B. Zhao, Y. Li, Z. Zhang, H. C. van der Mei, Y. Ren, L. Shi, L. *ACS Nano*, 2016, **10**, 4779–4789.

18 L. Zhang, F. X. Gu, J. M. Chan, A. Z. Wang, R. S. Langer, O. C. Farokhzad, *Clin. Pharmacol. Ther.*, 2008, **83**, 761–769.

19 V. P. Torchilin, *Adv. Drug Deliv. Rev.*, 2012, **64**, 302–315.

20 H. Lu, L. Fan, Q. Liu, J. Wei, T. Ren, J. Du, *Polym. Chem.*, 2012, **3**, 2217.

21 K. Zou, Q. Liu, J. Chen, J. Du, *Polym. Chem.*, 2014, **5**, 405–411.

22 H. Sun, L. Fan, K. Zou, H. Zhu, J. Du, *RSC Adv.*, 2014, **4**, 41331–41335.

23 C. Zhou, M. Wang, K. Zou, J. Chen, Y. Zhu, J. Du, *ACS Macro Lett.*, 2013, **2**, 1021–1025.

24 Z. Shi, K. G. Neoh, E. T. Kang, W. Wang, *Biomaterials*, 2006, **27**, 2440–2449.

25 C. Zhang, Y. Zhu, C. Zhou, W. Yuan, J. Du, *Polym. Chem.*, 2013, **4**, 255.

26 H. S. Zhu, Q. R. Geng, W. Q. Chen, Y. Q. Zhu, J. Chen, J. Du,. *J. Mater. Chem. B* 2013, **1**, 5496–5504.

27 Y. Li, X. Hu, S. Tian, Y. Li, G. Zhang, G. Zhang, S. Liu, *Biomaterials*, 2014, **35**, 1618–1626.

28 A. M. Carmona-Ribeiro, L. D. de Melo Carrasco, *Int. J. of Mol. Sci.*, 2013, **14**, 9906–9946.

29 F. Siedenbiedel, J. C. Tiller, *Polymers*, 2012, **4**, 46–71.

30 E.-R. Kenawy, S. D. Worley, R. Broughton, *Biomacromolecules*, 2007, **8**, 1359–1384.

31 A. Kanazawa, T. Ikeda, T. Endo, *J. Polym. Sci. Part A Polym. Chem.*, 1993, **31**, 335–343.

32 A. Kanazawa, T. Ikeda, T. Endo, *J. Polym. Sci. Part A Polym. Chem.*, 1993, **31**, 1441–1447.

33 A. Kanazawa, T. Ikeda, T. Endo, *J. Polym. Sci. Part A Polym. Chem.*, 1993, **31**, 3031–3038.

34 T. J. Cuthbert, T. D. Harrison, P. J. Ragogna, E. R. Gillies, *J. Mater. Chem. B* 2016, **4**, 4872–4883.

35 T. J. Cuthbert, R. Guterman, P. J. Ragogna, E. R. Gillies, *J. Mater. Chem. B*, 2015, **3**, 1474–1478.

36 S. Park, S. H. Cha, I. Cho, S. Park, Y. Park, S. Cho, Y. Park, *Mater. Sci. Eng. C*, 2016, **58**, 1160–1169.

37 V. R. Sinha, K. Bansal, R. Kaushik, R. Kumria, A. Trehan, *Int. J. of Pharm.*, 2004, **278**, 1–23.

38 A. Nazemi, R. C. Amos, C. V. Bonduelle, E. R. Gillies, *J. Polym. Sci. Part A Polym. Chem.*, 2011, **49**, 2546–2559.

39 Y. Mai, A. Eisenberg, *Chem. Soc. Rev.*, 2012, **41**, 5969.

40 N. A. Lynd, A. J. Mueler, M. A. Hillmyer, *Prog. Polym. Sci.*, 2008, **33**, 875-893.

41 J. H. Davies, P. Kirby, *J. Polym. Sci. Part. A, General Papers*, 1964, **1**, 3425–3429.

42 M. Tajkarimi, S. A. Ibrahim, *Food Control*, 2011, **22**, 801–804.

43 M. Hadadpour, J. Gwyther, I. Manners, P. J. Ragogna, *Chem. Mater.*, 2015, **27**, 3430–3440.

44 C. Fang, B. Shi, Y.-Y. Pei, M.-H. Hong, J. Wu, H.-Z. Chen, *Eur. J. Pharm. Sci.*, 2006, **27**, 27–36.

45 L. Timofeeva, N. Kleshcheva, *Appl. Microbiol. Biotechnol.*, 2011, **89**, 475–492.

46 E. F. Panarin, M. V. Solovskii, N. A. Zaikina, G. E. Afinogenov, *Makromol. Chemie, Suppl.*, 1985, **9**, 25–33.

47 A. Chen, H. Peng, I. Blakey, A. K. Whittaker, *Polym. Rev.*, 2017, **57**, 276-310.

48 H. Lu, L. Fan, Q. Liu, J. Wei, T. Ren, J. Du, *Polym. Chem.*, 2012, **3**, 2217–2227.

49 G. A. Sotiriou, S. E. Pratsinis, *Environ. Sci. Technol.*, 2010, **44**, 5649–5654.

50 Q. L. Feng, J. Wu, G. Q. Chen, F. Z. Cui, T. N. Kim, J. O. Kim, *J. Biomed. Mater. Res.*, 2000, **52**, 662–668.

51 M. Yamanaka, K. Hara, J. Kudo, *Appl. Environ. Microbiol.*, 2005, **71**, 7589–7593.

52 M. Wang, C. Zhou, J. Chen, Y. Xiao, J. Du, *Bioconjug. Chem.*, 2015, **26**, 725–734.

53 A. S. Abd-El-Aziz, C. Agatemor, N. Etkin, D. P. Overy, M. Lanteigne, K. McQuillan, R. G. Kerr, *Biomacromolecules*, 2015, **16**, 3694–3703.

54 V. Sambhy, B. R. Peterson, A. Sen, *Angew. Chemie Int. Ed.*, 2008, **47**, 1250–1254.

55 G. A. O'Toole, M. Wathier, M. E. Zegans, R. M. Q. Shanks, R. Kowalski, M. W. Grinstaff, *Cornea*, 2012, **31**, 810–816.

56 I. Chopra, M. Roberts, *Microbiol. Mol. Biol. Rev.*, 2001, **65**, 232–260.

Chapter 3

Hisey, B; Gillies, E. R.; Ragogna, P. J. *Langmuir*, **2017**, *33(51)*,pp 14738-14747.

Effect of Counter Ions on the Self-Assembly of Polystyrene-Polyphosphonium Block Copolymers

3.1 Introduction

The self-assembly of amphiphilic BCPs in solution is a phenomenon that is poised to address a wide range of important technical challenges such as new methods for drug delivery,[1-4] detection and imaging of cancer cells,[5,6] and compartmentalization of reactions.[7-9] Ground-breaking discoveries of the factors that influence the solution phase self-assembly phenomenon have provided the foundations to impact these diverse and highly technical areas. The assembled ordering of amphiphilic BCPs is a balance between the thermodynamic interactions between a copolymer and solvent,[10] the block components in the copolymer (hydrophilic/hydrophobic) and the interactions between individual polymer chains. The importance of the relative lengths of the blocks was well demonstrated in the study by Eisenberg and coworkers, in which it was found that even small changes in the relative volume fractions of the blocks of PAA-*b*-PS (**3.1**; Figure 3-1) had significant impacts on the morphological properties of the self-assembled materials.[11] The effects of these interactions had also been observed when self-assembled systems underwent changes in equilibrium structures in response to stimuli such as temperature, pH or the relative amounts of selective and non-selective solvents.[12]

Polyelectrolytes are polymers that contain repeating units with cation/anion pairs. Polyelectrolytes have a variety of uses as functional components in antimicrobial and antibacterial polymers,[13,14] self-healing polymers,[15] and many other areas.[16] Polyelectrolytes have been used in amphiphilic BCPs as the solvophilic block, thereby promoting solution phase self-assembly. Many groups have studied the self-assembly behavior of amphiphilic polyelectrolyte-*b*-polyneutral copolymers and it has been

established that polyelectrolyte blocks in the solution phase self-assembly of copolymers are sensitive to the ionic strength of the selective solvent because of the imposed solvation states of the corona, as determined by the theoretical work of Borisov and Zhulina.[17] Solomatin and coworkers showed that the stability of nanoparticles formed by complexes of poly(ethylene oxide)-*b*-poly(sodium methacrylate) (**3.2**; Figure 3-1) and hexadecyltrimethylammonium bromide was dependent on the identity and concentration of different added salts.[18,19] The effect of added salts on the morphology of nanoparticles formed from polyelectrolyte BCPs was also studied by Förster and coworkers on systems composed of polyethylethylene-*b*-poly(styrenesulfonic acid) (**3.3**; Figure 3-1).[20] The authors discovered that, by increasing the salt concentration, the charged micelles could be induced to fuse into toroidal networks.

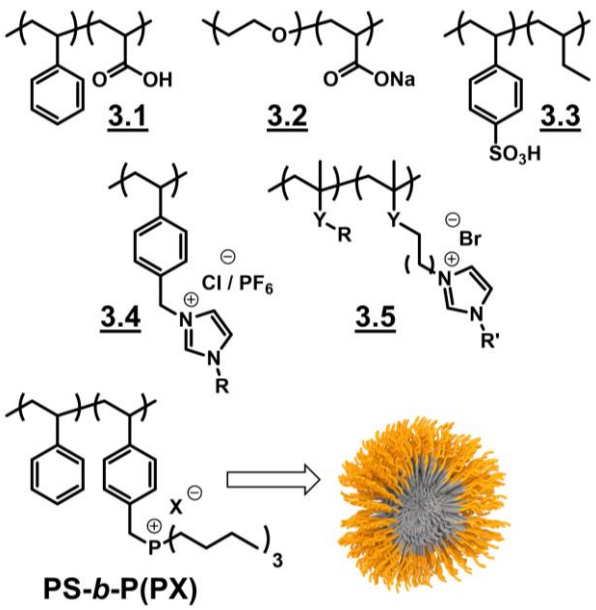

Figure 3-1. Chemical structures of polyelectrolyte-*b*-polyneutral copolymers (**3.1–5**) that were investigated in previous[11,18-22,] and those of the current work (**PS-*b*-P(PX)**).

More recently, poly(1-(4-vinylbenzyl)-3-methyl imidazolium chloride) (**3.4**, Figure 3.1) was subjected to partial ion exchange with hexafluorophosphate to produce a random copolymer of the same backbone repeat unit with randomly associated counterions.[21] These random copolymers then underwent self-assembly due to the differences in the solubilities of the repeat units, depending on the identity of the counter anion. The size of the particles was found to depend on the ratio of the two anions (Cl^-

and PF_6^-) associated with the polymer chains. Vijayakrishna and coworkers synthesized a series of BCPs comprising a methacrylate or methacrylamide block and an imidazolium block (**3.5**; Figure 3-1). The hydrophilicity of the methacrylate or methacrylamide block could be tuned through the degree of methylation and the hydrophobicity of the imidazolium was altered through anion exchange from a bromide counterion to a bis(trifluoromethane)sulfonimide anion.[22] The *in situ* exchange of the anion led to switching of the location of the block domains in the self-assembled nanostructures as well as alterations in morphological properties.

Most amphiphilic BCP systems rely on changing the degree of polymerization of the polymer blocks to affect the morphology of the nano-assemblies. With a hydrophilic block composed of permanently charged phosphonium repeat units, the morphological characteristics of the nano-assemblies can be altered through the presence of different anions. The identity of the counter ion alters the relative hydrophilic volume fraction through the size of the anion itself, as well as the separation of the anion and the cation. Unlike polyneutral solvophilic blocks, in polyelectrolytes the interaction between the same blocks becomes energetically unfavorable because of coulombic repulsion. The repulsion experienced between coronal chains will depend in part on the screening of the coronal charges not only by solvation but by the counter-ions present. While the above work with polymers such as **3.1**-**5** showed that the identity of the added salt influenced the morphological properties researchers were unable to ensure that there was only a single counterion present. Furthermore, the addition of salt also resulted in the addition of ions of the same charge as the polymer being studied, which may have also influenced the self-assembled material.

The effect of varying the anion type on the copolymer itself prior to the self-assembly of polyneutral-*block*-polycation into nano scale materials has not been reported to the best of my knowledge. In this context, I have prepared a library of polystyrene-*b*-polyphosphonium (**PS-*b*-P(PX),** Figure 3-1) copolymers using RAFT polymerization. Each **PS-*b*-P(PX)** system had the same DP, but a different counter anion. The effect of the differing cation-anion pairs on the self-assembly was explored. The self-assembly of the polymers was investigated by nano-precipitation of the core forming polystyrene block in the presence of increasing water content from a non-selective solvent. Several

morphological characteristics were examined. It was found that the identity of the counter-ion of the **PS-*b*-P(PX)** copolymer did influence the morphological properties of the self-assembled materials. The influence was a result of the differences in anion interaction with the phosphonium block, and differences in the solubility.

3.2 Results and Discussion

3.2.1 Synthesis of Phosphonium Monomers

The morphological properties of the self-assembled materials are dependent on the relative DP of the two blocks. In a study of the effect of anion identity on self-assembly, it was clear that there were two approaches to accessing polymers with the same DP of the blocks and different anions. The first was to make the polymers with monomers with different anions and the other was to make the polymer and to exchange the anions. The second method presents a challenge in confirming that complete conversion is achieved from one anion to the next and requires more difficult experimental conditions for achieving the exchange due to the amphiphilicity of the BCP. Therefore, in this work the first method was used, as this allowed the full characterization of the identity of the anion on the monomer as well as the investigation of the anion effect on some of the monomer properties.

Understanding the effect of solution phase cation-anion interactions on polymer self-assembly required some variation in the electronics and lipophilicity of the anionic species, so a series of anions was selected that provided different anion sizes and salt hydrophilicity. The halide anions (Cl^-, Br^-) have spherical charge distributions, the difference being that the bromide is much larger, more polarizable due to the larger ionic radius. Therefore **3.8-Br** exhibits a lower aqueous solubility than **3.8-Cl**. While the nitrate salt **3.8-NO_3** LogP is positive, the ionic radius is similar to that of bromide.[23] The triflate anion was much more lipophilic and thus **3.8-OTf** has limited aqueous solubility. Taken together, these anions represent different charge densities, sizes and aqueous solubilities; properties that impact the self-assembly of the resultant BCPs.

The chloride and bromide analogues (**3.8-Cl/Br**) were synthesized via quaternization of tri(*n*-butyl)phosphine with 4-vinylbenzyl chloride (**3.6**) or its bromide analogue 4-vinylbenzyl bromide (**3.7**), synthesized from the former via a Finkelstein

reaction (Scheme 3-1). The reaction proceeded to at least 98% conversion in each case, as determined by the relative integrations of the ^{1}H NMR spectra for the methylene protons at 4.57 ppm for **3.6** and 4.48 ppm for **3.7** (Figure B-1). The onwards quaternization reaction was carried out without separation of the chloride analogue because of the extremely similar nature of the vinylbenzyl halides. Nevertheless, the formation of **3.8-Br** was the preferred product because of the enhanced reactivity of **3.7** (i.e. heavy halide displacement).

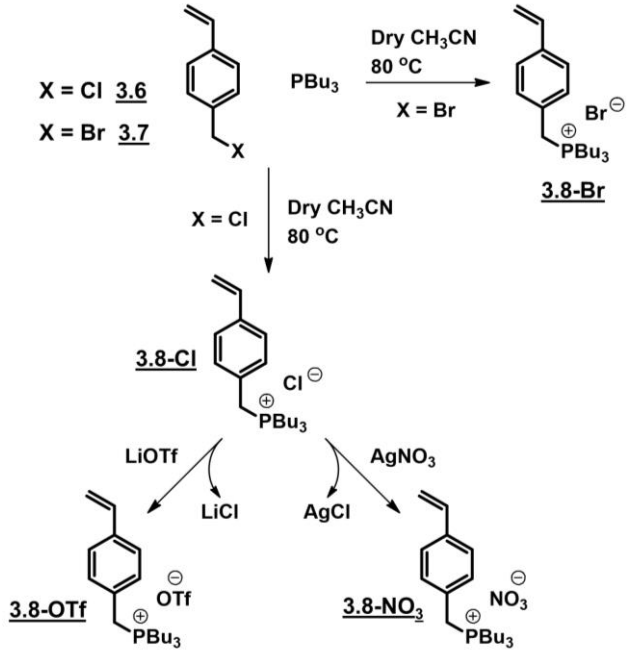

Scheme 3-1. Synthesis of phosphonium monomers

Compounds **3.8-NO$_3$** and **3.8-OTf** were produced through salt metathesis of the chloride monomer using $AgNO_3$ and LiOTf, respectively. In those cases, the removal of the chloride anion was confirmed through a precipitation test using lithium triflate or silver nitrate accordingly, where the absence of precipitate (AgCl or LiCl) was taken as complete Cl^- removal. The identity of the new salts was confirmed using ESI mass spectrometry in both positive and negative ion detection modes.

The phosphonium salts showed no difference in the IR active vibrations of the phosphonium cation (Figure B-2). The relative degree of anion-cation interaction for the monomers in $CDCl_3$ was determined from the relative chemical shifts of the peaks corresponding to the benzylic methylene protons in the ^{1}H NMR spectra. As the extent of

cation-anion interaction decreased going from the chloride to triflate counterion, the chemical shifts of those peaks decreased (Table 3-1, Figure 3-2). When salt **3.8-Cl** was exposed to solvents mixtures ranging from a low dielectric constant solvent (100% $CDCl_3$) to a higher one (100% CD_3OD), the chemical shift of the alpha methylene protons decreased with increasing solvent polarity (Figure 3-3). The decrease in chemical shifts may have been due to a greater interaction between the phosphonium and solvent dipoles as the anion moved away from the cation. These data show that there was little difference in the coordination between the chloride and bromide salts, whereas the nitrate association was much weaker than that of the halides and the triflate anion even less so in chloroform. While one might expect the change in chemical shifts to be more downfield from electronegativity arguments, it is possible that the paramagnetic contributions from the phosphorus atom are dominant and have a greater influence on the chemical shifts observed for the cation-anion pairs. The trend may also arise from stronger cation-π interactions[25,26] between the phosphonium and the phenyl rings in the case of the more weakly coordinating anions.

	Benzylic Methylene δ	LogP
3.8-Cl	4.28	-0.39 ± 0.02
3.8-Br	4.26	-0.19 ± 0.03
3.8-NO_3	3.93	0.13 ± 0.02
3.8-OTf	3.78	0.33 ± 0.05

Table 3-1. Chemical shift values (δ) of the benzylic methylene protons and the partition coefficients of the monomer salts (n=3, ±st. dev).

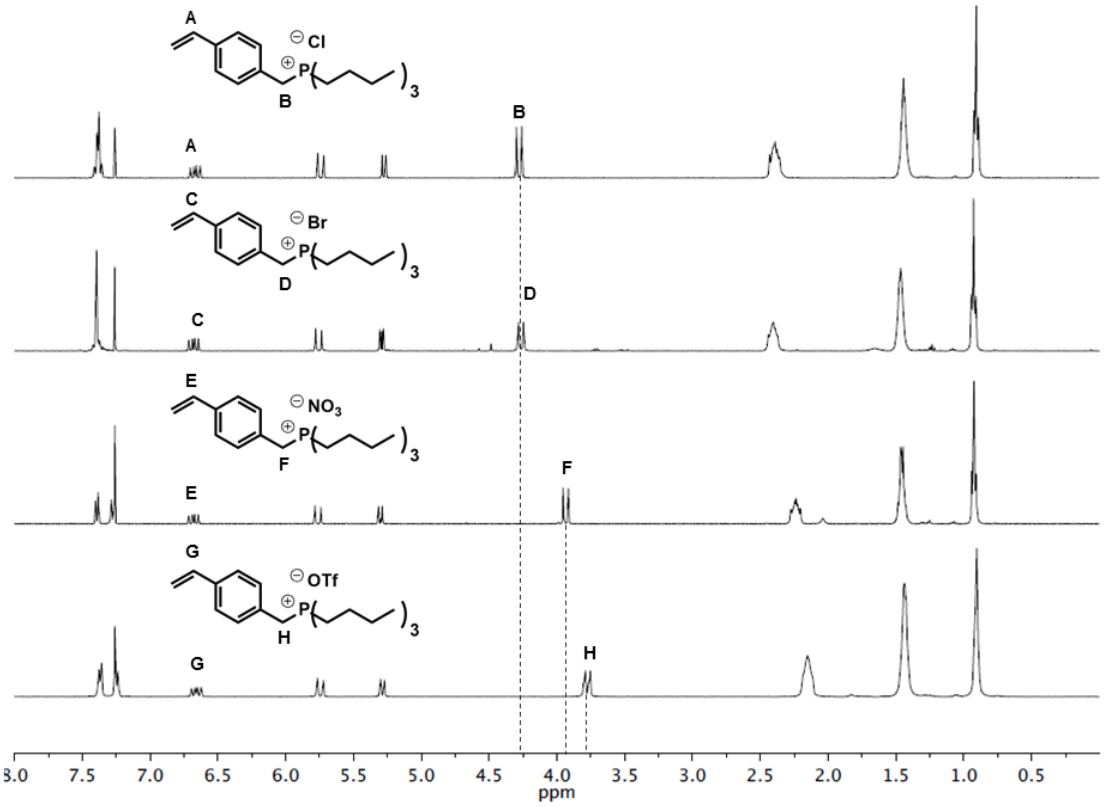

Figure 3-2. ^{1}H NMR spectra ($CDCl_3$, 400 MHz) of the phosphonium monomers indicating the change in chemical shift of the benzylic methylene protons with the change of the anion.

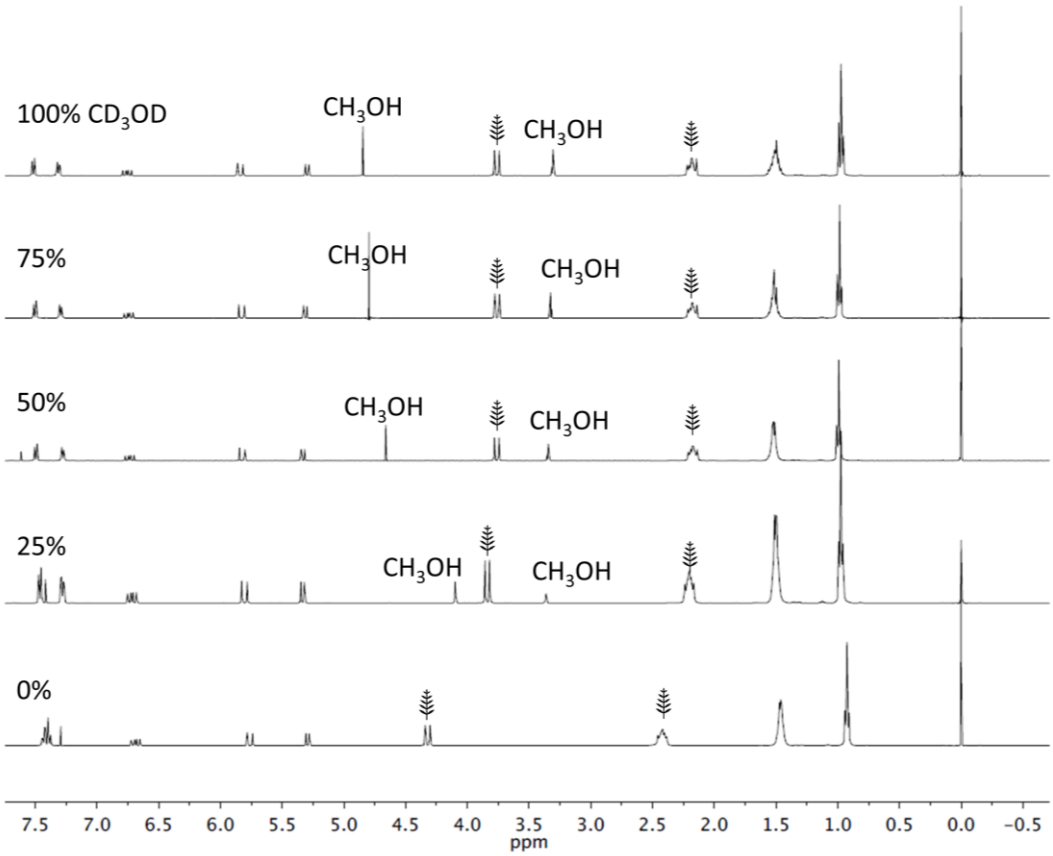

Figure 3-3. ^{1}H NMR (400 MHz) solvent titration of **3.8-Cl** in 100% CD_3OD to 0% CD_3OD (100% $CDCl_3$), referenced relative to Me_4Si. Branch symbol indicates the alpha methylene proton signals.

3.2.2 Octanol/Water Partition Coefficient

The solubility behavior of the different **3.8-X** repeat units played a key role in the self-assembly of the BCPs by altering the energy of interaction between the hydrophilic phosphonium block and the water. We selected the octanol/water partition coefficient (LogP as defined by equation 3.1) as an indicator of the monomer solubility and thus overall hydrophobicity. The presence of the phosphorus atom in the monomers provided a convenient handle for the spectroscopic determination of the amount of **3.8-X** in solution relative to an internal standard. This allowed the concentration of **3.8-X** to be measured in octanol after its partitioning between octanol and water. The LogP values are listed in Table 3-1. When the value LogP is greater than 0, as in the case of **3.8-OTf** or **3.8-NO3,** the compound is considered hydrophobic. Higher hydrophobicity should translate into an increased energy of interaction between the **P(PX)** block and water. This increased

energy of interaction should lead to a smaller corona as the interaction between **P(PX)** chains should became more favorable than their interaction with the solvent. On the other hand, **3.8-Cl** and **3.8-Br** could be considered hydrophilic and should have had favorable interactions with water.

3.2.3 Synthesis of a Polystyrene MacroRAFT Agent

The morphological properties of nano-materials formed by the aqueous self-assembly of amphiphilic BCPs are sensitive to the f_A of the blocks. The f_A of each block depends on both the identity of the polymer and its DP. As the goal was to explore the effects of the different anions, the differences in the DP of the different **PS-*b*-P(PX)** polymers needed to be negligible. Self-assembly is also dependent on the *Đ* of the BCPs so it was important to achieve a similar, and ideally low *Đ*, for each copolymer. This was achieved by RAFT polymerization using a previously reported fluorinated RAFT agent (Scheme 3-2).[27] The fluorine groups provided a handle to assist in characterization of the block polymers as described in appendix B. The PS macroRAFT agent was synthesized first, which allowed for the absolute determination of M_n and M_W using SEC calibrated with PS standards. A relatively high DP for the PS was desired, as the smallest monomer, **3.8-Cl**, has a 3.4-fold greater mass than that of styrene. The resulting polymer had a M_n of 39400 g/mol and a *Đ* of 1.17, which demonstrated good control over the polymerization. This corresponds to a DP_n of 390.

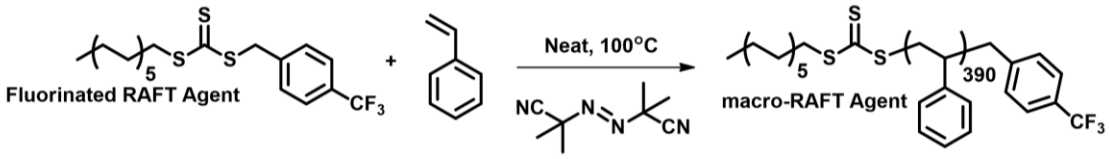

Scheme 3-2. Synthesis of polystyrene macro-RAFT agent.

3.2.4 Synthesis and Characterization of PS_{390}-*b*-$P(PX)_7$

The Eisenberg group has reported that relatively low volume fractions of the annealed polyelectrolyte polyacrylate (PAA) provided interesting and higher ordered morphologies of PS-*b*-PAA BCPs.[10] For this reason the **P(3.8X)** block was targeted at a short length of 7 repeat units. A length of 7 repeat units gives a hydrophilic mass fraction of approximately 6 - 9%, greater than those reported for the PS-*b*-PAA copolymers

reported by Eisenberg. The **PS$_{390}$-b-P(3.8-X)$_7$** BCPs were prepared from the polystyrene macroRAFT agent, and an excess of the **3.8-X** monomer was used to avoid undesirable side reactions typically seen at high monomer conversions (Scheme 3-3).[28]

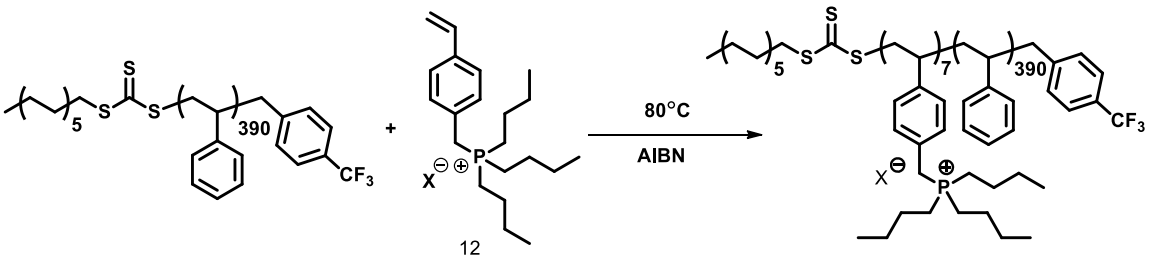

Scheme 3-3. Synthesis of **PS$_{390}$-b-P(3.7-X)$_7$**

The ability of the PS macro-RAFT agent to control the polymerization of the **3.8-OTf** was monitored by ^{1}H NMR spectroscopy using a previously reported procedure.[29] Briefly, the disappearance of the vinylic protons indicated the consumption of monomer relative to the methyl protons on the phosphonium. A linear relationship between the natural logarithm of the monomer conversion and time was observed indicating that the RAFT agent provided good control over the polymerization (Figure 3-4).

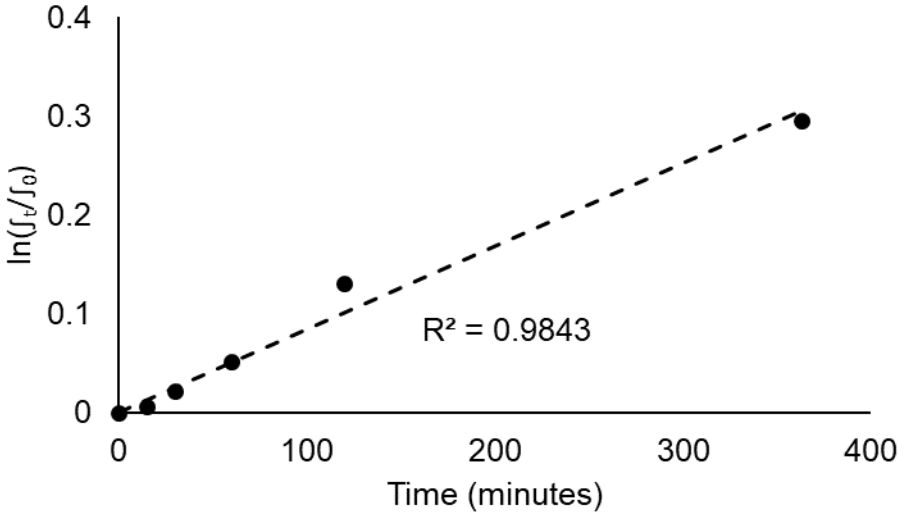

Figure 3-4. Pseudo- 1st order kinetics of the polymerization **3.8-OTf** by **PS** MacroRAFT agent determined from a single polymerization; where $\int_t$ is the integration of an alkene signal in the ^{1}H NMR spectrum of an aliquot of the reaction mixture and $\int_0$ is the initial integration of that same peak, relative to the integration of the phosphonium methyl groups, the chemical shift of which is unaltered between monomer and polymer. The slope of the line of fit is equal to the k value and is 8 x 10^{-4} min^{-1}.

Having demonstrated control over the polymerization, chain extension from the PS MacroRAFT agent with monomer **3.8-OTf** to afford the desired block copolymer was performed first because this monomer has two separate NMR spectroscopic handles available to determine the DP of the phosphonium block. The trifluoromethyl group on the RAFT agent combined with the trifluoromethyl group on the anion allow for end-group analysis of the **PS$_{390}$-*b*-P(3.8-OTf)$_7$** copolymer by ^{19}F NMR spectroscopy. In addition, the known DP of the PS block can be used to determine the DP of the **P(3.8-OTf)** block by comparing the relative integrations of the methyl protons from the phosphonium block with the total integration of all other alkyl protons (Figure B-11). Both methods yielded consistent DP_n values, demonstrating the reliability of the ^{1}H NMR spectroscopic method for the other copolymers, where the ^{19}F method could not be applied. It was confirmed that each of the product BCPs had a DP_n of 7 for the phosphonium block. The SEC traces of the BCPs also confirmed that low *Đ* values were maintained (Table 3-2); however, due to the nature of the standard used for the salt SEC system the M_n reported is from ^{1}H NMR spectroscopic data, which were more reliable. Thermal characterization of the polymers showed that the presence of the phosphonium generally resulted in an increased decomposition temperature, in all cases except for **PS$_{390}$-*b*-P(3.8-NO$_3$)$_7$**. No T_g for the phosphonium blocks was observed in the thermograms (Figures B-15 - B-19) likely due to the relatively low mass fraction of the phosphonium blocks in the polymers.

Polymer	M_n (kg/mol)	Decomposition Onset Point (°C)	T_g (°C)	*Đ*	CAC (μg/mL)
MacroRAFT agent	39.4[a]	300	103	1.1	N/A
PS$_{390}$-*b*-P(3.8-Cl)$_7$	41.9	332	101	1.4	39
PS$_{390}$-*b*-P(3.8-Br)$_7$	42.2	333	104	N/A	21
PS$_{390}$-*b*-P(3.8-OTf)$_7$	42.7	338	105	1.4	28
PS$_{390}$-*b*-P(3.8-NO$_3$)$_7$	42.1	304	98	1.4	24

Table 3-2. Polymer characterization. [a]M_n determined by SEC; all others determined by ^{1}H NMR spectroscopy of single samples.

3.2.5 Preparation and Characterization of Self-Assembled Particles

Aqueous nanoprecipitation of the BCPs was performed to investigate the effect the anions had on the aqueous self-assembly of the BCPs. DMF and THF were used not only for their ability to dissolve fully the polymer chains, but they provided differences in polarity while retaining water miscibility at any solvent ratio. DMF has a smaller polarity difference with water than THF does, and so the PS block was expected to precipitate at lower solvent:water ratios in the DMF:water system than in the THF:water systems. Additionally, two different rates of water addition were investigated to assess differences in kinetic and thermodynamic control of assembly formation. The rapid switch from organic to aqueous environment involved the addition of organic solvent into water, ensuring that there was always an excess of water. The excess water induced the BCPs to adopt kinetically trapped morphologies as the polystyrene core forming block remained insoluble throughout particle formation. The slow addition system involved slow water addition over ten minutes to allow the polymers to adopt a thermodynamically favorable morphology as the water content slowly increased and the PS remained solvated by the organic solvent before becoming trapped into a final morphology. Further solvent annealing for some samples also enabled the glassy PS core to remain partially solvated allowing for thermodynamic equilibrium to be reached for the morphologies. The dodecyl chain at the end of the phosphonium block was not removed prior to self-assembly as the chain is flexible enough to fold into the hydrophobic pocket created by the polyphosphonium backbone. TEM analysis of particles formed from BCP with the terminal RAFT group removed did not show a difference in morphological properties (see Figure B-19).

The effect of the anion on the aqueous self-assembly was explored by measuring the size distributions of the particles that formed during nanoprecipitation. The diameter distributions were measured by DLS. Table 3-3 lists the mean z-average diameters and polydispersity indices (PDIs) of the different systems determined by the cumulants analysis of the raw DLS data. The nanoprecipitation performed with slow addition of water resulted in the largest particles, as the particles had more time to reach thermodynamic equilibrium. As the water content was slowly increased, the polymers remained dissolved and the core-forming PS block remained partially solvated, allowing

the assemblies to grow larger. Comparing the z-average diameters produced from the different organic solvents also revealed that the particles produced by the DMF system were systematically smaller than the particles produced by the same polymers from the THF systems (Table 3-3). This was likely due to the smaller difference in polarity between water and DMF, which induced kinetic trapping to occur earlier in the process. The low variability (the highest is **PS$_{390}$-*b*-P(3.7-OTf)$_7$** with a standard deviation of 28%) for most of the samples showed that the nanoprecipitation method was highly reproducible for the kinetically trapped particles in terms of the resulting particle size distributions. The low mean PDI values for the samples also indicated that the particles had narrow size distributions, as measured by DLS.

	DMF				THF			
	Kinetic Trapping		Solvent Annealed		Kinetic Trapping		Solvent Annealed	
Counter anion	Slow H_2O addition	Fast addition to H_2O	Slow H_2O addition	Fast addition to H_2O	Slow H_2O addition	Fast addition to H_2O	Slow H_2O addition	Fast addition to H_2O
Chloride	77 ± 1^{b} (0.16 ± 0.01)	$58 \pm 3^{b,c,d}$ (0.25 ± 0.03)	169 ± 31 (0.10 ± 0.04)	$60 \pm 1^{b,c,d}$ (0.18 ± 0.01)	$176 \pm 2^{c,d}$ (0.27 ± 0.16)	$55 \pm 1^{b,c}$ (0.17 ± 0.02)	$503 \pm 74^{b,c,d}$ (0.23 ± 0.05)	$56 \pm 7^{b,c,d}$ (0.17 ± 0.06)
Bromide	$67 \pm 2^{a,c,d}$ (0.19 ± 0.01)	24 ± 1^{a} * (0.13 ± 0.02)	177 ± 21 (0.20 ± 0.04)	$27 \pm 2^{a,d}$ (0.19 ± 0.01)	$163 \pm 8^{a,d}$ (0.06 ± 0.02)	$39 \pm 4^{a,d}$ (0.27 ± 0.05)	$406 \pm 29^{a,c,d}$ (0.11 ± 0.03)	37 ± 1^{a} (0.25 ± 0.02)
Nitrate	$78 \pm 3^{b,d}$ (0.21 ± 0.03)	24 ± 1^{a} * (0.13 ± 0.01)	154 ± 44 (0.14 ± 0.02)	$26 \pm 1^{a,d}$ (0.18 ± 0.03)	$217 \pm 3^{a,d}$ (0.29 ± 0.21)	$38 \pm 2^{a,d}$ (0.31 ± 0.02)	$275 \pm 32^{a,b}$ (0.11 ± 0.06)	33 ± 2^{a} (0.22 ± 0.03)
Triflate	$84 \pm 4^{b,c}$ (0.19 ± 0.02)	23 ± 1^{a} (0.35 ± 0.06)	184 ± 12 (0.22 ± 0.08)	$42 \pm 1^{a,b,c}$ (0.16 ± 0.02)	$137 \pm 2^{a,b,c}$ (0.13 ± 0.03)	$49 \pm 5^{b,c}$ (0.28 ± 0.04)	$225 \pm 3^{a,b}$ (0.06 ± 0.02)	30 ± 1^{a} (0.26 ± 0.03)

Table 3-3. Mean z-average values ± the standard deviation and PDI values (indicated in brackets) measured by DLS in triplicate for the different solvent systems and addition rates. a) significantly different than Cl, b) significantly different than Br, c) significantly different than nitrate, d) significantly different than OTf. *Samples filtered through 0.22 μm filters.

The method of assembly influenced the size distributions of the particles formed (Table 3-3). In all different methods of assembly with the exception of the solvent annealed particles prepared by slow addition of water into the DMF BCP solution, the particle sizes obtained with the different anions were statistically different from one another (Tables B-1 and B-2). Particles formed from **PS_{390}-*b*-P(3.8-Cl)$_7$** were consistently larger than those formed from **PS_{390}-*b*-P(3.8-Br)$_7$** ($p < 0.05$, Table B-2). Given the relatively similar LogP of the chloride and bromide monomers ($LogP_{,3.8\text{-}Cl} = -0.39$, $LogP_{,3.8\text{-}Br} = -0.19$) and the relatively similar anion-cation interaction evidenced by the similar chemical shifts (Figure 3-2), the most relevant difference between the systems was the size of the anion. As Br^- is larger than Cl^-, the relative hydrophilic volume was expected to increase, requiring a greater curvature to pack into the self-assembled particles, thereby favoring smaller particle diameters. The same pattern was also observed between **PS_{390}-*b*-P(3.8-Cl)$_7$** and the remaining BCPs except for the kinetically trapped particles formed by the fast addition water into a THF solution of the BCPs where the particles formed by **PS_{390}-*b*-P(3.8-NO_3)$_7$** were larger than those formed by **PS_{390}-*b*-P(3.8-Cl)$_7$**. This result suggests that overall the size of the anion played an important role in the formation of the particles.

Comparing the particle diameters of **PS_{390}-*b*-P(3.8-Br)$_7$** assemblies with those formed by **PS_{390}-*b*-P(3.8-NO_3)$_7$**, the only instances when the distributions were statistically different were when the particles were formed by slow addition of water into the BCP solution (Table B-1). Given the similar sizes of these two anions[26] the difference in particle size likely arose from their different LogP values. In the particles formed by kinetic trapping, those formed by the **PS_{390}-*b*-P(3.8-Br)$_7$** BCP were smaller than those formed by **PS_{390}-*b*-P(3.8-NO_3)$_7$**. This can be explained by the higher hydrophilicity of the Br^- anion, which would increase the relative hydrophilic volume fraction of the BCP and result in a higher curvature to favour smaller particles.

In the case of particles formed from DMF BCP solutions, **PS_{390}-*b*-P(3.8-Br)$_7$** formed significantly smaller particles than **PS_{390}-*b*-P(3.8-OTf)$_7$** (Table B-2). The opposite was true for the THF systems of these block copolymers, except for the kinetically trapped particles formed by fast addition of water. The lack of consistent patterns may

result from differences in both the sizes and the hydrophilicities of these two anions. The data do not lend themselves to readily discernable patterns.

Particles formed from **PS_{390}-*b*-P(3.8-NO_3)$_7$** were significantly smaller than those formed from **PS_{390}-*b*-P(3.8-OTf)$_7$** when they were prepared kinetically except for slow water addition into a THF solution of the BCP. This is consistent with the lower hydrophobicity of the phosphonium NO_3^- salt, which would increase the relative hydrophilic block fraction for **PS_{390}-*b*-P(3.8-NO_3)$_7$** relative to **PS_{390}-*b*-P(3.8-OTf)$_7$**, leading to higher curvature and consequently smaller assemblies. On the other hand, NO_3^- is smaller than OTf^-, which would be expected to result in larger assemblies due to a decrease in hydrophilic volume fraction, and this was indeed observed when the assemblies were prepared by kinetic trapping following slow addition of water into a THF solution of the BCPs.

Particles formed by the fast addition of both THF and DMF BCP solutions into H_2O, followed by kinetic trapping, had very similar diameters for **PS_{390}-*b*-P(3.8-Br)$_7$**, **PS_{390}-*b*-P(3.8-NO_3)$_7$** and **PS_{390}-*b*-P(3.8-OTf)$_7$**. The fast addition of organic solvent to water with kinetic trapping was expected to result in the most rapid formation of the particles from the fully dissolved polymer chains, as at all points in the mixing of the solvent there was a large excess of water in the system. This shows that the effect of the anion was less important when the particles were formed by kinetic trapping. However, the solvent-annealed particles had greater variabilities in diameter. This is likely due to the greater role the anion played when the particles were allowed to reach a more thermodynamically stable state.

The particle sizes and morphologies were also investigated in the dried state using TEM imaging. Previous work on the self-assembly of low polycation content BCPs revealed the formation of higher-order morphologies such as vesicles or lamellae.[12] However, the present work shows that despite a very low hydrophilic content, the dominant morphologies are micelles and larger solid nanoparticles (NP) (Figure 3-5), (Table 3-4). Micellar morphologies as seen in Figure 3-5b, were present in most of the self-assembled suspensions (Table 3-4). When particles were allowed more time to reach equilibrium during formation, larger solid nanoparticles developed (Figure 3-5C-E). In some cases, very large particles were present, such as for the slow addition of water into a

THF solution of **PS$_{390}$-*b*-P(3.8-NO$_3$)$_7$** as shown in Figure 3-5C. In those cases, there was a clear distinction between the outer region and the inner region of the particles based on their differences in electron density. These particles have been assigned as solid nanoparticles, since they are too large to be true micelles. Interestingly they exhibited a distinct difference in electron density between the inner and outer regions of the particles. Attempts to determine the composition of the outer region of the particles were unsuccessful.

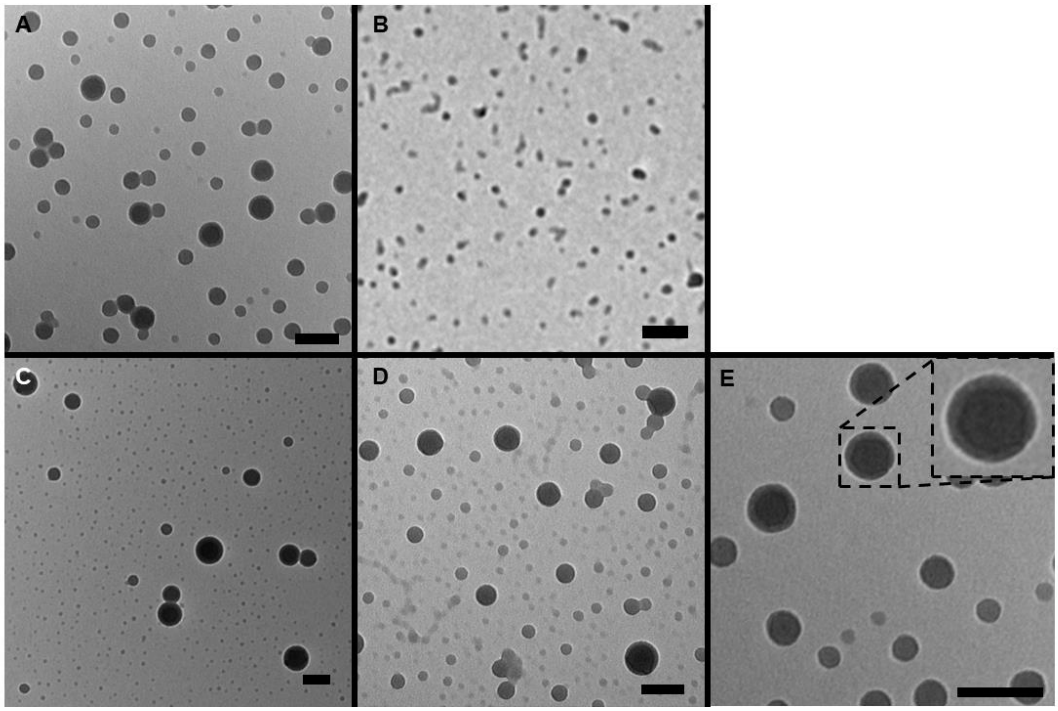

Figure 3-5. TEM images of A) **PS$_{390}$-*b*-P(3.8-Cl)$_7$** particles formed by slow addition of water into DMF; B) **PS$_{390}$-*b*-P(3.8-Br)$_7$** particles formed by fast addition of water into DMF; C) **PS$_{390}$-*b*-P(3.8-NO$_3$)$_7$** particles formed by slow addition of water into THF; D) **PS$_{390}$-*b*-P(3.8-OTf)$_7$** particles formed by fast addition of water into THF E) blow-up of 3-5A to show contrast difference on particles along with expanded view of one of the particle. Scale bars are 100 nm.

	DMF				THF			
	Kinetic Trapping		Solvent Annealed		Kinetic Trapping		Solvent Annealed	
Counter anion	Slow H_2O addition	Fast addition to H_2O	Slow H_2O addition	Fast addition to H_2O	Slow H_2O addition	Fast addition to H_2O	Slow H_2O addition	Fast addition to H_2O
Chloride	M	M	M, NP	M	M, NP	M, NP	M, NP	M
Bromide	M	M	M, NP	M	M, NP	M	M, NP	M
Triflate	M	M	M, NP	M	M, NP	M, NP	M, NP	M
Nitrate	M, NP	M	M, NP	M	M, NP	M	M, NP	M

Table 3-4. Morphology of particles formed by nanoprecipitation as determined by TEM; M = micelles, NP = solid nanoparticles.

The TEM image analysis showed that the diameter distribution of the particles for the fast addition of non-selective solvent into the water agreed best with those determined from DLS (Figure B-20). In general, the diameters measured by TEM were smaller than those measured by DLS. This may have arisen from two key factors: (i) in the solution phase the hydrophilic blocks were hydrated and in extended conformations, whereas in the dry state they collapsed; (ii) in DLS measurements the larger particles scatter light more effectively (scattered light intensity $\propto r^6$), which tends to emphasize a small population of larger particles, thereby increasing the z-average diameter. On the other hand, analysis of TEM images provides a number-based distribution. This is illustrated well in Figure 3-5C where there are two distinct distributions of particles from the slow addition of water into a THF solution of $\mathbf{PS_{390}}$-***b***-$\mathbf{P(3.8\text{-}NO_3)_7}$. As such, the diameters obtained from the TEM image analyses are smaller than those obtained from DLS, and in some cases the relative orders of mean sizes are also different for the different systems. Most importantly, however, is that there was no apparent effect of the anion identity on

the morphology of the particles. As stated earlier, the expectation was that by varying the anion identity, the changes in hydrophilicity and anion size would result in changes in the particle morphology This was not observed (Table 3-4). Instead, change in particle size, rather than morphology, was the dominant effect and ration explanations for the effect of the anion size and hydrophilicity could be made from the available data.

3.3 Summary

This study explored the physical properties of several phosphonium monomers and their relationship to the morphological properties of nano-materials assembled from their copolymers. The monomer salts displayed an interesting relationship in that the degree of interaction between the charges in lipophilic solution provided a good prediction of the LogP values for the salts. The choice of anions provided differences in size as well as hydrophilicity to allow for the investigation of the effects of these properties on the self-assembled particles. The ability to make low *Đ* BCPs from the phosphonium monomer salts and their aqueous self-assembly from dilute solutions in THF and DMF was explored and their self-assembly led to nanoparticles with diameters ranging from 30 nm to > 200 nm, based on DLS and TEM analysis. The anions had reproducible effects on the sizes but not the morphologies of the nanoparticles. The differences between the particle diameters of the **PS_{390}-*b*-P(3.8-Cl)$_7$** and the other anion systems showed that anions of small size resulted in larger particles. In contrast, the relationships between the diameters of assemblies formed from **PS_{390}-*b*-P(3.8-Br)$_7$**, **PS_{390}-*b*-P(3.8-NO_3)$_7$**, and **PS_{390}-*b*-P(3.8-OTf)$_7$** were more complex, arising from different and sometimes competing effects of anion size and hydrophilicity. Even with low phosphonium block volume fractions differences in particle size distribution was observed. This work is important in providing new insights into the effects of counterions on self-assembly of polyelectrolytes. Future work exploring the relationship may consider varying only the anion-cation interaction, or the hydrophilicity of similar sized anions in order to obtain a clearer picture of the relationship between anion identity and assembly size and morphology.

3.4 Experimental Section

General materials and procedures

Solvents were dried using an MBraun Solvent Purification System. Dried acetonitrile was collected under vacuum in a flame-dried Straus flask and stored over 3 Å molecular sieves. Ultrapure water was obtained using a Barnstead EASYPure II ultra pure water system (ThermoFisher Scientific). **3.8-Cl** was prepared according to a published procedure.[27] Nuclear Magnetic Resonance (NMR) spectroscopy was conducted on a Varian INOVA 400 MHz spectrometer (^{1}H 400.09 MHz, ^{31}P{^{1}H} 161.82 MHz, ^{13}C{^{1}H} 100.52 MHz) unless otherwise noted. All ^{1}H NMR chemical shifts are reported relative to $SiMe_4$ (residual solvent in $CDCl_3$; ^{1}H δ = 7.27). The chemical shifts for ^{31}P{^{1}H} NMR spectroscopy are referenced to an external standard (85% H_3PO_4; δ_P = 0). All ^{13}C{^{1}H} NMR chemical shift are reported relative to $SiMe_4$ (residual solvent in $CDCl_3$; δ_C = 77.0). Infrared spectra were recorded using a Bruker Tensor 27 spectrometer using attenuated total internal reflectance mode (ATR) on a ZnSe crystal. Electrospray Ionisation (ESI) Mass spectrometry was obtained on a Finnigan MAT 8400 mass spectrometer using electron impact ionization. Dynamic Light Scattering (DLS) and ζ-potential measurements were performed on a Zetasizer Nano ZS (Malvern Instruments) using a 633 nm laser. Solutions of approximately 0.1 mg/mL of polymer were used in DLS measurements. Ultraviolet-visible (UV-Vis) spectroscopy was performed using a Varian Cary 300 Bio UV-Visible spectrophotometer. Size exclusion chromatography (SEC) of the MacroRAFT agent was performed on a Viscotek GPC Max VE2001 solvent module (Malvern Instruments Ltd., Malvern, U.K.). Samples were analyzed using the Viscotek VE3580 RI detector operating at 30 °C. The separation technique employed two Agilent Polypore (300 × 7.5 mm) columns connected in series with a Polypore guard column (50 × 7.5 mm; Agilent Technologies). Samples were dissolved in tetrahydrofuran (glass distilled) at a concentration of approximately 5 mg/mL, filtered through 0.22 μm syringe filters, and then injected using a 100 μL loop. The THF eluent was filtered and eluted at 1 mL/min for a total of 30 min. The instrument was calibrated with PS standards. Dispersities (*Đ*) are listed to two decimal places, and the degree of polymerization (DP) for the styrene polymer was determined by SEC. The SEC of the BCPs was performed on a Malvern VISCOTEK GPCmax instrument equipped with a VISCOTEK VE 3580 RI

detector and two Inert series columns (P101609 and Q10183) at a constant temperature of 50 °C. The eluent was 0.4 M tetrabutylammonium triflate in DMF with a flow rate of 1 mL/min. Calibration was performed using narrow PMMA standards. TEM images were obtained using a Philips CM 10 Transmission Electron Microscope. Self-assembled samples were loaded onto Formvar coated copper grids by holding the grid with self-closing tweezers, placing a 5.0 μL drop of a 0.5 – 1.0 mg/mL solution onto the grid, and wicking away the excess after 1 min. Dialysis was performed using Spectra/Por® 6 pre-wetted dialysis tubing (Spectrum Laboratories Inc.).

Synthesis of 4-vinylbenzyl bromide, ***3.7***

To a stirring suspension of anhydrous lithium bromide (6.00 g, 69.1 mmol) in 15 mL of anhydrous THF, 4-vinylbenzyl chloride (6.00 mL, 38.3 mmol) was added in a N_2-filled glovebox. The suspension was stirred overnight at room temperature. The following day the solvent was removed under vacuum and the mixture was suspended in 30 mL dry CH_2Cl_2 and filtered. The filtrate was washed three times with water (20 mL). The organic layer was dried with $MgSO_4$ and the volatiles were removed under vacuum to yield a light-yellow oil. The product was used without further purification (5.80 g, 78% yield); ^{1}H NMR (400 MHz, $CDCl_3$): δ = 7.37 (m, *Ar*H, 4H); 6.70 (dd, ^{3}J(H,H) = 11.2 Hz, ^{3}J(H,H) = 17.6 Hz, =*C*H, 1H); 5.77 (d, ^{3}J(H,H) = 17.6 Hz, *trans*, 1H); 5.28 (d, ^{3}J(H,H) = 11.2 Hz, *cis*-, 1H); 4.57 (s, *C*H_2 *on 4-vinylbenzyl chloride*); 4.48 (s, *C*H_2, 2H).

Synthesis of tributyl-(4-vinylbenzyl)phosphonium bromide, ***3.8-Br***

To a stirring solution of 4-vinylbenzyl bromide (2.00 g, 10.1 mmol) in 10 mL of anhydrous CH_3CN in a pressure flask in a N_2-filled glovebox, tributyl phosphine (1.70 g, 8.4 mmol) was added dropwise. The reaction mixture warmed with the addition of the phosphine. The flask was capped and stirred at room temperature. After one hour, the ^{31}P-NMR showed the conversion of the phosphine to a single product. The volatiles were removed under vacuum. The resulting oil was dissolved in minimum CH_2Cl_2 and the product was precipitated out of solution in excess, cold stirring hexanes. The light orange powder was collected by vacuum filtration. (2.83g, 84% yield) ^{1}H NMR (400 MHz, $CDCl_3$): δ = 7.39 (s, Ar*H*, 4H); 6.67 (dd, ^{3}J(H,H) = 17.6 Hz, ^{3}J(H,H) = 11.2 Hz, CH_2=C*H*,

1H); 5.76 (d, ^{3}J(H,H) = 17.6 Hz, *cis*- alkene, 1H); 5.29 (d, ^{3}J(H,H) = 10.8 Hz, *trans*-alkene, 1H); 4.26 (d, ^{3}J(H,P) = 15.2 Hz, PC*H*$_2$C$_q$, 2H); 2.40 (m, PC*H*$_2$, 6H); 1.47 (m, C*H*$_2$, 12H); 0.92 (t, ^{3}J(H,H) = 6.6 Hz, C*H*$_3$, 9H). ^{13}C{^{1}H} (100.52 MHz, $CDCl_3$): δ = 137 (s, 3° alkene, 1C); 135 (d, ^{5}J(C,P) = 2 Hz, 4° aromatic, 1C); 130 (d, ^{3}J(C,P) = 5 Hz, 3° aromatic, 2C); 127 (d, ^{2}J(C,P) = 8.8 Hz, 4° aromatic, 1C); 127 (s, 3° aromatic, 2C); 114 (s, H_2C=, 1C); 27 (d, ^{1}J(C,P) = 45 Hz, CH_2P, 1C); 24 (d, ^{1}J(C,P) = 15 Hz, CH_2P, 3C); 23 (d, ^{2}J(C,P) = 4 Hz, CH_2, 3C); 18 (d, ^{3}J(C,P) = 46 Hz, CH_2, 3C); 13 (s, CH_3, 3C). ^{31}P{^{1}H} NMR (161.82 MHz, $CDCl_3$): δ = 31.8. ATR-IR: 1630 cm^{-1} (w, C=C-H); 2870 cm^{-1} (s, alkane C-H); 2920 cm^{-1} (m, aryl C-H); 2960 cm^{-1} (s, alkenyl C-H).

Synthesis of tributyl-(4-vinylbenzyl)phosphonium nitrate, ***3.8-NO$_3$***

To a rapidly stirring aqueous solution of tributyl-(4-vinylbenzyl)phosphonium chloride in 4 mL of water (2.00 g, 5.6 mmol) an aqueous solution of silver nitrate in 4 mL of water (1.00 g, 5.8 mmol) was slowly added. A white precipitate formed upon mixing and the solution was stirred for 1 hour. The suspension was filtered and a drop of aqueous silver nitrate solution was added. If a white precipitate formed, the process was repeated until no further precipitate formed.[29] Upon complete reaction of the chloride monomer, the aqueous phase was extracted ten times with 15 mL of CH_2Cl_2. The organic phases were combined, dried with $MgSO_4$, filtered, and the volatiles were removed in vacuo to yield a clear colourless oil which cooled to a waxy solid. (1.87 g, 88% yield). ^{1}H NMR (400 MHz, $CDCl_3$): δ = 7.39 (d, ^{3}J(H,H) = 8.0 Hz, 2H); 7.27 (dd, ^{3}J(H,H) = 8.6 Hz, ^{4}J(H,P) = 3.0 Hz, 2H); 6.68 (dd, ^{3}J(H,H) = 17.6 Hz, ^{3}J(H,H) = 11.2 Hz, CH_2=C*H*, 1H); 5.76 (d, ^{3}J(H,H) = 17.6 Hz, *cis*- alkene, 1H); 5.30 (d, ^{3}J(H,H) = 10.8 Hz, *trans*- alkene, 1H); 3.93 (d, ^{3}J(H,P) = 14.8 Hz, PC*H*$_2$C$_q$, 2H); 2.23 (m, PC*H*$_2$, 6H); 1.45 (m, C*H*$_2$, 12H); 0.92 (t, ^{3}J(H,H) = 6.8 Hz, C*H*$_3$, 9H). ^{13}C{^{1}H} (100.52 MHz, $CDCl_3$): δ = 138 (d, ^{6}J(C,P) = 3.9 Hz, 2° alkene, 1C); 135 (d, ^{5}J(C,P) = 1.9 Hz, 4° aromatic, 1C); 129 (d, ^{3}J(C,P) = 5.0 Hz, 3° aromatic, 2C); 127 (d, ^{2}J(C,P) = 8.8 Hz, 4° aromatic, 1C); 126 (d, ^{4}J(C,P) = 3.3 Hz, 3° aromatic, 2C); 113 (d, ^{7}J(C,P) = 1.5 Hz, 1° alkene, 1C); 25 (d, ^{1}J(C,P) = 45.1 Hz, PCH_2, 1C); 23 (d, ^{1}J(C,P) = 15.7 Hz, PCH_2, 3C); 22 (d, ^{2}J(C,P) = 4.7 Hz, CH_2, 3C); 17 (d, ^{3}J(C,P) = 47.3 Hz, CH_2, 3C); 12 (s, CH_3, 3C). ^{31}P{^{1}H} NMR (161.82 MHz, $CDCl_3$): δ =

31.8. ATR-IR: 1330 cm^{-1} (s, N-O); 1600 cm^{-1} (w, C=C-H); 2870 cm^{-1} (s, alkane C-H); 2935 cm^{-1} (m, aryl C-H); 2955 cm^{-1} (s, alkenyl C-H).

Synthesis of tributyl-(4-vinylbenzyl)phosphonium triflate, ***3.8-OTf***

To a rapidly stirring solution of tributyl-(4-vinylbenzyl)phosphonium chloride (2.50 g, 7.0 mmol) in CH_2Cl_2, a solution of lithium triflate in CH_2Cl_2 (2.18 g, in 5 mL) was added. A white precipitate formed upon mixing and the solution was stirred overnight. The suspension was filtered and a drop of lithium triflate solution in CH_2Cl_2 was added. If a white precipitate formed the process was repeated until no further precipitate formed. Upon complete reaction of the chloride monomer, the organic phase was washed three times with water (20 mL), dried over $MgSO_4$, filtered, and the volatiles were removed in vacuo. The product was a white powder. (3.03 g, 92% yield). ^{1}H NMR (400 MHz, $CDCl_3$): δ = 7.36 (d, ^{3}J(H,H) = 8.0 Hz, 2H); 7.25 (dd, ^{3}J(H,H) = 8.2 Hz, ^{4}J(H,P) = 2.2 Hz, 2H); 6.66 (dd, ^{3}J(H,H) = 17.8 Hz, ^{3}J(H,H) = 11.0 Hz, CH_2=C*H*, 1H); 5.74 (d, ^{3}J(H,H) = 17.6 Hz, *cis*- alkene, 1H); 5.29 (d, ^{3}J(H,H) = 11.2 Hz, *trans*- alkene, 1H); 3.78 (d, ^{3}J(H,P) = 15.2 Hz, PC*H*$_2$C$_q$, 2H); 2.15 (m, PC*H*$_2$, 6H); 1.14 (m, C*H*$_2$, 12H); 0.90 (m, C*H*$_3$, 9H). ^{13}C{^{1}H} (100.52 MHz, $CDCl_3$): δ = 137 (d, ^{6}J(C,P) = 4 Hz, 2° alkene, 1C); 135 (d, ^{5}J(C,P) = 2 Hz, 4° aromatic, 1C); 130 (d, ^{3}J(C,P) = 5 Hz, 3° aromatic, 2C); 127 (d, ^{2}J(C,P) = 9 Hz, 4° aromatic, 1C); 127 (d, ^{4}J(C,P) = 3 Hz, 3° aromatic, 2C); 120 (q, ^{1}J(C,F) = 320 Hz, F_3CSO_3, 1C); 115 (s, H_2C=, 1C); 26 (d, ^{1}J(C,P) = 45 Hz, CH_2P, 1C); 23 (d, ^{1}J(C,P) = 15 Hz, CH_2P, 3C); 23 (d, ^{2}J(C,P) = 5 Hz, CH_2, 3C); 18 (d, ^{3}J(C,P) = 47 Hz, CH_2, 3C); 13 (s, CH_3, 3C). ^{31}P{^{1}H} NMR (161.82 MHz, $CDCl_3$): δ = 32.3. ATR-IR: 635 cm^{-1} (s, S-O); 1030 cm^{-1} (s, S-O); 1160 cm^{-1} (m, CF_3); 1225 cm^{-1} (m, CF_3); 1270 cm^{-1} (s, SO_3); 1625 cm^{-1} (w, C=C-H); 2875 cm^{-1} (s, alkane C-H); 2935 cm^{-1} (m, aryl C-H); 2955 cm^{-1} (s, alkenyl C-H).

Synthesis of the polystyrene macro-RAFT agent

The synthesis of the dodecyl-(4-trifluoromethylbenzyl)trithiocarbonyl RAFT agent followed a previously reported procedure with the following differences.[27] After quenching the reaction, the reaction mixture was poured into rapidly stirring excess methanol and a light-yellow precipitate formed. The precipitate was collected as a light

yellow powder but contained large amounts of styrene monomer. The polymer was re-dissolved in CH_2Cl_2 and precipitated in excess stirring methanol. This process was repeated until the complete removal of styrene monomer was achieved as determined by the absence of the monomer signals in the ^{1}H-NMR spectrum of the macro-RAFT agent. The product was a light yellow powder. (9.4 g, 96% yield). ^{1}H NMR (400 MHz, $CDCl_3$): δ = 7.09 (m, 3H, *para*- and *meta*- aryl); 6.50 (m, 2H, *ortho*- aryl); 2.30 – 1.30 (m, 3H, alkyl). DP = 390, $Đ$ = 1.14, M_w = 40,500 g/mol

General synthetic procedure of macro-RAFT polymerization of phosphonium copolymers

The macro-RAFT agent (1.00 g, 25 μmol) and **3.8-Cl** as an example (110 mg, 308 μmol) were dissolved in (10 mL) of degassed THF (3 × freeze-pump-thaw). Sonication was used to ensure the macro-RAFT agent and monomer were fully dissolved. AIBN (1.4 mg, 8 μmol) was added to the reaction mixture and the solution was purged with N_2 at room temperature for five minutes with stirring. After purging, the flask was placed in an 80 °C oil bath for 20 hours. The flask was removed from the oil bath and placed in liquid nitrogen for one minute. The product was obtained by precipitating the copolymer in isopropanol and unreacted monomer was removed by washing with isopropanol. The product was an off-white powder.

PS$_{390}$*-b-*P(3.8-Cl)$_7$ (958 mg, 90.4 % yield). ^{1}H NMR (400 MHz, $CDCl_3$): δ = 7.2 – 7.0 (m, aryl *ortho*- and *para*- to backbone); 6.9 – 6.3 (m, 794H, aryl *meta*- to backbone); 2.43 (m, benzylic, *α* to P); 2.21 (m, methylene *α* to P); 2.18 – 1.30 (m, 1275H, alkyl not otherwise assigned); 0.91 (m, 61H, CH_3). ^{31}P{^{1}H} NMR (161.82 MHz, $CDCl_3$): δ = 31.8. $Đ$ = 1.36, M_n (by SEC) = 31,500 g/mol, M_n (by ^{1}H-NMR) = 37,060 g/mol

PS$_{390}$*-b-*P(3.8-Br)$_7$ (968 mg, 91.2 % yield). ^{1}H NMR (400 MHz, $CDCl_3$): δ = 7.1 – 6.9 (m, aryl *ortho*- and *para*- to backbone); 6.8 – 6.2 (m, 794H, aryl *meta*- to backbone); 2.44 (m, methylene *α* to P); 2.2 – 1.3 (m, 1275H, alkyl not otherwise assigned); 0.94 (m, 61H, CH_3). ^{31}P{^{1}H} NMR (161.82 MHz, $CDCl_3$): δ = 31.5. M_n (by ^{1}H-NMR) = 37,700 g/mol

PS$_{390}$*-b-*P(3.8-NO$_3$)$_7$ (852 mg, 86.7 % yield). ^{1}H NMR (400 MHz, $CDCl_3$): δ = 7.2 – 6.9 (m, aryl *ortho*- and *para*- to backbone); 6.8 – 6.2 (m, 794H, aryl *meta*- to backbone); 2.27 (m, methylene *α* to P); 2.2 – 1.3 (m, 1275H, alkyl not otherwise assigned); 0.92 (m, 61H, CH_3). ^{31}P{^{1}H} NMR (161.82 MHz, $CDCl_3$): δ = 31.9. $Đ$ = 1.4, M_n (by SEC) = 35,300 g/mol, M_n (by ^{1}H-NMR) = 37,600 g/mol

PS$_{390}$*-b-*P(3.8-OTf)$_7$ (862 mg, 88.6 % yield). ^{1}H NMR (400 MHz, $CDCl_3$): δ = 7.1 – 6.9 (m, aryl *ortho*- and *para*- to backbone); 6.8 – 6.2 (m, 794H, aryl *meta*- to backbone); 2.15 (m, methylene *α* to P); 2.1 – 1.3 (m, 1275H, alkyl not otherwise assigned); 0.89 (m, 61H, CH_3). $^{31}P\{^1H\}$ NMR (161.82 MHz, $CDCl_3$): δ = 31.4. ^{19}F NMR (376.50 MHz, $CDCl_3$): δ = -62.5 (s, 3F, RAFT end-group); -78.4 (s, 21F, triflate). *Đ* = 1.4, M_n (by SEC) = 36,500 g/mol, M_n (by ^{1}H-NMR) = 38,200 g/mol

Kinetically trapped self-assembly of phosphonium BCPs

PS-*b*-P(PX) (2.5 mg) was dissolved in 0.5 mg of DMF or THF as non-selective solvents. For the organic-into-water addition, the BCP solution was quickly added to rapidly stirring ultra-pure water (2.0 mL). For the water-into-organic addition, the ultra-pure water (2.0 mL) was added stirred BCP solution slowly over ten minutes. In the case of THF as the non-selective solvent, the suspension was placed in a 35°C sand bath overnight to evaporate the THF. In the case of DMF as the non-selective solvent, the suspension was transferred to a 10 kg/mol molecular weight cut-off dialysis membrane (Spectra/Por® 6 Standard RC Pre-wetted dialysis tubing, 28 mm flat width) and dialyzed against 100 mL of ultra-pure water with one replacement of the dialysate over a 14 hour period.

Solvent annealed self-assembly of phosphonium BCPs

PS-*b*-P(PX) (2.5 mg) was dissolved in 0.5 mg of DMF or THF as non-selective solvents. For the organic-into-water addition, the BCP solution was quickly added to rapidly stirring ultra-pure water (2.0 mL). For the water-into-organic addition, the ultra-pure water (2.0 mL) was added to a stirring BCP solution slowly over ten minutes. The resulting suspensions were allowed to anneal at room temperature for 96 hours. 100 μL of the annealed suspension was added into 1900 μL of ultra-pure water to quench the annealing and give a final concentration of 0.5 mg/mL of BCP and a 1% solution of the non-selective solvent.

Determination of CAC

Note that only the fast water addition to THF systems were used. The assemblies were prepared as stated above except approximately 5 mg of copolymer was used. The resulting suspension was diluted by two-fold steps, 10 times. The dilutions were added into vials containing nile red dye, introduced by the evaporation of 100 μL of a 6.03 μM CH_2Cl_2 solution. The nile red solution was prepared by dissolution of 1.92 mg in 10.0 mL of CH_2Cl_2. The vials were agitated overnight on a wrist action shaker and the following day the fluorescence of the diluted suspensions was measured. The fluorescence intensity was plotted against the log of the concentration of the samples and the CAC was taken as the concentration at the point of intersection of the two lines generated from the two regions of slope on the plot.

Determination of LogP

The partition of the **3.8-X** salts between 1-octanol and ultrapure water was determined spectroscopically with ^{31}P NMR and in triplicate. The 1-octanol was washed three times with a 1M NaOH solution and dried over $MgSO_4$ before use. A ^{31}P NMR standard of Ph_3P was made by dissolving 179 mg of Ph_3P into 5.00 mL of 1-octanol. The **3.8-Cl** and **3.8-Br** salts were dissolved in ultra pure water to give a concentration of 10.0 mg/mL. Due to the low water solubility of **3.8-NO_3** and **3.8-OTf**, they were dissolved in 1-octanol at a concentration of 10.0 mg/mL. In a centrifuge tube, 1 mL of the stock **3.8-X** solution was added to 1 mL of the opposing solvent. These were gently stirred on a wrist action shaker at room temperature for 16 hours. The samples were then centrifuged the following morning and 500 μL of the 1-octanol phase was added to 300 μL of the Ph_3P standard solution and 200 μL of 1-octanol. The relative integration of the **3.8-X** ^{31}P NMR signal to the Ph_3P ^{31}P NMR signal was used to determine the concentration of **3.8-X** in the octanol phase. The octanol-water partition coefficient (LogP) is determined with the following equation:

$$LogP = Log([solute]_{OctOH}) - Log([solute]_{H2O}) \qquad \text{Equation 3.1}$$

3.5 References

1 G. Chen, I. Roy, C. Yang, P. N. Prasad, *Chem. Rev.*, 2016, **116**, 2826–2885.

2 S. Mura, J. Nicolas, P. Couvreur, *Nat. Mater.*, 2013, **12**, 991–1003.

3 N. Kamaly, B. Yameen, J. Wu, O. Farokhzad. *Chem. Rev.*, 2016, **116**, 2602-2663

4 R. Duncan, *Nat. Rev. Drug Discov.*, 2003, **2**, 347–360.

5 M. Elsabahy, G. S. Heo, S. Lim, G. Sun, K. L. Wooley, *Chem. Rev.*, 2015, **115**, 10967–11011.

6 A. B. Chinen, C. M. Guan, J. R. Ferrer, S. N. Barnaby, T. J. Merkel, C. A. Mirkin, *Chem. Rev.*, 2015, **115**, 10530–10574.

7 J. Lu, J. Dimroth, M. Weck, *J. Am. Chem. Soc.*, 2015, **137**, 12984-12989

8 L. C. Lee, J. Lu, M. Weck, C. W. Jones, *ACS Catal.*, 2016, **6**, 784–787.

9 J. Lu, L. Liang, M. Weck, *J. Mol. Catal. A Chem.*, 2016, **417**, 122–125.

10 Y. Mai, A. Eisenberg, *Chem. Soc. Rev.*, 2012, **41**, 5969–5985.

11 N. S. Cameron, M. K. Corbierre, A. Eisenberg, *Can. J. Chem.*, 1999, **77**, 1311–1326.

12 D. E. Discher, A. Eisenberg, *Science.*, 2002, **5583**, 967-973.

13 R. Nigmatullin, F. Gao, *Macromol. Mater. Eng.*, 2012, **297**, 1038–1074.

14 A. M. Carmona-Ribeiro, L. D. de Melo Carrasco, *Int. J. Mol. Sci*., 2013, **14**, 9906–9946.

15 M. A. Aboudzadeh, M. E. Muñoz, A. Santamaría, R. Marcilla, D. Mecerreyes, *Macromol. Rapid Commun.*, 2012, **33**, 314–318.

16 A. Eisenberg, J. Kim, *Introduction to Ionomers*; John Wiley & Sons, Inc.: New York, 1998.

17 O. V. Borisov, E. B. Zhulina, *Macromolecules*, 2002, **35**, 4472–4480.

18 S. V. Solomatin, T. K. Bronich, T. W. Bargar, A. Eisenberg, V. Kabanov, A. Kabanov, *Langmuir*, 2003, **19**, 8069–8076.

19 S. V. Solomatin, T. K. Bronich, A. Eisenberg, V. Kabanov, A. Kabanov, *Langmuir*, 2004, **20**, 2066–2068.

20 S. Förster, N. Hermsdorf, W. Leube, H. Schnablegger, M. Regenbrecht, S. Akari, P. Lindner, C. Böttcher, *J. Phys. Chem. B*, 1999, **103**, 6657–6668.

21 J. Guo, Y. Zhou, L. Qiu, C. Yuan, F. Yan, *Polym. Chem.*, 2013, **4**, 255-259

22 K. Vijayakrishna, D. Mecerreyes, Y. Gnanou, D. Taton, *Macromolecules*, 2009, **42**, 5167–5174.

23 W. L. Masterton, D. Bolocofsky, T. P. Lee, *J. Phys. Chem.*, 1971, **75**, 2809–2815.

24 D. A. Dougherty, *Science*, 1996, **271**, 163-168

25 P. C. Kearney, L. S. Mizoue, R. A. Kumpf, J. E. Forman, A. McCurdy, D. A. Dougherty, *J. Am. Chem. Soc.*, 1993, **115**, 9907-9919

26 G. Moad, E. Rizzardo, S. H. Thang, *Polymer*, 2008, **49**, 1079-1131

27 M. Hadadpour, J. Gwyther, I. Manners, P. J. Ragogna, *Chem. Mater.*, 2015, **27**, 3430–3440.

28 T. J. Cuthbert, T. D. Harrison, P. J. Ragogna, E. R. Gillies, *J Mater. Chem. B*, 2016, **4**, 4872–4883.

29 J. J. Tindale, K. D. Hartlen, A. Alizadeh, M. S. Workentin, P. J. Ragogna, *Chem. Eur. J.*, 2010, **16**, 9068–9075.

Chapter 4

Two of a Kind. Incorporating Phosphines and Phosphonium Salts into a Single Amphiphilic BCP

4.1 Introduction

Properties of polymeric materials have been improved from the incorporation of inorganic elements into the monomer side chains and polymer backbone. Well-known examples include the highly conductive polythiophenes and related materials, ferrocene-containing polymers and polysiloxanes.[1-4] The incorporation of phosphorus has also had a considerable impact on the structural and chemical properties of polymers in recent years. Synthetic polymers containing phosphorus demonstrate improved functionality. Examples include dental resins that have made use phosphorus to bind to tooth enamel,[5] anticorrosion coatings for metals,[6] bone adhesives,[7] anti-fouling surfaces with phosphorylcholines,[8] and antibacterial phosphonium-containing polymers.[9] Most materials with phosphorus in either the backbone or on pendant groups of the polymer utilize phosphorus in the +5 oxidation state. While the material properties are enhanced from the incorporation of the P(V) atoms, the P(V) is unable to undergo chemical transformations.

Amphiphilic BCPs are copolymers which are composed of polymer blocks of different solubilities. These materials undergo self-assembly in the bulk, thin film and solution phases. The material properties of amphiphilic BCPs have also been positively impacted through the incorporation of phosphorus compounds such as phosphates[10-13] and phosphonium salts.[14-16] Amphiphilic BCPs incorporating phosphines have also been prepared by various groups. The incorporation of phosphines into BCPs is desirable due to the ability of phosphines to act as ligands, and the numerous transformations they can undergo.

An advantage of incorporating phosphorus into amphiphilic copolymers is the presence of the phosphorus in the resulting self-assembled materials. This introduces the functionality of the phosphorus into the primary structure and enables new chemistries and material properties to be explored. To introduce phosphine functionalities into

amphiphilic block copolymers, several research groups have made use of the 4-(diphenylphosphino) styrene (DPPS) monomer (Figure 4-1). In 2017, the Stones research group detailed the synthesis of an amphiphilic pegylated poly(ionic liquid)-*b*-polyphosphine BCP (**4.3** in Figure 4-1).[17] The copolymer was able to support palladium nanoparticles suspended in the aqueous phase through interaction of the phosphine block with the surface of the Pd nanoparticles. The authors also demonstrated the highly active and selective hydrogenation of α,β-unsaturated aldehydes. The Long group has also incorporated the DPPS monomer into amphiphilic copolymers. In a 2016 communication, they demonstrated the controlled living anionic polymerization of the DPPS as one block with the addition of styrene or isoprene (**4.1** and **4.2** in Figure 4-1).[18] The authors quaternized the phosphine and performed bulk self-assembly of the materials to investigate the different quaternizing agents. In related work, the same group synthesized polystyrene-*b*-polyisoprene-*b*-polyphosphine copolymers (**4.5** in Figure 4-1) and investigated the thin film self-assembly and the effects of different block lengths on the mechanical properties.[19]

The Huang group has demonstrated the ability to form a brush copolymer with a poly(methyl acrylate) backbone bearing brushes of poly(lactic acid)-*b*-poly(DPPS-*r*-styrene) (**4.6** in Figure 4-1).[20] In solution the outer poly(DPPS-*r*-styrene) block was hyper-cross-linked and the core etched away leaving a 42 nm long hollow tube of phosphine-rich polymer network. The authors loaded this material with Pd and investigated its use as a catalyst in a Suzuki-Miyaura coupling reaction. Julcour and coworkers synthesized a complex poly(methylacrylate)-*b*-poly(styrene-*r*-DPPS)-*b*-poly(styrene-*r*-methylacrylate) copolymer (**4.4** in Figure 4-1).[21] This material was self-assembled under controlled conditions with cross-linking agents into a variety of nano-materials. The DPPS repeat units allowed the incorporation of ruthenium into the nano-materials and the authors were able to demonstrate the biphasic hydroformylation of 1-octene with their material.

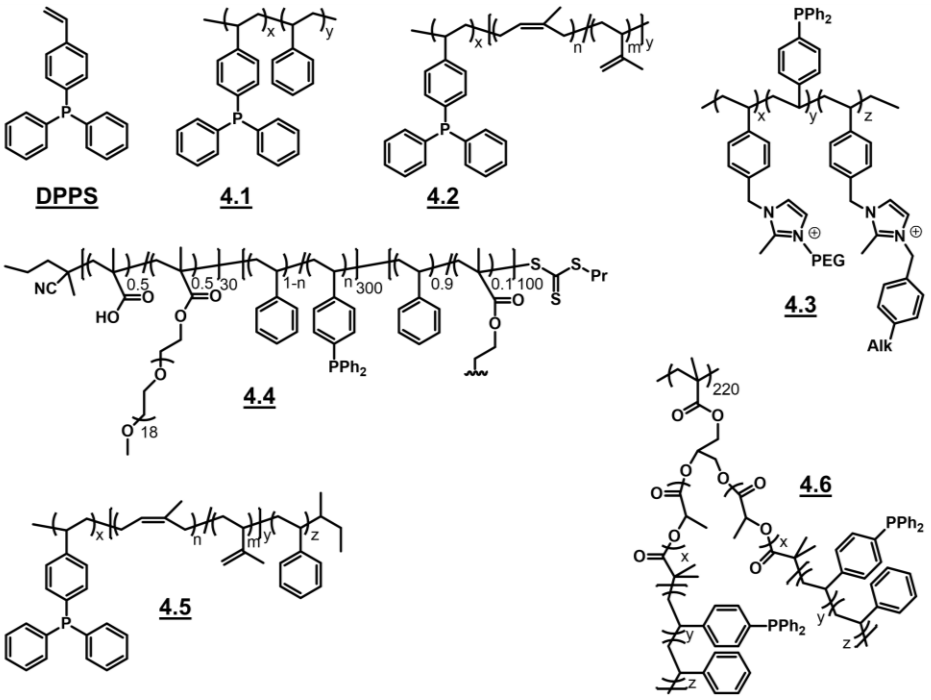

Figure 4-1. DPPS and DPPS containing amphiphilic block copolymers found in the literature.

Phosphonium salts contain a positively charged P(V) central atom, a property that affects the solubility of these compounds, often resulting in hydrophilicity. Despite this, there are a limited number of investigations into the incorporation of phosphonium salts into amphiphilic block copolymers. Investigations that incorporated polyphosphonium salts into the amphiphile structure did not focus on the self-assembly of such polymers.[18,22–24] Long and coworkers reported a poly(phosphonium salt)-*b*-poly(butyl acrylate)-*b*-poly(phosphonium salt) tri-BCP and investigated the self-assembly of the polymer in the thin film state.[25] The same group investigated the ability of a polyacrylate-*b*-poly(phosphonium salt) BCP to complex with plasmid DNA for delivery into cells.[16] Recently the Ragogna and Gillies groups have demonstrated the effect of different anions on the aqueous phase self-assembly of polystyrene-*b*-polyphosphonium block copolymers.[14]

In my efforts to expand the utility of phosphorus-containing polymers and novel functional nano-materials I noted a lack of any amphiphilic BCPs that incorporated phosphorus in more than a single chemical form, such as phosphines and phosphonium salts. In this context, I report here the synthesis of poly[(4-tributylphosphonium chloride)styrene]-*b*-poly[(4-diphenylphosphino)styrene] (P(PCl)-*b*-P(DPP)) by RAFT

polymerization of the commercially available DPPS and the previously reported monomer 4-vinylbenzyltributylphosphonium chloride (Scheme 4-1).[14] The resulting polymer incorporates Lewis basic triarylphosphines in the hydrophobic block and the positively charged phosphonium salts in the hydrophilic block. The ability to use orthogonal chemistries to place different metals onto the hydrophilic and hydrophobic blocks is demonstrated.

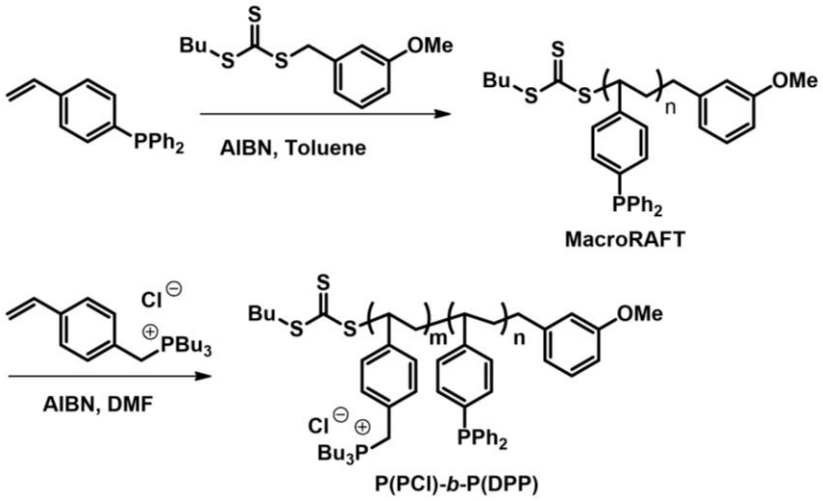

Scheme 4-1. RAFT synthesis of P(PCl)-*b*-P(DPP) using 3-methoxybenzyl butyl trithiocarbonate (RAFT agent) and the phosphine and phosphonium monomers

4.2 Results and Discussion

4.2.1 MacroRAFT Agent Synthesis

RAFT polymerization was utilized to prepare the BCP as this method allowed purification of the first block prior to synthesis of the second block as well as the determination of the DP from spectroscopic analysis of the RAFT agent end-group. Use of a RAFT agent with a methoxy group (Scheme 4-1) provided an NMR spectroscopic handle for the end-group analysis of the polymers (Figure 4-2). Specifically, the methoxy hydrogens have a chemical shift that does not overlap with any signals generated from the polymerized monomers.

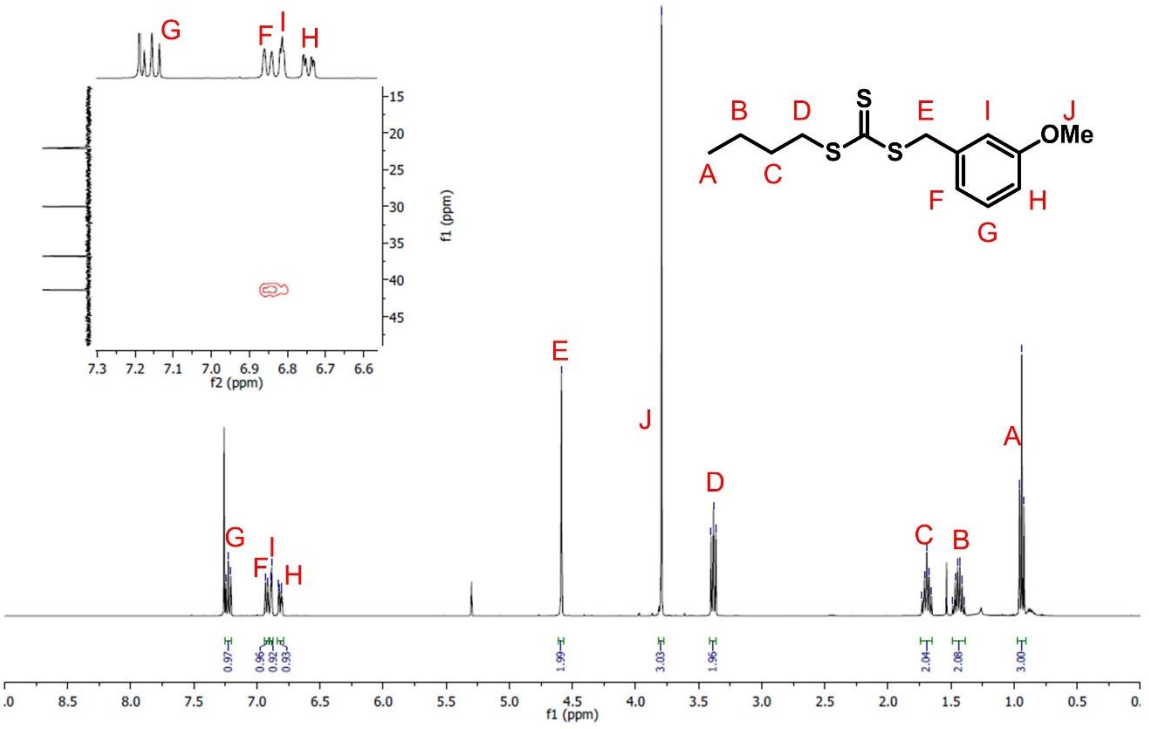

Figure 4-2 ^{1}H NMR ($CDCl_3$, 400 MHz) spectrum of the RAFT agent used in this experiment. The inset shows a region of the Heteronuclear Multiple Bond Correlation NMR spectrum used to assign the identity of the signals labelled F and I based on coupling to the benzylic carbon.

The DP could also be determined based on the monomer conversion from the ^{31}P NMR spectrum after quenching the polymerization, and before removing the monomer. The conversion of the vinyl group into an aliphatic chain alters the electronics at the phosphine to such an extent that baseline resolution is possible between the monomeric and polymeric forms of the DPPS. This allowed for the determination of the conversion by comparing the relative integrations of the two peaks during polymerization. The MacroRAFT agent was synthesized with a DP of 45, an M_n based on ^{1}H NMR spectroscopy of 13,000 g/mol and a *Đ* of 1.4 from SEC. As anticipated, comparison of the integrations of the peaks corresponding to the methoxy protons and the backbone methines allowed for the determination of the DP (45 units by conversion percent from

^{31}P NMR spectroscopy and 46 units by end-group analysis from ^{1}H NMRspectroscopy).

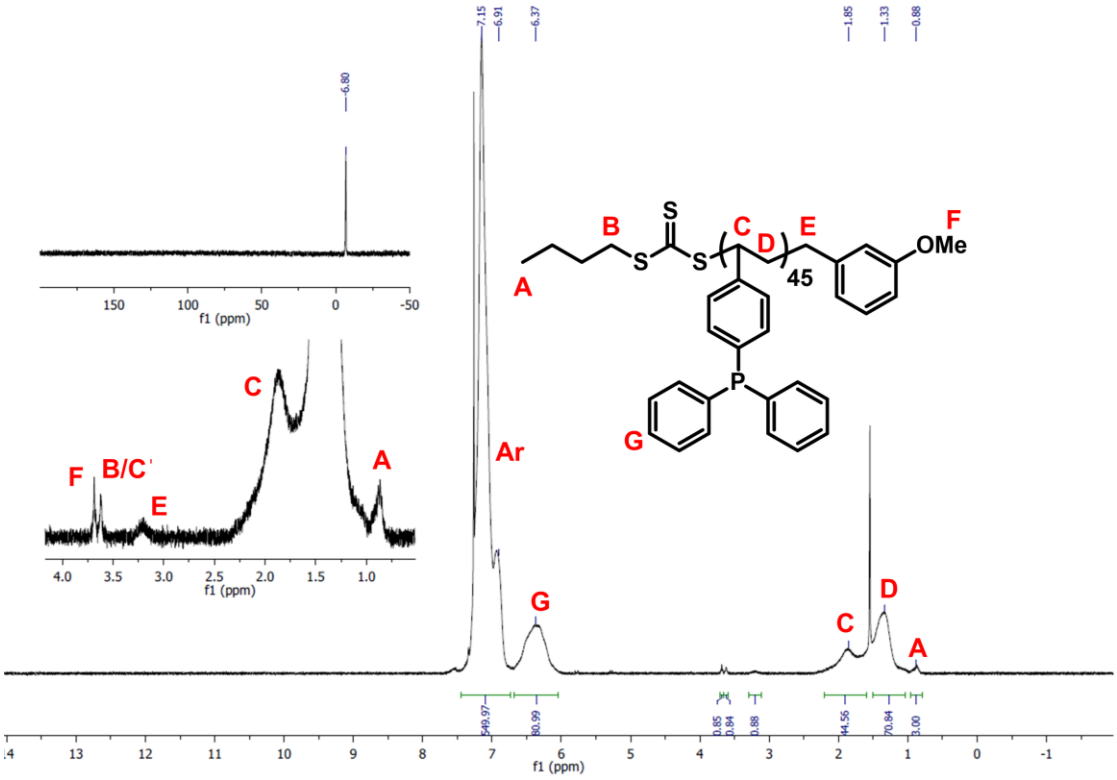

Figure 4-3. ^{1}H NMR ($CDCl_3$, 400 MHz) spectrum of the MacroRAFT agent. Top inset is ^{31}P{^{1}H} NMR spectrum. Bottom inset is a blow-up of the ^{1}H NMR spectrum where C' represents the protons of the methine unit adjacent to the trithiocarbonate group.

It should be noted that following the polymerization, a new peak, labelled C' in Figure 4-3 appeared in the region expected for the methoxy group. The new peak was confirmed to be inherent to the MacroRAFT agent structure, as the RAFT agent was stirred for three days at 80 °C with no radical source, and new peaks were observed similar to those observed in the MacroRAFT agent spectrum. Triphenylphosphine stirred with the RAFT agent and AIBN also showed no new peaks in the same region. This suggests that the signals did not result from a side reaction between the monomer and the RAFT agent. Based on this information, the additional peak at ~3.7 ppm was assigned to the methine proton of the monomer adjacent to the RAFT agent.

4.2.2 BCP Synthesis

The phosphonium block was initially to be composed of the previously reported monomer 4-vinylbenzyltriethylphosphonium chloride. The short alkyl chains provide high hydrophilicity. 4-Vinylbenzyltriethylphosphonium chloride, however, is only slightly soluble in DMF, the best solvent for dissolving both the monomer and MacroRAFT agent. Additionally, the poly(4-vinylbenzyltriethylphosphonium chloride) was not DMF-soluble and so the reaction required low monomer concentrations (undesirable) and it was not possible to generate block copolymers of sufficient polyphosphonium block lengths. Therefore, 4-vinylbenzyltributylphosphonium chloride was used instead as it had much better DMF solubility and the polymeric form was also soluble in DMF. This allowed for the controlled polymerization of the butyl monomer as demonstrated by the pseudo-first order kinetics (Figure 4-4).

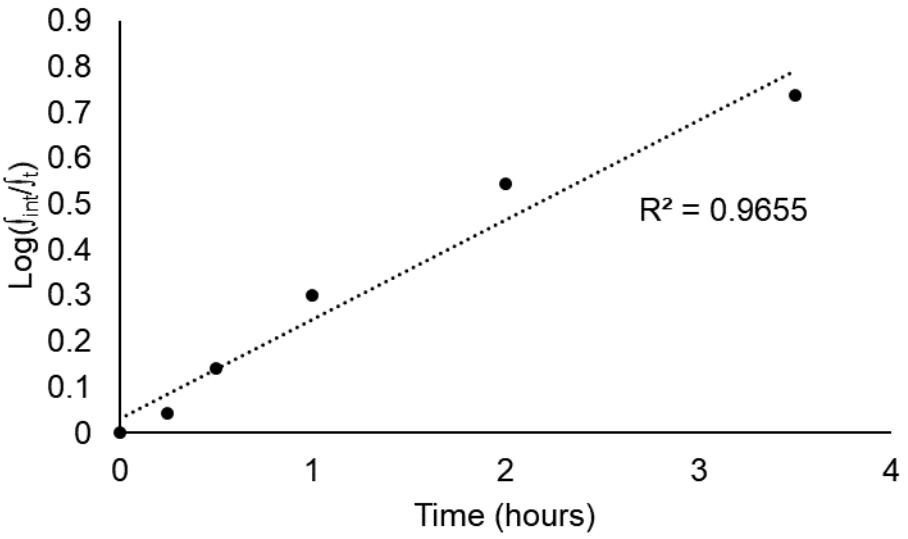

Figure 4-4. Pseudo-first order kinetics of the polymerization of the phosphonium salt monomer by the MacroRAFT agent.

Three different BCPs were prepared with varying lengths of the phosphonium salt block. These different phosphonium block lengths were prepared with the aim to determine if their different relative hydrodynamic volumes have a substantive impact on the sizes and morphologies of the self-assembled particles. We targeted mole fractions of one third, one half, and parity and the resulting polymers were: **P(PCl)$_{15}$-*b*-P(DPP)$_{45}$**, **P(PCl)$_{23}$-*b*-P(DPP)$_{45}$**, and **P(PCl)$_{45}$-*b*-P(DPP)$_{45}$** (Table 4-1). The DPs of the

phosphonium salt blocks were determined by comparing the integrations of the phosphonium methyl peaks with those of the baseline resolved phosphine aryl peaks in the ^{1}H NMR spectra.

Polymer	M_n (g/mol)[a]	DP P(PCl)	T_{onset} (°C)	T_g (°C)
P(DPP)$_{45}$	13,000	N/A	355	112
P(PCl)$_{15}$-*b*-P(DPP)$_{45}$	17,200	15	338	123
P(PCl)$_{23}$-*b*-P(DPP)$_{45}$	21,500	23	339	120, 166†
P(PCl)$_{45}$-*b*-P(DPP)$_{45}$	30,000	45	330	122, 181†

Table 4-1. Physical characterization of the polymers prepared in this chapter. a) M_n determined by H NMR conversion. †) two T_g observed

The SEC data for the **P(PCl)$_{45}$-*b*-P(DPP)$_{45}$** polymer demonstrated only a small change in the retention time of the polymer (Figure 4-5). SEC for the comparison of the BCP and the MacroRAFT agent was performed using a 0.4 M tetrabutylammonium triflate in DMF eluant. The small relative shift of the distribution is likely a result of strong interactions between the phosphine and the column material. This was corroborated by the lower than expected measured M_w values of 12,500 g/mol for the **P(PCl)$_{45}$-*b*-P(DPP)$_{45}$** and 11,000 g/mol for the **P(DPP)$_{45}$**. The *Đ* values were large (2.4 and 2.5, respectively) and likely not accurate, as the MacroRAFT agent *Đ* measured by SEC without the tetrabutylammonium triflate salt was 1.4.

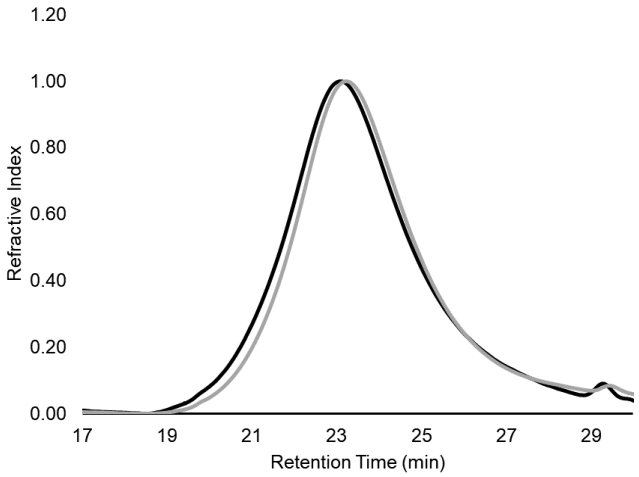

Figure 4-5. SEC data for the P(DPP)$_{45}$ MacroRAFT agent (grey line) and P(PCl)$_{45}$-*b*-P(DPP)$_{45}$ (black line).

The thermal properties of the polymers reflected the relative amount of P(PCl) block in the polymer sample. The T_g of **P(DPP)$_{45}$** was observed at 112 °C. Introduction of the phosphonium block changes the temperature at which the T_g is observed, as demonstrated by **P(PCl)$_{15}$-*b*-P(DPP)$_{45}$**, which displayed a single T_g at 123 °C. Both **P(PCl)$_{23}$-*b*-P(DPP)$_{45}$** and **P(PCl)$_{45}$-*b*-P(DPP)$_{45}$** had two T_g values, a lower one (120 °C and 122 °C, respectively) and a higher T_g (166 °C and 181 °C, respectively). Again, the T_g of the **P(DPP)$_{45}$** was altered by the presence of the phosphonium salt block, as this likely altered the interactions between the polymer chains, affecting the energy required to allow the polymer backbone to move freely. And with sufficient amounts of the phosphonium salt block, a higher T_g was observed, which corresponds to the T_g of the phosphonium salt block.

4.2.3 Self-Assembly of the BCPs

Self-assembly was initially investigated by nano-precipitation of the BCP from a DMF solution into water. All copolymers resulted in small micellar nanoparticles (Figure 4-6). Since the length of the phosphonium block did not appear to affect significantly the morphology of the particles, the **P(PCl)$_{45}$-*b*-P(DPP)$_{45}$** BCP was chosen for further study due to the desirable 1:1 phosphine:phosphonium molar ratio and the potential for greater core coverage to enhance kinetic stability of the micelles.[26] Due to the propensity for such a system to form micelles, the self-assembly was performed using aqueous nano-precipitation by fast addition of a BCP DMF solution into rapidly stirring water. The particles formed this way had a z-average diameter of 26.2 ± 4.7 nm as measured by DLS.

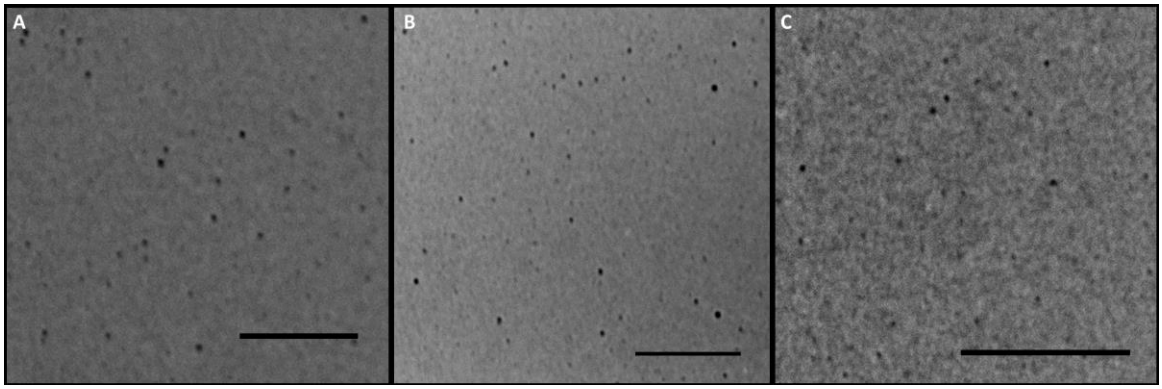

Figure 4-6 A) **P(Ph$_{2P}$ Sty)$_{45}$-*b*-P(Bu$_3$P Sty)$_{15}$** nanoparticles. B) **P(Ph$_{2P}$ Sty)$_{45}$-*b*-P(Bu$_3$P Sty)$_{23}$** nanoparticles. C) **P(Ph$_{2P}$ Sty)$_{45}$-*b*-P(Bu$_3$P Sty)$_{45}$** nanoparticles. Scale bars are 500 nm.

4.2.4 Core Loading with Metals

Several reports have demonstrated the incorporation of metals into the cores of self-assembled nano-particles. There are two main approaches to metal incorporation: 1) pre-stirring the molecularly dissolved BCP with the metal complex containing a labile ligand or 2) stirring solvent-swelled self-assembled nano-particles with the metal complex containing a labile ligand. The second method requires that the metal complex is inert to the solvent used to suspend the nano-particles, which is usually water. The other requirement is that the metal complex is able to diffuse through the corona and into the core of the particles. Since few labile metallic species are soluble in the same solvent as the corona, pre-loading of the core forming block was used in this study.

To install the Mo and W onto the core forming block $Mo(CO)_6$ and $W(CO)_6$ were photolyzed and subsequent stirring of $M(CO)_5(THF)$ with the BCP resulted in the disappearance of the peaks corresponding to the free phosphines in the ^{31}P $\{^1H\}$ NMR spectra which coincided with the appearance of **P(DPP M(CO)$_5$)** peaks. In the case of reaction with $Mo(CO)_5(THF)$ the new chemical shift of the metal coordinated phosphine was at 37 ppm (Figure 4-7B). This new chemical shift was similar to that observed in the reaction between the MacroRAFT agent and photolyzed $Mo(CO)_6$ (Figure 4-7C). When the material was exposed to oxidizing conditions the signal at 37 ppm disappeared and a new signal appeared at 26 ppm. The signal had a similar chemical shift to that observed in the ^{31}P $\{^1H\}$ NMR spectrum of the product from the reaction between the MacroRAFT agent and hydrogen peroxide, which should form the phosphine oxide (Figure 4-7D).

Attachment of tungsten carbonyl to the BCP required the use of a solvent other than acetonitrile as that did not lead to functionalization. THF provided a good solvent for the photolysis of the $W(CO)_6$ and solvated the phosphine block without solvating the phosphonium salt block. Mixing resulted in precipitation of the functionalized polymer from the solution as the $W(CO)_5$(THF) functionalized BCP became insoluble in the THF. Following the removal of the unreacted photolyzed $W(CO)_6$ by centrifugation the resulting material was not soluble. The MacroRAFT agent was able to coordinate $W(CO)_5$ and showed a new chemical shift of the coordinated complex (20 ppm, J(W,P) = 123 ppm).

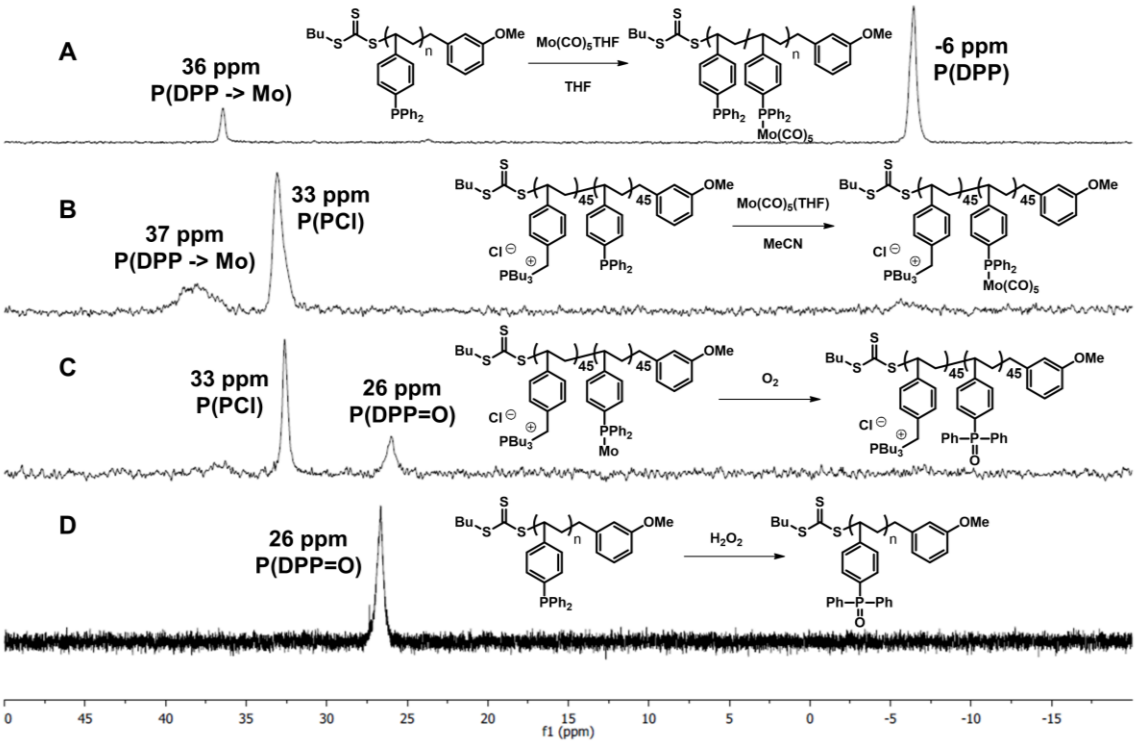

Figure 4-7. ^{31}P {^{1}H} NMR (161.5 MHz) stack A) (THF-H_8) MacroRAFT agent with photolyzed $Mo(CO)_6$, B) (CH_3CN) BCP with photolyzed $Mo(CO)_6$ C) ($CDCl_3$) Product of B after exposure to ambient room conditions D) (THF) MacroRAFT agent after oxidation with H_2O_2.

The BCP coordinated to Pd after stirring of the BCP in an acetonitrile suspension with $(Ph_3P)_2Pd(II)Cl_2$. Interestingly the ^{31}P NMR spectrum of the Pd loaded material showed only the peak corresponding to the phosphonium slat block (Figure 4-8A). The ^{31}P {^{1}H} NMR spectrum of the reaction mixture showed the disappearance of the free

phosphine peak of the BCP and the appearance of free Ph_3P (Figure 4-8B). In Figure 4-8C the new peak from coordination of the phosphine with the $Pd(II)Cl_2$ can be observed as a broad signal at 23-27 ppm. This peak only appeared in systems where there was a low amount of $Pd(II)Cl_2$ bound to the polymer. The two available coordination sites of the Pd allow for phosphine groups from two different polymer chains to bind. This allowed for the cross-linking of the core forming polyphosphine. In Figure 4-8A, only the signal for the polyphosphonium salt is observed, as the phosphine is in the core of the cross-linked nano-particles and is unable to tumble at rates which allow for its detection by NMR spectroscopy. The loading of Pd into the core of the nanoparticles is supported by the dark core observed in the TEM images of the particles (Figure 4-9). Comparing the Pd loaded nanoparticles to the unloaded particles the difference in contrast in the images indicated the loading of the nanoparticles with Pd. This finding is confirmed by EDS data from the same sample showing the concurrence of P with Pd (Figure 4-10). Figure 4-8A and B show that outside of the core of the particle P is present without Pd. Figures 4-8C and D show that in the core of the particles there is a concurrence of P with Pd, demonstrating the loading of the particles.

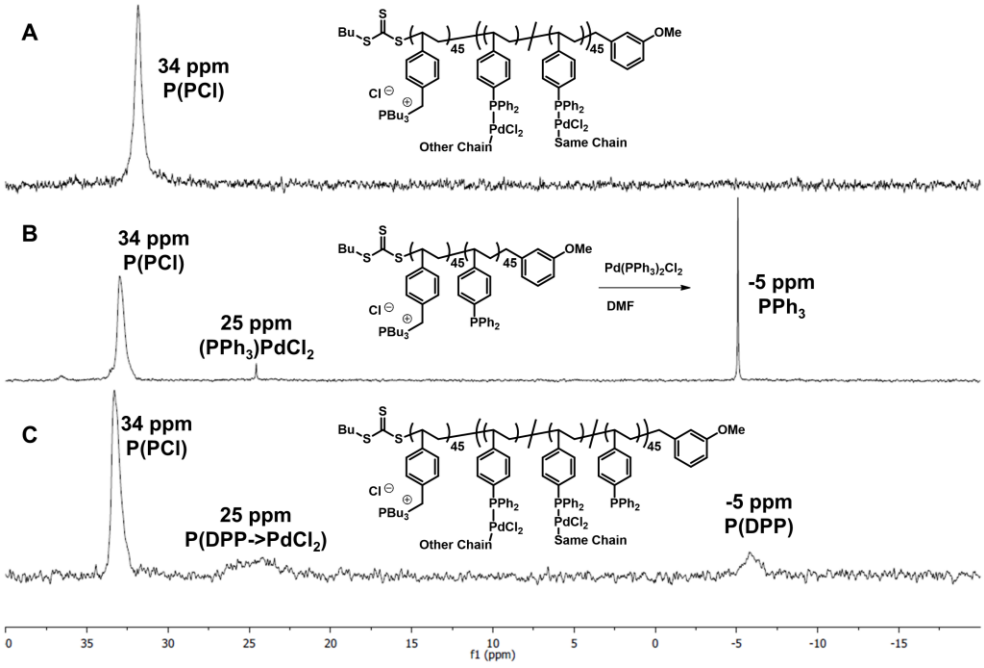

Figure 4-8. ^{31}P $\{^1H\}$ NMR (161.5 MHz) spectra of A) (H_2O) $Pd(II)Cl_2$ loaded nanoparticles B) (DMF-H_6) reaction mixture of BCP with $(Ph_3P)_2Pd(II)Cl_2$, the sharp peaks are the Ph_3P bound to Pd (25 ppm) and free (-5 ppm) C) (DMF-H_6) suspension of BCP functionalized with low amounts of $Pd(II)Cl_2$.

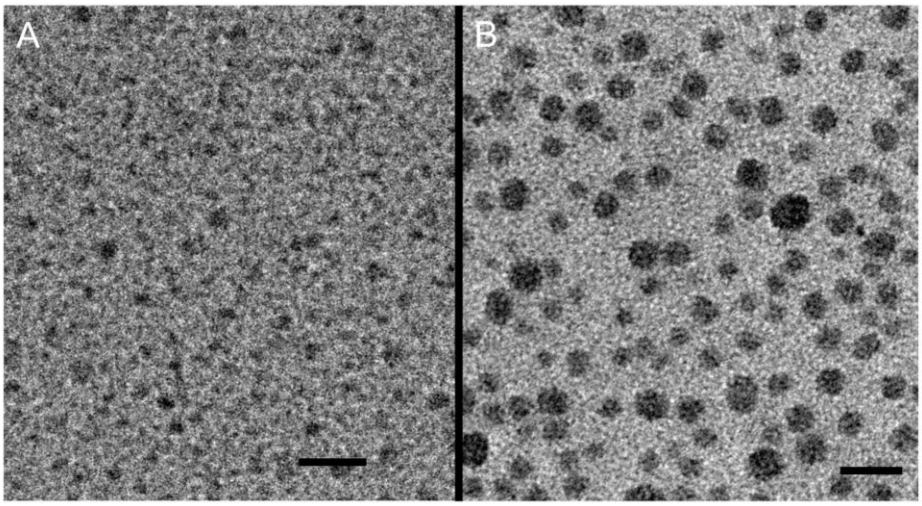

Figure 4-9. TEM image (A) unloaded particles (B) the Pd loaded particles. No stain has been applied. Scale bars are 50 nm.

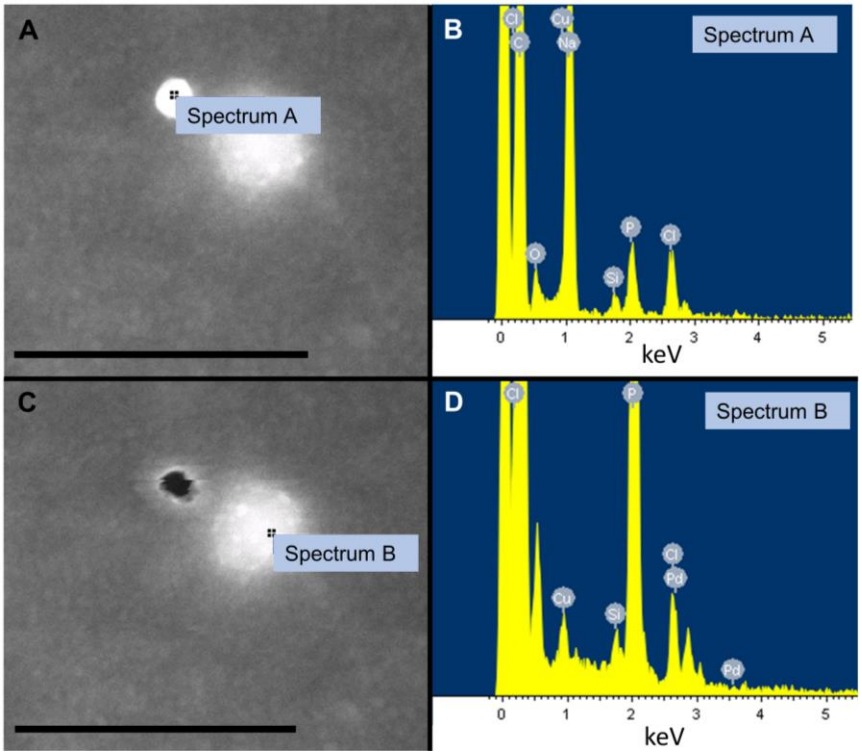

Figure 4-10. A) SEM image of Pd loaded nanoparticles (scale bar 900 nm). B) EDS spectrum at the indicated site in A. C) SEM image of Pd loaded nanoparticles (scale bar 900 nm). D) EDS spectrum at the indicated site in C.

The formation of cross-linked core sections was corroborated by the existence of persistent nanoparticles, as measured by DLS, when the polymer is in DMF (Figure 4-11). The DLS data showed the existence of nanoparticles in a solvent that was able to

dissolve both polymer chains. This demonstrated that the core was cross-linked. The bimodal distribution is likely due to the uncontrolled nature of the core cross-linking enabled by the coordination to Pd.

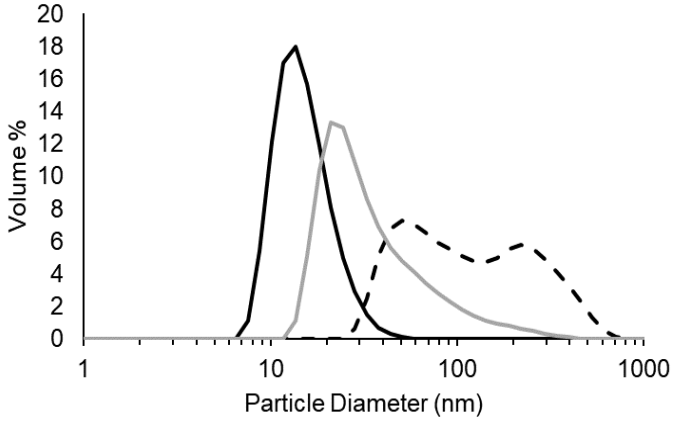

Figure 4-11. DLS volume distribution of the unloaded nanoparticles in aqueous solution (solid line), $AuCl_4$ loaded nanoparticles in aqueous solution (grey line), and the Pd cross-linked BCP in DMF (dashed line)

4.2.5 Corona Loading

Previous work in the Ragogna and Gillies groups demonstrated an association of $AuCl_4^-$ with the corona of phosphonium salt containing nano-particles. Initial attempts to associate $AuCl_4^-$ with the corona of the nano-particles by using an aqueous solution of $HAuCl_4$ as the selective solvent to cause nanoprecipitation resulted instead in the precipitation of the BCP from solution. This is likely due to the increased hydrophobicity of the $AuCl_4^-$ anion compared to that of the Cl^- anion. This suggested that performing anion exchange prior to nano-precipitation would also be likely to result in poor control over self-assembly. To alleviate this undesirable consequence of $AuCl_4^-$ exchange with Cl^-, the particles were formed prior to exchange. After particle formation an aqueous solution of $HAuCl_4$ was added slowly to the particles with rapid stirring. When too great an amount of $HAuCl_4$ was added (excess of 1 molar equivalents to the phosphonium salt repeat units) precipitation of the BCP from solution occured. At equivalents lower than 1, precipitation did not occur, and the DLS data (Figure 4-11) suggested that the particles underwent some morphological changes likely in order to accommodate the $AuCl_4$ anions. However, the change may also be due to a different salt concentration of the solution.

4.2.6 Au Nanoparticle Formation

An odd behaviour was noted for some of the suspensions of self-assembly nanoparticles containing $AuCl_4^-$. Several days following the dialysis of the suspension to remove DMF and excess $HAuCl_4^-$, colour began to appear. The colour formed in the vials was somewhat dependent on the amount of Au added to the coronas, and the UV-vis spectra (Figure 4-11) showed a broad absorption in the visible range. The colour and the broad absorption are characteristic of Au nanoparticles. No precipitation was observed in these solutions and so it would seem that the BCP provided a good environment to stabilize the Au. Previous research has shown that polymeric materials alone are able to reduce $AuCl_4^-$ to Au nanoparticles, particularly for PEO containing systems.[27–32]

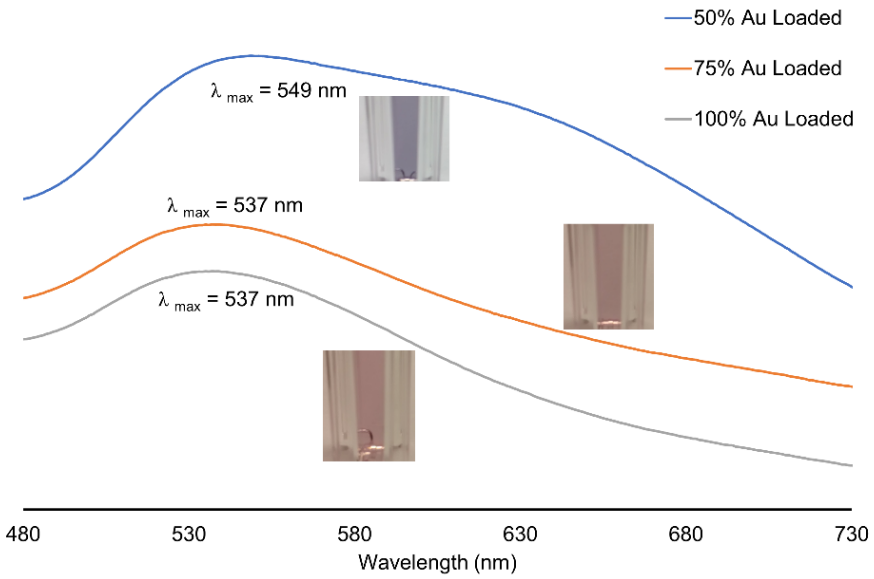

Figure 4-12. Surface plasmon resonance absorbances of Au nanoparticles formed from the reduction of $AuCl_4^-$ in the Au loaded particles after dialysis. The loading percent refers to added molar equivalents.

4.3 Summary

This work has demonstrated the ability to produce a novel phosphorus-containing amphiphilic block copolymer. The copolymer contained phosphorus(III) as a phosphine, and phosphorus(V) as a phosphonium salt. The phosphonium salt block enabled the BCP to undergo self-assembly in solution as well as to associate $AuCl_4^-$ with the corona, and

the phosphine provided a site for the binding of other metals. Pd, Mo and W have been shown to coordinate to the polyphosphine block, and in the case of Pd loaded BCP we have demonstrated the formation of nanoparticles with the loaded metal.

3.4 Experimental

General materials and procedures

Solvents were dried using an MBraun Solvent Purification System. Dried acetonitrile was collected under vacuum in a flame-dried Straus flask and stored over 3 Å molecular sieves. Ultrapure water was obtained using a Barnstead EASYPure II ultra pure water system (ThermoFisher Scientific). Tributyl(4-vinylbenzyl)phosphonium chloride was synthesized according to previous reports from the Ragogna and Gillies groups.[14] Nuclear Magnetic Resonance (NMR) spectroscopy was conducted on a Varian INOVA 400 MHz spectrometer (^{1}H 400.09 MHz, ^{31}P{^{1}H} 161.82 MHz, ^{13}C{^{1}H} 100.52 MHz) unless otherwise noted. All ^{1}H NMR spectra were referenced relative to $SiMe_4$ (residual solvent in $CDCl_3$; ^{1}H δ = 7.27). The chemical shifts for ^{31}P{^{1}H} NMR spectroscopy were referenced using an external standard (85% H_3PO_4; δ_P = 0). All ^{13}C{^{1}H} NMR spectra were referenced relative to $SiMe_4$ (residual solvent in $CDCl_3$; δ_C = 77.0). Infrared spectra were recorded using a Bruker Tensor 27 spectrometer using attenuated total internal reflectance mode (ATR) on a ZnSe crystal. Electrospray Ionisation (ESI) Mass spectrometry was obtained on a Finnigan MAT 8400 mass spectrometer using electron impact ionization. Dynamic Light Scattering (DLS) and ζ-potential measurements were performed on a Zetasizer Nano ZS (Malvern Instruments) using a 633 nm laser. Solutions of approximately 0.1 mg/mL of polymer were used in DLS measurements. Ultraviolet-visible (UV-Vis) spectroscopy was performed using a Varian Cary 300 Bio UV-Visible spectrophotometer. Size exclusion chromatography (SEC) of the MacroRAFT agent was performed on an instrument equipped with a Waters 515 HPLC pump and a Waters In-line Degasser AF. Materials were detected using the Wyatt miniDawn Treos Light Scattering detector and a Wyatt Optilab Rex RI detector operating at 658 nm and 25°C. The method employed two PLgel 5um (300 × 1.5mm) columns connected to a PLgel guard column. Solvent used for separation was DMF 10 mM LiBr and 1% TEA flowing

at 1 ml/min for 30 minute run times at 85°C. Samples were dissolved in the above mobile phase at approximately 5 mg/mL concentrations and filtered through 0.22 µm PTFE syringe filters prior to injection using a 50 µL loop (56 µL volume). The DMF eluent was filtered and eluted at 1 ml/min for a total of 30 minutes. Polystyrene samples ranging in molecular weight from 580 to 170800 were used as calibration standards. The SEC of the BCPs was performed on a Malvern VISCOTEK GPCmax instrument equipped with a VISCOTEK VE 3580 RI detector and two Inert series columns (P101609 and Q10183) at a constant temperature of 50 °C. The eluent was 0.4 M tetrabutylammonium triflate in DMF with a flow rate of 1 mL/min. Calibration was performed using narrow PMMA standards. Dialysis was performed using Spectra/Por® 6 pre-wetted dialysis tubing (Spectrum Laboratories Inc.). Pd loaded nanoparticles were sent to the Canadian Center for Electron Microscopy (McMaster University) and were imaged using a Titan 80-300 LB HRTEM/STEM microscope operating at an accelerating voltage of 200 kV and energy dispersive X-ray spectroscopy (EDS) was used to determine the co-occurrence of P with Pd.

Synthesis of 3-methoxybenzyl butyl trithiocarbonate, RAFT agent

To a stirring solution of dry triethylamine in dry tetrahydrofuran, dry butanethiol was added and the reaction stirred for 10 min. CS_2 was added dropwise, the reaction went from clear colourless to a clear bright yellow solution, the solution was allowed to stir for 20 min. 3-methoxybenzyl chloride was added dropwise and a white precipitate began forming. Aliquots were removed and the reaction was monitored decrease in the ^{1}H NMR signal of the methoxy group in the 3-methoxybenzyl chloride. When the signal of the starting material in the ^{1}H NMR was no longer present, water was added to the reaction mixture and the two phases were separated. Dichloromethane was added to the organic phase and was washed 3× with 20 mL of deionized water. The organic phase was dried over sodium sulphate and the solvent removed in vacuum to afford a yellow oil. ^{1}H NMR (400 MHz, $CDCl_3$): δ = 7.23 (dd, ^{3}J(H,H) = 8.0 Hz, Ar-H, 1H); 6.92 (d, ^{3}J(H,H) = 8.0 Hz, Ar-H, 1H); 6.89 (s, Ar-H, 1H); 6.82 (d, ^{3}J(H,H) = 8.0 Hz, Ar-H, 1H); 4.60 (s, S-CH_2-benzyl, 2H); 3.80 (s, CH_3O, 3H); 3.38 (m, S-CH_2, 2H); 1.69 (m, S-CH_2-CH_2, 2H); 1.44 (tq, ^{3}J(H,H) = 8.0 Hz, ^{3}J(H,H) = 8.0 Hz, CH_3-CH_2, 2H); 0.94 (t, ^{3}J(H,H) = 8.0 Hz, CH_3,

3H). ^{13}C NMR (600 MHz, $CDCl_3$): δ = 224 (S*C*S$_2$, 1C); 160 (MeO-*C*, 1C); 136 (CH$_2$*C$_q$*, 1C); 130 (1C, Ar); 121 (1C, Ar); 115 (1C, Ar); 113 (1C, Ar); 55 (*C*H$_3$O, 1C); 41 (S-*C*H$_2$-Ar, 1C); 37 (S-*C*H$_2$-pr, 1C); 30 (S-CH$_2$-*C*H$_2$, 1C); 22 (CH$_3$-*C*H$_2$, 1C); 14 (CH$_3$, 1C).

Synthesis of Poly(4-diphenylphosphino styrene) MacroRAFT agent

In a 10 mL round bottom flask 4-diphenyphosphino styrene (1.16 g, 4.02 mmol) and CTA (21 mg, 0.07 mmol) were dissolved in 5.5 mL of DMF and 1.0 mL of a 4 mg/mL DMF solution of azobisisobutyronitrile (0.02 mmol) was added to the flask and the solution was purged with N_2 for 30 min. in a 0 ℃ ice bath. The solution was then allowed to warm to room temperature for 10 min. the flask was then placed in an 80 ℃ oil bath. Aliquots were removed and the reaction was monitored by ^{31}P NMR spectroscopy by comparison of the monomer signal to the polymer signal, at 80% conversion the flask was placed into a $N_{2(l)}$ bath for 3 min. The product was precipitated in excess stirring methanol, the precipitate was collected by vacuum filtration. The process was repeated by dissolving the precipitate in minimal CH_2Cl_2. Remaining solvent was removed under vacuum in an 80 ℃ oil bath. The product was a light-yellow powder. ^{1}H NMR (400 MHz, $CDCl_3$): δ = 7.2 – 6.8 (m, Ar-H, 12H); 6.6 – 6.0 (m, Ar-H *ortho*-, 2H); 2.1 – 1.6 (m, methine, 1H); 1.6 – 1.0 (m, methylene, 2H). ^{31}P NMR (400 MHz, 85% H_3PO_4): δ = -6 (1, phosphine). M_n (H NMR) = 13,000 g/mol, M_n (SEC, 1% Et_3N in DMF) = 4,300 g/mol, M_w (SEC, 1% Et_3N in DMF) = 5,800 g/mol, $Đ$ = 1.4. T_{onset} = 355 ℃, T_g = 112 ℃.

General Synthesis of Poly(4-diphenylphosphino styrene)-b-*Poly(tributyl(4-vinylbenzyl)phosphonium chloride)*

In a 10 mL round bottom flask MacroRAFT agent (200 mg, 15 μmol) and tributyl(4-vinylbenzyl)phosphonium chloride were dissolved in 2 mL of DMF and 1.0 mL of a 0.85 mg/mL DMF solution of azobisisobutyronitrile (5 μmol) was added to the flask and the solution was purged with N_2 for 30 min. in a 0 ℃ ice bath. The solution was then allowed to warm to room temperature for 10 min. the flask was then placed in an 80 ℃ oil bath. Aliquots were removed, and the reaction was monitored by ^{1}H NMR spectroscopy by comparison of the monomer signal to the polymer signal, at 80% conversion the flask was placed into a $N_{2(l)}$ bath for 3 min. The solution was diluted with 5 mL of water and placed

in a 6 – 8 kg/mol molecular weight cut-off (MWCO) membrane and dialysed against water for 24 hours. The water was removed via lyophilisation and a white powder was obtained as the product.

P(PPh2Sty)$_{45}$-b-*P(Bu$_3$vbPCl)$_{15}$*

^{1}H NMR (400 MHz, $CDCl_3$): δ = 7.2 – 6.8 (m, Ar-H, 12H); 6.6 – 6.0 (m, Ar-H *ortho*-, 2H); 2.1 – 1.6 (m, methine, 1H); 1.6 – 1.0 (m, methylene, 2H). ^{31}P NMR (400 MHz, 85% H_3PO_4): δ = -6 (1, phosphine). M_n (H NMR) = 18,300 g/mol. T_{onset} = 355 °C, T_g = 112 °C.

P(PPh2Sty)$_{45}$-b-*P(Bu$_3$vbPCl)$_{23}$*

^{1}H NMR (400 MHz, $CDCl_3$): δ = 7.2 – 6.8 (m, Ar-H, 12H); 6.6 – 6.0 (m, Ar-H *ortho*-, 2H); 2.1 – 1.6 (m, methine, 1H); 1.6 – 1.0 (m, methylene, 2H). ^{31}P NMR (400 MHz, 85% H_3PO_4): δ = -6 (1, phosphine). M_n (H NMR) = 21,200 g/mol. T_{onset} = 355 °C, T_g = 112 °C.

P(PPh2Sty)$_{45}$-b-*P(Bu$_3$vbPCl)$_{45}$*

^{1}H NMR (400 MHz, $CDCl_3$): δ = 7.2 – 6.8 (m, Ar-H, 12H); 6.6 – 6.0 (m, Ar-H *ortho*-, 2H); 2.1 – 1.6 (m, methine, 1H); 1.6 – 1.0 (m, methylene, 2H). ^{31}P NMR (400 MHz, 85% H_3PO_4): δ = -6 (1, phosphine). M_n (H NMR) = 31,000 g/mol. T_{onset} = 355 °C, T_g = 112 °C.

Synthesis of Pd-loaded P(PPh2Sty)$_{45}$-b-*P(Bu$_3$vbPCl)$_{45}$*

To a stirring 15 mL CH_3CN solution of *P(PPh2Sty)$_{45}$*-b-*P(Bu$_3$vbPCl)$_{45}$* (150 mg, 3.5 μmol) a 1 mL CH_3CN suspension of $(Ph_3P)_2Pd(II)Cl_2$ (55 mg, 78.4 μmol) was added. The solution was allowed to stir for 24 hours. The $^{31}P\{^1H\}$ NMR showed the formation of free Ph_3P and the consumption of the polyphosphine peak. The solution was decanted and placed into a 6-8 kg/mol molecular weight cut-off membrane for dialysis. The solution was dialysed against 1:1 CH_3CN:H_2O with two solvent replacements, and then two more times against pure H_2O. The DLS of the particles were recorded from the solution.

General Synthesis of Metal Carbonyl-Loaded P(PPh2Sty)$_{45}$-b-*P(Bu$_3$vbPCl)$_{45}$*

Metal hexacarbonyl (250 μmol) was dissolved in anhydrous THF and stirred under UV light for 30 minutes, the solution went from clear colourless to a clear yellow. The photolyzed metal hexacarbonyl solution was added to a stirring suspension of *P(PPh2Sty)$_{45}$*-b-*P(Bu$_3$vbPCl)$_{45}$* (150 mg, 225 mmol of phosphine) in anhydrous THF. The suspension was allowed to stir for 24 hours

$Mo(CO)_5$-Loaded $P(PPh2Sty)_{45}$-b-*$P(Bu_3vbPCl)_{45}$*. After reaction the suspension became a clear solution and solvent and excess $Mo(CO)_x$ species were removed in vacuo.

$W(CO)_5$-Loaded $P(PPh2Sty)_{45}$-b-*$P(Bu_3vbPCl)_{45}$*. The product precipitated out of solution and was separated by centrifugation, the solid was washed once with THF and the solid collected.

3.5 References

1. U. Mehmood, A. Al-Ahmed, I. A. Hussein, *Renewable and Sustainable Energy Reviews*, 2016, **57**, 550-561.
2. C. Paquet, P. W. Cyr, E. Kumacheva, I. Manners, *Chem. Commun.*, 2004, **0**, 234-235.
3. D. A. Rider, I. Manners, *Polym. Rev.*, 2007, **47**, 165-195.
4. I. Manners, *Angew. Chem. Int. Ed.*, 1996, **35**, 1602-1621.
5. Y. Lei, T. Wang, J. W. Mitchell, L. Zaidel, J. Qiu, L. Kilpatrick-Liverman, K. Le, J. Hedger, F. Qi, M. Anderson, B. Rutherford, B. Wu, S. Tetradis, W. Shi, *RSC Adv.*, 2014, **4**, 49053–49060.
6. S. Banerjee, M. Wehbi, A. Manseri, A. Mehdi, A. Alaaeddine, A. Hachem, B. Ameduri, *ACS Appl. Mater. Interfaces*, 2017, **9**, 6433–6443.
7. V. Bhagat, E. O'Brien, J. Zhou, M. L. Becker, *Biomacromolecules*, 2016, **17**, 3016–3024.
8. X. Lin, K. Fukazawa, K. Ishihara, *ACS Appl. Mater. Interfaces*, 2015, **7**, 17489–17498.
9. A. Kanazawa, T. Ikeda, T. Endo, *J. Polym. Sci. Part A Polym. Chem.*, 1993, **31**, 1441–1447.
10. Z. E. Yilmaz, S. Vanslambrouck, S. Cajot, J. Thiry, A. Debuigne, P. Lecomte, C. Jérôme, R. Riva, *RSC Adv.*, 2016, **6**, 42081–42088.
11. S. Vanslambrouck, B. Clément, R. Riva, L. H. Koole, D. G. M. Molin, G. Broze, P. Lecomte, C. Jérôme, *RSC Adv.*, 2015, **5**, 27330–27337.
12. C.-J. Chen, Q. Jin, G.-Y. Liu, D.-D. Li, J.-L. Wang, J. Ji, *Polymer*, 2012, **53**, 3695–3703.

13. J. Liu, W. Huang, Y. Pang, P. Huang, X. Zhu, Y. Zhou, D. Yan, *Angew. Chemie Int. Ed.*, 2011, **50**, 9162–9166.
14. B. Hisey, J. V. Buddingh, E. R. Gillies, P. J. Ragogna, *Langmuir*, 2017, **33**, 14738–14747.
15. B. Hisey, P. J. Ragogna, E. R. Gillies, *Biomacromolecules*, 2017, **18**, 914–923.
16. S. T. Hemp, A. E. Smith, J. M. Bryson, M. H. Allen, T. E. Long, *Biomacromolecules*, 2012, **13**, 2439–2445.
17. S. Doherty, J. G. Knight, T. Backhouse, E. Abood, H. Alshaikh, I. J. S. Fairlamb, R. A. Bourne, T. W. Chamberlain, R. Stones, *Green Chem.*, 2017, **19**, 1635–1641.
18. A. R. Schultz, G. B. Fahs, C. Jangu, M. Chen, R. B. Moore, T. E. Long, *Chem. Commun.*, 2016, **52**, 950–953.
19. A. R. Schultz, M. Chen, G. B. Fahs, G. R. B. Moore, T. E. Long, *Polym. Int.*, 2017, **66**, 52–58.
20. Y. Xu, T. Wang, Z. He, A. Zhong, W. Yu, B. Shi, K. Huang, *Polym. Chem.*, 2016, **7**, 7408–7415.
21. E. Lobry, A. F. Cardozo, L. Barthe, J.-F. F. Blanco, H. Delmas, S. Chen, F. Gayet, X. Zhang, M. Lansalot, F. D'Agosto, R. Poli, E. Manoury, C. Julcour, *J. Catal.*, 2016, **342**, 164–172.
22. R. Wang, A. B. Lowe, *J. Polym. Sci. Part A Polym. Chem.*, 2007, **45**, 2468–2483.
23. Y. P. Borguet, N. V. Tsarevsky, *Polym. Chem.*, 2012, **3**, 2487.
24. P. Cotanda, G. Sudre, M. A. Modestino, X. C. Chen, N. P. Balsara, *Macromolecules*, 2014, **47**, 7540–7547.
25. S. Cheng, F. L. Beyer, B. D. Mather, R. B. Moore, T. E. Long, *Macromolecules*, 2011, **44**, 6509–6517.
26. S. C. Owen, D. P. Y. Chan, M. S. Shoichet, *Nano Today*, 2012, 7, 53–65.
27. J.-J. Yuan, A. Schmid, S. P. Armes, A. L. Lewis, *Langmuir*, 2006, **22**, 11022–11027.
28. P. Khullar, A. Mahal, V. Singh, T. S. Banipal, G. Kaur, M. S. Bakshi, *Langmuir*, 2010, **26**, 11363–11371.
29. P. Khullar, V. Singh, A. Mahal, H. Kaur, V. Singh, T. S. Banipal, G. Kaur, M. S.

Bakshi, *J. Phys. Chem. C*, 2011, **115**, 10442–10454.

30. P. Khullar, V. Singh, A. Mahal, H. Kumar, G. Kaur, M. S. Bakshi, *J. Phys. Chem. B*, 2013, **117**, 3028–3039.
31. T. S. Sabir, L. K. Rowland, J. R. Milligan, D. Yan, A. W. Aruni, Q. Chen, D. S. Boskovic, R. S. Kurti, C. C., Perry, *Langmuir*, 2013, **29**, 3903–3911.
32. A. A. Bogdanov, S. Gupta, N. Koshkina, S. J. Corr, S. Zhang, S. A. Curley, G. Han, *Bioconjug. Chem.*, 2015, **26**, 39–50.

Chapter 5

Raft Agents with Phosphonium Salt-Containing R Groups

5.1 Introduction

Polymers with functional or reactive end-groups have received research attention as functional polymers and have become more ubiquitous in daily life. The introduction of end-group functionalities on a polymer serves many useful purposes. In synthesis, end-functional polymers are used to synthesize block-copolymers, graft-copolymers macro-monomers, or polymer nano-composites.[1] These materials are also able to interact with biological molecules, inorganic materials as well as behave as surfactants, or probe molecules.[1] The benefit of having a functional end-group on the polymer is that the functionality of the end-group can be limited to a single unit per polymer chain, and be orthogonal to any functionality present in the polymer repeat units.[1,2] Many approaches have been developed to produce end-functional polymers and include the use of functional initiators or controlled polymerization agents.[1,2]

RAFT agents provide a convenient handle to add end-group functionality to polymeric materials prepared by RAFT polymerizations. One approach to functionalizing the termini of polymers prepared by RAFT polymerization is to alter or cleave the RAFT end group. This approach benefits from extensive precedence reported in the literature (Figure 5-1).[3,4] RAFT end-group functionalization often results in hetero-functional end groups, as there is often only a single thiocarbonyl group at the end of a polymer. This technique has been used recently by Abel and co-workers to append maleimide functionality to dithiobenzoate-terminated poly(*N*,*N*-dimethylacrylamide).[5] This was accomplished by the removal of the dithiobenzoate group by reaction with a nucleophile and the initiation of the reaction between the remaining thiol group with the maleimide. The authors demonstrated that this could be achieved in a “one-pot” procedure, as the nucleophile which removed the ditiobenzoate was also able to initiate the reaction between the remaining thiol and the maleimide.[5] Other examples are present in the literature and make use of maleimido functionalization, hormones, biotin, proteins,

saccharides, donor and acceptor dyes for Förster resonance energy transfer and malto-oligosaccharides.[6–10]

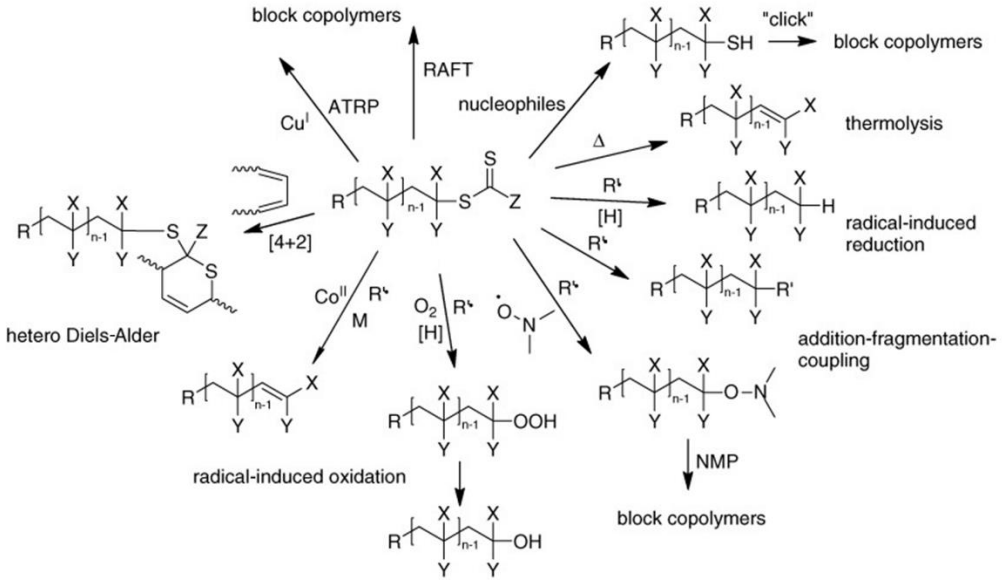

Figure 5-1 Functionalization of RAFT agent end-group via transformation or removal. Reproduced with permission from reference 3.

The post-polymerization functionalization of the RAFT end-group has a rich chemistry allowing for a variety of functionalities to be installed. However, post-polymerization functionalization requires doing chemistry on the polymer, introducing difficulties in determining the extent of reaction as well as the avoidance of side-products, such as the oxidative coupling of thiols. The extensive literature on the synthesis of RAFT agents, as well as the tolerance of RAFT polymerization to a wide variety of functional groups has allowed researchers to introduce useful and varied functional groups to the termini of polymers. These have included hydroxy, carboxylic acid or amino groups, activated esters for protein conjugation, “click-able” end groups such as azides or alkynes, and even light-harvesting groups such as coumarin.[11–15] RAFT agents offer a unique ability to introduce hetero-functionality on the α- and ω- termini of RAFT-made polymers.[7,9,11,16,17] This is because the polymer chains can be considered to insert between the thiocarbonyl with the covalently bound Z group and the R-group.

Heteroatoms have been incorporated into RAFT end-groups to provide novel properties to polymers produced from RAFT polymerization. For example Chakrabarty and co-workers demonstrated the use of an ammonium salt containing RAFT agent (**5.1** in Figure 5-2) in the Pickering mini-emulsion polymerization of several monomers.[18] The fluorinated random copolymer was synthesized without the use of additional surfactants, which is uncommon in emulsion polymerization but made possible by the cationic RAFT agent interacting with suspended negatively charged clay particles. The cationic head group from the RAFT agent was present on the final polymer and was able to stabilize the Pickering emulsion of negatively charged laponite clay discs.[18] Moughton and O'Reilly showed in 2010 that an ammonium salt-containing RAFT agent (**5.2**) allowed for the aqueous stabilization of a poly(*tert*-butyl acrylate)-*b*-poly(*N*-isopropyl acrylamide) (Figure 5-2). The BCP formed self-assembled nanoparticles in an aqueous dispersion. The poly(*N*-isopropyl acrylamide) block has a lower critical solution temperature (LCST), above which the polymer becomes hydrophobic. The cationic end-group was able to stabilize the particles as the BCP transitioned from amphiphilic to double-hydrophobic.[19]

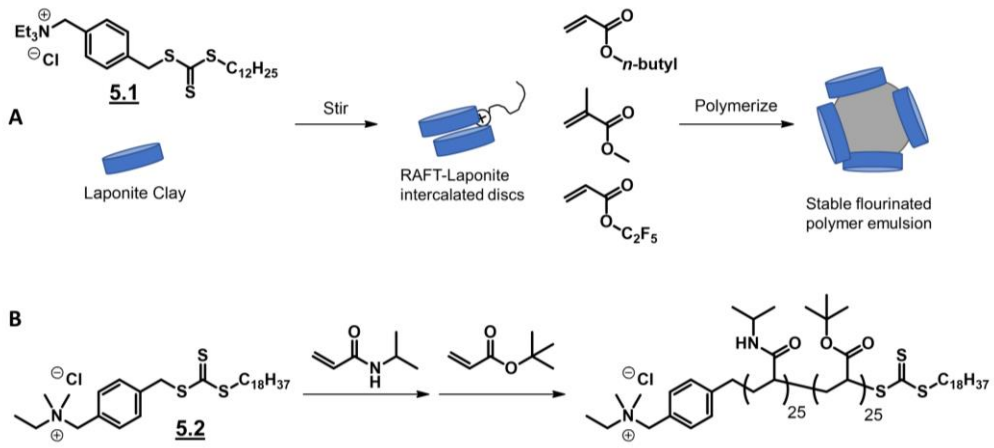

Figure 5-2. A) Schematic representation of the Pickering emulsion polymerization of a fluorinated random copolymer from reference 18. B) Cationic headgroup on a LCST BCP allows for stabilization of nanoparticles above the LCST. From reference 19.

Incorporation of hetero-atoms, including phosphorus, into polymer end-groups has also provided end-group functionality. Placement of a dialkoxyphosphoryl group (**5.3** in Figure 5-3) in the Z group as the atom connecting to the thiocarbonyl group allowed the

Barner-Kowollik group to add dienes to the thiocarbonyl end group through a photo-induced Diels-Alder reaction.[20,21] Phosphorus in the Z-group of the RAFT agent also allowed for its use in a Staudinger ligation reaction to create BCPs by clicking together two polymers (**5.4** in Figure 5-3).[22] Other groups have also included phosphonic acid into the Z-group in order to stabilize and functionalize iron-oxide nanoparticles through binding at the particle surfaces,[23] as well as to include interesting bonding motifs at the polymer end.[24,25] Inclusion of phosphorus into the R-group of RAFT agents as trialkylphosphine oxides (**5.5** in Figure 5-3) by the Emrick group and the Barros-Timmins group have shown that polymers could be grown from the surface of cadmium chalcogenide nanoparticles.[26,27] Other work has shown the incorporation of phosphonate groups at the α terminus of the polymer.[28] RAFT agents with phosphonium salts incorporated into the R-group (**5.6** in Figure 5-3) have been used by the Cavicchi group to control the polymerization of styrene and allow the polymers to behave as phase transfer catalysts.[29]

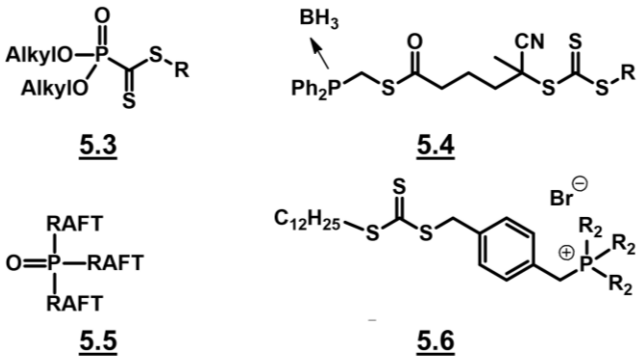

Figure 5-3. A) Dialkoxyphosphoryl containing RAFT agents as seen in references 20 and 21. B) Phosphine containing RAFT able to undergo a Staudinger ligation, reference 22. C) Trialkylphosphine RAFT agents from references 26 and 27. D) phosphonium containing RAFT agents from reference 29.

The few published examples of phosphorus-containing RAFT agents and the lack of study of their effect on macromolecular self-assembly motivated me to investigate the phosphonium salt RAFT agents similar to **5.6**. The work in Chapter 3 also showed that extremely low incorporation of phosphonium salt onto the PS macroRAFT agent still allowed for the self-assembly of the polymers, despite the very low DP of phosphonium salt monomer. This prompted investigation of the incorporation of more hydrophilic

phosphonium salts to explore the possibility of self-assembly of a telechelic homopolymer of poly(*n*-butyl acrylate) (PBuA). Additionally, we wanted to investigate if the inclusion of a phosphonium salt at the PBuA terminus of a PBuA-*b*-poly(phosphonium) BCP would result in the formation of vesicles due to unequal hydrophilic volumes at either end of the polymer.

5.2 Results and Discussion

5.2.1 Phosphonium Salt-Containing RAFT Agents

Incorporating the phosphonium salt into the RAFT agent prior to polymerization allows for separation of non-functionalized material. The synthetic approach was designed to allow for variability in the capping phosphonium salt as well as the relative lengths of the polymer blocks. This method provided the ability to investigate the effects of the alkyl chain on the behaviours of the RAFT agent as well as the self-assembly of the BCP and the PBuA.

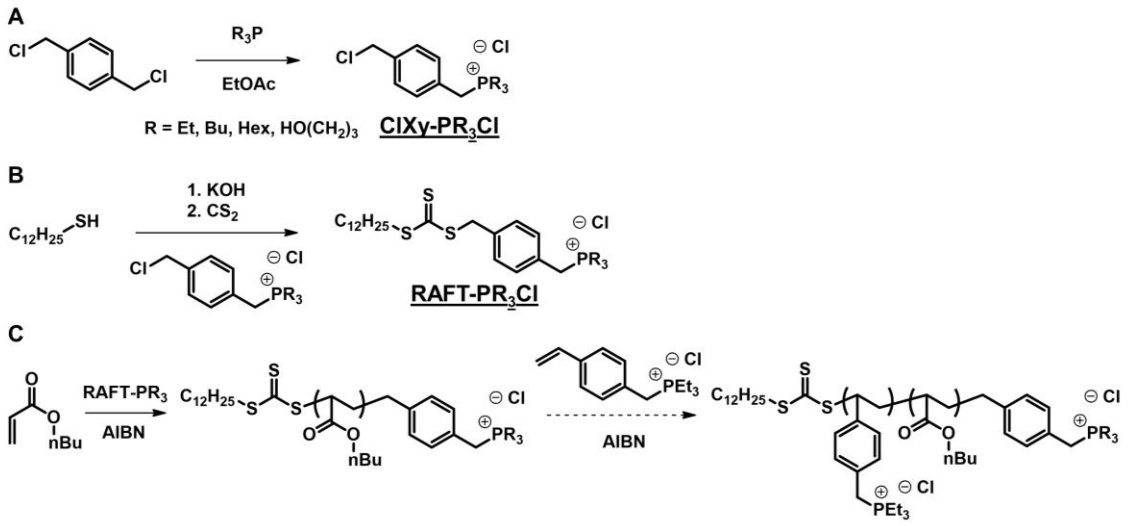

Scheme 5-1. A) Synthesis of 4-bromomethylbenzyltrialkylphosphonium bromide with the method detailed in reference 27. B) synthesis of phosphonium salt RAFT agents. C) RAFT polymerization of butyl acrylate and chain extension with 4-vinylbenzyltriethylphosphonium chloride to generate the phosphonium salt capped PBuA-*b*-PP^+ BCPs.

The asymmetric functionalization of the starting 1,4-bischloromethylbenzene with a trialkylphosphine makes excellent use of solubility changes upon the formation of the

phosphonium salt.[29] In that work, tributylphosphine and triphenylphosphine were used to generate the respective phosphonium salts. All the reagents were soluble in the ethyl acetate, but the product was not. The removal of the product from the reaction mixture avoided the double displacement of chlorine. I was able to reproduce the results with tributylphosphine and show that triethylphosphine could also be used in this reaction (Figure 5-4). Efforts with trihexylphosphine and tris(3-hydroxypropyl)phosphine did not produce the same effect. The product of the addition of trihexylphosphine to the dichloride starting material led to a mixture of single and doubly functionalized systems. The tris(3-hydroxypropyl)phosphine was insoluble in the xylylene solvent, and in biphasic mixtures the phosphonium was more soluble in the phosphine phase, resulting in exclusively double functionalization. Alternative methods of formation of the **RAFT-Phex$_3$Cl** and **RAFT-P(nPrOH)$_3$Cl** were explored. However, they did not lead to isolable compounds and were not explored further (see Figure D-7 for an example of the RAFT reaction with a phosphine). Following the synthesis of the triethyl and tributyl versions of the phosphonium salts, the respective **RAFT-PR$_3$Cl** agents were synthesized according to previous report (Figures D-4 and D-5).[27]

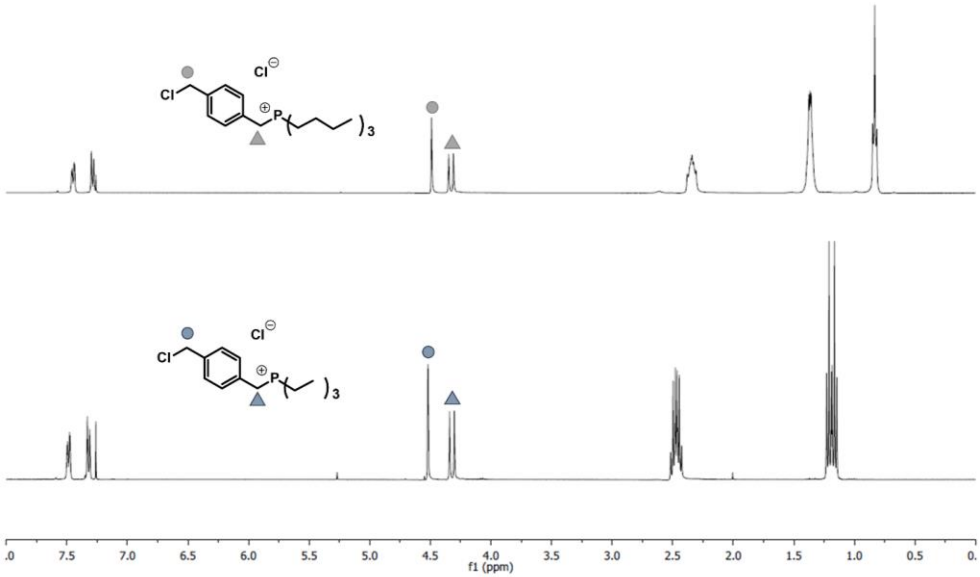

Figure 5-4. ^{1}H NMR ($CDCl_3$, 400 MHz) spectra of 4-chloromethylbenzyltributylphosphoinum chloride and 4-chloromethylbenzyltriethylphosphonium chloride. The highlighted peaks have a 1:1 ratio of integration and demonstrate the successful synthesis of the desired compound.

5.2.2 RAFT Polymerization of *n*-Butyl Acrylate

The choice of hydrophobic polymer was prompted by the low T_g of PBuA. Due to the self-assembly behaviour coming from a single charged group at the end of the polymer, a non-crystalline and non-glassy core-forming block was desirable, so that the core would not 'freeze-out' when a large amount of the anti-solvent was added. Particles with high T_g polymer cores form quickly during selective solvent addition and are unable to relax to thermodynamic equilibrium. Additionally, a smaller core-forming segment was required as the relative volume fraction of the phosphonium salt would be small even for low DP values of the PBuA. Thus, two DPs of PBuA were targeted: DP = 10 and DP = 80. The polymerizations of the DP = 10 polymers were monitored by removing aliquots of the reaction mixture and taking the ^{1}H NMR integrations of the alkene peaks and the methylene units α to the ester oxygen. The α-methylene exhibited relatively little chemical shift change between the polymer and the monomer, allowing it to serve as an internal standard. As the polymerization proceeded, the relative integration of the alkene peaks decreased, and the conversion could be monitored. Figure 5-5 shows the pseudo-1st order kinetics of the polymerization of BuA with **RAFT-PEt$_3$Cl** and **RAFT-PBu$_3$Cl**. The deviation from a linear fit demonstrates the need to optimize polymerization conditions. The lines of best fit for both the tributyl and triethyl RAFT agents are almost identical (RAFT-PEt$_3$ y = 0.2312x; RAFT-PBu$_3$ y = 0.2318x). This suggests that the nature of the phosphonium has little to no effect on the polymerization. However, not all of the RAFT agents reacted with growing polymer chains and so the DP could not be determined by end-group analysis. Figures D-8 and D-9 show the chemical shift and splitting pattern of the benzylic methylene adjacent to the trithiocarbonate group unchanged. This would not be the case if the R group re-initiated polymer chain growth.

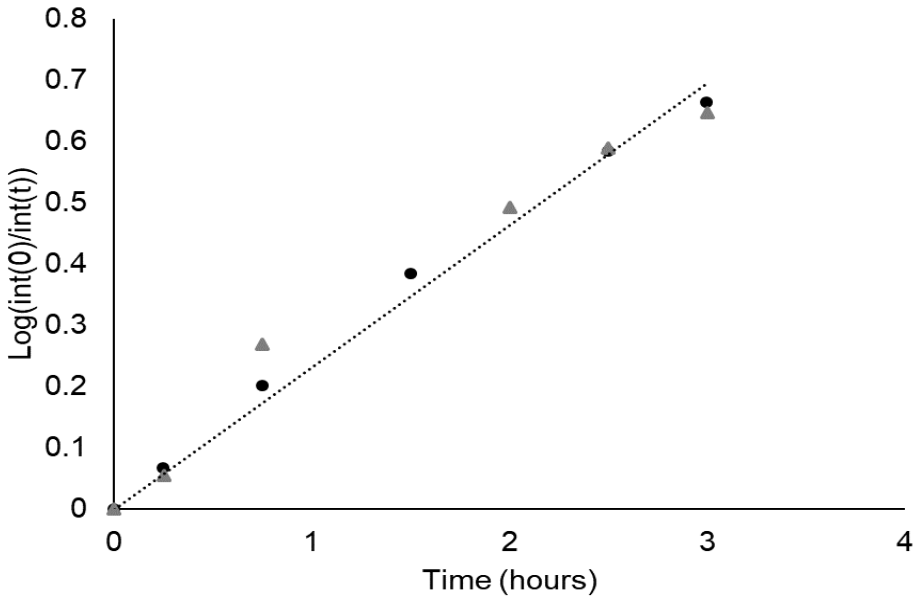

Figure 5-5 Pseudo-1st order kinetics of the polymerization of BuA by RAFT-PEt_3Cl (●) and RAFT-PBu_3Cl (▲). The dotted line represents the linear regression of both sets of data (they are incidental). The R^2 values are 0.991 for RAFT-PEt_3Cl and 0.967 for RAFT-PBu_3Cl.

The phosphonium salt-containing RAFT agents can be used for end-group analysis in the resulting polymeric materials, as there are certain peaks that are noted in the ^1H NMR spectrum (Figure 5-6). By comparing the integration of the α-methylene protons from the phosphorus containing block to the α-methylene protons on the PBuA the DP can be determined to be ~78 units. The control over the polymerization was confirmed with SEC with a $Đ$ = 1.3 and M_w of 12,200 g/mol relative to poly(methyl methacrylate), which is a DP of 95.

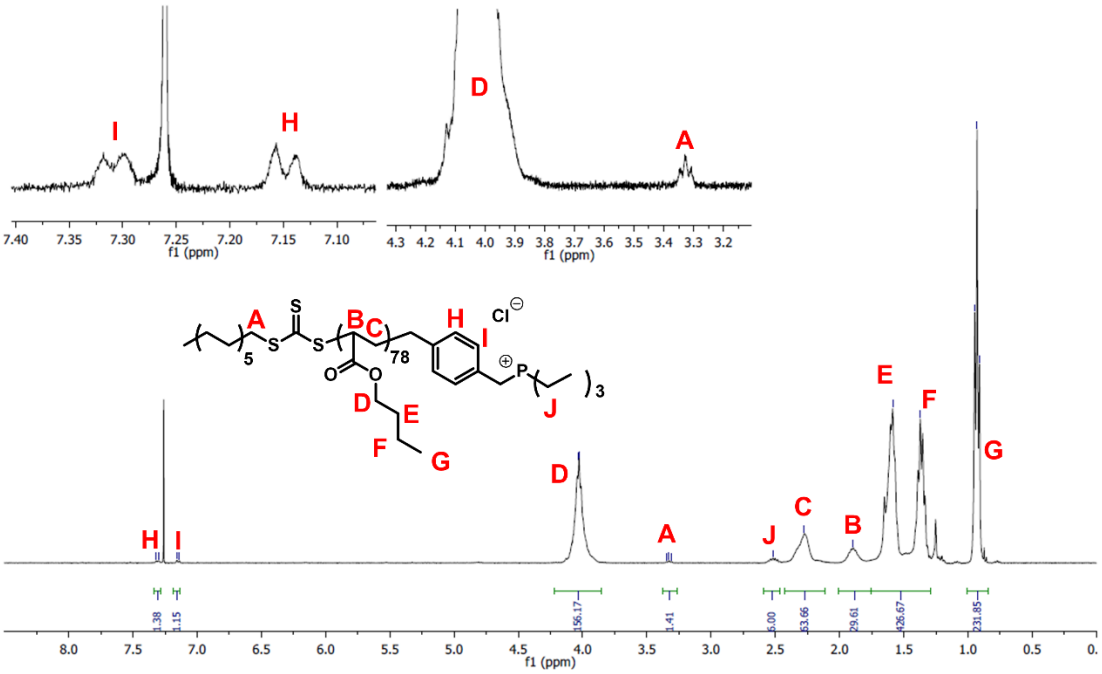

Figure 5-6. ^{1}H NMR ($CDCl_3$, 400 MHz) spectrum of the $PBuA_{78}$-PEt_3Cl. Inserts are blow-ups regions showing the RAFT end-groups.

5.2.3 Self-Assembly of Phosphonium-Capped PBuA

To investigate the ability of the phosphonium end-group to stabilize self-assembled nanoparticles of the PBuA, the polymer was dissolved in DMF and was added to water to achieve four different final concentrations: 5.0, 3.3, 2.5 and 1.6 mg/mL. The different concentrations can be used to determine the effect of the concentration of the PBuA in the initial solution phase self-assembly. Following the removal of the DMF from the solutions by dialysis, the solutions were translucent and the DLS investigations of the suspensions showed the formation of particles. The z-average sizes of the particles showed variation of the particle size with concentration where the z-average sizes were ordered inversely with the concentrations (Figure 5-7, Table 5-1).

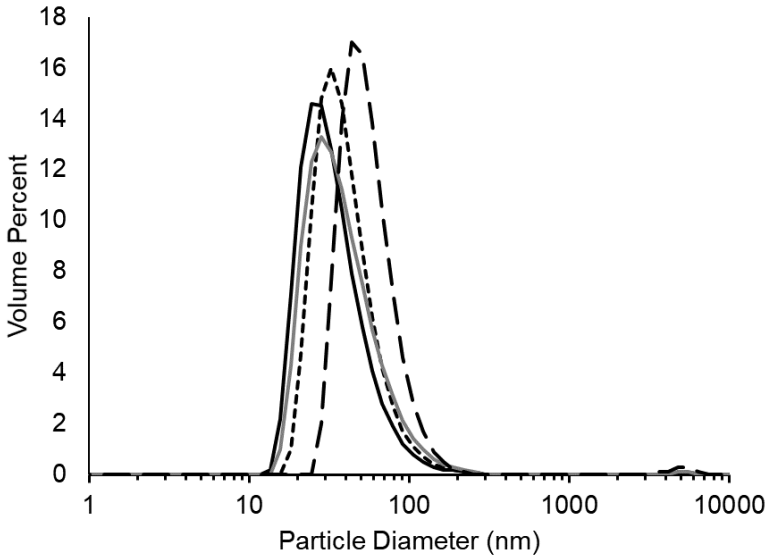

Figure 5-7. DLS distributions of different concentrations of self-assembled particles from $PBuA_{78}$-PEt_3Cl; 5.0 mg/mL (solid black line), 3.3 mg/mL (dotted black line), 2.5 mg/mL (solid grey line), 1.6 mg/mL (dashed black line).

Concentration (mg/mL)	z-average (nm) (PDI)
5.0	59.4 (0.232)
3.3	62.6 (0.222)
2.5	70.2 (0.239)
1.6	73.5 (0.182)

Table 5-1. Summary of DLS measured z-average particle diameters

5.3 Summary

This work has demonstrated the synthesis of phosphonium salt- containing RAFT agents and their application towards the polymerization of *n*-butyl acrylate. Good control over the polymerization of *n*-butyl acrylate resulted in polymers with low *Đ*. Attempts to produce a BCP containing a fluorinated phosphonium salt were pursued.

RAFT agents have also been nearly ubiquitous in the use of a carbon-sulfur bond as the homolytic cleavable group on the R-group. Phosphorus-centered radicals readily add to unsaturated carbon-carbon bonds generating new carbon centered radicals following addition. There are currently no studies which investigate the use of a

phosphorus centered radical as the leaving group from a RAFT agent. Phosphorus-sulfur bonds can cleave homolytically to provide a phosphorus-centered radical able to undergo addition to olefins.[30] Phosphonyl groups have been shown for several decades to add readily to polymerizable monomers and are used currently as common photoinitiated radical sources for polymerization.[31,32] To date, this chemistry has not been incorporated into a RAFT agent. This chapter demonstrates the progress made towards the incorporation of phosphorus into RAFT agents and some studies of polymer self-assembly.

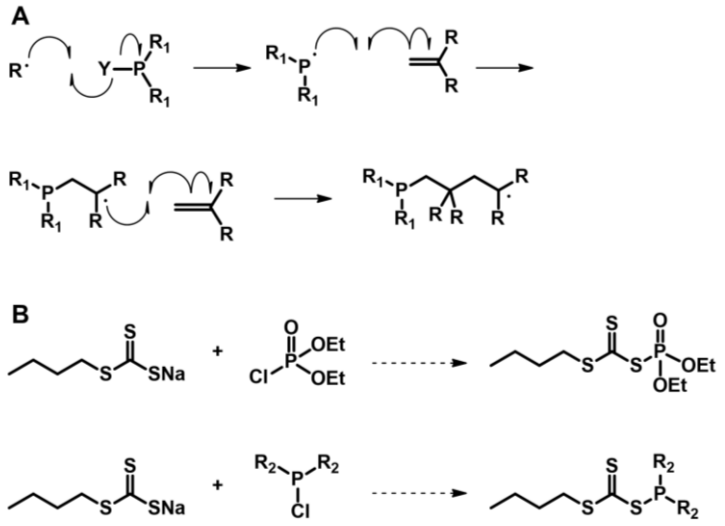

Scheme 5-2. A) mechanism of radical phosphine addition to carbon-carbon double bonds demonstrating the ability to initiate polymerization. B) proposed synthetic approach to phosphoryl RAFT agents and phosphine RAFT agents.

5.4 Experimental

General materials and procedures

Solvents were dried using an MBraun Solvent Purification System. Dried acetonitrile was collected under vacuum in a flame dried Straus flask and stored over 3 Å molecular sieves. Ultrapure water was obtained using a Barnstead EASYPure II ultra pure water system (ThermoFisher Scientific). 4-chloromethylbenzyltributylphosphonium chloride was prepared according to a published procedure.[27]. Butyl acrylate was passed through an alumina column prior to use to remove inhibitor. Nuclear Magnetic Resonance (NMR)

spectroscopy was conducted on a Varian INOVA 400 MHz spectrometer (^{1}H 400.09 MHz, ^{31}P{^{1}H} 161.82 MHz, ^{13}C{^{1}H} 100.52 MHz) unless otherwise noted. All ^{1}H NMR spectra were referenced relative to $SiMe_4$ (residual solvent in $CDCl_3$; ^{1}H δ = 7.27). The chemical shifts for ^{31}P{^{1}H} NMR spectroscopy were referenced using an external standard (85% H_3PO_4; δ_P = 0). All ^{13}C{^{1}H} NMR spectra were referenced relative to $SiMe_4$ (residual solvent in $CDCl_3$; δ_C = 77.0). Electrospray Ionisation (ESI) Mass spectrometry was obtained on a Finnigan MAT 8400 mass spectrometer using electron impact ionization. Dynamic Light Scattering (DLS) measurements were performed on a Zetasizer Nano ZS (Malvern Instruments) using a 633 nm laser. SEC was performed on a Malvern VISCOTEK GPCmax instrument equipped with a VISCOTEK VE 3580 RI detector and two Inert series columns (P101609 and Q10183) at a constant temperature of 50 °C. The eluent was 0.4 M tetrabutylammonium triflate in DMF with a flow rate of 1 mL/min. Calibration was performed using narrow PMMA standards. Dialysis was performed using Spectra/Por® 6 pre-wetted dialysis tubing (Spectrum Laboratories Inc.).

Synthesis of 4-chloromethylbenzyltributylphosphonium chloride

Title compound was prepared according to literature procedure from reference 27 and yielded a white powder (81 % yield); ^{1}H NMR (400 MHz, $CDCl_3$); δ = 7.45 (dd, ^{4}J(H,P) = 4 Hz, ^{3}J(H,H) = 8 Hz, Ar-H, 2H); 7.30 (d, ^{3}J(H,H) = 8 Hz, Ar-H, 2H); 4.5 (s, CH_2Cl, 2H); 4.33 (d, ^{2}J(H,P) = 16 Hz, $ArCH_2P$, 2H); 2.34 (m, CH_2P, 6H); 1.37 (m, CH_2, 12H); 0.83 (t, ^{3}J(H,H) = 8 Hz, CH_3, 9H). ^{13}C{^{1}H} NMR (100.6 MHz, $CDCl_3$); δ = 137 (d, ^{5}J(C,P) = 4 Hz, BrMeC, 1C); 130 (d, ^{4}J(C,P) = 5 Hz, Ar C-H, 2C); 129 (d, ^{3}J(C,P) = 3 Hz, Ar C-H, 2C); 129 (d, ^{2}J(C,P) = 9 Hz, *quat* C, 1C); 45 (s, CBr, 1C); 26 (d, ^{1}J(C,P) = 45 Hz, $PhCH_2P$, 1C); 24(d, ^{3}J(C,P) = 15 Hz, CH_2, 3C); 23 (d, ^{2}J(C,P) = 5 Hz, CH_2, 3C) 18 (d, ^{1}J(C,P) = 47 Hz, CH_2P, 3C); 13 (s, CH_3, 3C).

Synthesis of 4-chloromethylbenzyltriethylphosphonium chloride

Title compound was prepared according to literature procedure from reference 27 except triethylphosphine was used and yielded a white powder (73 % yield); ^{1}H NMR (400 MHz, $CDCl_3$); δ = 7.49 (dd, ^{4}J(H,P) = 4 Hz, ^{3}J(H,H) = 8 Hz, Ar-H, 2H); 7.32 (d, ^{3}J(H,H) = 8 Hz, Ar-H, 2H); 4.52 (s, CH_2Cl, 2H); 4.32 (d, ^{2}J(H,P) = 16 Hz, $ArCH_2P$, 2H);

2.47 (dq, $^{2}J(H,P)$ = 16 Hz, $^{3}J(H,H)$ = 8 Hz, $MeCH_2P$, 6H); 1.19 (dt, $^{3}J(H,P)$ = 20 Hz, $^{3}J(H,H)$ = 8Hz, CH_3, 9H). $^{13}C\{^{1}H\}$ NMR (100.6 MHz, $CDCl_3$); δ = 137 (d, $^{5}J(C,P)$ = 4 Hz, BrMeC, 1C); 130 (d, $^{4}J(C,P)$ = 5 Hz, Ar C-H, 2C); 129 (d, $^{3}J(C,P)$ = 3 Hz, Ar C-H, 2C); 128 (d, $^{2}J(C,P)$ = 9 Hz, *quat* C, 1C); 45 (s, CBr, 1C); 25 (d, $^{1}J(C,P)$ = 45 Hz, $ArCH_2P$, 1C); 11 (d, $^{1}J(C,P)$ = 48 Hz, CH_2P, 3C); 6 (d, $^{2}J(C,P)$ = 5 Hz, CH_3, 3C). $^{31}P\{^{1}H\}$ NMR (161.8 MHz, $CDCl_3$); δ = 36.

S-*1-dodecyl*-S'-*(methylbenzyltributylphosphonium chloride) trithiocarbonate*

Prepared according to literature procedure from reference 27 and yielded a yellow oil (2.39 g, 94 % yield). ^{1}H NMR (400 MHz, $CDCl_3$); δ = 7.40 (dd, $^{4}J(H,P)$ = 4 Hz, $^{3}J(H,H)$ = 8 Hz, Ar-H, 2H); 7.29 (d, $^{3}J(H,H)$ = 8 Hz, Ar-H, 2H); 4.56 (s, SCH_2Ar, 2H); 4.29 (d, $^{2}J(H,P)$ = 16 Hz, $ArCH_2P$, 2H); 3.34 (t, $^{3}J(H,H)$ = 8 Hz, CH_2S, 2H); 2.37 (m, PCH_2, 6H); 1.67 (dd, $^{3}J(H,H)$ = 8 Hz, $^{3}J(H,H)$ = 8 Hz, $SCH_2\underline{CH_2}$, 2H); 1.41 (m, CH_2, 14H); 1.26 (m, CH_2, 18H); 0.89 (t, $^{3}J(H,H)$ = 8 Hz, CH_3, 9H); 0.85 (t, $^{3}J(H,H)$ = 8 Hz, CH_3, 3H). $^{31}P\{^{1}H\}$ NMR (161.8 MHz, $CDCl_3$); δ = 32.

S-*1-dodecyl*-S'-*(methylbenzyltriethylphosphonium chloride) trithiocarbonate*

To a stirred solution of dodecanethiol (1.00 mL, 4.17 mmol) and CS_2 (1.30 mL, 21.5 mmol) in 5 mL of CH_2Cl_2 triethylamine (0.70 mL, 5.0 mmol) was added dropwise. The solution stirred for 2 hours at room temperature and went from clear and colourless to clear yellow. The 4-chloromethylbenzyltriethylphosphonium chloride (1.22 g, 4.16 mmol) was added as a 2 mL solution in CH_2Cl_2 and stirred for 30 min. The addition caused the solution to become a cloudy orange suspension. 30 mL of CH_2Cl_2 was added and the organic layer washed with a mixture of 25 mL of water and 3 mL of brine twice. The aqueous wash was extracted once with 20 mL of CH_2Cl_2 and the organic phases combined. The organic layer was dried over $MgSO_4$ and the CH_2Cl_2 was removed *in vacuo* to yield a yellow powder. (1.79 g, 80 % yield) ^{1}H NMR (400 MHz, $CDCl_3$); δ = 7.42 (dd, $^{4}J(H,P)$ = 3 Hz, $^{3}J(H,H)$ = 8 Hz, Ar-H, 2H); 7.29 (d, $^{3}J(H,H)$ = 8 Hz, Ar-H, 2H); 4.56 (s, SCH_2Ar, 2H); 4.26 (d, $^{2}J(H,P)$ = 16 Hz, $ArCH_2P$, 2H); 3.35 (t, $^{3}J(H,H)$ = 6 Hz, CH_2S, 2H); 2.47 (dq, $^{2}J(H,P)$ = 12 Hz, $^{3}J(H,H)$ = 8 Hz, PCH_2, 6H); 1.68 (dd, $^{3}J(H,H)$ = 8 Hz, $^{3}J(H,H)$ = 8 Hz, $SCH_2\underline{CH_2}$, 2H); 1.38 (m, CH_2, 2H); 1.24 (m, CH_2, 18H); 1.19 (dt,

$^{3}J(H,P)$ = 20 Hz, $^{3}J(H,H)$ = 8 Hz, CH_3, 9H); 0.86 (t, $^{3}J(H,H)$ = 8 Hz, CH_3, 3H). $^{31}P\{^{1}H\}$ NMR (161.8 MHz, $CDCl_3$); δ = 36.

RAFT polymerization of n-*butyl acrylate, targeted DP = 80*

n-Butyl acrylate (2.99 g, 23.3 mmol), RAFT-PEt_3 (0.125 g, 0.233 mmol) and AIBN (0.013 g, 0.079 mmol) were dissolved in acetonitrile and purged with N_2 for 10 min. in a 0 ℃ ice bath. The mixture came to room temperature before being placed in a 75 ℃ oil bath. The conversion of monomer was monitored by ^{1}H NMR spectroscopy. At a conversion of 80% consumption of the monomer, the flask was removed and placed in a liquid N_2 bath. Solvent and monomer were removed from the reaction mixture over several days at high vacuum. The product was a transparent yellow very viscous oil (2.41 g, 81 % yield). ^{1}H NMR (400 MHz, $CDCl_3$); δ = 7.31 (d, $^{3}J(H,H)$ = 8 Hz, Ar-H, 2H); 7.15 (d, $^{3}J(H,H)$ = 8 Hz, Ar-H, 2H); 4.03 (m, O-CH_2, 156H); 3.33 (t, $^{3}J(H,H)$ = 8 Hz, SCH_2, 2H); 2.52 (m, CH_2P, 6H); 2.28 (m, CH_2 *backbone*, 64H); 1.90 (m CH *backbone*, 30H); 1.59 (m, $OCH_2\underline{CH_2}$, 240H); 1.37 (m, $\underline{CH_2}CH_3$ *butyl*, 200H); 0.93 (t, $^{3}J(H,H)$ = 8 Hz, CH_3 *butyl*, 230H). DP (By ^{1}H NMR) = 78, M_n = 10,000 g/mol

General RAFT polymerization of butyl acrylate, targeted DP = 10

n-Butyl acrylate (0.38 g, 3.0 mmol), RAFT-PR_3 (0.23 mmol) and AIBN (0.013 g, 0.079 mmol) were dissolved in *N*,*N*-dimethylformamide and purged with N_2 for 15 minutes in a 0 ℃ ice bath. The mixture was allowed to come to room temperature before being placed in a 75 ℃ oil bath. The conversion of monomer was monitored by ^{1}H NMR spectroscopy. At a conversion of 80% consumption of the monomer the flask was removed and placed in a liquid N_2 bath. Solvent and monomer were removed from the reaction mixture over several days at high vacuum.

PBuA-PEt_3

The product was a yellow waxy solid (0.23 g, 63 % yield). ^{1}H NMR (Polymer) (400 MHz, $CDCl_3$); δ = 3.9 – 4.1 (m, O-CH_2, 2H); 1.8 – 2.0 (m, CH_2 *backbone*, 2H); 1.90 (m CH *backbone*, 1H); 1.43 (m, $OCH_2\underline{CH_2}$, 2H); 1.29 (m, $\underline{CH_2}CH_3$ *butyl*, 2H); 0.93 (m, CH_3 *butyl*, 3H).

PBuA-PBu$_3$

The product was a yellow waxy solid (0.26 g, 60 % yield). ^{1}H NMR (Polymer) (400 MHz, $CDCl_3$); δ = 3.8 – 4.1 (m, O-CH_2, 2H); 1.75 – 2.0 (m, CH *backbone*, 1H); 1.59 (m CH_2 *backbone*, 2H); 1.41 (m, $OCH_2\underline{CH_2}$, 2H); 1.26 (m, $\underline{CH_2}CH_3$ *butyl*, 2H); 0.95 (t, ^{3}J(H,H) = 8 Hz, CH_3 *butyl*, 3H).

Nanoparticle self-assembly

The polymer was dissolved in DMF passed through a 0.22 μm PTFE syringe filter to produce a solution of 20 mg/mL of polymer in DMF. The polymer solution was introduced into rapidly stirred filtered high purity water. The volumes were adjusted to produce the desired volume. The suspension was placed into a 6-8 kg/mol molecular-weight cut-off membrane and dialysed against water for 16 hours. The suspension was removed from the membrane and the DLS measurements were made at full concentration.

5.5 References

1. D. Vinciguerra, J. Tran, J. Nicolas, *Chem. Commun.*, 2018, **54**, 228–240.
2. F. Lo Verso, C. N. Likos, *Polymer*, 2008, **49**, 1425–1434.
3. G. Moad, E. Rizzardo, S. H. Thang, *Polym. Int.*, 2011, **60**, 9–25.
4. H. Willcock, R. K. O'Reilly, *Polym. Chem.*, 2010, **1**, 149–157.
5. B. A. Abel, C. L. McCormick, *Macromolecules*, 2016, **49**, 6193–6202.
6. S. M. Henry, A. J. Convertine, D. S. W. Benoit, A. S. Hoffman, P. S. Stayton, *Bioconjug. Chem.*, 2009, **20**, 1122–1128.
7. P. J. Roth, F. D. Jochum, R. Zentel, P. Theato, *Biomacromolecules*, 2010, **11**, 238–244.
8. V. Vázquez-Dorbatt, Z. P. Tolstyka, H. D. Maynard, *Macromolecules*, 2009, **42**, 7650–7656.
9. P. J. Roth, M. Haase, T. Basché, P. Theato, R. Zentel, *Macromolecules*, 2010, **43**, 895–902.
10. D. Togashi, I. Otsuka, R. Borsali, K. Takeda, K. Enomoto, S. Kawaguchi, A. Narumi, *Biomacromolecules*, 2014, **15**, 4509–4519.

11. N. A. Cortez-Lemus, R. Salgado-Rodríguez, A. Licea-Claveríe, *J. Polym. Sci. Part A Polym. Chem.*, 2010, **48**, 3033–3051.
12. H. Li, A. P. Bapat, M. Li, B. S. Sumerlin, *Polym. Chem.*, 2011, **2**, 323–327.
13. K. Zhang, L. Gao, Y. Chen, *Polymer*, 2010, **51**, 2809–2817.
14. K. T. Wiss, P. Theato, *J. Polym. Sci. Part A Polym. Chem.*, 2010, **48**, 4758–4767.
15. M. Chen, K. P. Ghiggino, A. W. H. Mau, E. Rizzardo, W. H. F. Sasse, S. H. Thang, G. J. Wilson, *Macromolecules*, 2004, **37**, 5479–5481.
16. K. L. Heredia, L. Tao, G. N. Grover, H. D. Maynard, *Polym. Chem.*, 2010, **1**, 168-170.
17. P. W. Reader, R. Pfukwa, S. Jokonya, G. E. Arnott, B. Klumperman, *Polym. Chem.*, 2016, **7**, 6450–6456.
18. A. Chakrabarty, L. Zhang, K. A. Cavicchi, R. A. Weiss, N. K. Singha, *Langmuir*, 2015, **31**, 12472–12480.
19. A. O. Moughton, R. K. O'Reilly, *Chem. Commun.*, 2010, **46**, 1091–1093.
20. M. Glassner, G. Delaittre, M. Kaupp, J. P. Blinco, C. Barner-Kowollik, *J. Am. Chem. Soc.*, 2012, **134**, 7274–7277.
21. M. Langer, J. O. Mueller, A. S. Goldmann, F. H. Schacher, C. Barner-Kowollik, *ACS Macro Lett.*, 2016, **5**, 597–601.
22. R. Pötzsch, S. Fleischmann, C. Tock, H. Komber, B. I. Voit, *Macromolecules*, 2011, **44**, 3260–3269.
23. C. Boyer, V. Bulmus, P. Priyanto, W. Y. Teoh, R. Amal, T. P. Davis, *J. Mater. Chem.*, 2009, **19**, 111–123.
24. S. Mazières, I. Kulai, R. Geagea, S. Ladeira, M. Destarac, *Chem. Eur. J.*, 2015, **21**, 1726–1734.
25. R. Geagea, S. Ladeira, S. Mazières, M. Destarac, *Chem. Eur. J.*, 2011, **17**, 3718–3725.
26. H. Skaff, T. Emrick, *Angew. Chemie Int. Ed.*, 2004, **43**, 5383–5386.
27. A. C. C. Esteves, P. Hodge, T. Trindade, A. M. M. V. Barros-Timmons, *J. Polym. Sci. Part A Polym. Chem.*, 2009, **47**, 5367–5377.

28. P.-E. Dufils, G. David, B. Boutevin, G. Woodward, G. Otter, A. Guinaudeau, S. Mazières, M. Destarac, *J. Polym. Sci. Part A Polym. Chem.*, 2012, **50**, 1997–2007.

29. L. Zhang, Q. Tang, R. A. Weiss, K. A. Cavicchi, *Polym. Chem.*, 2014, **5**, 5492–5500.

30. P. Carta, N. Puljic, C. Robert, A.-L. Dhimane, L. Fensterbank, E. Lacôte, M. Malacria, *Org. Lett.*, 2007, **9**, 1061-1063.

31. S. C. Ligon, K. Seidler, C. Gorsche, M. Griesser, N. Moszner, R. Liska, *J. Polym. Sci. Part A Polym. Chem.*, 2016, **54**, 394–406.

32. T. Sumiyoshi, W. Schnabel, A. Henne, *J. Photochem.*, 1986, **32**, 191–201.

Chapter 6 Conclusions and Future Work

6.1 Conclusions

The work presented in this dissertation has demonstrated the utility and interesting results available from the incorporation of phosphorus into amphiphilic BCPs. The experimental chapters demonstrate the variety of different applications phosphorus can serve in amphiphilic BCPs.

In the first experimental chapter I demonstrated that a low weight percentage of covalently bound phosphonium salt on the surface of amphiphilic drug carriers can provide antibacterial activity that is comparable to other work in the field. The incorporation uses a method that is already used to functionalize many existing nano-assembly platforms.[1] The method of incorporation used in chapter 2 for the bio-active species is important, as previously published antibacterial micelle work relied on the use of generating new ammonium containing polymeric materials that are not already common in the drug delivery research field.[2,3] This requires then that new platforms be made in order to provide antibacterial activity, instead of the simpler method of altering existing systems. Additionally, the reliance of some systems on the use of nano-silver creates another limitation to incorporating antibacterial activity into drug nano-carrier systems.[4] This is because the particles must be able to bind and stabilize the formation of Ag nanoparticles.

The knowledge generated by this work should allows researchers to functionalize already existing ‘click-able’ BCP systems with antibacterial phosphonium salts. The relatively low incorporation amount required to see bio-activity. Future work in this area should explore the incorporation of targeting groups on the surface of these particles, to increase affinity for bacterial cell walls as well as potentially target specific bacteria, similar to targeting of cancer cells.[5,6]

Considering together the results from chapters 2 and 3 of this work can also prompt investigators in the field BCP self-assembly to utilize phosphonium salts in a dual role in these systems. By incorporating the phosphonium salts into a core-shell-corona type nanoparticle with the phosphonium salt block as the shell, anionic drugs could be

introduced into the shell of the self-assembled nanoparticles. This system would be able to release the ionically bound drug as a response to pH changes, and then provide antibacterial activity.

My second experimental chapter reported work that answered an important question in the role anions on the self-assembly of polyneutral-*b*-polyion BCPs. The literature available concerning the self-assembly of polyneutral-*b*-polyion BCPs has demonstrated the influence of: relative chain lengths, degree of ionization, added salt concentration, added salt identity, and several others.[7,8] Despite the research published in this field, the influence of the intrinsic counterion had yet to be investigated. Knowing how the counterion influences the morphological properties of the self-assembled material allows researchers to rationally design a system from the ground up to target specific particle sizes, and potentially morphologies. As in other material chemistry and nano-chemistry fields one of the important goals of these fields is to be able to design materials of targeted size and morphology.

The obvious direction for the field to take the work of chapter 3 in is to investigate different anions, or perhaps varying poly(phosphonium salt) chain lengths. What is likely more interesting, however, is the inclusion of these types of polymers into mixed BCP systems in an attempt to form Janus particles, and is discussed in further detail in the future work section. The identity of the anion, as demonstrated by the varying LogP values for the different phosphonium salt monomers, changes the hydrophilicity of the phosphonium salt block. By including phosphonium salt BCP materials in polyneutral-*b*-polyneutral systems, tuning the hydrophilicity of the phosphonium salt block can allow for the exclusion of the two hydrophilic blocks from one another.

The work reported in chapter 4 demonstrates the versatility of phosphorus in a single BCP. The phosphorus provided not only hydrophilicity to cause self-assembly and a charge that can ionically bind $AuCl_4$, the phosphine in the core was able to bind metals. This dual modality for phosphorus in the material is novel for phosphorus-containing BCPs. The most important contribution this makes to the field of BCP self-assembly is the demonstration that phosphorus can be incorporated to fulfill multiple roles in the same material. Often published work demonstrates the utility of phosphorus through a single chemical species of phosphorus, playing a unique and singular role in the material.

Continued growth of incorporation of inorganic elements into BCPs requires work which demonstrates the variety of roles inorganic elements can play.

The ability to incorporate two different transition metal elements into the assemblies provides a path forward to the greater special control of elements in self-assembled nanoparticles. Greater spatial control can then lead to improved material properties. For example, several reports have detailed catalysis achieved by transition metal elements in the cores of nanoparticles formed from amphiphilic BCPs.[9,10] By incorporating two metals with spatial separation it may become possible to perform several catalyzed reactions in the same media with little to no interaction of the two catalytic species. This type of compartmentalization may also allow for the formation of core-shell ceramics following the patterning and pyrolysis of bimetallic self-assembled amphiphilic BCPs. The work in this chapter represents an important step in the progress towards the systems mentioned above as well as new avenues for such materials.

While the work in chapter 5 is limited to a homopolymer system, the ability to use a single phosphonium salt unit to produce surfactant behaviour can perhaps be translated into improved morphological control through the polymerization of a second, hydrophilic, block. By separating the phosphonium salt head group from a hydrophilic block with a separating hydrophobic block, unequal forces would act upon each end of the BCP during self-assembly and can lead to particle morphologies with the phosphonium salt forming one hydrophilic surface while the hydrophilic block of the BCP forms another. These materials may preferentially form bilayer-type structures, such as vesicles, without the need for finely tuned control of the block ratios or assembly conditions. This technique would allow the generation of libraries of amphiphilic BCP materials able to form higher-order morphologies without the need for screening a wide range of block ratios or assembly conditions. This can move the field forward by allowing researchers to instead focus efforts on producing BCPs with interesting functionality in the repeat units.

This dissertation represents several distinct attempts to increase the perceived functionality of phosphorus in BCPs. Each experimental chapter represents an expanding and unique vision for the ways in which the incorporation of phosphorus can provide improved functionality to BCPs. The self-assembly of these materials demonstrates that there is important synthetic and material design space for individuals working in this area

to explore. To continue addressing the scientific and social challenges that we face, materials that do more, have improved properties, and that researchers are able to rationally design need to be investigated. As the field continues to innovate on the design of polymer architectures the need for monomers that contain functionality beyond the limitations of carbon are required. Phosphorus is an excellent element to meet many challenges due to its ability to exist in several varied and unique chemical forms. The work presented in this dissertation is a demonstration of that and should be considered as a showing how a single element can have an important impact on the structure and behaviour of amphiphilic BCP self-assembled systems.

6.2 Future Work

6.2.1 Encapsulating Antibacterial Micelles

While the decoration of the corona of nanoparticles provides intrinsic antibacterial behaviour, the ability to coordinate different anions to the phosphonium salt was not explored. The phosphonium salt, as shown in chapter 3, ought to be able to coordinate a variety of anions. Recent work in the Ragogna and Gillies groups has investigated the ability of phosphonium salts in hydrogels to ionically bind to drug model and drug compounds. This behaviour can be introduced into phosphonium salt containing micelles.

The incorporation of an anionic or multi-anionic drug compound can increase the hydrophobicity of the phosphonium block. A triBCP with the phosphonium salt block as the middle block with PEO as the hydrophilic can serve as a drug delivery platform (Figure 6-1). The incorporation of an anionic drug compound can be made into the phosphonium block, likely decreasing the hydrophilicity; however, the PEO chains will allow the nanoparticles to remain suspended. As the drug is released the micelles become antibacterial. The synthesis could be achieved using a PEO-functionalized RAFT agent (**6.1**) previously reported in the literature by dos Santos *et al*.[11] The subsequent blocks can be polymerized from styrenic monomers as the Z group of that RAFT agent has been shown to provide good control over styrene-like monomers.[12] The resulting material should be able to undergo self-assembly in aqueous solution and associate with anionic drugs, while the volume fraction of the hydrophilic block would decrease, the frozen PS core would likely keep the particles from changing morphology. The PEO would also

ensure that the particles remain dispersed in water. The release of the drug would allow the poly(phosphonium salt) to interact with and disrupt bacterial cell walls.

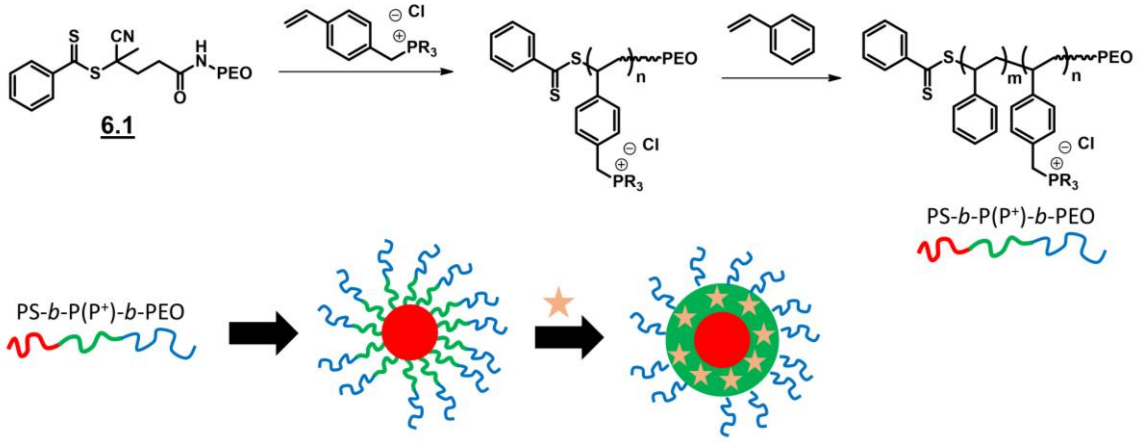

Figure 6-1. Synthesis of a PS-*b*-poly(phosphonium salt)-*b*-PEO block copolymer. The BCP could undergo SA to form nanoparticles able to load an anionic drug (yellow star).

6.2.2 Versatile Alkene-pendant Polymer for Phosphine Incorporation

While chapter 4 demonstrated the incorporation of phosphine as the hydrophobic block into an amphiphilic BCP, the design relied on a commercially available monomer, DPPS. A polymer that features pendant alkene chains should be able to undergo hydrophosphination, to create a polymer with pendant phosphine groups. This would allow researchers to generate a library of polymers that feature a variety of phosphines, all produced with that same precursor polymer. The synthetic route to such a polymer is already mostly published and the system has not been used for the formation of phosphine-containing polymers. BCPs can be made if a multifunctional RAFT agent (**6.2**) such as the one in Figure 6-2 are used, the synthesis of which has been described by the O'Reilly group.[13] The RAFT agent can be used to synthesize a hydrophilic block through radical polymerization, including phosphonium salts. The benzyl hydroxy group initiated polymerization of lactone **6.3** in the presence of an aluminum salophen catalyst **6.4**.[14] The resulting polyalkene can undergo hydrophosphination to become a polyphosphine. If the phosphine used is a secondary phosphine, then no cross-linking will occur. If the phosphine is primary, or PH_3, then cross-linking can occur of the polyalkene block. This

may be desirable for making phosphine containing gels, or nanogels stabilized by the presence of the RAFT polymerized block.

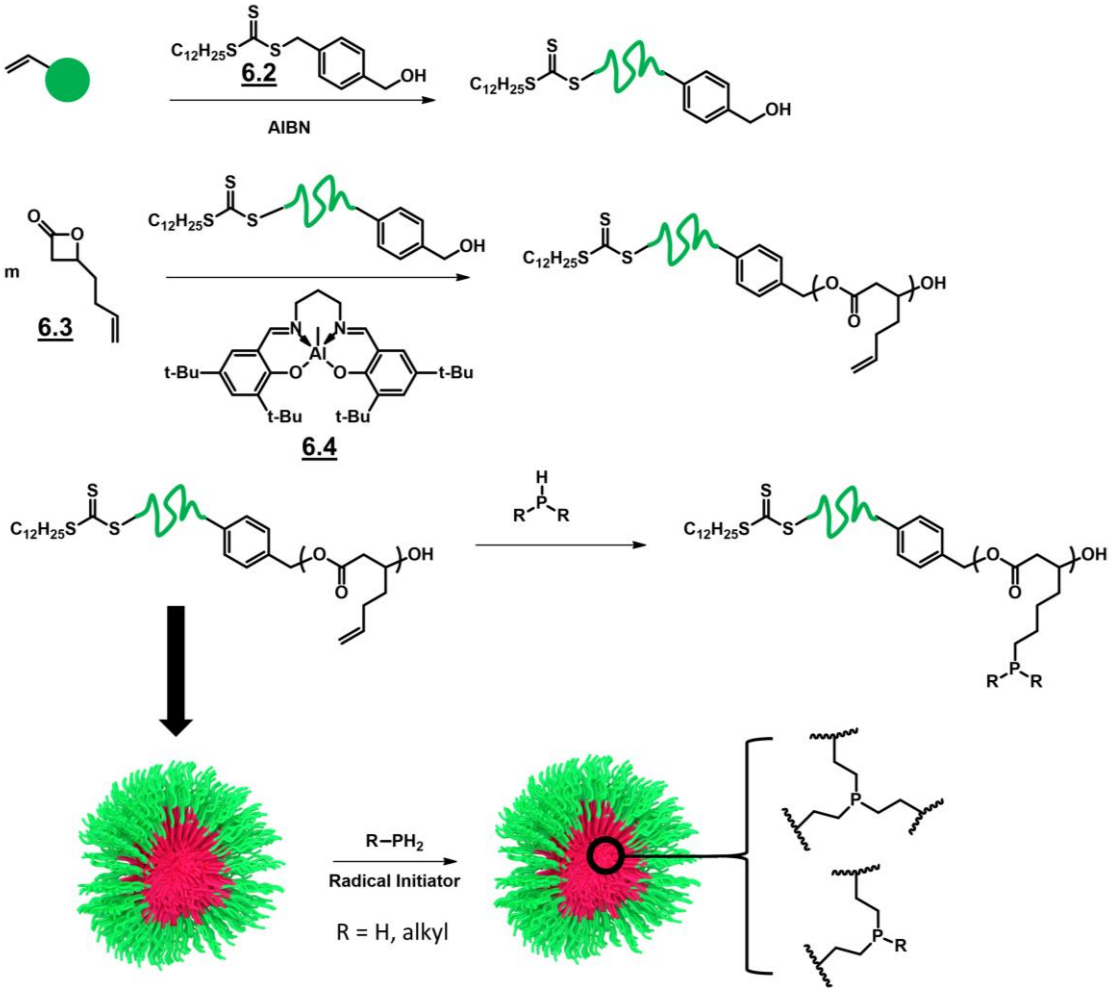

Figure 6-2. Proposed synthetic route to alkene functional amphiphilic BCP for phosphine functionalization. The hydrophilic monomer and polymer are represented by green.

6.2.3 Janus Particles Featuring Phosphonium Salts

Janus particles, particles with two distinct volumes of material in the same organizational structure (Figure 6-3), have gained recent research interest due to their promise to provide materials able to meet applications that symmetric micellar systems cannot.[15] The most promising synthetic route to Janus particles is through the self-assembly of ABC triBCPs.[16] This strategy guarantees that given the appropriate conditions, the self-assembly of ABC triBCPs will result in particles that have the

necessary components for the formation of the Janus particles. While a variety of strategies exist for the formation of Janus particles, generally the B block of the BCP is the core forming block and there ought to be a high degree of incompatibility between the A and C blocks that form the particle corona.[15,16] Other strategies include the cross-linking of one of the corona forming blocks in a fashion that will not cross-link micelles together.[16]

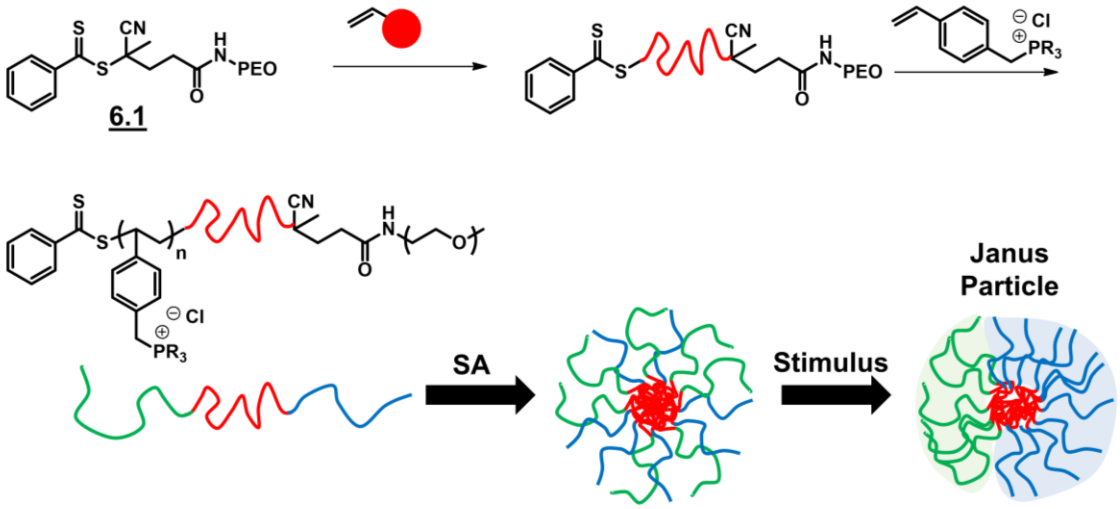

Figure 6-3. Proposed synthesis towards an amphiphilic ABC tri-BCP aimed at forming Janus particles.

Phosphonium salts can be incorporated into Janus particles through the synthesis of ABC BCPs with a poly(phosphonium salt) block. The incorporation of phosphonium salt is beneficial as it can impart antibacterial behaviour to Janus particle drug or probe carriers. It also provides a patch of positive charge on what may otherwise be a neutral structure; this can be harnessed for supramolecular assembly of the Janus particles. The RAFT agent **6.1** can be used to synthesize the BCP, synthesizing the core-forming B block first followed by the polymerization of the phosphonium salt block. Ideally the BCP would be able to undergo self-assembly in appropriate conditions. Following the successful formation of mixed corona particles the formation of Janus particles can be encouraged by the addition of a dianion, reversibly cross-linking the poly(phosphonium salt) chains on the corona similar to other studies.[17] Addition of hydrophobic anions may also be available to achieve this, and in such a case the Janus nature of the particles may be reversible if the core-forming block is non-crystalline and has a low T_g.

6.2.4 Aldehyde Degradable Polymer

Polymeric Wittig reagents have been known for several decades now.[18,19] They exist to provide a solid-state anchor for the generation of phosphonium ylide species for the heterogenous production of the desired alkene products. A common feature of these systems is the pendant ylide functionality, which allows the polymer to react without degradation of the backbone. Recent work in the Ragogna, Kerr and Workentin groups has shown that the phospha-Michael addition of phosphines to maleimide is possible, and the resulting compound is a phosphonium ylide, able to undergo Wittig reactions. That work focused on the generation of materials suitable for the use of Wittig reactions on the surface of gold nanoparticles. This inspired the idea that a similar system may be able to undergo polymerization if the maleimide was covalently bound to the phosphine, prior to undergoing phospha-Michael addition.

Scheme 6-1 shows the proposed synthetic route to these poly-ylides. The *N*-allyl maleimide (**6.5**) can be synthesised according to published procedures, from the corresponding allyl amine and maleic anhydride.[20] The alkene can be used for hydrophosphination to install the phosphine moiety capable of acting as a nucleophile in the phospha-Michael addition. The maleimide can be protected from the phospha-Michael addition during hydrophosphination by reacting the maleimide with furan to produce the protected compound **6.6**.[21] This species can react with the phosphine, and the furan removed with a retro Diels-Alder reaction to allow the monomers to undergo polymerization.

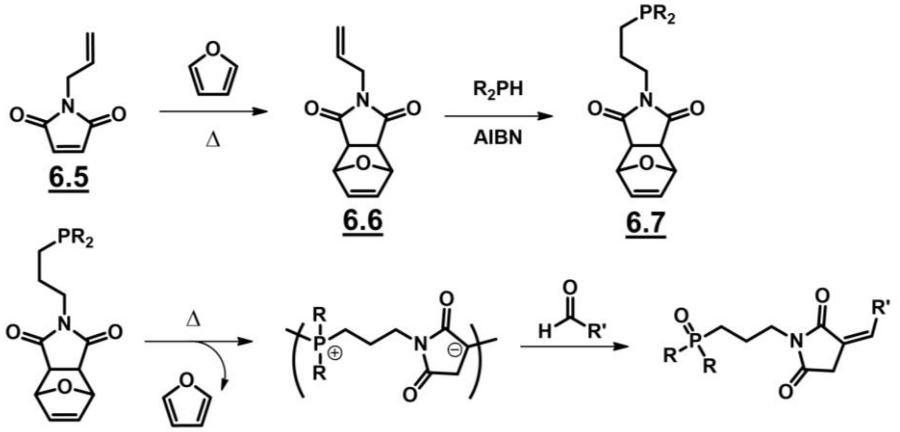

Scheme 6-1. Proposed synthetic route to a poly(phosphonium ylide). Addition of an aldehyde would degrade the polymer backbone through the Wittig reaction.

Ideally, the resulting poly(phosphonium ylide) is able to undergo Wittig reactions with aldehyde containing compounds. The Wittig reaction would degrade the backbone of the polymer and because of the covalent bond between the maleimide and the phosphorus, the resulting phosphine oxide would also become part of the product. The degradation of polymer backbone by an aldehyde has been only reported once before by Chimpibul and co-workers in a dextran system.[22]

6.3 References

1. R. K. O'Reilly, M. J. Joralemon, K. L. Wooley, C. J. Hawker, *Chem. Mater.*, 2005, **17**, 5976-5988
2. Q. L. Feng, J. Wu, G. Q. Chen, F. Z. Cui, T. N. Kim, J. O. Kim, *J. Biomed. Mater. Res.*, 2000, **52**, 662–668.
3. M. Yamanaka, K. Hara, J. Kudo, *Appl. Environ. Microbiol.*, 2005, **71**, 7589–7593.
4. H. Lu, L. Fan, Q. Liu, J. Wei, T. Ren, J. Du, *Polym. Chem.*, 2012, **3**, 2217.
5. S. D. Steichen, M. Caldorera-Moore, N. A. Peppas, *Eur. J. Pharm. Sci.*, 2013, **48**, 416-427
6. C. Oerlemans, W. Bult, M. Bos, G. Storm, J. F. W. Nijsen, W. E. Hinnik, *Pharm. Res.*, 2010, **27**, 2569-2589
7. I. W. Hamley, *Block Copolymers in Solution: Fundementals and Applications*, John Wiley & Sons, Inc., Chichester, 2005.
8. P. Alexandridis, B. Lindman, *Amphiphilic Block Copolymers: Self-Assembly and Applications*, Elsevier Science B.V., Amsterdam, 2000.
9. S. Doherty, J. G. Knight, T. Backhouse, E. Abood, H. Alshaikh, I. J. S. Fairlamb, R. A. Bourne, T. W. Chamberlain, R. Stones, *Green Chem.*, 2017, **19**, 1635–1641.
10. E. Lobry, A. F. Cardozo, L. Barthe, J.-F. F. Blanco, H. Delmas, S. Chen, F. Gayet, X. Zhang, M. Lansalot, F. D'Agosto, R. Poli, E. Manoury, C. Julcour, *J. Catal.*, 2016, **342**, 164–172.
11. A. M. dos Santos, J. Pohn, M. Lansalot, F. D'Agosto, *Macromol. Rapid Commun.*, 2007, **28**, 1325-1332

12. D. J. Keddie, G. Moad, E. Rizzardo, S. H. Thang, *Macromolecules*, 2012, **45**, 5321-5342

13. N. Petzatakis, A. P. Dove, R. K. O'Reilly, *Chem. Sci.*, 2011, **2**, 955-960

14. F. Sinclair, L. Chen, B. W. Greenland, M. P. Shaver, *Macromolecules*, 2016, **49**, 6826-6834

15. Y. Sheng, X. Yang, N. Yan, Y. Zhu, *Soft Matter*, 2013, **9**, 6254-6262

16. R. Deng, F. Liang, J. Zhu, Z. Yang, *Mater. Chem. Front.*, 2017, **1**, 431-443

17. J. Du, S. P. Armes, *Soft Matter*, 2010, **6**, 4851-4857

18. W. Heitz, R. Michels, *Angew. Chem. Int. Ed.*, 1972, **2**, 298-299

19. A. Akelah, *Reactive Polymers, Ion Exchanges, Sorbents*, 1988, **8**, 273-284

20. A. Gómez-SanJuan, N. Sotomayor, E. Lete, *Eur. J. Org. Chem.*, 2013, **2013**, 6722-6732

21. W. K. Anderson, A. S. Milowsky, *J. Org. Chem.*, 1985, **50**, 5423-5424

22. W. Chimpibul, T. Nagashima, F. Hayashi, N. Nakajima, S.-H. Hyon, K. Matsumura, *J. Poly. Sci. Part A Poly. Chem.*, 2016, **54**, 2254-2260

Appendix A – Supplementary Information for Chapter 2

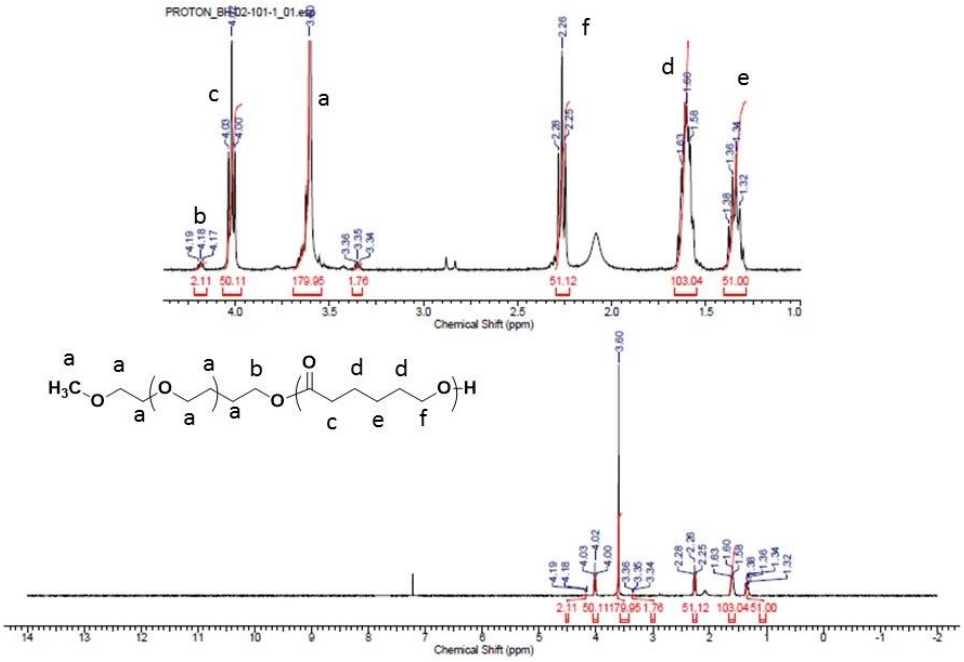

Figure A-1. ^{1}H NMR spectrum of **MeO-BCP** ($CDCl_3$, 400 MHz).

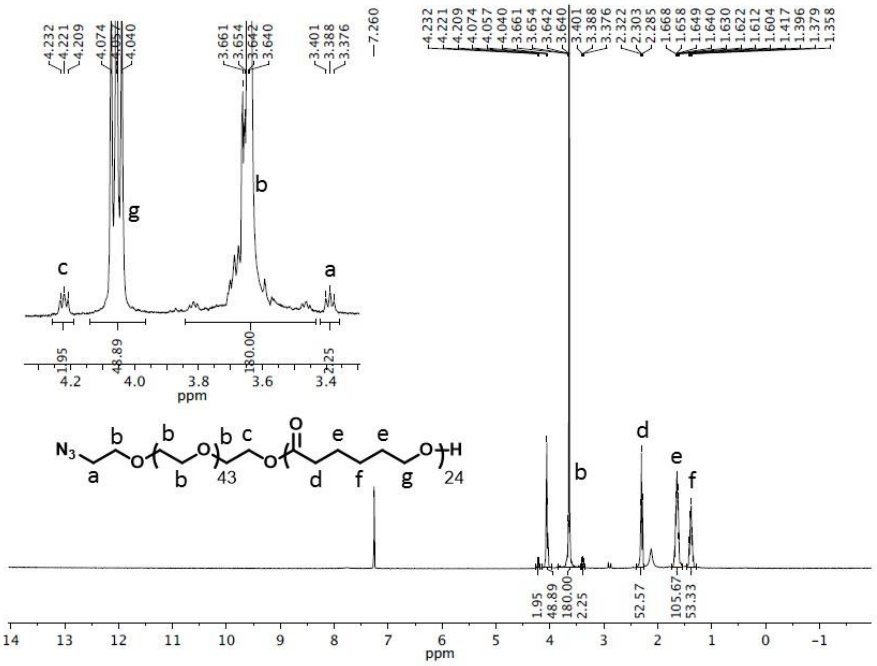

Figure A-2. ^{1}H NMR spectrum of **N_3-BCP** ($CDCl_3$, 400 MHz).

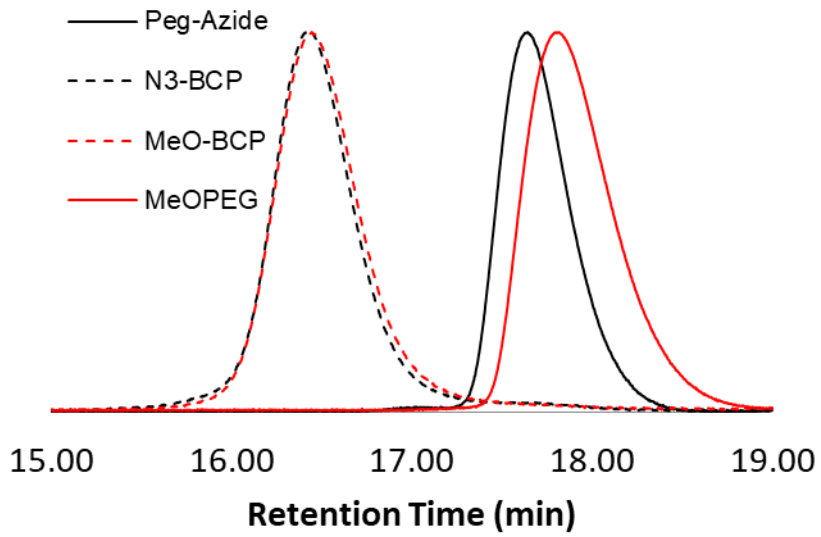

Figure A-3. SEC traces of **MeO-PEO** (M_n = 2000 g/mol, *Đ* = 1.01), **N_3-BCP** (M_n = 2200 g/mol, *Đ* = 1.01), **MeO-BCP** (M_n = 5750 g/mol, *Đ* = 1.11), **N_3-BCP** (M_n = 5950 g/mol, *Đ* = 1.12).

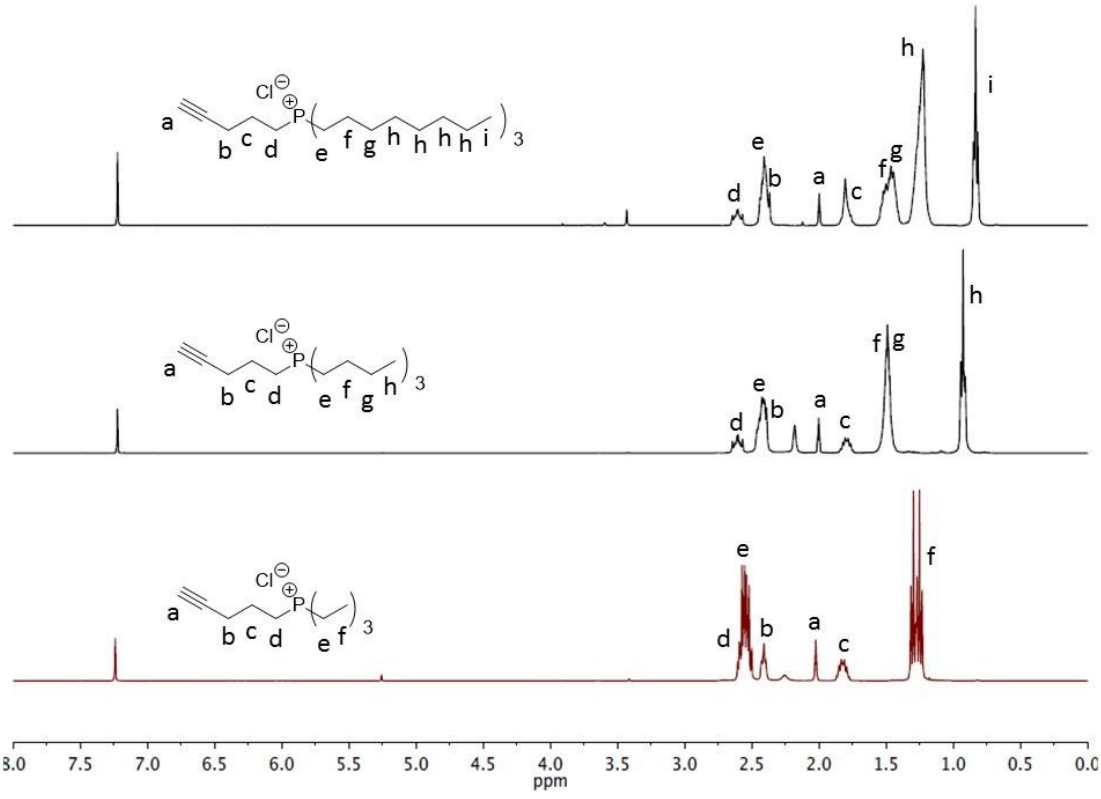

Figure A-4. Full ^{1}H NMR spectra of Alk_3P-yne chlorides ($CDCl_3$, 400 MHz).

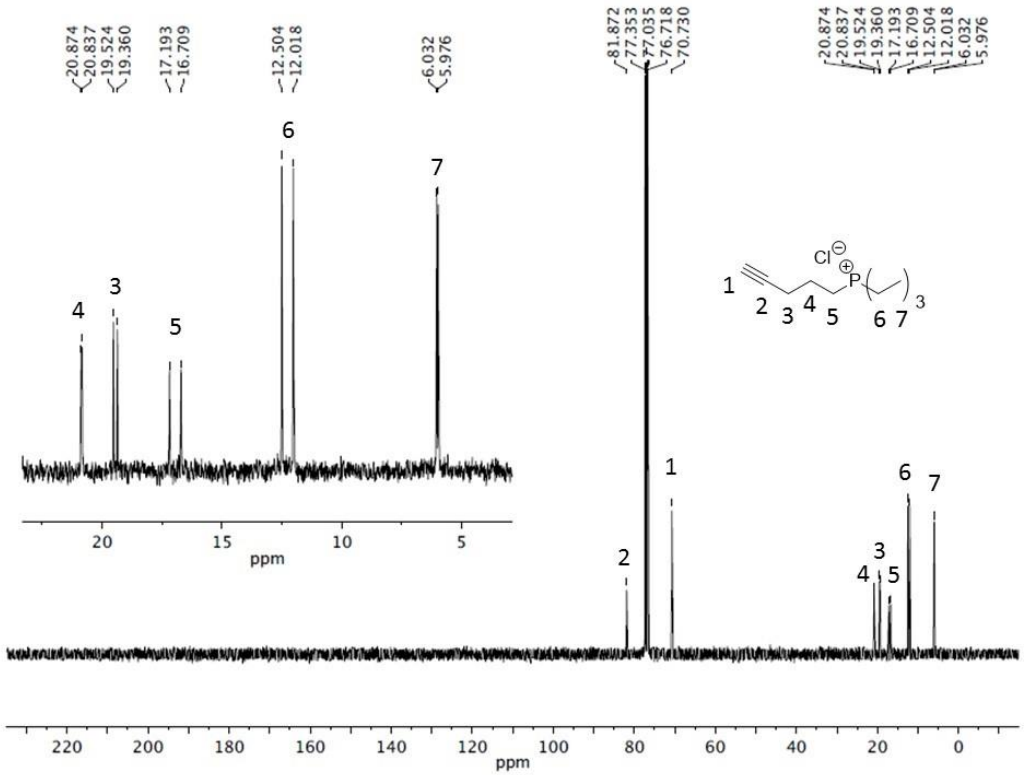

Figure A-5. ^{13}C NMR spectrum of **Et$_3$P-yne** ($CDCl_3$, 100 MHz).

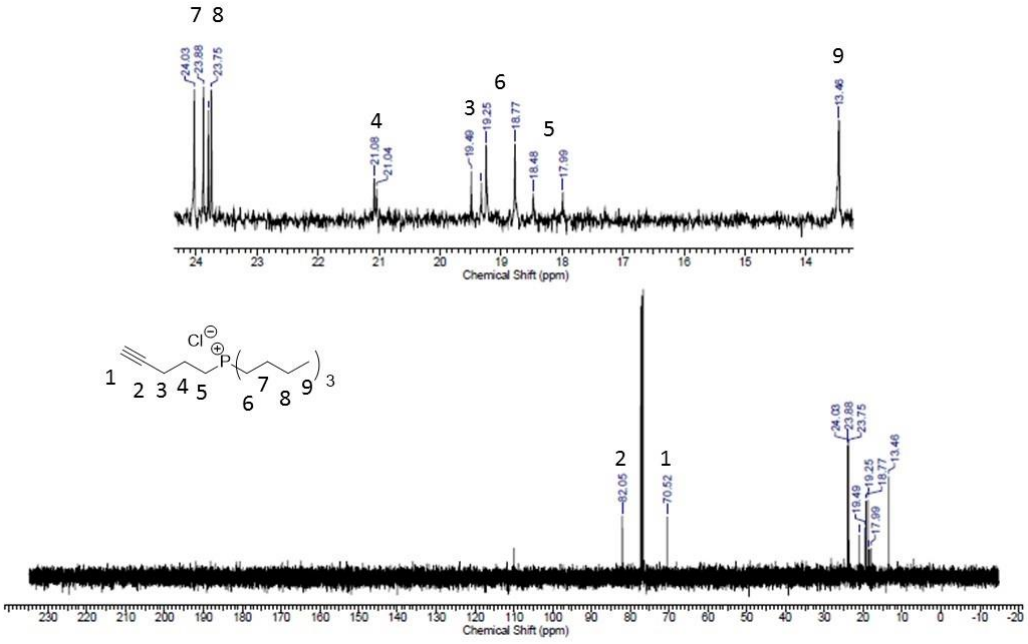

Figure A-6. ^{13}C NMR spectrum of **Bu$_3$P-yne** ($CDCl_3$, 100 MHz).

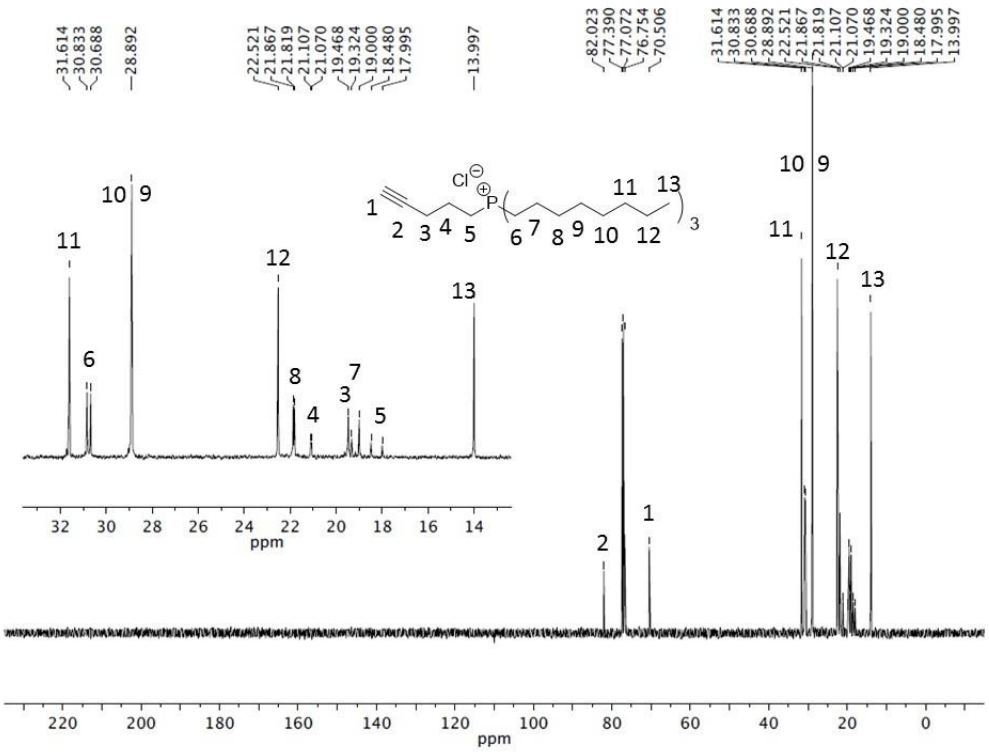

Figure A-7. ^{13}C NMR spectrum of **Oct$_3$P-yne** ($CDCl_3$, 100 MHz).

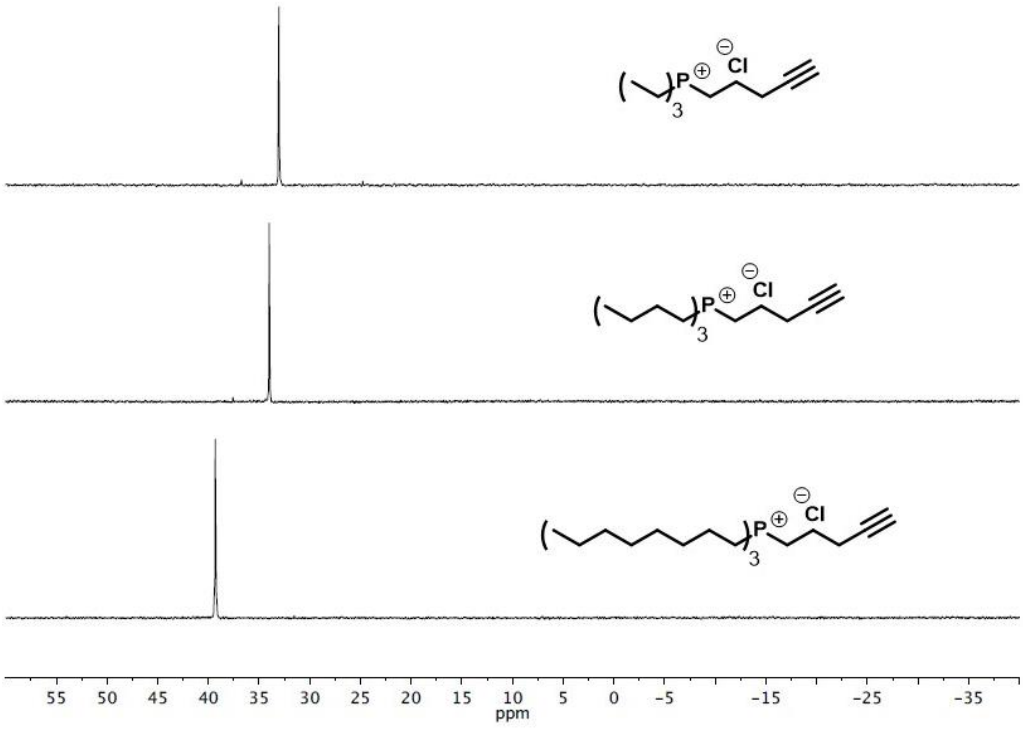

Figure A-8. Stack plot of ^{31}P NMR spectra of Alk$_3$P-ynes ($CDCl_3$, 161 MHz).

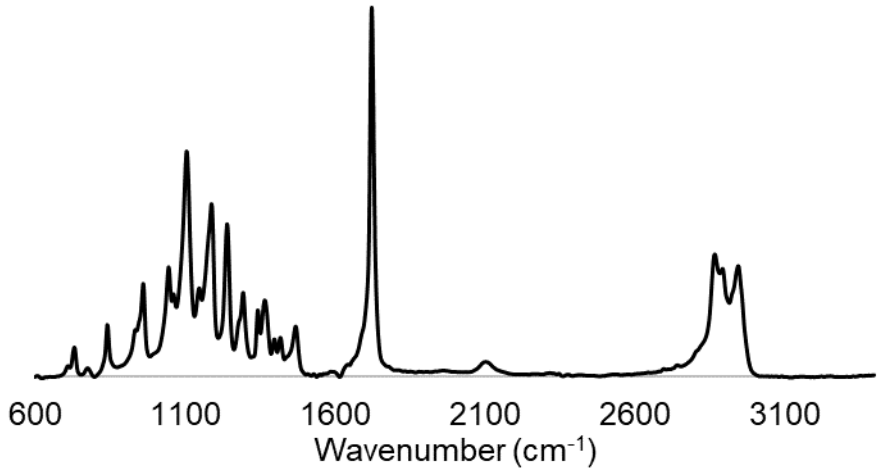

Figure A-9. ATR-IR spectrum of **N_3-BCP**

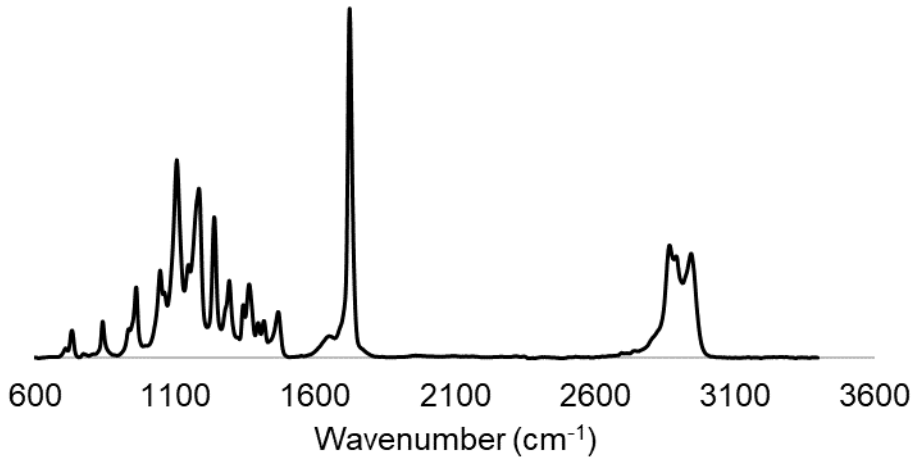

Figure A-10. Representative ATR-IR spectrum of **Et_3P-BCP** after cycloaddition with the alkyne-functionalized phosphonium, followed by dialysis.

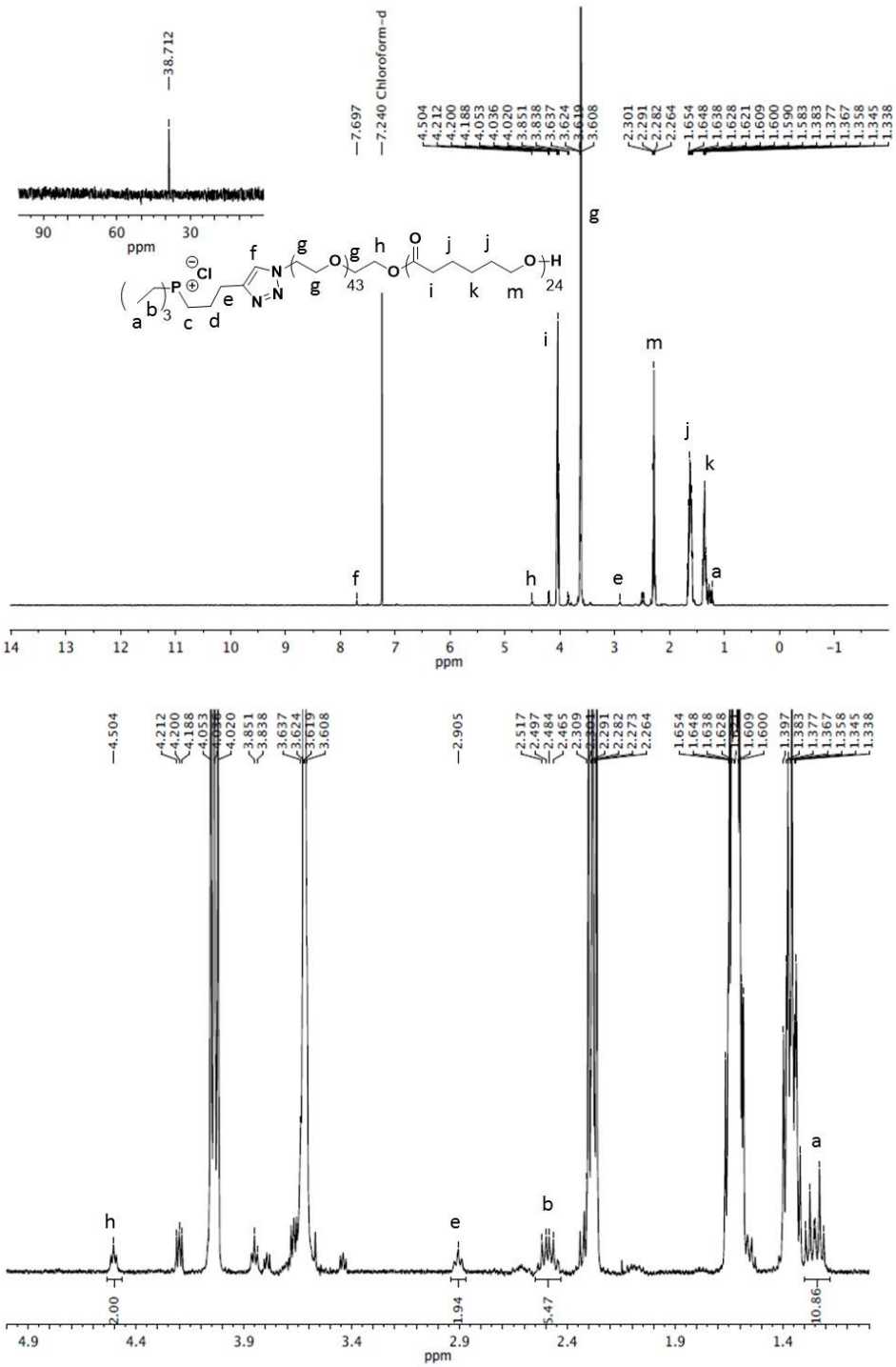

Figure A-11. ^{1}H NMR spectrum (400 MHz, $CDCl_3$) of **Et$_3$P-BCP** with a blow-up of the region from 1 – 4.6 ppm and an inset of ^{31}P NMR spectrum (161 MHz, $CDCl_3$).

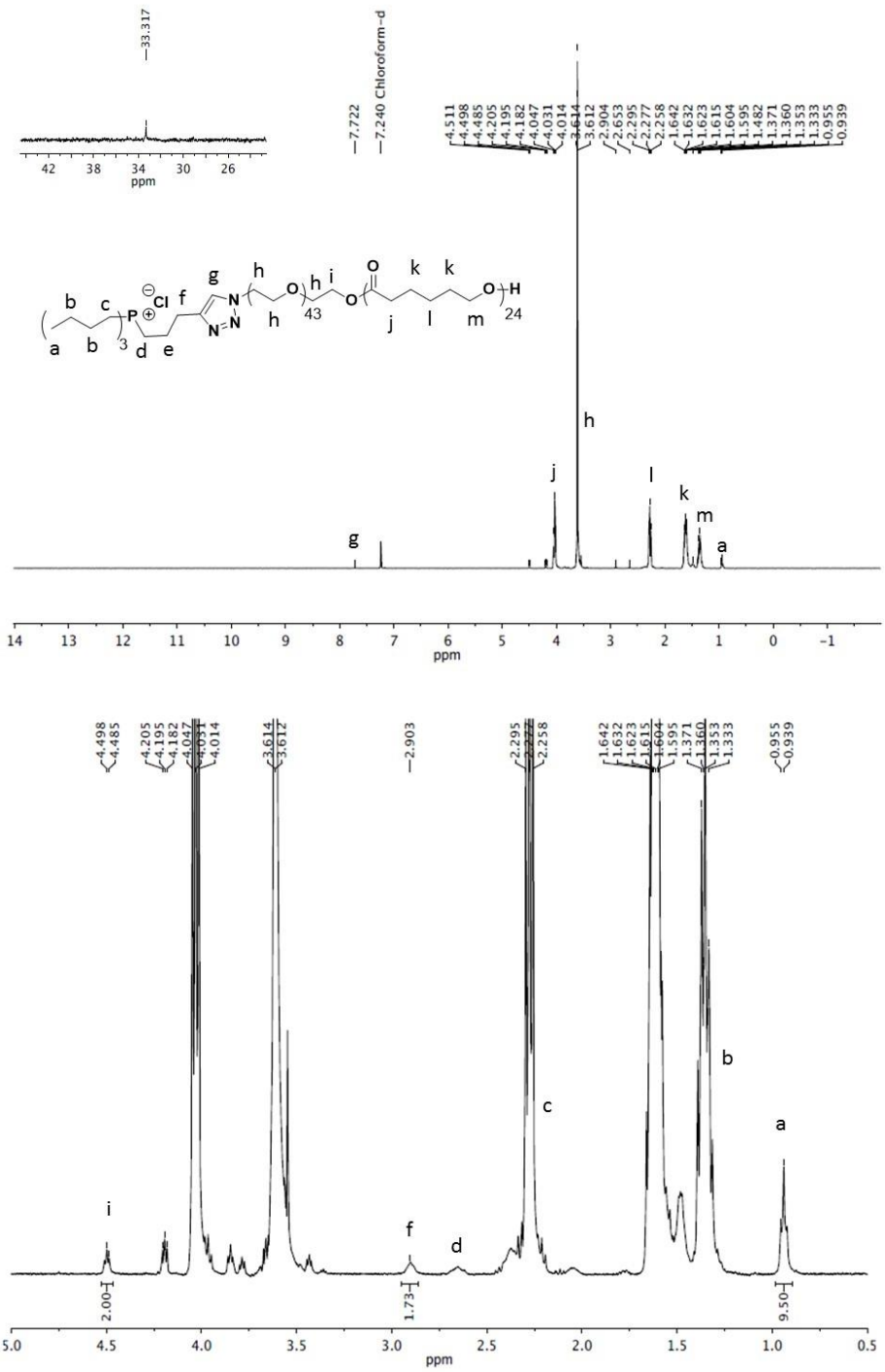

Figure A-12. ^{1}H NMR spectrum (400 MHz, $CDCl_3$) of **Bu_3P-BCP** with a blow-up of the region from 0.5 – 5.0 ppm and an inset of ^{31}P NMR spectrum (161 MHz, $CDCl_3$).

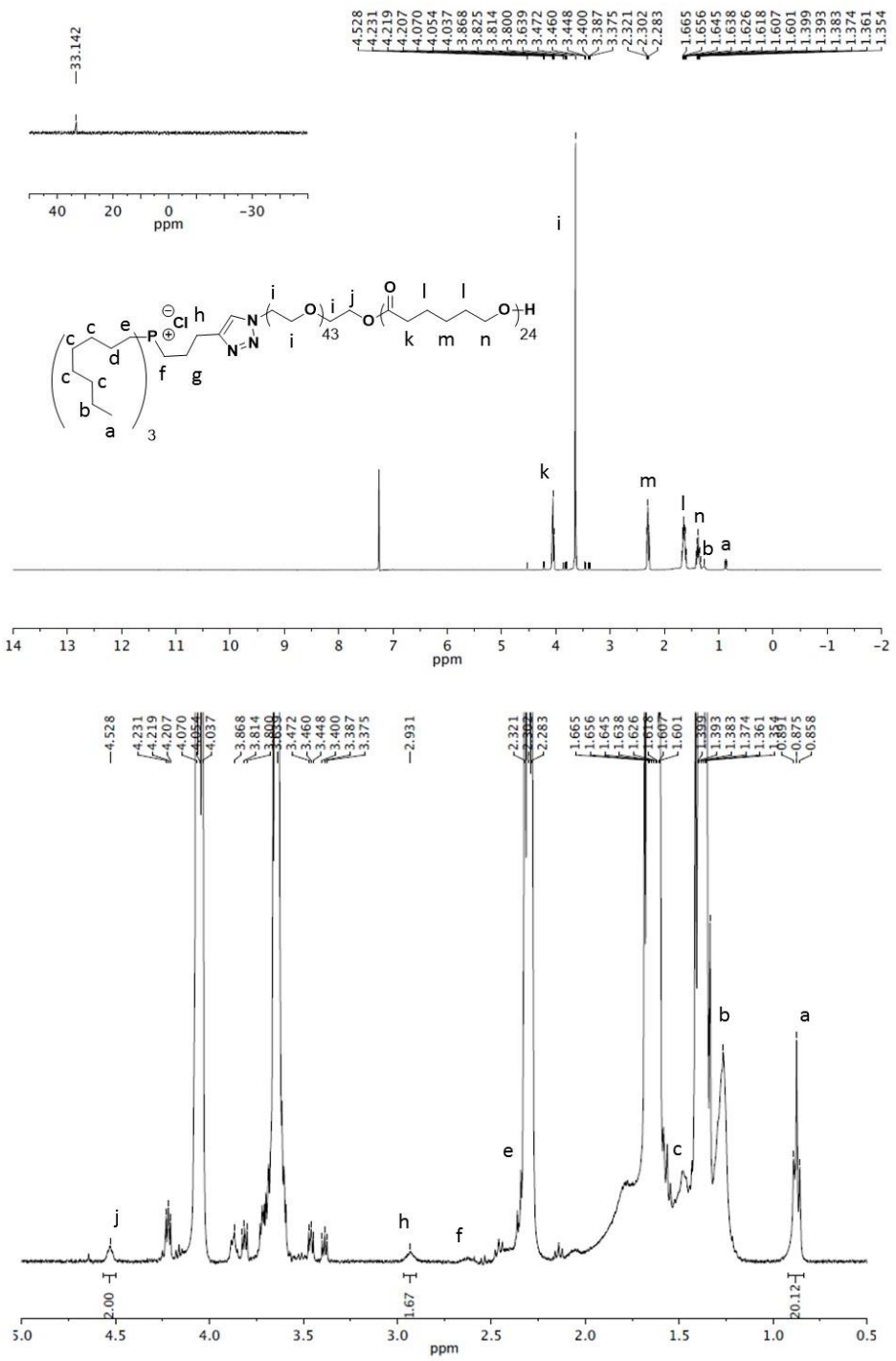

Figure A-13. ^{1}H NMR spectrum (400 MHz, $CDCl_3$) of **Oct_3P-BCP** with a blow-up of the region from 0.5 – 5.0 ppm and an inset of ^{31}P NMR spectrum (161 MHz, $CDCl_3$).

Compound	Concentration (mg/mL)						
	10.00	5.00	2.50	1.25	0.63	0.31	0.016
Et_3P-yne	+ / + / +	+ / + / +	+ / + / +	+ / + / +	+ / + / +	+ / + / +	N/A
Bu_3P-yne	- / - / -	- / - / -	- / - / -	- / - / -	+ / + / +	+ / + / +	N/A
MeO-BCP	N/A	+ / + / +	+ / + / +	+ / + / +	+ / + / +	+ / + / +	N/A
Et_3P-BCP	N/A	- / - / -	- / - / -	- / - / -	+ / + / +	+ / + / +	N/A
Bu_3P-BCP	N/A	- / - / -	- / - / -	- / - / -	- / - / -	+ / + / +	N/A
Oct_3P-BCP	N/A	- / - / -	- / - / -	- / - / -	- / - / -	- / - / -	- / - / -

Table A-1. Bacterial growth for tests against *S. aureus* a "-" indicates no colony forming units observed, a "+" indicates colony forming units observed. Measurements were performed in triplicate.

Compound	Concentration (mg/mL)					
	10.00	5.00	2.50	1.25	0.63	0.31
Et_3P-yne	+ / + / +	+ / + / +	+ / + / +	+ / + / +	+ / + / +	+ / + / +
Bu_3P-yne	- / - / -	+ / + / +	+ / + / +	+ / + / +	+ / + / +	+ / + / +
MeO-BCP	N/A	+ / + / +	+ / + / +	+ / + / +	+ / + / +	+ / + / +
Et_3P-BCP	N/A	- / - / -	- / - / -	+ / + / +	+ / + / +	+ / + / +
Bu_3P-BCP	N/A	- / - / -	- / - / -	- / - / -	- / - / -	+ / + / +
Oct_3P-BCP	N/A	- / - / -	+ / + / +	+ / + / +	+ / + / +	+ / + / +

Table A-2. Bacterial growth for tests against *E. coli* a "-" indicates no colony forming units observed, a "+" indicates colony forming units observed. Measurements were performed in triplicate.

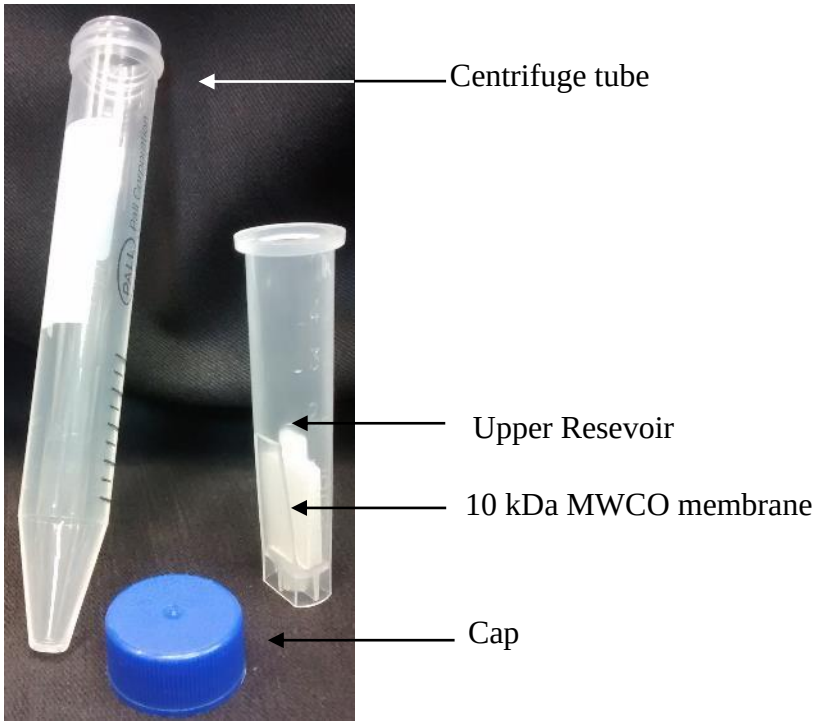

Figure A-14. Centrifugal ultrafiltration device

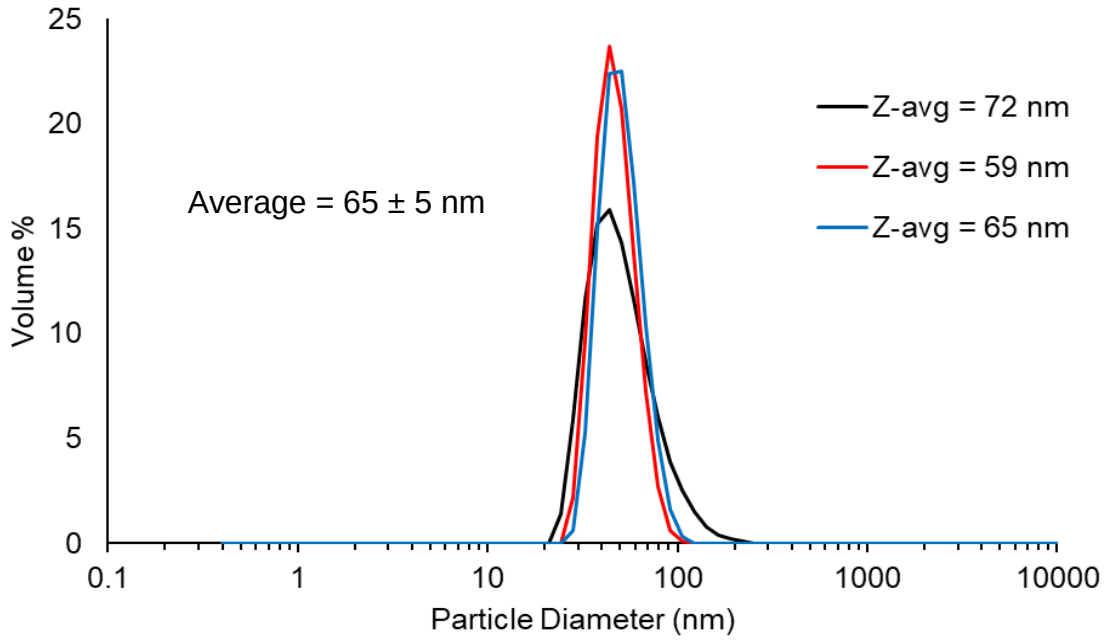

Figure A-15. DLS volume % plots of MeO-BCP micelles encapsulated with tetracycline, after removal of excess tetracycline.

Appendix B – Supplemental Information for Chapter 3

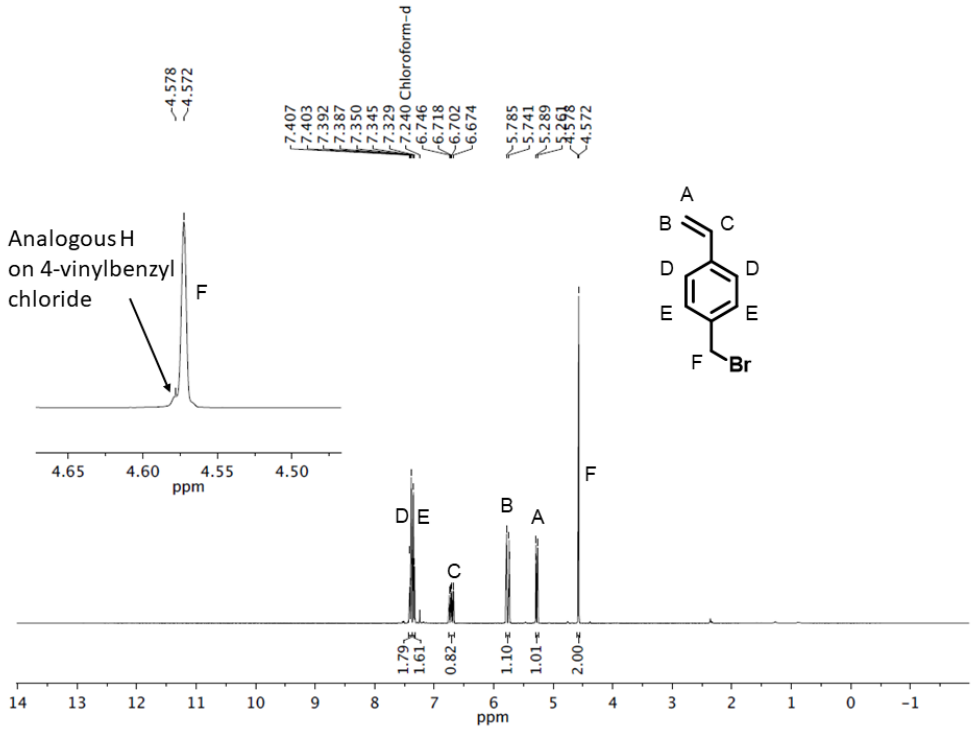

Figure B-1. ^{1}H NMR of **3.7** showing remaining 4-vinylbenzyl chloride (400 MHz, $CDCl_3$).

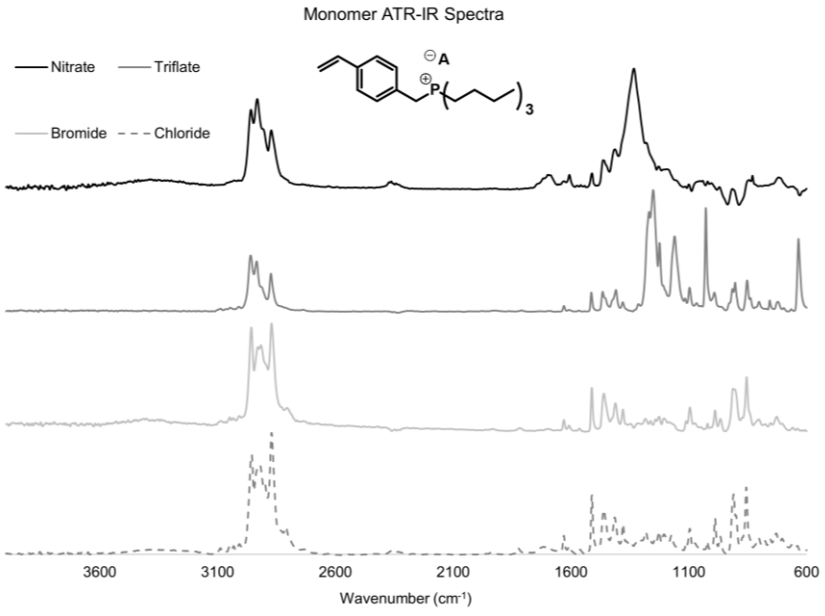

Figure B-2. ATR-IR spectra of the monomer salts

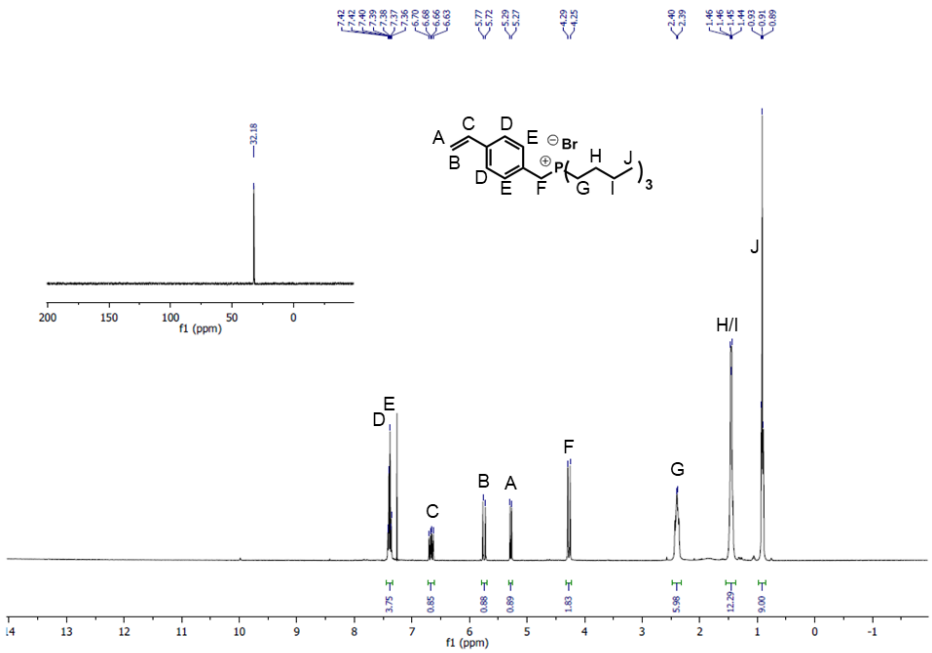

Figure B-3. ^{1}H NMR spectrum of **3.8-Br**. Inset $^{31}P\{^{1}H\}$ NMR spectrum (400 MHz, $CDCl_3$).

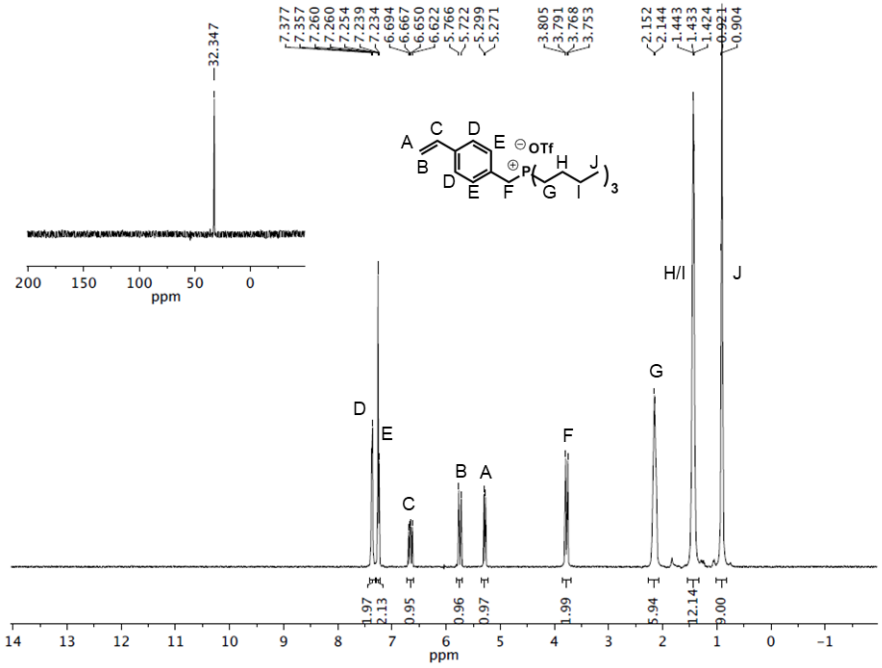

Figure B-4. ^{1}H NMR spectrum of **3.8-OTf**. Insert $^{31}P\{^{1}H\}$ NMR spectrum (400 MHz, $CDCl_3$).

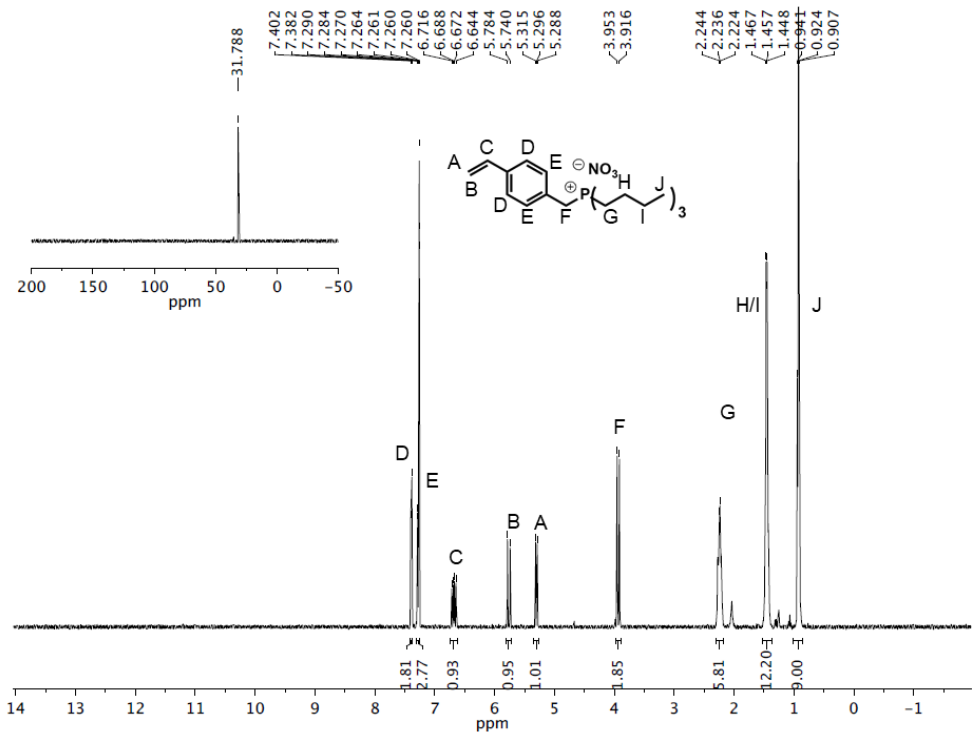

Figure B-5. ^{1}H NMR spectrum of **3.8-NO$_3$**. Insert $^{31}P\{^{1}H\}$ NMR spectrum (400 MHz, $CDCl_3$).

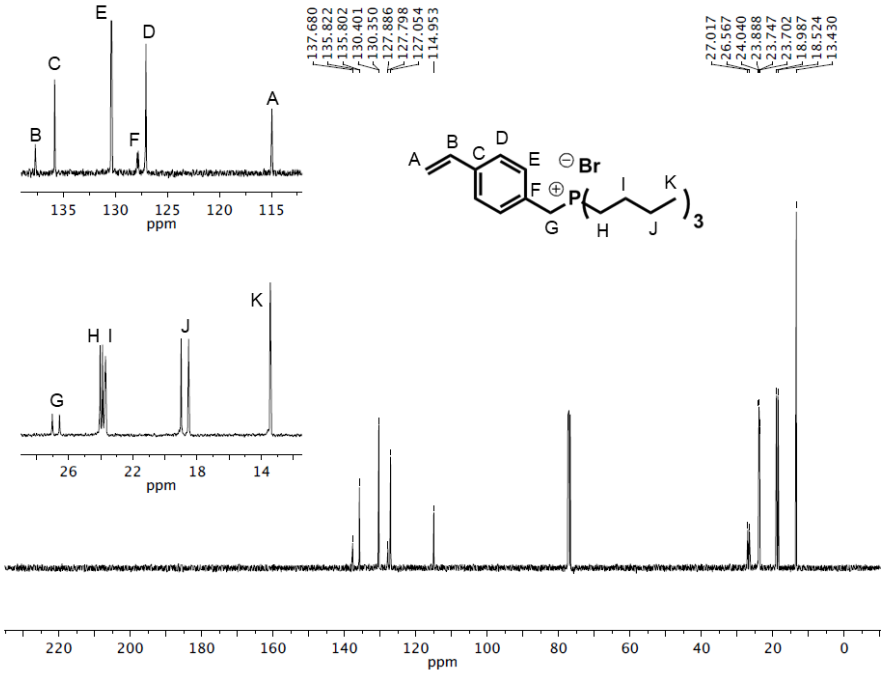

Figure B-6. ^{13}C NMR spectrum of **3.8-Br** (400 MHz, $CDCl_3$).

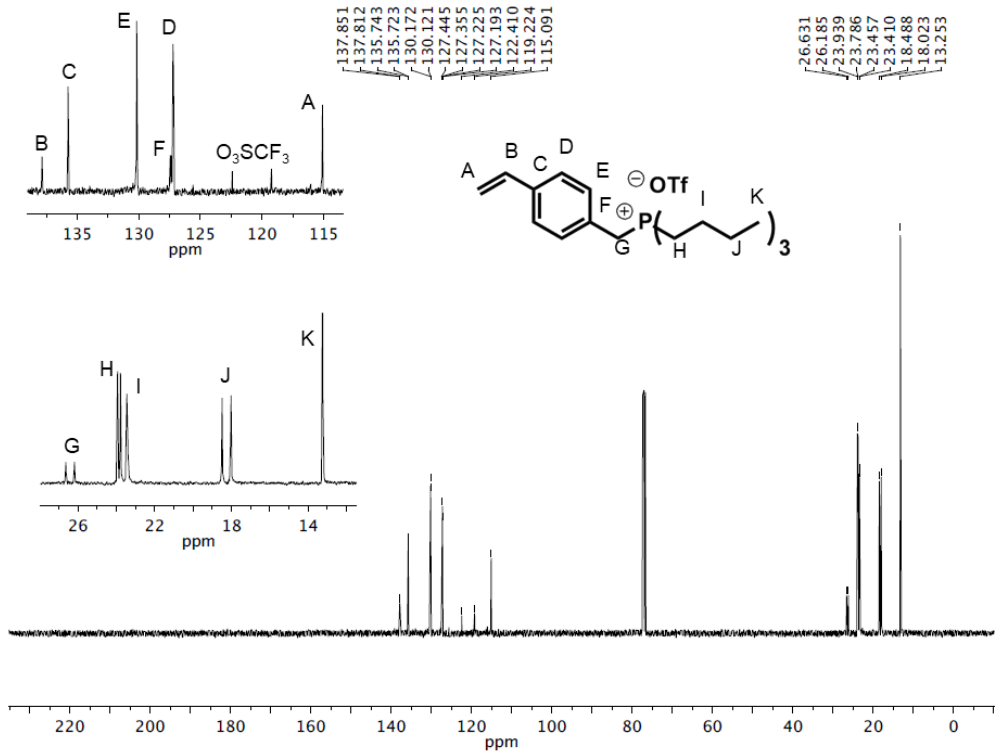

Figure B-7. ^{13}C NMR spectrum of **3.8-OTf** (400 MHz, $CDCl_3$).

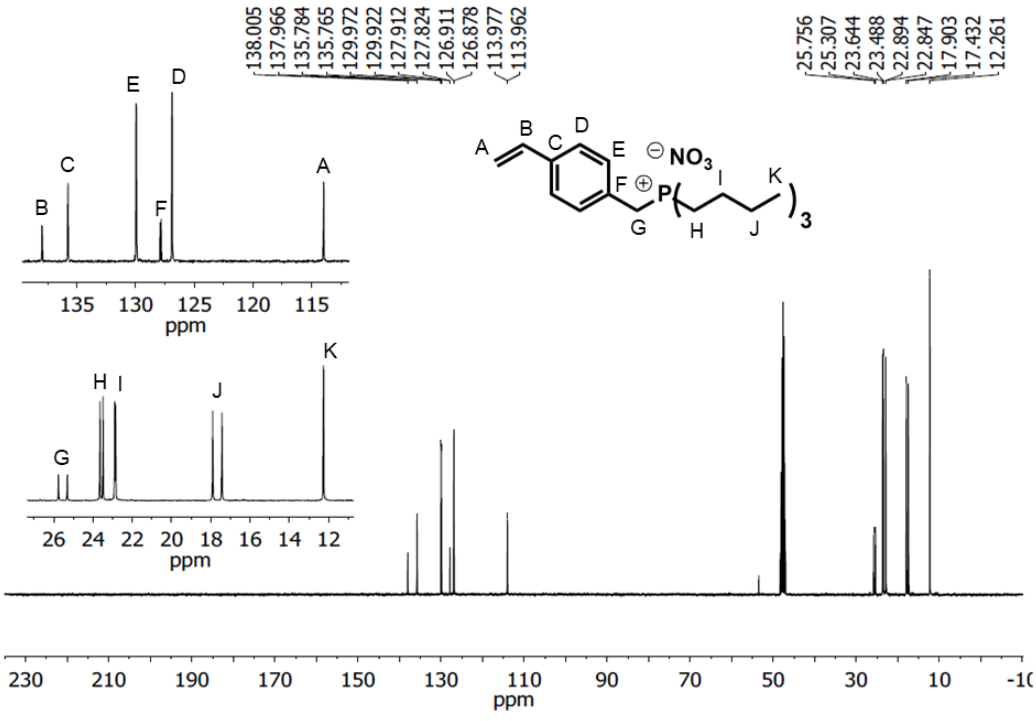

Figure B-8. ^{13}C NMR spectrum of **3.8-NO_3** (400 MHz, $CDCl_3$).

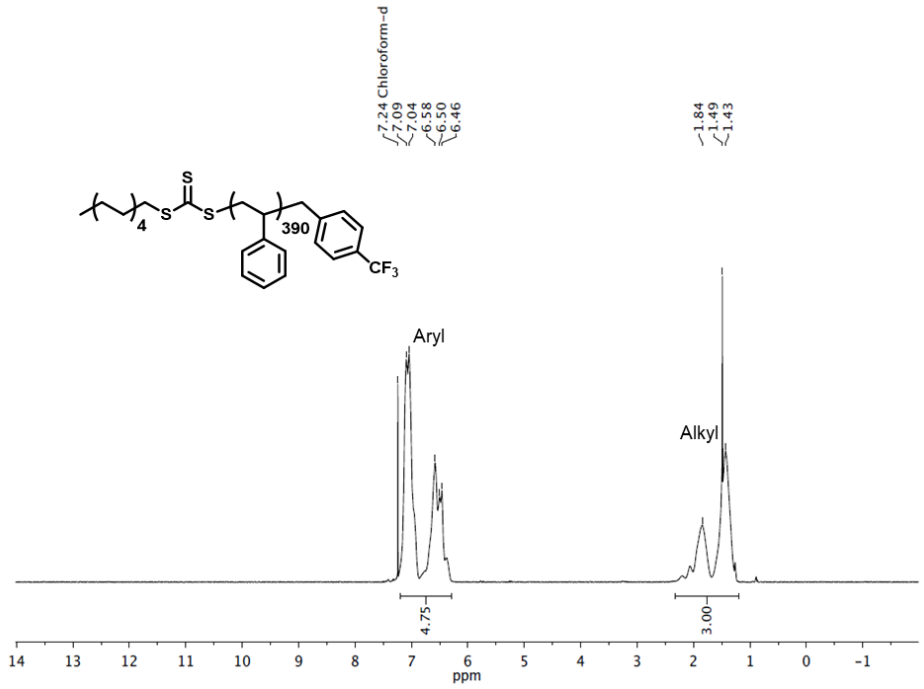

Figure B-9. ^{1}H NMR spectrum of the polystyrene macroRAFT agent. The end-groups are not seen due to the DP of the polymer. (400 MHz, $CDCl_3$)

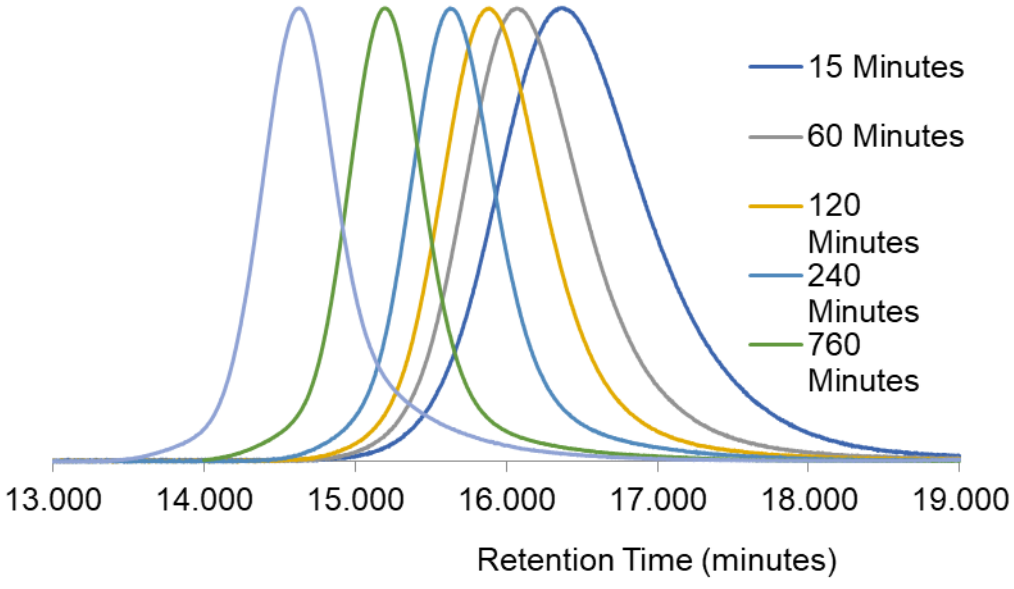

Figure B-10. SEC traces of RAFT polymerization of neat styrene

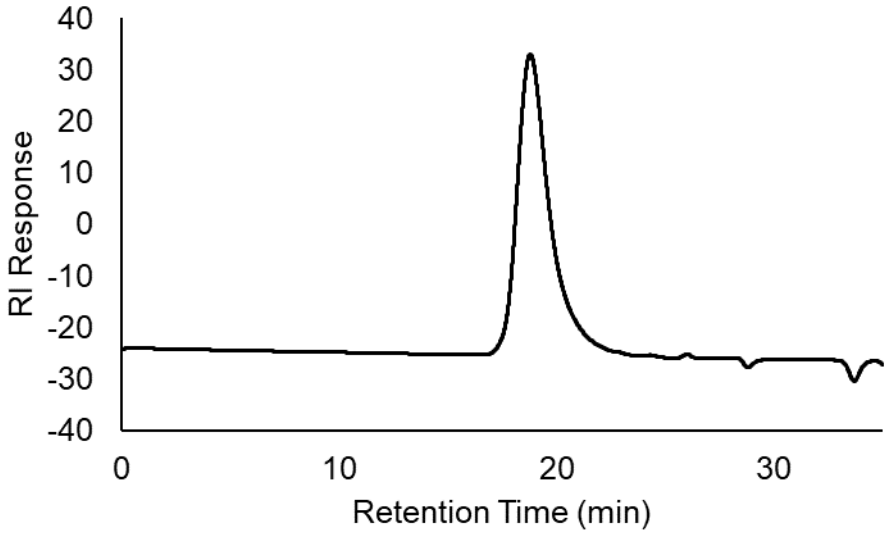

Figure B-11. SEC trace of **PS$_{390}$-*b*-P(3.8-Cl)$_7$**

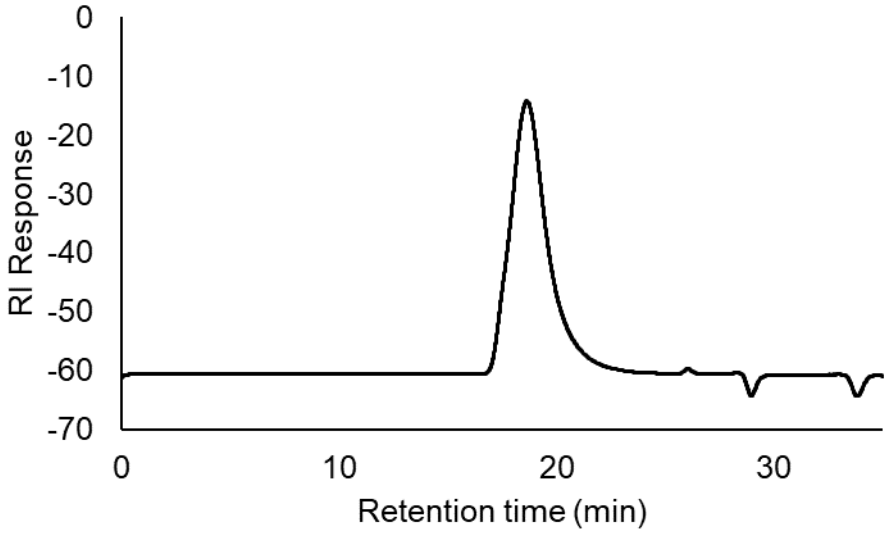

Figure B-12. SEC trace of **PS$_{390}$-*b*-P(3.8-NO$_3$)$_7$**

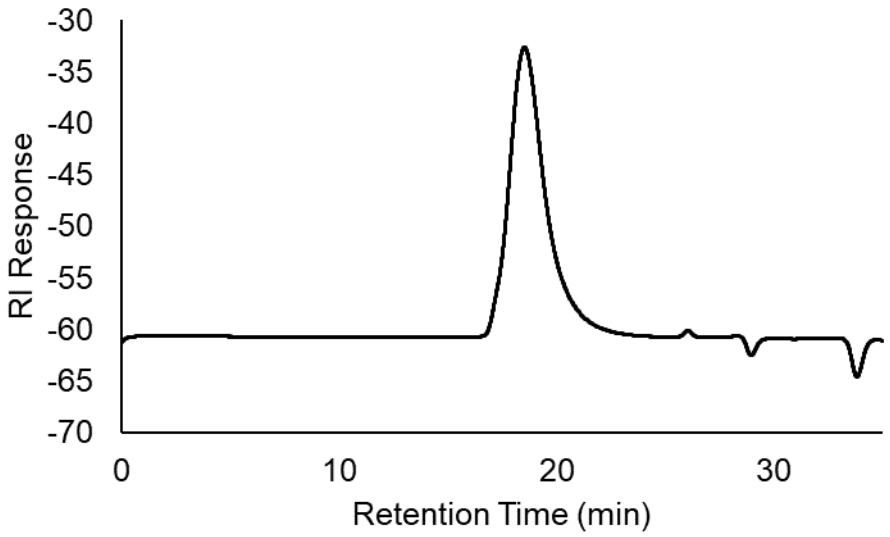

Figure B-13. SEC trace of **PS$_{390}$-*b*-P(3.8-OTF)$_7$**

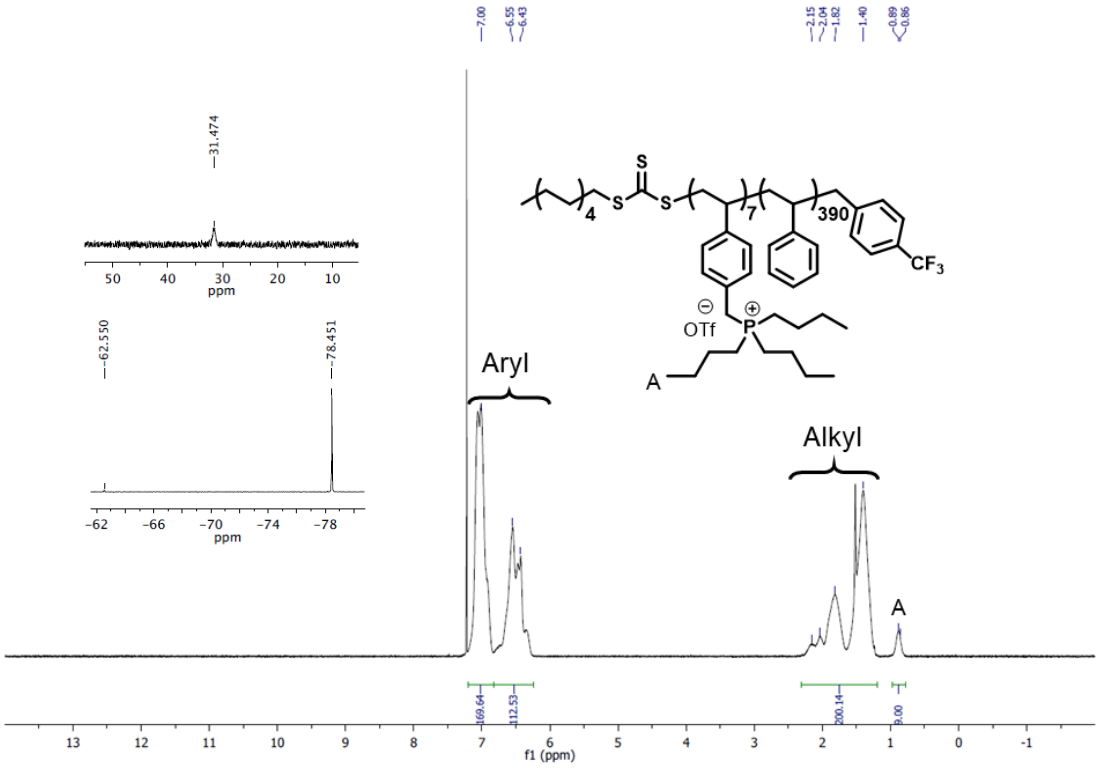

Figure B-14. ^{1}H NMR (400 MHz, $CDCl_3$) spectrum of **PS$_{390}$-*b*-P(3.8-OTf)$_7$**. The top inset is the ^{31}P{^{1}H} NMR (161 MHz) spectrum. The bottom inset is the ^{19}F NMR (376 MHz) spectrum.

Determination of phosphonium block DP from ^{1}H NMR spectroscopy

The length of the phosphonium block was determined relative to the length of the polystyrene block. The peak labelled A in the spectrum represents the 9 methyl protons of the phosphonium salt repeat unit. The remainder of the 200 alkyl protons (relative to the phosphonium salt methyl protons) are due to the backbone of the styrene block, as well as the 23 other protons present on the phosphonium repeat unit. This means there are 177 alkyl protons on styrene repeat units relative to each phosphonium repeat unit giving a ratio of 59 styrene units per phosphonium unit. From the size exclusion chromatogram the DP of the styrene unit is 390, meaning there is a total of approximately 7 phosphonium units per polymer chain.

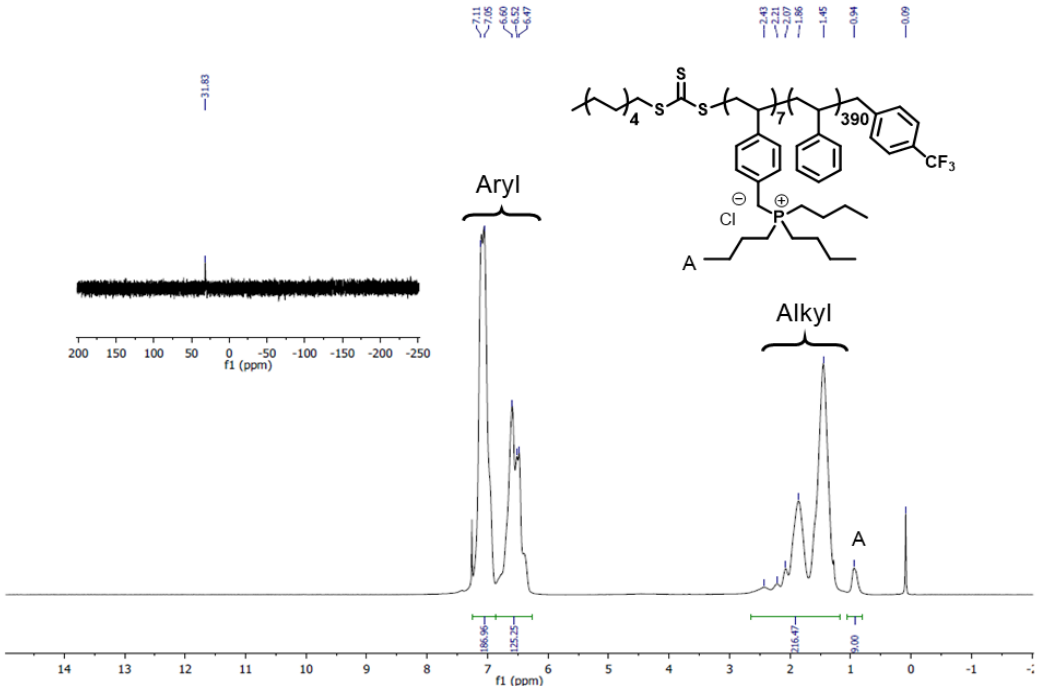

Figure B-15. ^{1}H NMR (400 MHz, $CDCl_3$) spectrum of **PS-*b*-P(3.8-Cl)**. The inset is the $^{31}P\{^{1}H\}$ NMR (161 MHz) spectrum.

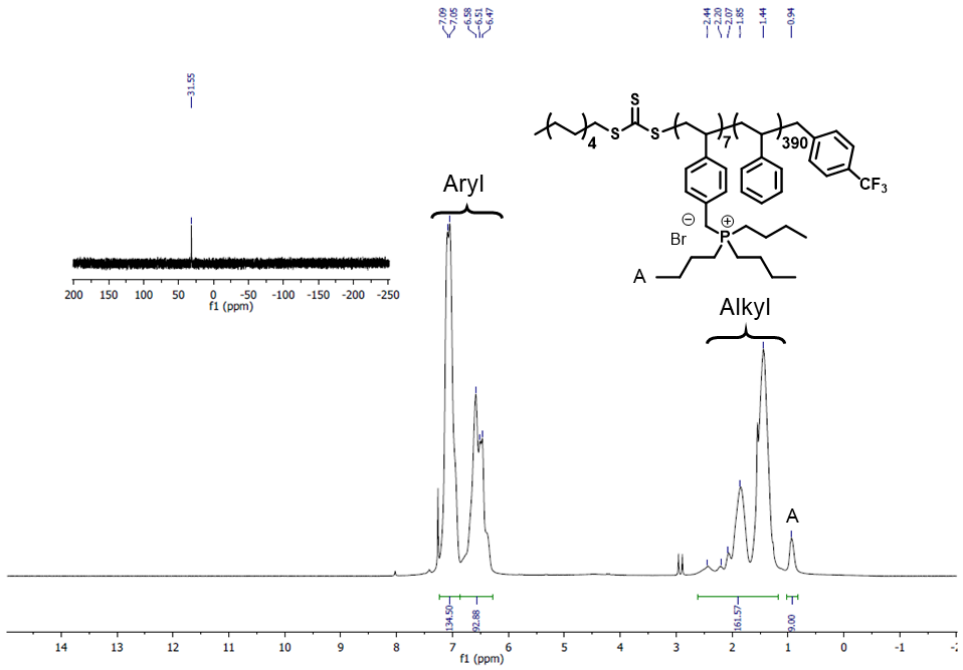

Figure B-16. ^{1}H NMR ($CDCl_3$, 400 MHz). spectrum of **PS-*b*-P(3.8-Br)** The inset is the $^{31}P\{^{1}H\}$ NMR spectrum (161 MHz).

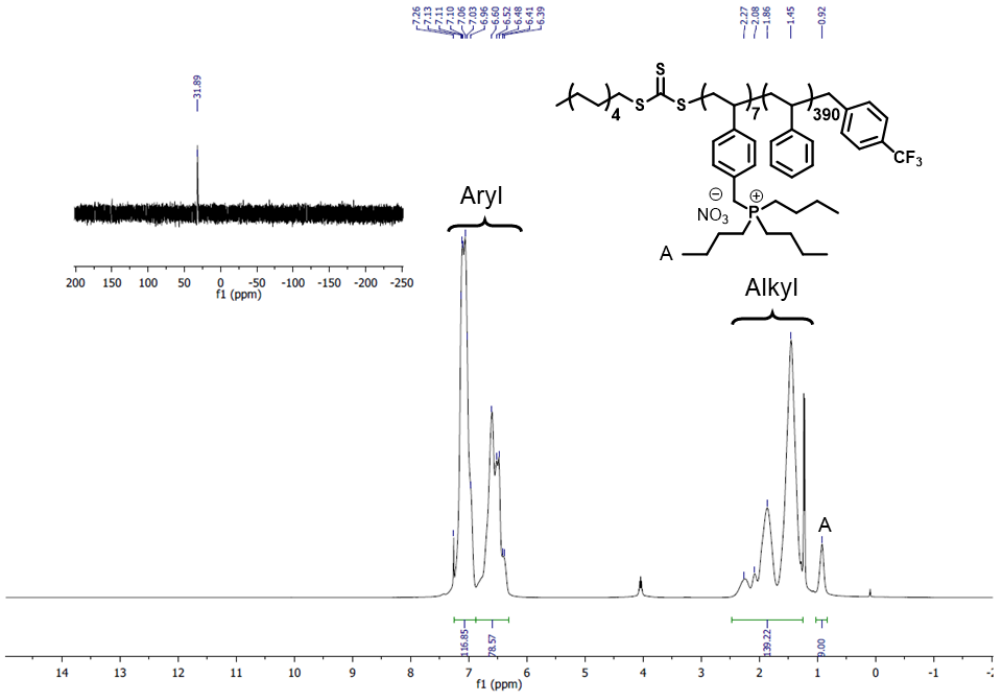

Figure B-17. ^{1}H NMR ($CDCl_3$, 400 MHz) spectrum of **PS-*b*-P(3.8-NO_3)**. Insert is $^{31}P\{^{1}H\}$ NMR spectrum (161 MHz).

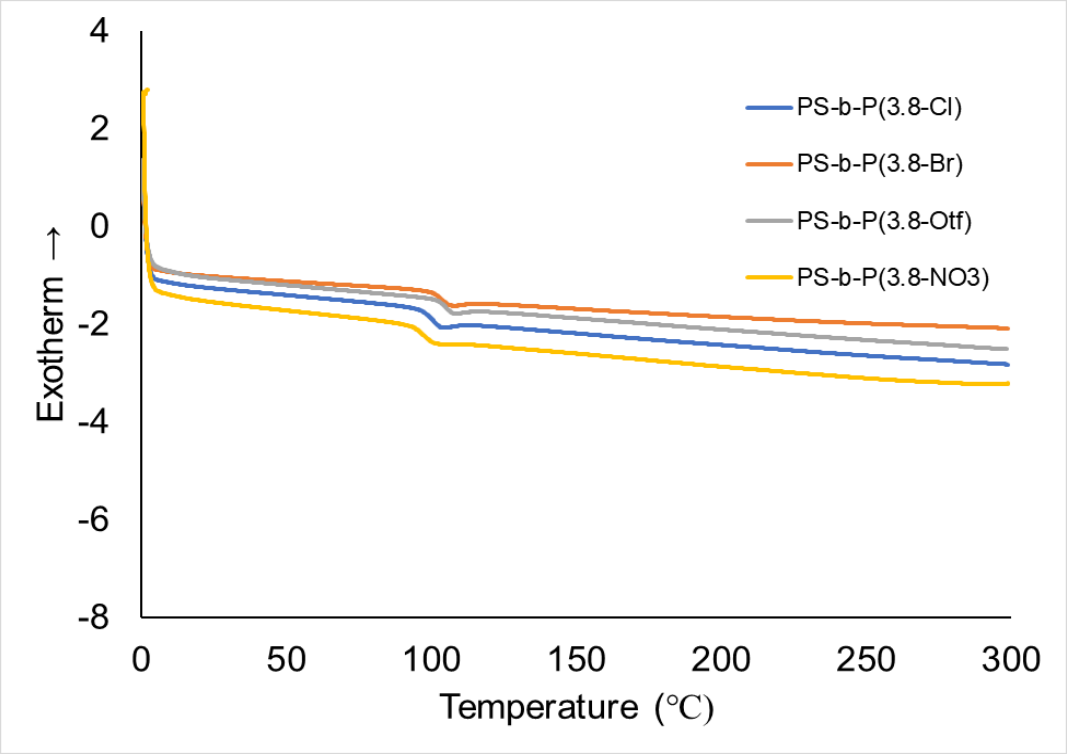

Figure B-18 DSC thermograms from heating cycle.

	DMF		THF	
	Slow H_2O Addition	Fast addition to H_2O	Slow H_2O Addition	Fast addition to H_2O
Kinetically Trapped	$p < 0.001$	$p < 0.001$	$p < 0.001$	$p < 0.001$
Solvent Annealed	$p = 0.241$	$p < 0.001$	$p < 0.001$	$p < 0.001$

Table B-1. Summary of the results of the one-way ANOVA involving BCP assembly diameters for different anions. $p < 0.05$ means the null hypothesis is rejected and that there was a significant effect of the anion identity on the z-average measured size from DLS. In these cases, the data was further analyzed by a Tukey's post-hoc test (Table B-2 below)

	DMF				THF			
	Kinetically Trapped		Solvent Annealed		Kinetically Trapped		Solvent Annealed	
	Slow H_2O Addition	Fast Addition to H_2O	Slow H_2O Addition	Fast Addition to H_2O	Slow H_2O Addition	Fast Addition to H_2O	Slow H_2O Addition	Fast Addition to H_2O
Cl ↔ Br	p = 0.002	p < 0.001	p = 0.944	p < 0.001	p = 0.988	p = 0.001	p = 0.009	p < 0.001
Cl ↔ NO_3	p = 0.094	p < 0.001	p = 0.750	p < 0.001	p < 0.001	p = 0.002	p < 0.001	p < 0.001
Cl ↔ OTf	p = 1.000	p < 0.001	p = 0.759	p < 0.001	p < 0.001	p = 0.225	p < 0.001	p < 0.001
Br ↔ NO_3	p < 0.001	p = 0.89	p = 0.417	p = 0.79	p < 0.001	p = 0.979	p = 0.001	p = 0.35
Br ↔ OTf	p < 0.001	p = 0.90	p = 0.973	p < 0.001	p = 0.001	p = 0.038	p < 0.001	p = 0.05
NO_3 ↔ OTf	p = 0.045	p = 0.60	p = 0.214	p < 0.001	p < 0.001	p = 0.044	p = 0.298	p = 0.55

Table B-2. Results of $p \geq 0.05$ from the post-hoc Tukey test performed with the one-way ANOVA. For readability values of $p < 0.05$ have been indicated by light grey cells.

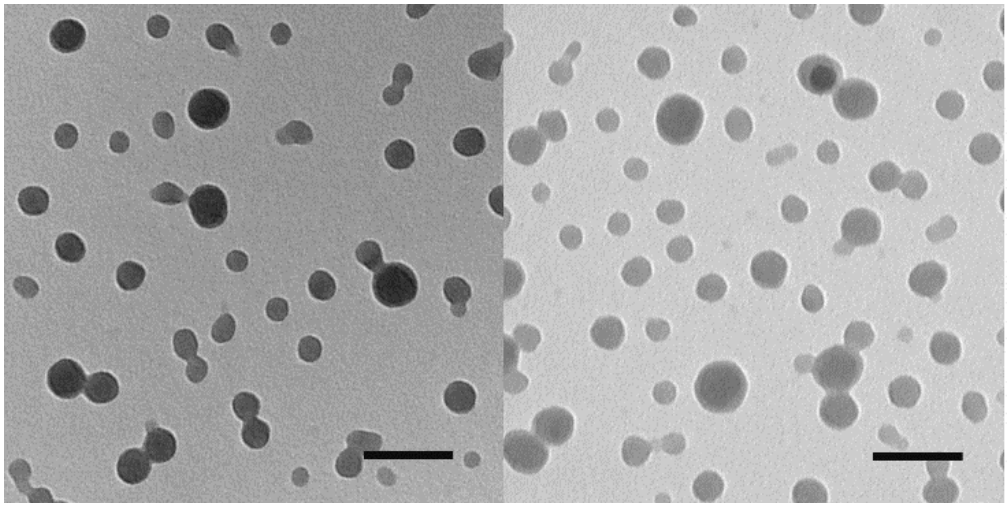

Figure B-19. Morphological comparison of **PS_{390}-b-P(3.8-Cl)$_7$** *with RAFT end-group* (Left image) and **PS_{390}-*b*-P(3.8-Cl)$_7$** *with RAFT end-group removed* by stirring of the polymer with propylamine[1] (Right image). Both suspensions were formed by slow addition of water into a 1 mg/mL DMF BCP solution, scale bars 100 nm.

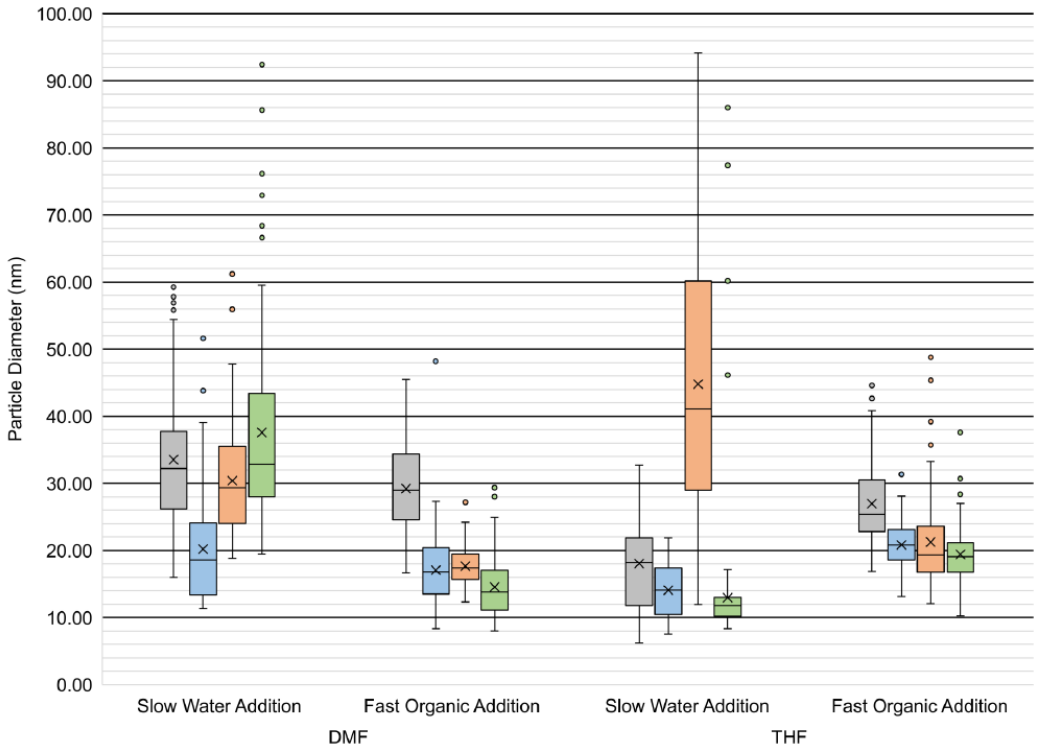

Figure B-20. Box and whisker plot of the particle distribution obtained from the TEM images of the kinetically trapped particles (see Figure B-21 for the explanation of box and whiskers plots). Grey - **PS_{390}-*b*-P(3.8-Cl)$_7$**, blue - **PS_{390}-*b*-P(3.8-Br)$_7$**, orange - **PS_{390}-*b*-P(3.8-OTf)$_7$**, green - **PS_{390}-*b*-P(3.8-NO_3)$_7$**.

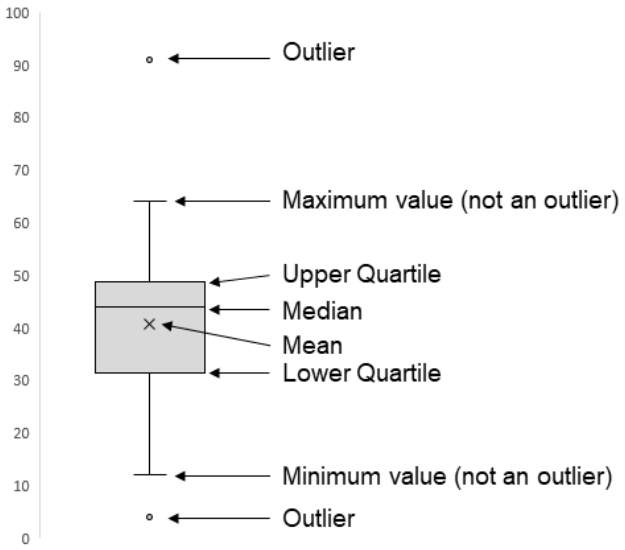

Figure B-21. How to read a box and whisker plot. The lower quartile (LQ) is the greatest value of the lowest 25% of values, the upper quartile (UQ) is the greatest value of the lowest 75% of values. The interquartile range (IQR) is defined as the difference between the upper and lower quartiles. A value is an outlier if it is less than LQ – (1.5 × IQR) or if it is greater than UQ + (1.5 × IQR).

References

1 Q. Zhang, L. Voorhaar, B. G. De Geest, R. Hoogenboom, *Macromol. Rapid Commun.*, 2015, **36**, 1177-1183

Appendix C – Supplemental Information for Chapter 4

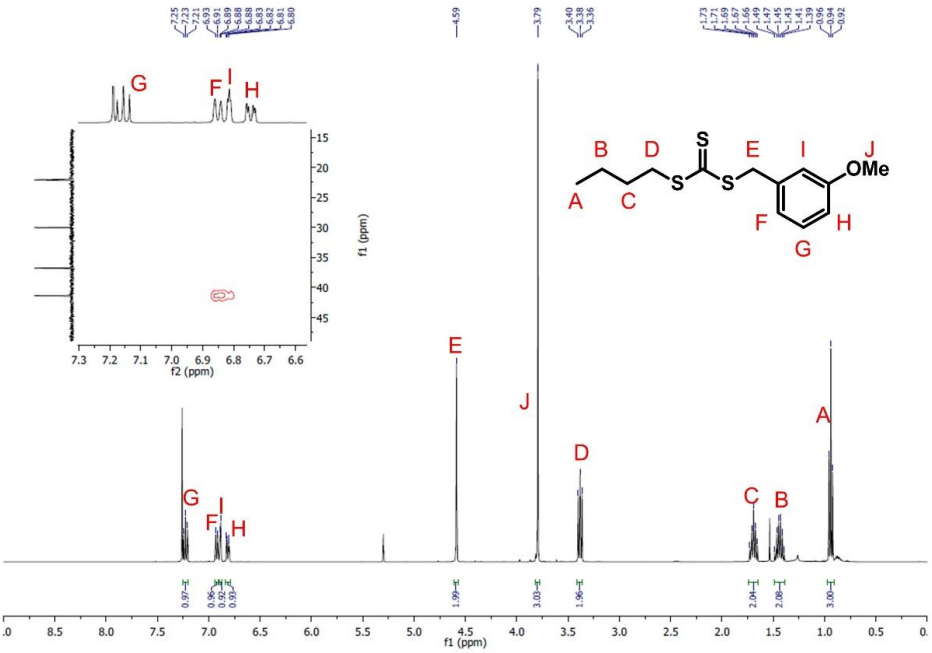

Figure C-1. ^{1}H NMR ($CDCl_3$, 400 MHz) spectrum of butyl(3-methoxybenzyl)trithiocarbonate, the inset is of the HMBC and demonstrates coupling between the benzylic carbon and one of the aryl protons to aid in assignment.

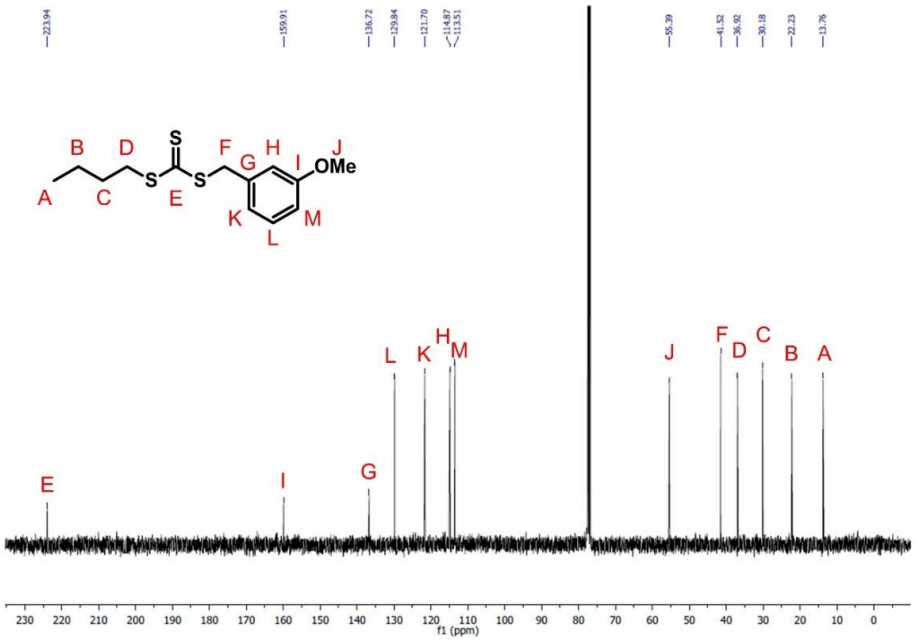

Figure C-2. ^{13}C NMR ($CDCl_3$, 100 MHz) spectrum of butyl(3-methoxybenzyl)trithiocarbonate

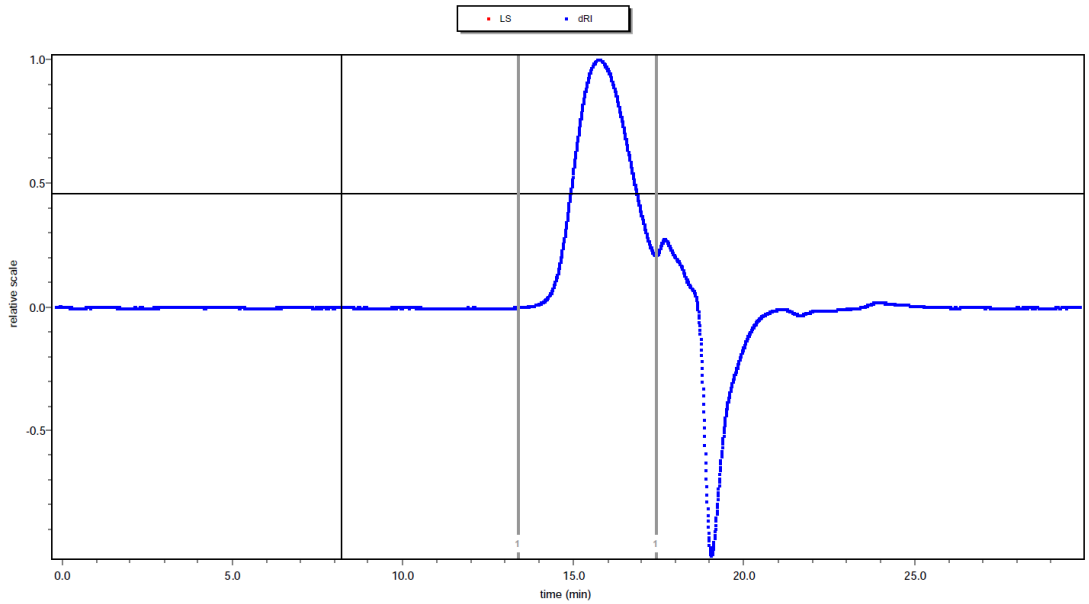

Figure C-3. SEC (1% Et_3N in DMF, refractive index detector) trace of the MacroRAFT agent

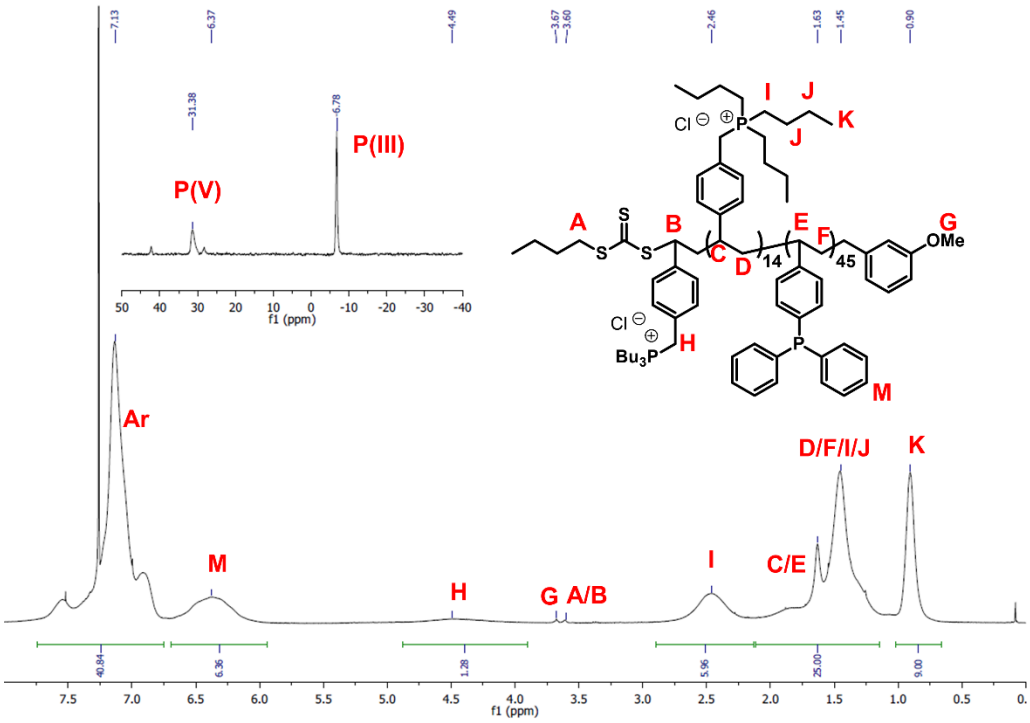

Figure C-4 ^1H NMR ($CDCl_3$, 400 MHz) spectrum of **P(PCl)$_{15}$-*b*-P(DPP)$_{45}$** BCP. Relative integration of the butyl methyl groups to the protons labeled H was used to determine the DP of the P(PCl) block.

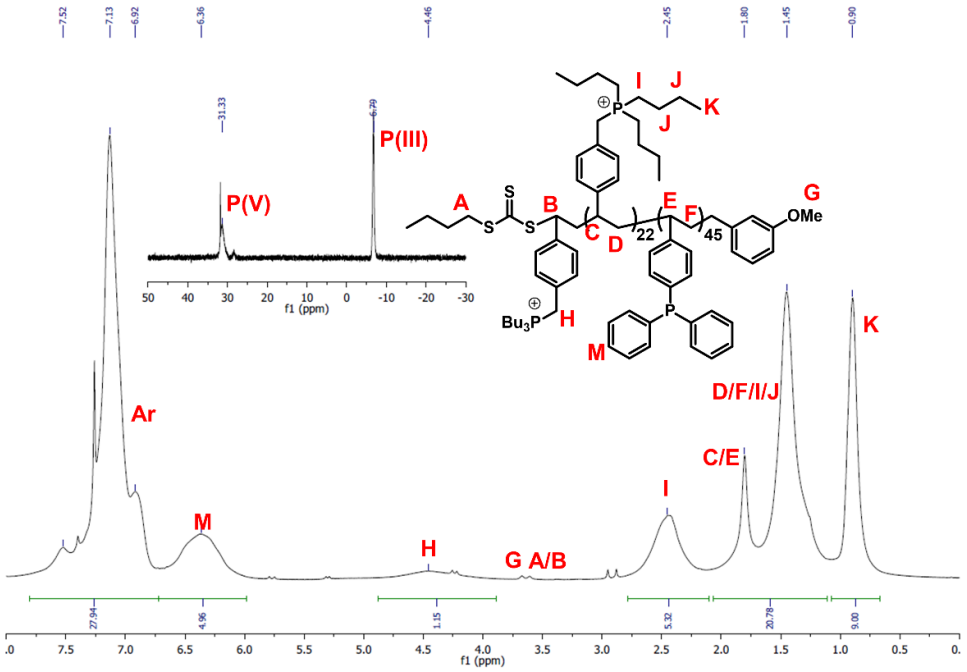

Figure C-5 ^{1}H NMR ($CDCl_3$, 400 MHz) spectrum of **P(PCl)$_{23}$-*b*-P(DPP)$_{45}$** BCP. Relative integration of the butyl methyl groups to the protons labeled H was used to determine the DP of the P(PCl) block.

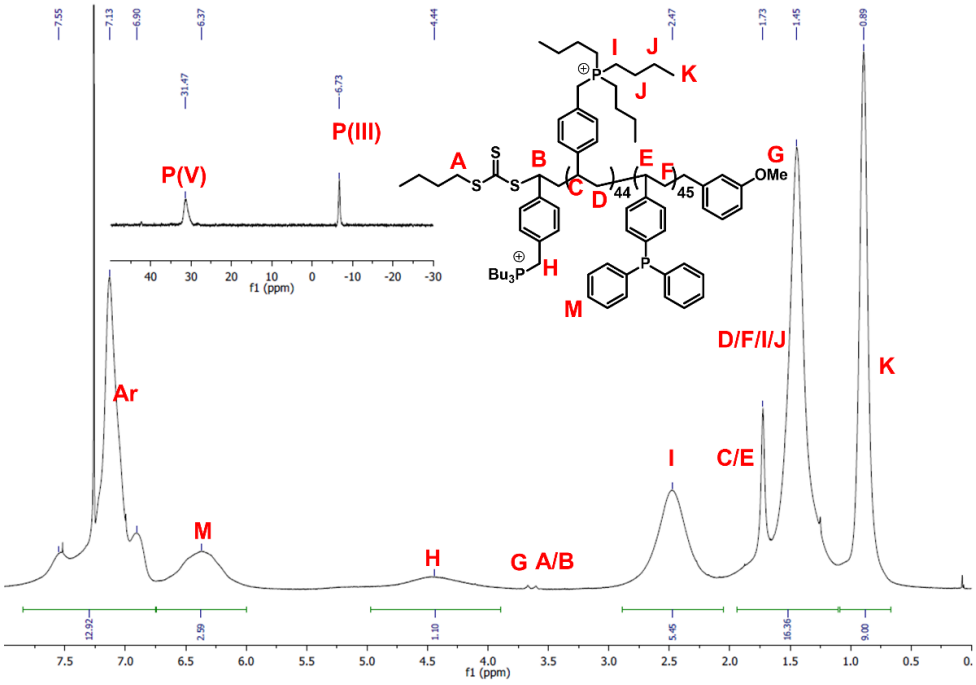

Figure C-6 ^{1}H NMR ($CDCl_3$, 400 MHz) spectrum of **P(PCl)$_{45}$-*b*-P(DPP)$_{45}$** BCP. Relative integration of the butyl methyl groups to the protons labeled H was used to determine the DP of the P(PCl) block.

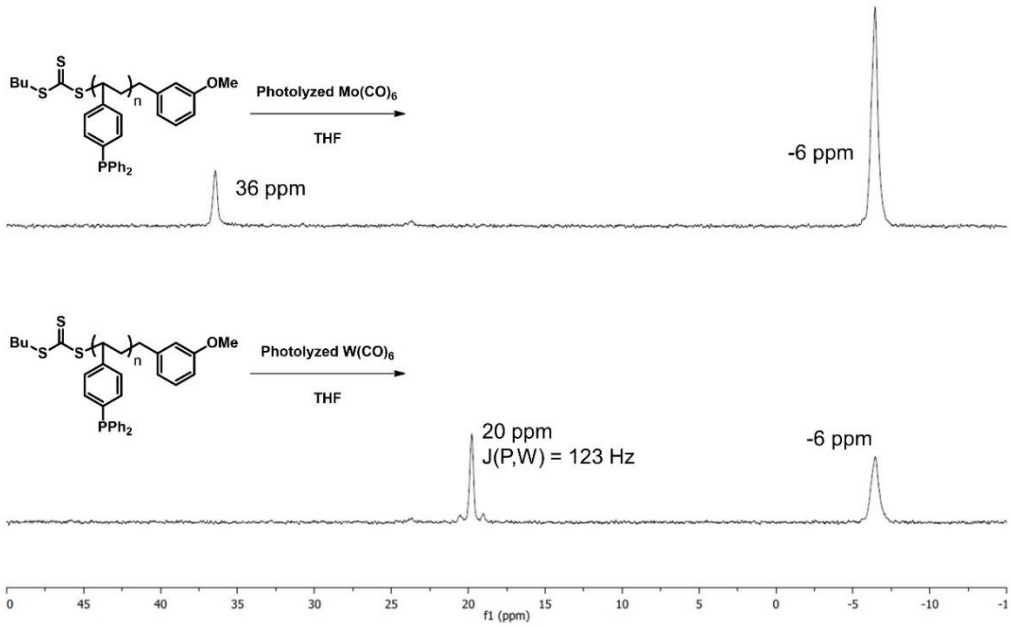

Figure C-7. $^{31}P\{^{1}H\}$ NMR (THF-H_8, 161 MHz) spectra of reaction mixtures of polyphosphine with the photolyzed metal carbonyls.

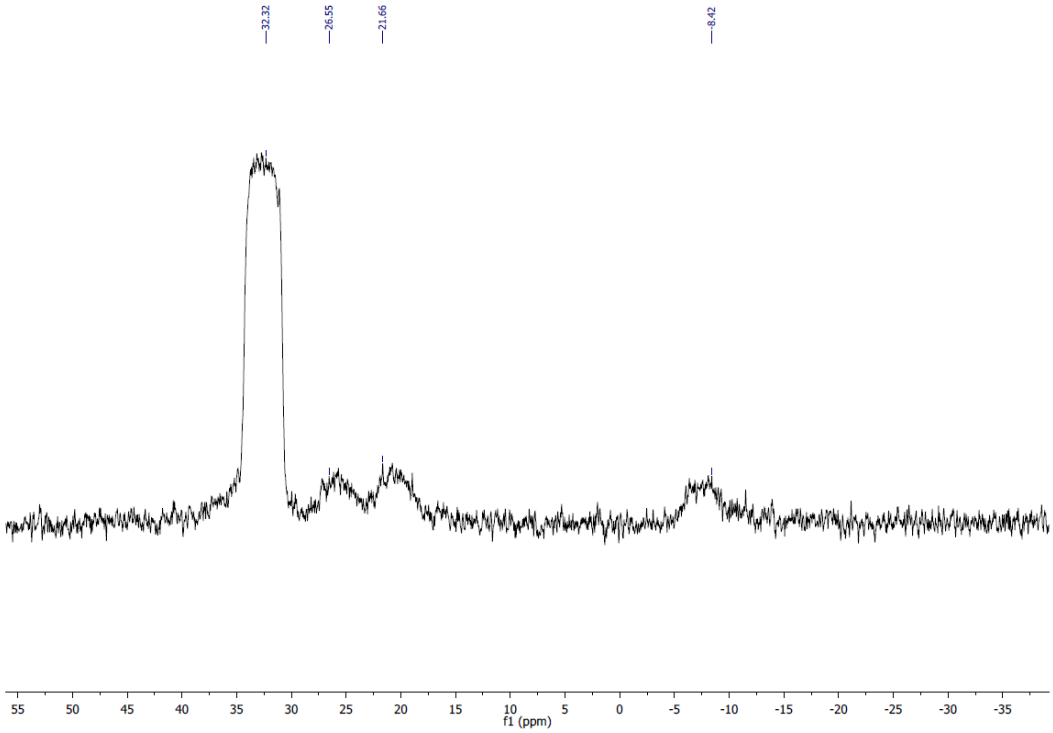

Figure C-8 $^{31}P\{^{1}H\}$ NMR (THF-H_8, 161 MHz) spectrum of the precipitate from the reaction of the BCP with photolyzed $W(CO)_6$. Unreacted phosphine is present at -8 ppm, and phosphine oxide is present at 26 ppm.

Appendix D – Supplemental Information for Chapter 5

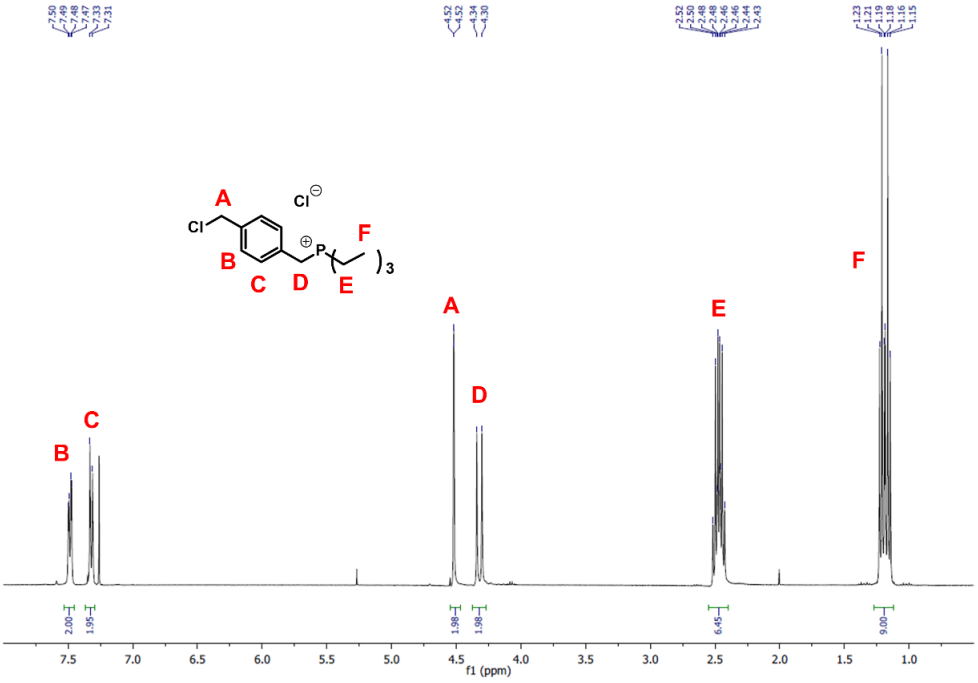

Figure D-1 ^{1}H NMR ($CDCl_3$, 400 MHz) spectrum of the 4-chloromethylbenzyltriethylphosphonium chloride

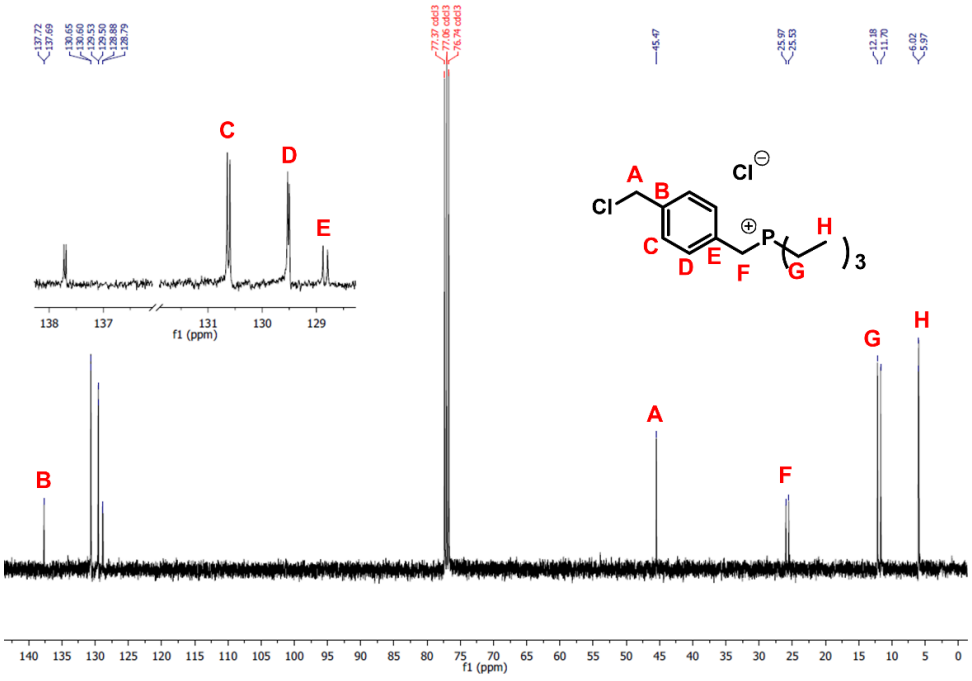

Figure D-2 $^{13}C\{^{1}H\}$ NMR ($CDCl_3$, 400 MHz) spectrum of 4-chlromethylbenzyltriethylphosphonium chloride. Insert is blow-up of the aromatic region.

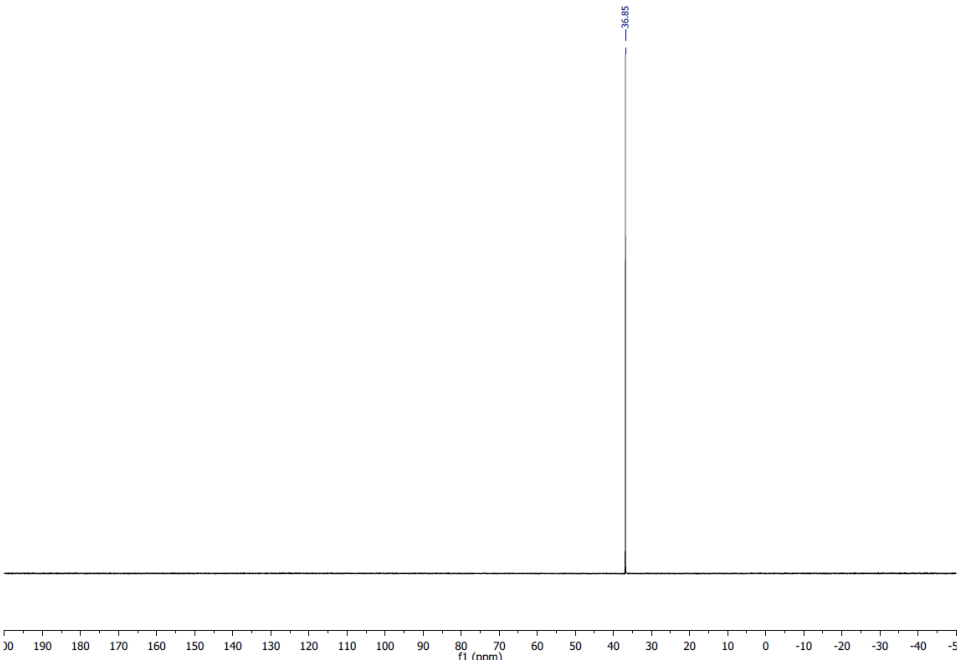

Figure D-3 $^{31}P\{^{1}H\}$ NMR ($CDCl_3$, 161 MHz) spectrum of 4-chlromethylbenzyltriethylphosphonium chloride.

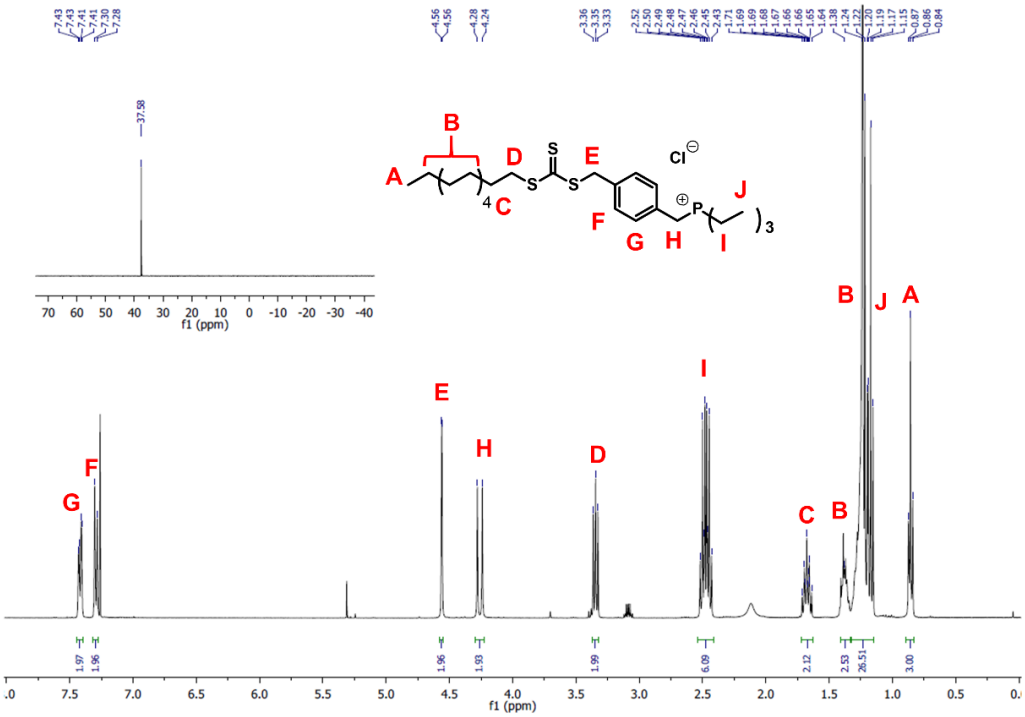

Figure D-4 ^{1}H NMR ($CDCl_3$, 400 MHz) spectrum of the S-1-dodecyl-S'-(methylbenzyltriethylphosphonium chloride) trithiocarbonate. Insert is the $^{31}P\{^{1}H\}$ NMR ($CDCl_3$, 161 MHz) spectrum.

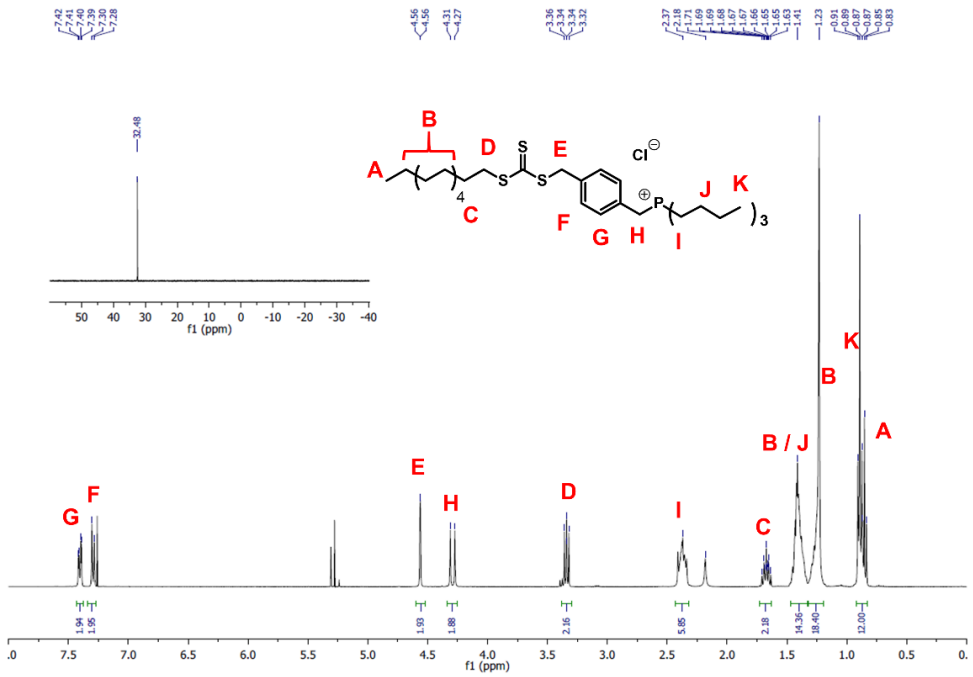

Figure D-5 ^{1}H NMR ($CDCl_3$, 400 MHz) spectrum of S-1-dodecyl-S'-(methylbenzyltributylphosphonium chloride) trithiocarbonate. The inset shows the $^{31}P\{^{1}H\}$ NMR ($CDCl_3$, 161 MHz) spectrum.

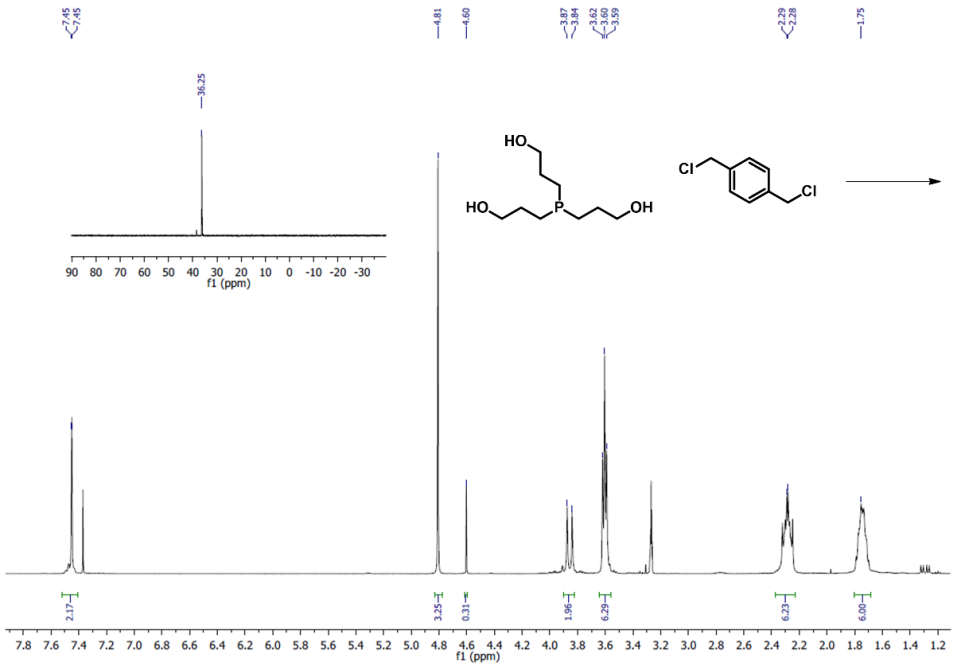

Figure D-6 ^{1}H NMR ($CDCl_3$, 400 MHz) spectrum of the reaction between tri(3-hydroxypropyl)phosphine and xylylene dichloride, typical of products from several reaction conditions. Inset is the $^{31}P\{^{1}H\}$ NMR ($CDCl_3$, 161 MHz) spectrum.

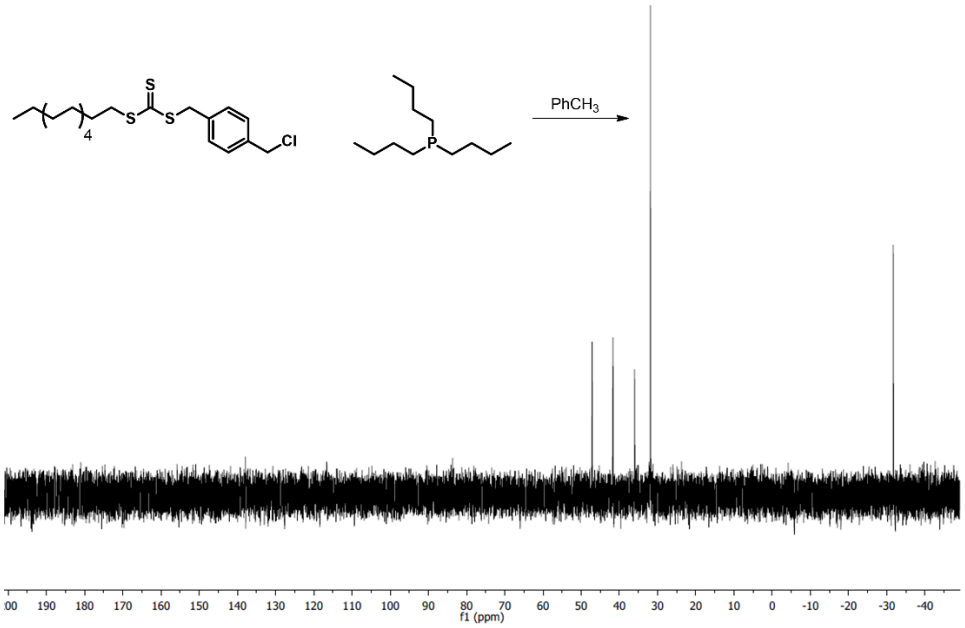

Figure D-7 $^{31}P\{^{1}H\}$ NMR (Toluene-H_8, 161 MHz) spectrum of the crude reaction mixture of tributylphosphine with a chloride functionalized RAFT agent.

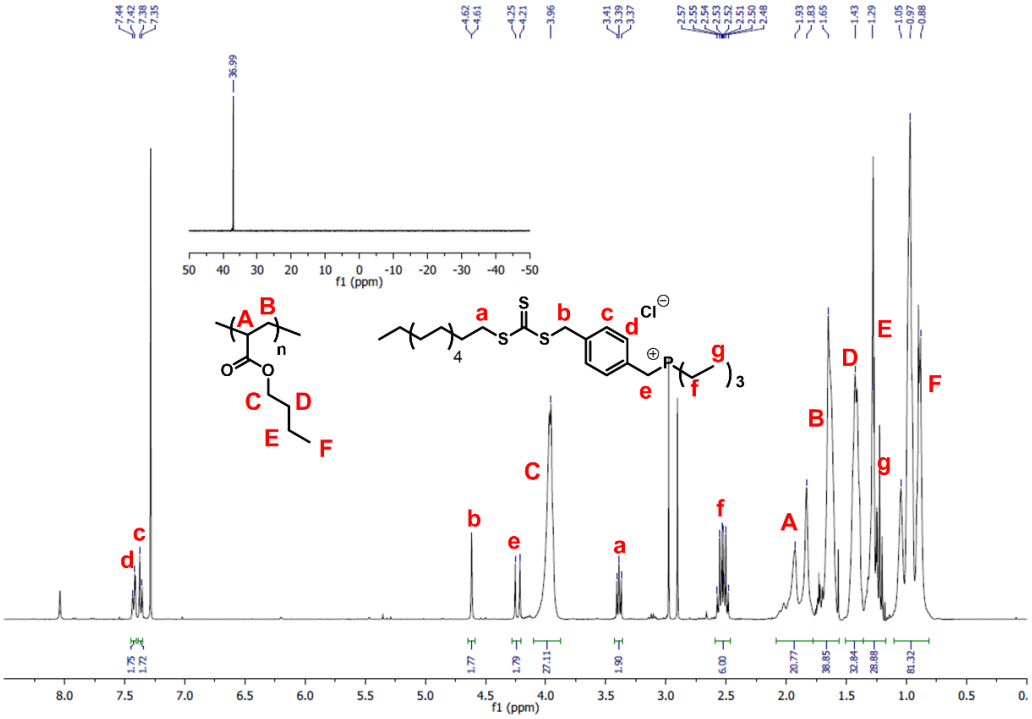

Figure D-8 ^{1}H NMR ($CDCl_3$, 400 MHz) spectrum of the resulting material from the polymerization butyl acrylate in the presence of RAFT-PEt_3. Inset if the $^{31}P\{^{1}H\}$ NMR ($CDCl_3$, 161 MHz) spectrum of the mixture.

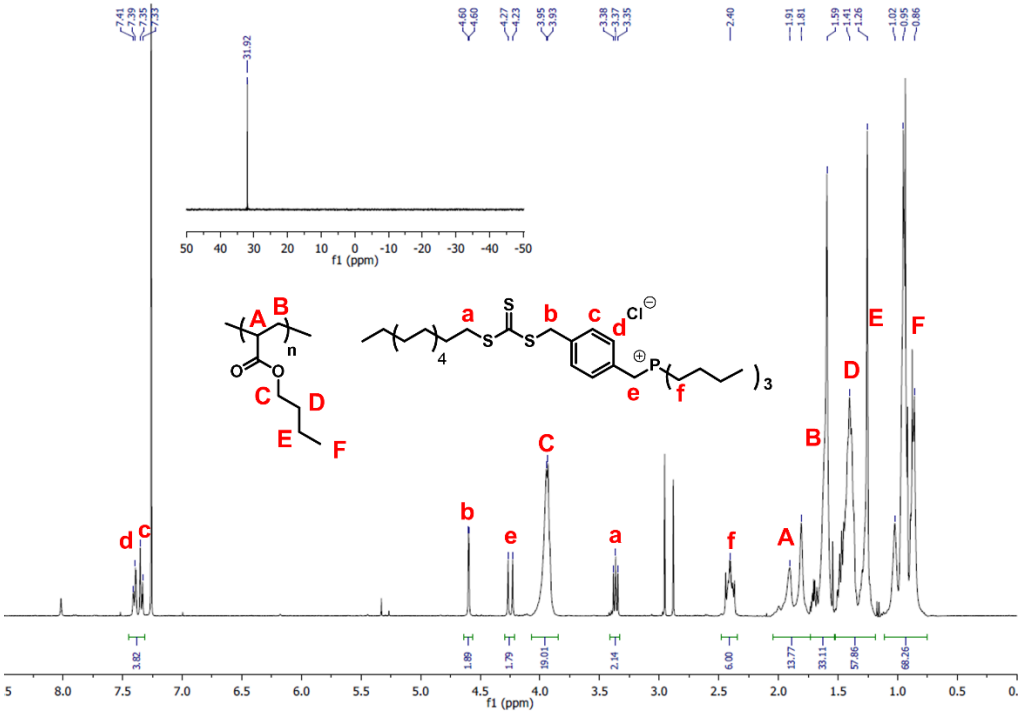

Figure D-9 ^{1}H NMR ($CDCl_3$, 400 MHz) spectrum of the resulting material from the polymerization butyl acrylate in the presence of RAFT-PBu_3. Inset of the $^{31}P\{^{1}H\}$ NMR ($CDCl_3$, 161 MHz) spectrum of the mixture.

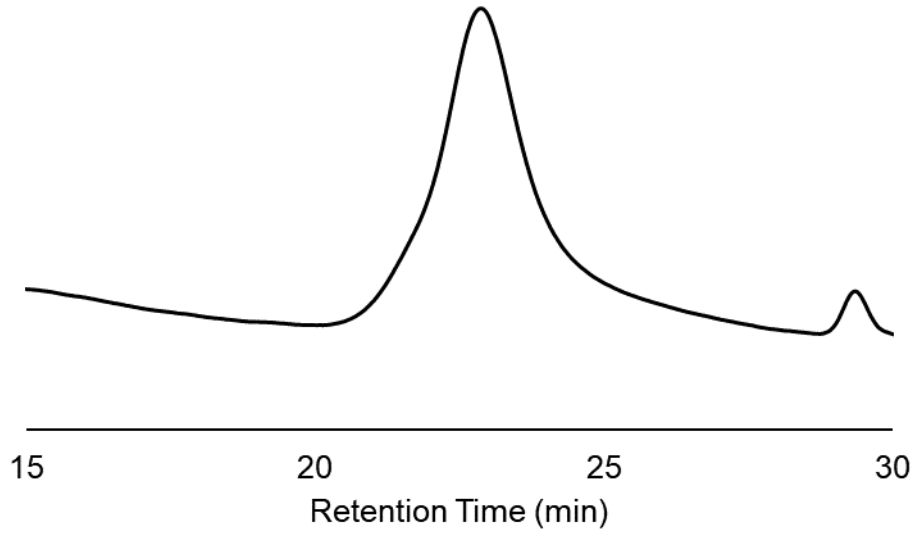

Figure D-10. SEC trace of the $PBuA_{78}$-PEt_3Cl, the peak at 29 minutes is a system peak.

Appendix E – Permissions

Permission for Figure 1-9

ROYAL SOCIETY OF CHEMISTRY LICENSE TERMS AND CONDITIONS

Apr 26, 2018

This Agreement between Western University -- Benjamin Hisey ("You") and Royal Society of Chemistry ("Royal Society of Chemistry") consists of your license details and the terms and conditions provided by Royal Society of Chemistry and Copyright Clearance Center.

License Number	4336040791686
License date	Apr 25, 2018
Licensed Content Publisher	Royal Society of Chemistry
Licensed Content Publication	Chemical Society Reviews
Licensed Content Title	Self-assembly of block copolymers
Licensed Content Author	Yiyong Mai,Adi Eisenberg
Licensed Content Date	Jul 9, 2012
Licensed Content Volume	41
Licensed Content Issue	18
Type of Use	Thesis/Dissertation
Requestor type	academic/educational
Portion	figures/tables/images
Number of figures/tables /images	1
Format	print and electronic
Distribution quantity	10
Will you be translating?	no
Order reference number	
Title of the thesis/dissertation	Incorporation of phosphorus into block copolymers for solution phase self-assembly
Expected completion date	Jun 2018
Estimated size	200
Requestor Location	Western University 1151 Richmond Street London, ON N6a3K7 Canada Attn: Western University
Billing Type	Invoice
Billing Address	Western University 1151 Richmond Street London, ON N6a3K7 Canada

Permission for Figure 1-11

ELSEVIER LICENSE
TERMS AND CONDITIONS

Apr 26, 2018

This Agreement between Western University -- Benjamin Hisey ("You") and Elsevier ("Elsevier") consists of your license details and the terms and conditions provided by Elsevier and Copyright Clearance Center.

License Number	4317110319599
License date	Mar 27, 2018
Licensed Content Publisher	Elsevier
Licensed Content Publication	Advanced Drug Delivery Reviews
Licensed Content Title	Advanced drug delivery devices via self-assembly of amphiphilic block copolymers
Licensed Content Author	Annette Rösler,Guido W.M Vandermeulen,Harm-Anton Klok
Licensed Content Date	Dec 3, 2001
Licensed Content Volume	53
Licensed Content Issue	1
Licensed Content Pages	14
Start Page	95
End Page	108
Type of Use	reuse in a thesis/dissertation
Portion	figures/tables/illustrations
Number of figures/tables /illustrations	1
Format	both print and electronic
Are you the author of this Elsevier article?	No
Will you be translating?	No
Original figure numbers	Figure 1
Title of your thesis/dissertation	Incorporation of phosphorus into block copolymers for solution phase self-assembly
Expected completion date	Jun 2018
Estimated size (number of pages)	200
Requestor Location	Western University 1151 Richmond Street London, ON N6a3K7 Canada Attn: Western University
Publisher Tax ID	GB 494 6272 12

Permission for Figure 5-1

JOHN WILEY AND SONS LICENSE TERMS AND CONDITIONS

Apr 26, 2018

This Agreement between Western University -- Benjamin Hisey ("You") and John Wiley and Sons ("John Wiley and Sons") consists of your license details and the terms and conditions provided by John Wiley and Sons and Copyright Clearance Center.

License Number	4320900771224
License date	Apr 02, 2018
Licensed Content Publisher	John Wiley and Sons
Licensed Content Publication	Polymer International
Licensed Content Title	End-functional polymers, thiocarbonylthio group removal/transformation and reversible addition–fragmentation–chain transfer (RAFT) polymerization
Licensed Content Author	Graeme Moad, Ezio Rizzardo, San H Thang
Licensed Content Date	Dec 23, 2010
Licensed Content Volume	60
Licensed Content Issue	1
Licensed Content Pages	17
Type of use	Dissertation/Thesis
Requestor type	University/Academic
Format	Print and electronic
Portion	Figure/table
Number of figures/tables	3
Original Wiley figure/table number(s)	Scheme 3
Will you be translating?	No
Title of your thesis / dissertation	Incorporation of phosphorus into block copolymers for solution phase self-assembly
Expected completion date	Jun 2018
Expected size (number of pages)	200
Requestor Location	Western University 1151 Richmond Street London, ON N6a3K7 Canada Attn: Western University
Publisher Tax ID	EU826007151
Total	0.00 CAD
Terms and Conditions	

Curriculum Vitae

Name:	Benjamin Hisey
Post-Secondary Education and Degrees:	University of Waterloo Waterloo, Ontario, Canada 2009-2013 B.Sc.
Honours and Awards:	Chemistry Upper Year Scholarship 2012-2013, Waterloo Lipson-Baines Award 2015-2016, Western
Related Work Experience:	Research Assistant The University of Waterloo 2012 Graduate Teaching Assistant The University of Western Ontario 2013-2018

Publications:

1. Benjamin Hisey, Paul J. Ragogna, Elizabeth R. Gillies. Phosphonium functionalized polymer micelles with intrinsic antibacterial activity. *Biomacromolecules*. **2017**, *18* (3), 914-923
2. Benjamin Hisey, Jasmine Buddingh, Elizabeth R. Gillies, Paul J. Ragogna. Effect of counter ions of the self-assembly of polystyrene-polyphosphonium block. *Langmuir*. **2017**, *33*(51), 14738-14747